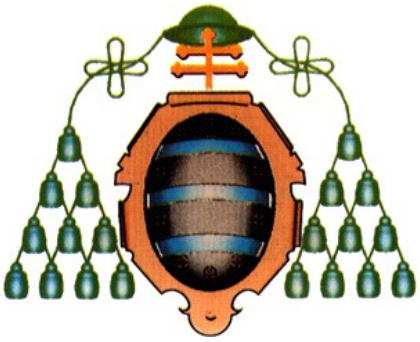

UNIVERSIDAD DE OVIEDO

Programa de Doctorado de Ciencia y Tecnología de Materiales

"Comportamiento en frío y en caliente de aceros con bajo contenido de carbono obtenidos a través de procesos de laminación controlada"

TESIS DOCTORAL

MARÍA JOSÉ QUINTANA HERNÁNDEZ

MARZO 2013

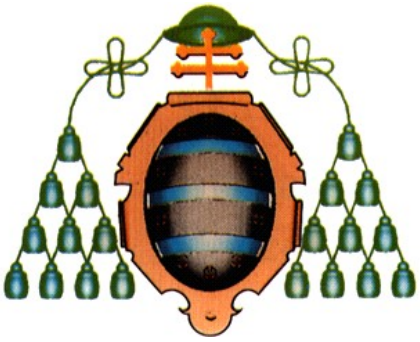

UNIVERSIDAD DE OVIEDO

Programa de Doctorado de Ciencia y Tecnología de Materiales

"Comportamiento en frío y en caliente de aceros con bajo contenido de carbono obtenidos a través de procesos de laminación controlada"

TESIS DOCTORAL

Nombre de directores de tesis

José Ignacio Verdeja González

Luis Felipe Verdeja González

RESUMEN DEL CONTENIDO DE TESIS DOCTORAL

1.- Título de la Tesis	
Español: Comportamiento en frío y en caliente de aceros con bajo contenido de carbono obtenidos a través de procesos de laminación controlada	Inglés: Room temperature and high temperature behavior of low carbon steels manufactured by controlled rolling processes

2.- Autor	
Nombre: María José Quintana Hernández	
Programa de Doctorado: Ciencia y Tecnología de Materiales	
Órgano responsable: Departamento de Ciencia de los Materiales e Ingeniería Metalúrgica	

RESUMEN (en español)

Los aceros con bajo contenido de carbono microaleados con Ti y Nb fabricados en la planta de Arcelor Mittal en Asturias, España usando el método avanzado de control termomecánico para laminación (ATMCRP) de aceros se pueden dividir en dos rubros: aceros de fase dual (enfriados con agua) y aceros HSLA (cuando el enfriamiento se realiza más lentamente). Dentro de las ventajas de este proceso se encuentran las propiedades mecánicas que permiten su aplicación industrial y el bajo costo en comparación a aceros aleados; los aceros con estas características se pueden utilizar en procesos como estirado y embutido en aplicaciones automotrices (largueros, piezas de refuerzo, etc.) o navales.

Los aceros de fase dual son una excelente alternativa para la fabricación de piezas automotrices que requieran alta resistencia mecánica, alta resistencia al impacto y elongaciones elevadas. Este tipo de materiales se fabrican a partir de aceros de baja aleación en procesos ATMCRP y agregando otros aleantes para inducir la creación de precipitados, reducir costos y que el producto final tenga una microestructura de martensita y ferrita de grano ultrafino. Todas estas características se logran controlando ciertos parámetros del proceso: la velocidad de deformación, la velocidad de enfriamiento y el templado del material. Esta tesis presenta los resultados de ensayos de tracción de dos aceros de fase dual (DP600 y DP780), así como la caracterización microestructural para poder entender el efecto de este tipo de laminación controlada en la creación de la microestructura responsable de las propiedades mecánicas exhibidas por estos aceros.

Los aceros HSLA con estructuras de grano ultrafino fabricados por métodos ATMCRP pueden presentar comportamiento superplástico a ciertas temperaturas y velocidades de deformación tales que permitan que se activen los procesos de deslizamiento de fronteras de grano. Esta tesis muestra los resultados de ensayos de tracción a temperaturas elevadas hechos en un acero de bajo carbono y baja aleación que presenta a 800°C elongaciones de hasta 200%. La microestructura del acero se analizó para calcular el tamaño de grano y su distribución, así como su interacción después de la deformación de las probetas, encontrándose descohesiones, granos de ferrita restaurados y la eliminación de la estructura bandeada, que son evidencias de la superplasticidad del material. Además, mediante microscopia electrónica de barrido se identificaron los diferentes tipos de precipitados presentes en el material, así como los subgranos formados dentro de los cristales de ferrita. Particularmente para este acero, la ventana superplástica se encuentra en esfuerzos de cedencia entre 30 y 70 MPa y velocidades de deformación de 10^{-2} a 10^{-3} s^{-1}. Por otra parte, este comportamiento corresponde a los modelos propuestos por Ashby-Verrall y Vasin et al. lo que confirma el carácter superplástico de este comportamiento.

Para ambos casos, aceros DP o HSLA, la microestructura tiene una función muy importante: para aceros DP la martensita es la responsable de disminuir el cociente esfuerzo de cedencia / esfuerzo de tracción y para aceros HSLA, la ferrita requiere una fase dura (perlita) que evita el crecimiento del grano, sin endurecer el material permitiendo a los granos deslizar y rotar como lo requiere el comportamiento superplástico.

RESUMEN (en Inglés)

Commercial weldable low carbon steels microalloyed with titanium and niobium manufactured in the Arcelor Mittal factories in Asturias, Spain through the Advanced Thermomechanical Controlled Rolling Processes (ATMCRP) can be divided into dual-phase steels (using a faster cooling method through the use of pulverized water) or HSLA steels (using a slower cooling method). The advantage of such manufacturing process is the mechanical properties as well as the cost, and that steels obtained from this method are used in drawing and bending processes in automotive (reinforced parts, beams, etc.) or shipbuilding applications.

Dual-phase steels are an excellent alternative in the production of automotive parts that require high mechanical resistance, high impact strength and elevated elongation. These materials are produced using low-alloy steels as a basis (through ATMCRP) and using other elements in order to create precipitates, reducing costs and resulting in a combination of martensite and ferrite structures with ultrafine grain sizes. These characteristics are accomplished through a strict control of rolling conditions: strain rate, cooling rate and direct quenching. This thesis presents the results of tension testing of two types of double phased steels, along with microstructural characterization, in order to understand the effect of the advanced thermomechanical controlled rolling processes on the formation of the microstructure and the resulting mechanical properties.

HSLA steels with ultrafine grained structure may present superplastic behavior at specific temperatures and strain rates that allow the grain boundary sliding mechanisms to be activated. This thesis presents high temperature tension tests in a low carbon, low alloy steel obtained by advanced thermomechanical controlled rolling processes (slow cooling), showing at 800°C elongations as high as 200%. The microstructure of the steel was analyzed in order to identify ferrite and pearlite grain boundaries, and their interaction after the specimens were deformed, showing intergranular decohesions, restored ferrite grains and elimination of banded structure, which are evidence of superplastic mechanisms in this material which is, in fact, ultrafine grained as demonstrated by quantitative metallographic techniques and grain size distribution analysis. Also, analysis by scanning electron microscope was used to identify different types of precipitates present in the material, as well as subgrains formed inside the ferrite crystals. In particular the superplastic window lies between 30 and 70 MPa (in yield stress) and 10^{-5} to $10^{-3}\ s^{-1}$ (in strain rate). Furthermore, the behavior of this steel agrees with the Ashby-Verrall and Vasin et al. models which indicate that in fact this steel behaves superplastically in certain conditions.

For both cases, DP and HSLA steels, the microstructure plays a very important role: for DP steels, the martensite is responsible for decreasing the yield stress / tension stress ratio (in order to increase the strain hardening coefficient *n* and allowing the material to be used in manufacturing applications), while for HSLA steels, the ferrite requires a hard phase (pearlite) to maintain the fine grain size without hardening the material and allowing the sliding and rotation of grains in order to achieve superplasticity.

SR. PRESIDENTE DE LA COMISIÓN ACADÉMICA DEL PROGRAMA DE DOCTORADO DE CIENCIA Y TECNOLOGIA DE MATERIALES

A mis padres, Jaime y Ana Marcela,

y a mis hermanas, Marcela y Ana,

por su apoyo incondicional

Agradecimientos

Agradezco a mis padres tanto su apoyo incondicional como por creer en mí, a pesar de no saber muy bien qué hacía, a lo largo de todos estos años para que yo pudiera seguir por un camino profesional desconocido y no convencional para ellos. Temo decirles que no tienen hijas normales y yo no soy la excepción.

A mis hermanas por ponerme atención cuando platicaba de lo que hacía en los experimentos y resultados, y su presencia en ponencias en congresos, a pesar de no entender mucho o casi nada de lo que decía, y sí hay ingenieros guapos, a ver si ahora sí me hacen caso.

A Roberto González por haberme introducido a este mundo increíble del estudio de los materiales y por motivarme siempre a continuar en él. Además agradezco profundamente su ayuda en la revisión de la redacción y ortografía en inglés de este escrito. Así como todos sus consejos que me han permitido dedicarme a la investigación y poder publicar en revistas internacionales, a lo largo de varios años y sobre muchos temas.

A José Ignacio Verdeja por su ayuda personal y profesional para hacer las investigaciones y artículos que llevaron a la escritura de esta tesis. Así como por la dirección e inspiración que llevaron a los ensayos y los capítulos a realizar, y por la revisión del contenido de toda la tesis.

A Luis Felipe Verdeja por todo el tiempo que invirtió para que yo lograra la escritura y publicación de esta tesis y por todo el trabajo administrativo, tanto en México como en España, que implicó esta titulación.

A José Ovidio García, por su ayuda invaluable en la obtención de resultados, muestras y micrografías presentes en esta tesis. También por todo el espacio de ordenador y múltiples carpetas en el escritorio que implicaron la realización de esta investigación.

A Julio Riba, por su ayuda en la obtención de micrografías con microscopio electrónico de barrido, incluyendo el tiempo que dedicó a buscar todas las descohesiones y precipitados que deseábamos ver en las muestras.

A Sara Fernández por la cooperación a distancia, con diferencia de horas y hasta con cambio de horario desfasado, para poder transmitirnos los resultados obtenidos, con todo y correcciones en ambos sentidos.

A la Universidad Panamericana y a Félix Martínez por el financiamiento de las estancias de investigación y la disponibilidad de tiempo para que hiciera tanto los ensayos como la escritura de esta tesis.

A la Universidad de Oviedo y al Centro Internacional de Postgrado por su ayuda y apoyo para poder obtener el grado de doctor.

A ArcelorMittal por proporcionar los aceros investigados para esta tesis, así como por la innovación en el proceso ATMCRP que ha llevado a la caracterización desde hace varios años de los aceros creados por este método y que además de esta tesis ha resultado en múltiples artículos y ponencias en congresos.

A todos los que me motivaron para que esta publicación fuera posible.

El mundo de los materiales no tiene edad, fronteras o nacionalidad, sólo existe la pasión de un nuevo descubrimiento que motive la tecnología, esto es algo que noté al hacer esta tesis y por esto me enorgullece pertenecer a él.

Abstract

Commercial weldable low carbon steels microalloyed with titanium and niobium manufactured in the Arcelor Mittal factories in Asturias, Spain through the Advanced Thermomechanical Controlled Rolling Processes (ATMCRP) can be divided into dual-phase steels (using a faster cooling method through the use of pulverized water) or HSLA steels (using a slower cooling method). The advantage of such manufacturing process is the mechanical properties as well as the cost, and that steels obtained from this method are used in drawing and bending processes in automotive (reinforced parts, beams, etc.) or shipbuilding applications.

Dual-phase steels are an excellent alternative in the production of automotive parts that require high mechanical resistance, high impact strength and elevated elongation. These materials are produced using low-alloy steels as a basis (through ATMCRP) and using other elements in order to create precipitates, reducing costs and resulting in a combination of martensite and ferrite structures with ultrafine grain sizes. These characteristics are accomplished through a strict control of rolling conditions: strain rate, cooling rate and direct quenching. This thesis presents the results of tension testing of two types of double phased steels, along with microstructural characterization, in order to understand the effect of the advanced thermomechanical controlled rolling processes on the formation of the microstructure and the resulting mechanical properties.

HSLA steels with ultrafine grained structure may present superplastic behavior at specific temperatures and strain rates that allow the grain boundary sliding mechanisms to be activated. This thesis presents high temperature tension tests in a low carbon, low alloy steel obtained by advanced thermomechanical controlled rolling processes (slow cooling), showing at $800°C$ elongations as high as 200%. The microstructure of the steel was analyzed in order to identify ferrite and pearlite grain boundaries, and their interaction after the specimens were deformed, showing intergranular decohesions, restored ferrite grains and elimination of banded structure, which are evidence of superplastic mechanisms in this material which is, in fact, ultrafine grained as demonstrated by quantitative metallographic techniques and grain size distribution analysis. Also, analysis by scanning electron microscope was used to identify different types of precipitates present in the material, as well as subgrains formed inside the ferrite crystals. In particular the superplastic window lies between 30 and 70 MPa (in yield stress) and 10^{-5} to 10^{-3} s^{-1} (in strain rate). Furthermore, the behavior of this steel agrees with the Ashby-Verrall and Vasin et al. models which indicate that in fact this steel behaves superplastically in certain conditions.

For both cases, DP and HSLA steels, the microstructure plays a very important role: for DP steels, the martensite is responsible for decreasing the yield stress / tension stress ratio (in order to increase the strain hardening coefficient n and allowing the material to be used in manufacturing applications), while for HSLA steels, the ferrite requires a hard phase (pearlite) to maintain the fine grain size without hardening the material and allowing the sliding and rotation of grains in order to achieve superplasticity.

Resumen

Los aceros con bajo contenido de carbono microaleados con Ti y Nb fabricados en la planta de Arcelor Mittal en Asturias, España usando el método avanzado de control termomecánico para laminación (ATMCRP) de aceros se pueden dividir en dos rubros: aceros de fase dual (enfriados con agua) y aceros HSLA (cuando el enfriamiento se realiza más lentamente). Dentro de las ventajas de este proceso se encuentran las propiedades mecánicas que permiten su aplicación industrial y el bajo costo en comparación a aceros aleados; los aceros con estas características se pueden utilizar en procesos como estirado y embutido en aplicaciones automotrices (largueros, piezas de refuerzo, etc.) o navales.

Los aceros de fase dual son una excelente alternativa para la fabricación de piezas automotrices que requieran alta resistencia mecánica, alta resistencia al impacto y elongaciones elevadas. Este tipo de materiales se fabrican a partir de aceros de baja aleación en procesos ATMCRP y agregando otros aleantes para inducir la creación de precipitados, reducir costos y que el producto final tenga una microestructura de martensita y ferrita de grano ultrafino. Todas estas características se logran controlando ciertos parámetros del proceso: la velocidad de deformación, la velocidad de enfriamiento y el templado del material. Esta tesis presenta los resultados de ensayos de tracción de dos aceros de fase dual (DP600 y DP780), así como la caracterización microestructural para poder entender el efecto de este tipo de laminación controlada en la creación de la microestructura responsable de las propiedades mecánicas exhibidas por estos aceros.

Los aceros HSLA con estructuras de grano ultrafino fabricados por métodos ATMCRP pueden presentar comportamiento superplástico a ciertas temperaturas y velocidades de deformación tales que permitan que se activen los procesos de deslizamiento de fronteras de grano. Esta tesis muestra los resultados de ensayos de tracción a temperaturas elevadas hechos en un acero de bajo carbono y baja aleación que presenta a $800°C$ elongaciones de hasta 200%. La microestructura del acero se analizó para calcular el tamaño de grano y su distribución, así como su interacción después de la deformación de las probetas, encontrándose descohesiones, granos de ferrita restaurados y la eliminación de la estructura bandeada, que son evidencias de la superplasticidad del material. Además, mediante microscopia electrónica de barrido se identificaron los diferentes tipos de precipitados presentes en el material, así como los subgranos formados dentro de los cristales de ferrita. Particularmente para este acero, la ventana superplástica se encuentra en esfuerzos de cedencia entre 30 y 70 MPa y velocidades de deformación de 10^{-5} a 10^{-3} s^{-1}. Por otra parte, este comportamiento corresponde a los modelos propuestos por Ashby-Verrall y Vasin et al. lo que confirma el carácter superplástico de este comportamiento.

Para ambos casos, aceros DP o HSLA, la microestructura tiene una función muy importante: para aceros DP la martensita es la responsable de disminuir el cociente esfuerzo de cedencia / esfuerzo de tracción y para aceros HSLA, la ferrita requiere una fase dura (perlita) que evita el crecimiento del grano, sin endurecer el material permitiendo a los granos deslizar y rotar como lo requiere el comportamiento superplástico.

Index

Index of figures

Index of tables

1 Introduction

1.1 Objective

1.1.1 General objective

The general objective of the present thesis is the characterization of the mechanical properties of two dual-phase steels manufactured by Advanced Thermomechanical Controlled Rolling Processes and an HSLA steel also manufactured by the same process; also, finding the range of temperature and strain rate at which the HSLA steel microalloyed with Ti and Nb, would present superplasticity, including the optimum conditions to obtain the best superplastic behavior.

Furthermore, the analysis of the mechanisms of superplastic deformation, including the effect of ultrafine microstructure and other microstructural features (phases, precipitates and formation of decohesions) is also sought.

1.1.2 Particular objectives

1. Confirm that the ultrafine structure results in adequate mechanical properties to allow the forming of automotive parts (drawing or bending). To assure this, the strain hardening n coefficient must be higher than 0.1.

2. Determine the temperatures and strain rates at which the HSLA steel behaves superplastically, reaching elongations of 100% or higher.
3. Verify that during deformation at high temperatures and under superplastic deformation, microstructural mechanisms take place, such as sliding and rotation of grains. Analyze the effect of the ultrafine microstructure, banding, precipitates and phases present.
4. Compare the mechanical behavior at high temperature of the HSLA steel to the superplasticity model proposed by Ashby and Verrall in 1973 (Grain Boundary Sliding, Diffusion Accommodated Flow Rate Controlling Model).

1.2 Work hypothesis

The manufacture of steels with ultrafine grained structures at an industrial level (and not only at a laboratory scale) is possible if stringed control of the rolling parameters result in a combination of phases and grain sizes with an adequate room temperature mechanical properties that allow drawing and bending in order to use these steels in automotive and other metal-mechanical industries.

Moreover, these ultrafine structures will show superplastic behavior at high temperature given that the combination of temperature and strain rate allows the rotation and sliding of grains.

1.3 HSLA and Dual-phase steels

Construction steels (materials used in civil engineering) are cheap, weldable and have a good mechanical resistance and fracture toughness. Their microstructures are usually formed by ferrite and pearlite, and sometimes include bainite, martensite, room temperature retained austenite (base of the TRIP steels) and even nanoprecipitates of Ti,

Nb and V, though the main phase of these steels is ferrite; certain construction steels can be dual-phase steels (or DP steels), which present two phases: a soft phase such as ferrite and a hard one which is commonly martensite with traces of bainite usually in the form of dispersion; showing excellent mechanical properties leading to mechanical parts (usually of the automotive industry) that have a thinner section compared to those of conventional steels. The mechanical properties include high strength – elongation ratio, excellent impact response, soft yield behavior, low yield stress – tension stress ratio and elevated formability. The strength of these steels is related to the amount of plastic deformation applied during the thermomechanical processes (see Section 1.4 Controlled rolling processes) in the intercritic region due to the formation of substructures in the ferrite. The epitaxial ferrite (phase that grows with the thermomechanical processes) is the cause for the improvement in tension stress when increasing the reduction in the transverse area during rolling, all this happens without significant reduction in the ductility of the steel [1; 2; 3].

Furthermore, the ferrite grain size (d) is the only parameter capable of increasing at the same time the mechanical resistance (yield stress) and tenacity (decrease of temperature of the ductile-fragile transition, ITT) of the steels; moreover, the grain refinement of a steel increases the value of the yield stress/ITT ratio, optimizing the thicknesses and costs, making the material structurally and economically more efficient. In other words, these three variables (grain size, yield stress and ITT) can be expressed in the following formulas [4; 5; 6; 7]:

$$\sigma_y \approx 54 + 17d^{1/2} \quad \textbf{[1.1]}$$

$$ITT \approx -19 - 11.5\, d^{-1/2} + 2.2\,(pearlite\ \%) \quad \textbf{[1.2]}$$

where d is expressed in μm, and the resulting yield stress in MPa and ITT in °C.

Thusly, a ferritic-pearlitic steel with a grain size ASTM G of 10 ($d \approx 10\ \mu m$) and 15% of pearlite (approximately 0.1% C) would have a $\sigma_y \approx 225$ MPa and an $ITT \approx -100$°C. These ferritic grain sizes ($10\ \mu m$) are usually obtained by a thermal treatment of normalizing after hot forging of the steel. The ultrafine ferritic steels (UFF) have grain sizes lower than $5\ \mu m$ (12 ASTM G) which are usually manufactured by Advanced Thermomechanical Controlled Rolling Processes (ATMCRP) or by Continuous Annealing

Processing Line (CAPL), which are technologies being used at the ArcelorMittal Factories in Asturias, Spain.

In the last 20 years it has been possible to enhance the productivity, quality, cost control and efficiency of the steel; furthermore, today more than 50% of the steels in use were unknown in 1985. A conservative calculation of use per capita of the steel in a country in development and considering the increase in the world population would lead us to an approximate of 3000 Mt/year for the year 2010. The future of the steel is, as it appears, consolidated and long-lasting; influencing the economy (shareholders) of both developed and developing countries, as well as changing the ecological negativity of this material through recycling and sustainability in both products and operations. The availability of its raw materials, its peculiarity of physical, chemical and mechanical properties, as well as its versatility in its use (as shown in recent developments in areas such as extractive metallurgy, physical metallurgy, materials science and solid state physics) have similarities with biological being; moreover, if the steel would have been found in this era it would certainly be qualified as a nanotechnological material [7; 8; 9; 10; 11].

1.4 Controlled rolling processes

1.4.1 Definition

A good example of these processes are DP steels. Also known as Advanced Thermomechanical Controlled Rolling Processes (ATMCRP) at temperatures close to Ar_3; they consist in strict control of the rolling process variables, as well as the cooling rates in order to allow the formation of grain sizes close to 1 μm, or, ultrafine grained steels (UFG) [12; 13; 14].

Through direct quenching (by applying pulverized water over the hot material), the amount of martensite present in DP steels can be modified, as well as the size and distribution of ferrite (soft phase), thusly producing finished products with tension stresses that may reach $800\ \mathrm{MPa}$ [15].

These processes include a careful control of: chemical composition (including microalloying elements such as Ti, Nb and V), deformation sequences, austenitic non-recrystallization temperatures, and $\gamma \rightarrow \alpha$ allotropic transformation temperature during cooling [16].

1.4.2 Manufacture

ATMCRP processes made on high strength low alloy (HSLA) steels improve their properties and reduce the costs of parts manufactured with them. They improve strength, fracture toughness and weldability through the refinement of ferrite grain size (in final products) [16; 17].

Thermomechanical processing minimizes and/or eliminates heat treatments after the hot deformation, reducing costs and increasing the productivity of the materials being manufactured. Moreover, it leads to a more advanced material, for example a steel with lesser amount of alloying elements [16].

The manufacture of DP steel through this method, according to some authors, includes four steps as shown in Figure 1.1 [18]:

1. Rolling in roughing and finishing mills, refining the austenite grain size due to the repeating static recrystallization as well as deformed austenite in the non-recrystallization region.
2. Water cooling.
3. Isothermal holding at intercritic temperatures.

4. Fast continuous cooling to the required coiling temperature. The martensitic transformation takes place if bainite is undesired.

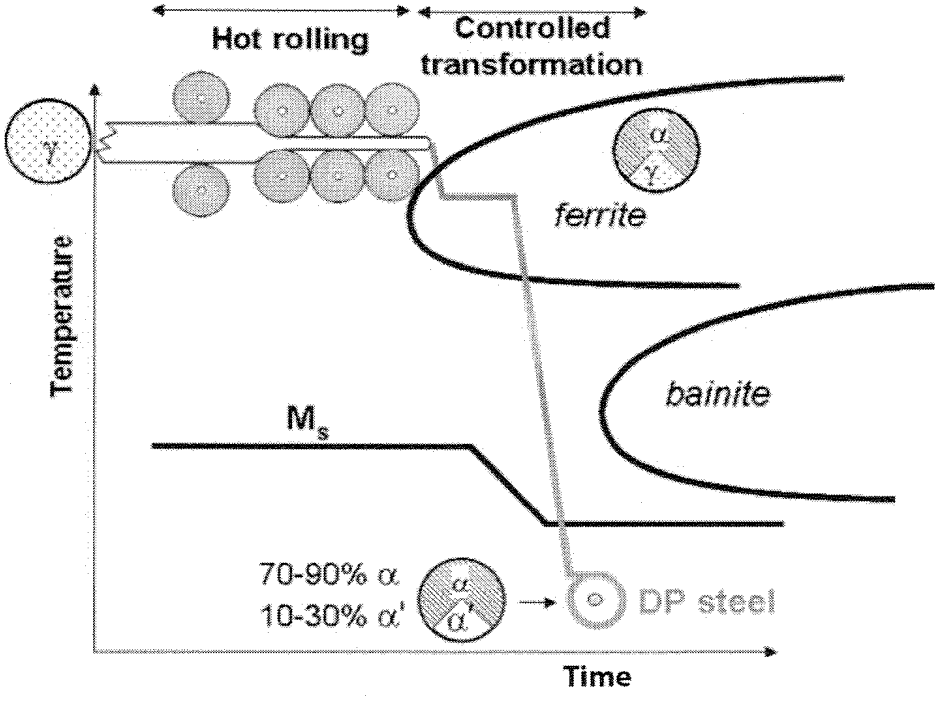

Figure 1.1 A sketch for the processing of DP steels [18]

Other authors consider the ATMCRP as six steps (as shown in Figure 1.2), in order to obtain DP steels with a strain hardening coefficient n high enough to allow the forming of the parts made with this material. The steps are as follows [14]:

1. Homogenization. In order to start with a recrystallized structure, the continuous casting slabs ($200\sim250$ mm) are kept at $1200\sim1250$°C.
2. Roughing. In order to reduce the thickness (~20 mm), approximately 10 passes are made in reversible rolling mills at $1200\sim1100$°C.
3. Waiting. The material is cooled to $1100\sim1000$°C.
4. Finishing. Reducing the thickness (~1.5 mm) through a mill of hot or semi-continuous bands, the temperature drops to 850°C.
5. Controlled cooling. In order to reach coiling temperature (~600°C) atomized water is used as a cooling method. At this step, the partial transformation $\gamma \rightarrow \alpha$ takes place; if the cooling rate increases, the ferrite percentage diminishes.

6. Coiling. The material is coiled at ~600°C. Below this temperature, the untransformed austenite becomes bainite-martensite (even if the steel is already coiled). It is required that the coiling window between the ferritic-pearlitic zone (upper) and the bainitic-martensitic one (lower) coincides with the mentioned temperature.

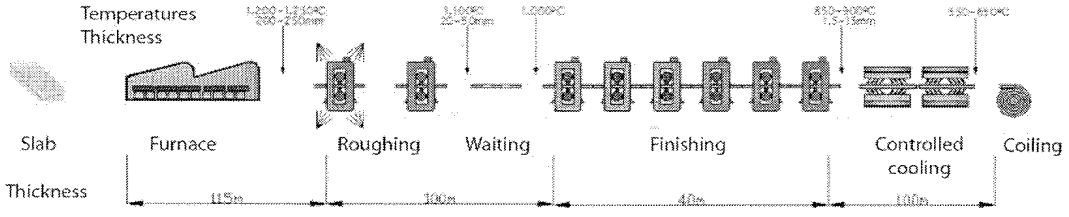

Figure 1.2 General scheme of the Hot rolling process used in Arcelor-Mittal factory in Avilés, Spain

Other authors propose three options of ATMCRP as follows [7; 19]:

- *Option 1*. Starting from a reheated austenite (after the thermal treatment of homogenization), followed by successive straining and recrystallization at temperatures higher than Ar_3 producing ferrite with grain sizes lower than 10 μm.
- *Option 2*. Starting from the same austenite, it is successively deformed and recrystallized between the different rolling passes, except at the last finishing passes, obtaining a non-recrystallized austenite that is latter transformed into a very fine ferrite (grain size lower than 5 μm, 12 ASTM G).
- *Option 3*. Is equivalent to *Option 2*, but the finishing rolling is prolonged below the $\gamma \rightarrow \alpha$ transformation. In other words, strain and allotropic transformation may occur simultaneously at the last boxes of the finishing train (hot rolling mill) obtaining an ultrafine ferrite with a dual-phase microstructure and a mean grain size lower than 5 μm (13 ASTM G).

1.4.3 Microstructure and Mechanical Properties

The most common microalloying elements for HSLA steels are Ti, Nb and V; while DP steels obtained by ATMCRP are also microalloyed Mn, Si, Cr, Mo and B. When the roughing processes are taking place, these materials are soaked at high temperatures and the microalloying elements remain in solution (partially or completely), afterwards (finishing deformations) they start to precipitate as the temperature lowers. The microalloying elements Nb, Ti and V combined with C and/or N during cooling produce carbide, nitride and/or carbonitride precipitates. These hard particles play a retardation role in the recrystallization that follows the deformation and help to retain the accumulated strain and deformed structures inside the austenite grains [16].

Figure 1.3 shows a schematic representation of the three stages of the ATMCRP and the microstructural change due to deformation in each stage [16; 20]:

- *Stage 1*: starts with the refinement of coarse austenite (a) through repeated deformation and recrystallization (b). The steel transforms to relatively coarse ferrite (b') except when using microalloyed Ti that allows the refinement of homogenized austenite before rolling.
- *Stage 2*: formation of elongated and non-recrystallized austenite bands (c) made by deformation and the nucleation of ferrite both in the deformation bands as well as in the γ grain boundaries. This produces fine ferrite grains. The Nb could be used to favor the accumulation of deformation inside the austenite when the rolling process takes place at a temperature below the non-recrystallization temperature (T_{nr}). This temperature is a key factor to be controlled in the ATMCRP.
- *Stage 3*: continuation of the deformation that takes place in the ferrite-austenite dual-phase region that produces a substructure. If the steel is microalloyed with V, the precipitation hardening by V_4C_3 will take place in the ferrite phase.

Sometimes there is a delay on the rolling between stages *1* and *2*, as well as accelerated cooling after stage *3*. This cooling along with deformation takes place in the $\gamma \rightarrow \alpha$ transformation temperature range just after the controlled rolling; refining the ferritic and the martensitic grain sizes and thusly improving the strength and toughness of

the steel. When the deformation takes place at temperatures below the non-recrystallization temperature, the austenite grains become elongated and deformation bands are introduced inside the grains (pancaking). Therefore the non-recrystallization temperature is the main controlling factor in ATMCRP [16; 20].

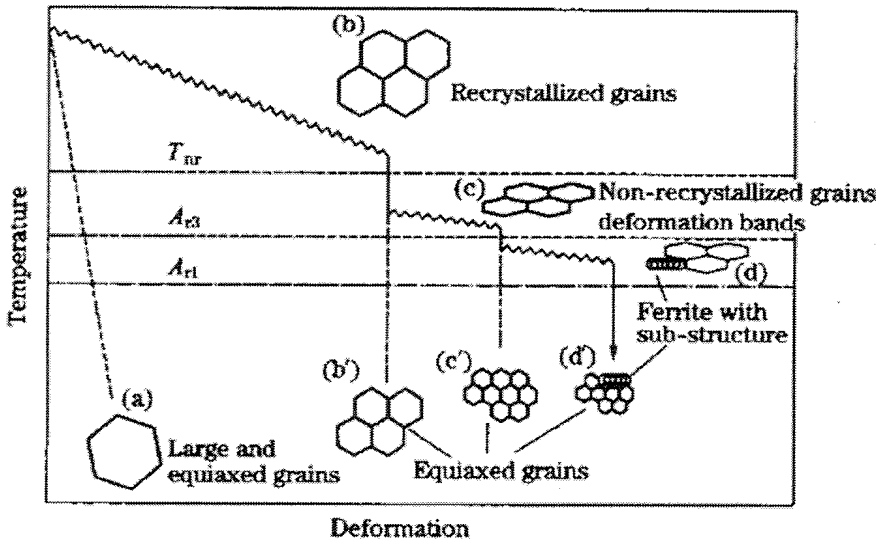

Figure 1.3 Schematic diagram of controlled rolling process (16)

In the temperature range of interest for the ATMCRP, the diffusion of carbon and nitrogen is order of magnitude faster than the one for titanium and niobium. Therefore, Ti and Nb are the rate controlling elements for these processes [16; 21; 22; 23].

ATMCRP produce elongated (pancake structure) grains in the rolling direction (Figure 1.4 shows DP steels and Figure 1.5 shows a HSLA steel) which explains higher yield strength and ultimate tensile strength as shown in Figure 1.6. This is specifically due to the amount of small ferrite grains and is independent from the amount of second phase particles (martensite) [16].

However, grain size reduction accompanies a problem: low ductility as work-hardenability is lost in the process, accompanied by "Lüdering effect" or "Lüders bands"

that will lead to fracture. On the other hand, steels microalloyed with Ti, Nb and V obtained by ATMCRP avoid this problem as the stress/strain induced $\gamma \rightarrow \alpha$ transformation favors work hardening and the anisotropy in the grains increases the amount of interfaces per unit volume [16; 24].

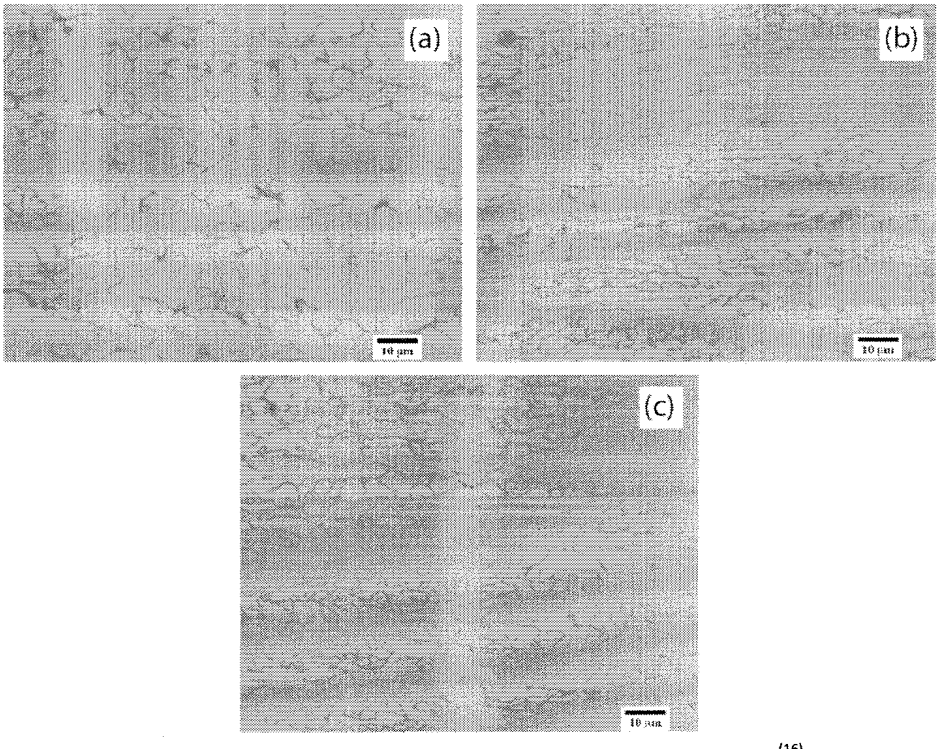

Figure 1.4 Optical micrographs of a) S355, b) S460 and c) S550 steels [16]

Commercial UFF steels obtained by ATMCRP can be found with grain sizes of $2{\sim}3$ μm and yield stresses close to 700 MPa. These materials can be welded due to their low carbon content and, as such, used in the automotive industry as construction and/or reinforcement parts as they produce lighter vehicles without losing safety standards [16].

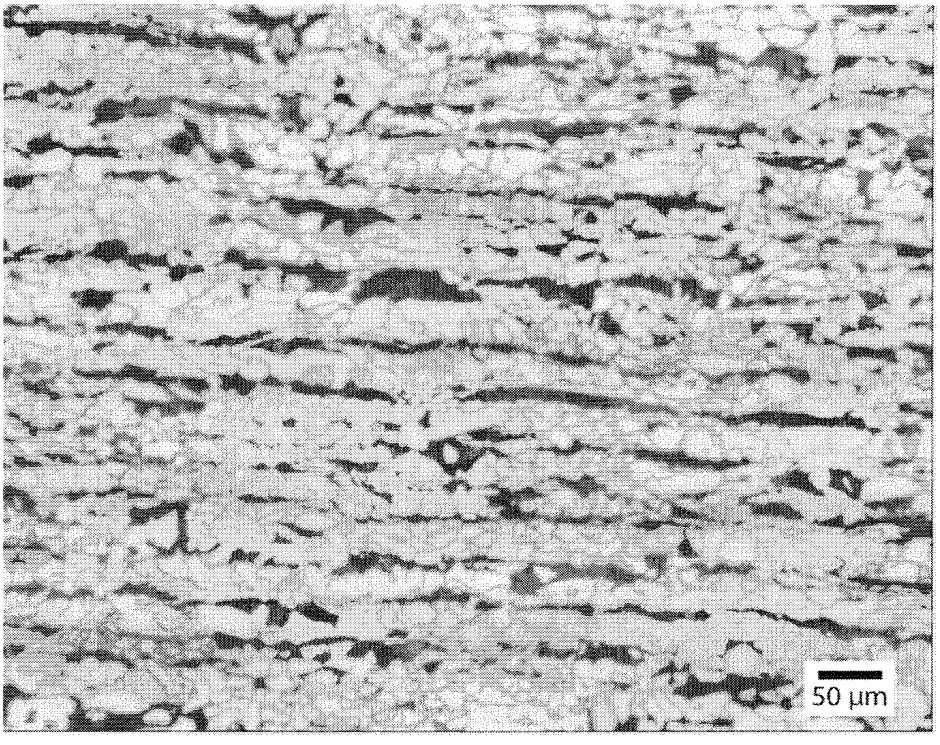

Figure 1.5 Microstructure of a HSLA obtained by ATMCRP

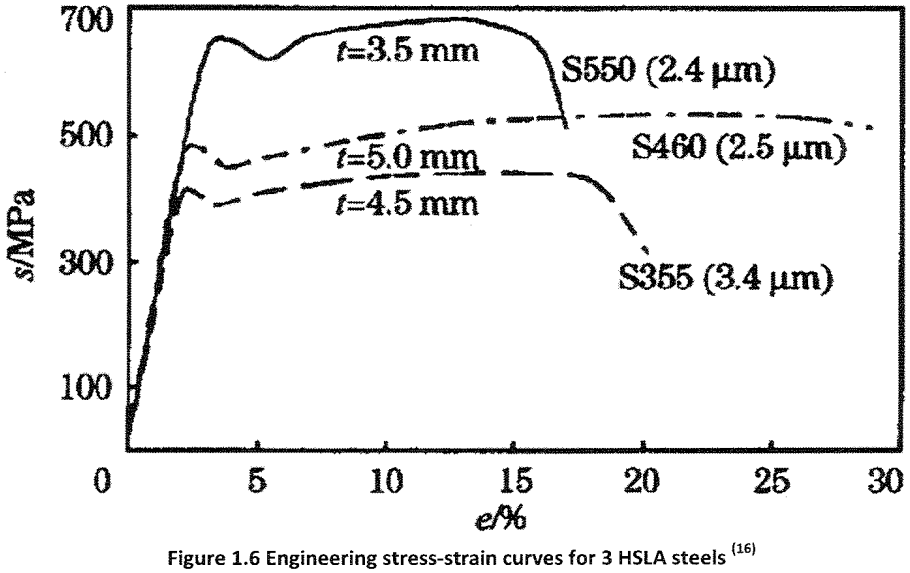

Figure 1.6 Engineering stress-strain curves for 3 HSLA steels [16]

1.5 Superplasticity

1.5.1 Definition

A material can be considered superplastic when, due to the high dependency between the creep tension stress and the strain rate, the necking is null or very subtle (a series of diffuse necks) along a part or test zone of a specimen. In other words, the material elongates uniformly when traction tested reaching elongations higher than 100% and in some cases higher than 1000%. Furthermore, superplasticity is the ability of crystalline solids (metals) to achieve extremely high uniform elongations when tension tested: for these materials strength is highly sensitive to strain rate. This phenomenon surpasses plasticity and, therefore, the presence of dislocations (linear defects that slide over crystallographic planes in lattice directions) provoke the plastic and irreversible deformations in each crystal or grain of the material [7; 25; 26; 27].

From a microstructural point of view, superplasticity is achieved when two phenomena take place in the material: grain boundary migration and grain boundary shearing/sliding. Theoretical and microstructural models agree that the most important feature in this behavior is grain boundary sliding (GBS), nevertheless, dislocations or diffusion in grains or in zones near grain boundaries are necessary in order to maintain the superplasticity of the material [27; 28].

1.5.2 Superplasticity and creep

Creep is known as the flow of a material under constant load and at a constant temperature which has to be higher than $0.3\,T_M$. A typical creep curve (Figure 1.7) has three stages: a primary transitory creep (parabolic), a secondary stationary creep (linear) and a tertiary exponential creep (where cavitations occur). At the second stage the strain

rate is constant and is related to the load (stress) applied and the diffusional phenomena (matter transport) activated with temperature following an Arrhenius type law [29].

There are two laws for the behavior of creep by sliding (conservative movement) and climbing (non-conservative movement) of dislocations [30; 31; 32]:

- *Power law creep or Weertman creep* [33]:

$$\dot{\varepsilon} = A\sigma^n \exp\left(\frac{-Q}{RT}\right) \quad [1.3]$$

being A and n constants, σ the stress, Q the activation energy (equal to self-diffusion) of creep, R the ideal gas constant and T the absolute temperature.

- *Exponential law creep or Dorn creep* [34]:

$$\dot{\varepsilon} = ASh(\beta\sigma) \exp\left(\frac{-Q}{RT}\right) \quad [1.4]$$

being A, S, h and B constants, σ the stress, Q the activation energy (equal to self-diffusion) of creep, R the ideal gas constant and T the absolute temperature.

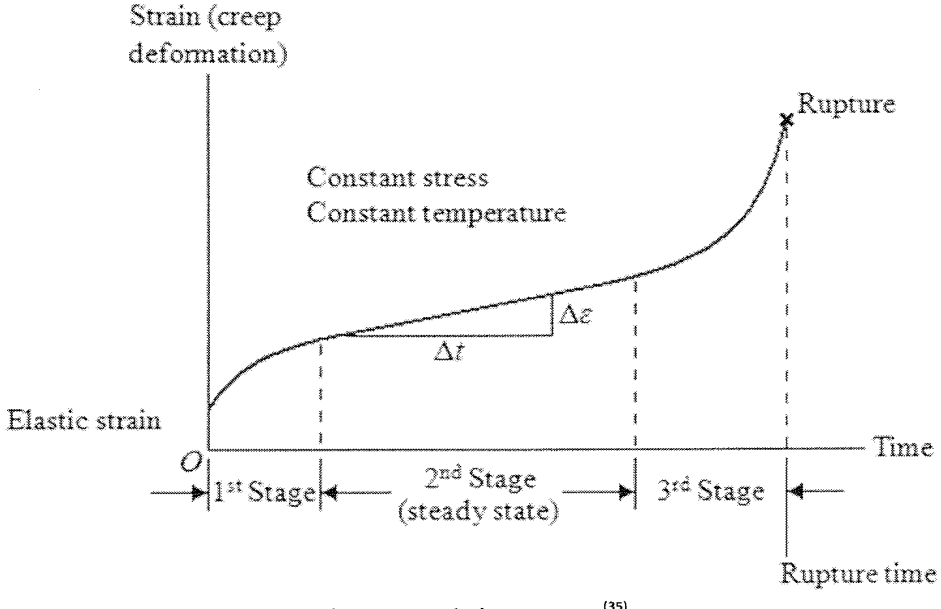

Figure 1.7 Typical creep curve [35]

Both laws require high stresses but always lower than the yield stress, intermediate ($0.3T_m < T < 0.5T_m$) or high ($T > 0.5T_m$) temperatures. At intermediate temperatures, the matter transport may take place through processes such as grain boundary diffusion, whose coefficient (D_{it}) would be:

$$D_{it} \cong D_v \left(1 + \frac{\delta}{d}\frac{D_{gb}}{D_v}\right) \quad [1.5]$$

where D_v is the volume diffusion coefficient, D_{gb} is the grain boundary diffusion coefficient, δ is the width of the grain boundary qpproximately equal to two interatomic distances $2b$ and d the grain size. While at low temperature the controlling process is the grain boundary coefficient, at higher or intermediate ones is the volume diffusion [30; 31; 32].

The diffusion creep mechanism happens at low applied stresses (lower than the one required for sliding or dislocation climbing) compared to other types of diffusion but at similar intermediate or high temperatures as previously mentioned. The grains, under the effect of the applied stress deformed either by intergranular diffusion (intermediate temperatures) or by volume diffusion (high temperatures) without the intervention of dislocations in the process. Moreover, there is an immediate generation of cavities or voids that can be related to the sliding of the grain boundaries generated through the diffusion processes necessary to achieve, at least temporarily, the continuity of the material (matter). The behavior law for this process (Herring-Nabarro creep) is of the Newtonian or viscous flow type [36; 37]:

$$\dot{\varepsilon} = \frac{B\sigma \exp(-Q/RT)}{d^2} \quad [1.6]$$

being B a constant, σ the applied stress, Q the activation energy, R the ideal gas constant, T the absolute temperature and d the grain size.

As these processes (sliding, dislocation climbing and diffusion) influence the behavior of a possible superplastic material, Ashby and Verrall take them into account for their model as will be mentioned in the following section [38].

1.5.3 Behavior laws, equations and models

One of the first researches on this subject was made in 1920 by Roseham et al.; they, however, studied the alloy Zn - 7% Al - 4% Cu at 250°C and discovered that the material was more ductile at room temperature when slowly folded or bended, but was almost fragile when the strain rate increased. In other words, resistance and ductility were particularly sensitive to this parameter (directly proportional to the resistance and indirectly proportional to the ductility). Moreover, the alloy behaved similar to a viscoplastic material (such as subcooled liquids, tar, etc.) including the stress relaxation and elastic after-effect [39].

Later on, in 1945, Bochvar et al. named the term superplasticity for the first time when working with a 80% Zn - 20% Al at 250°C and discovering its extremely high ductility (close to 700%). Figure 1.8 shows that the test conditions were made on the $\alpha + \beta$ region of the diagram. The explanation proposed by Bochvar et al. for the superplastic behavior is the "re-dissolution and precipitation processes" theory based on diffusional processes (thermally activated matter transport processes) inside the crystalline lattices mainly happening at the α/β interphase (intergranular diffusion) as a consequence of the limited solubility of Zn in Al and Al in Zn. Furthermore, they concluded that the test temperature must not be below 30% of the melting point in order for the diffusion-linked superplasticity to occur [40].

Presnyakov et al. continued the experiments using the Al-Zn system with hypoeutectoid and hypereutectoid alloys tempered from 375°C and concluded that [41]:

- Tempering made above 275°C accentuated the superplasticity of the material: the higher the temperature the higher the superplasticity.
- Tempering made below the eutectoid temperature eliminated the superplasticity.
- Annealing of homogenized alloys above 275°C and slowly cooled created normal ductilities.

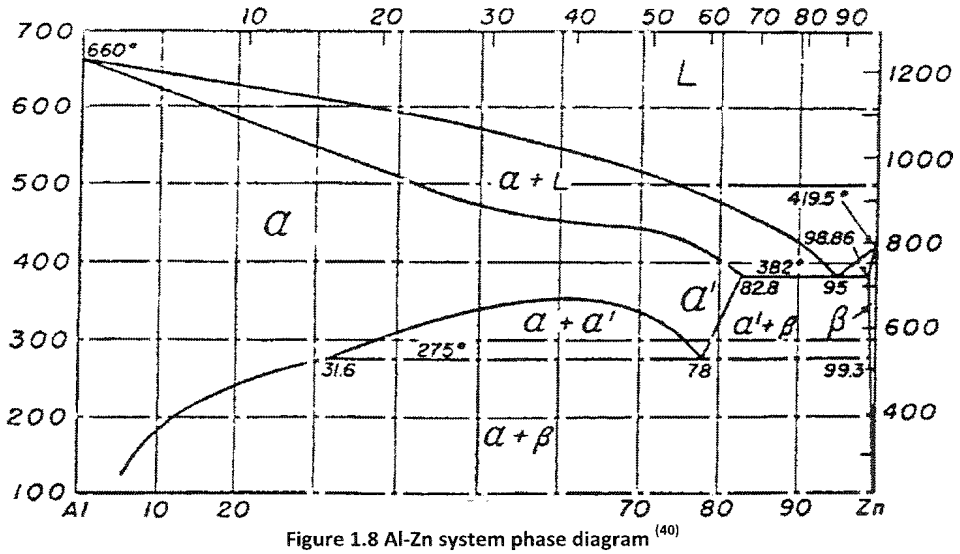

Figure 1.8 Al-Zn system phase diagram [40]

In other words, superplasticity occurred starting from a metastable structure (supersaturated solid solution of Zn in Al) obtained by tempering followed by subcritical ($T > 275°C$) straining that recrystallized the equilibrium ($\alpha + \beta$) structure. Furthermore, Presnyakov supposed that superplasticity was related to the weakness of the atomic bonds at the α/β interphases during recrystallization (nucleation and growth) which provoked the extremely high ductility [41].

Two years later, Underwood published that high ductility can be obtained when deforming mechanically during an allotropic transformation, solubility change or recrystallization processes in metallic alloys, and it is even higher when the transformations take place at high temperatures. In other words, temperature is a determining factor for superplasticity. Similar to what Presnyakov believed, Underwood considered that superplasticity happens due to the transitory breaking of atomic bonds when suffering tension and its subsequent reforming at the old/new or recrystallized interfaces favoring the increase in ductility. Furthermore, Bochvar established that the required stresses would be lower and the ductility higher during the transformation itself, neither before nor after; thusly, the material recovers its original properties when the transformations stops (nowadays known as reversible, transitory or internal stresses induced superplasticity) [40; 42].

Later on, in 1964, Backofen et al. worked in the same alloy as Bochvar et al did in 1945 confirming its superplastic behavior; they concluded that the necessary conditions for a polycrystalline material to experience superplastic deformations are low mechanical stresses and a capacity to achieve very large elongations free of localized necks. These requirements must be in terms of stresses and more importantly on the strain rate ($\dot{\varepsilon}$) sensitivity of the material [40; 43].

The general law for high temperature behavior of materials with standard grain sizes is as follows:

$$\dot{\varepsilon} \cdot e^{Q/RT} = Z \qquad [1.7]$$

being $\dot{\varepsilon}$ the strain rate, Q the activation energy for dynamic restoration, R the ideal gas constant, T the temperature (Kelvin) used during processing (forming) and Z the Zener-Hollomon parameter. This formula is valid when stress is constant [7].

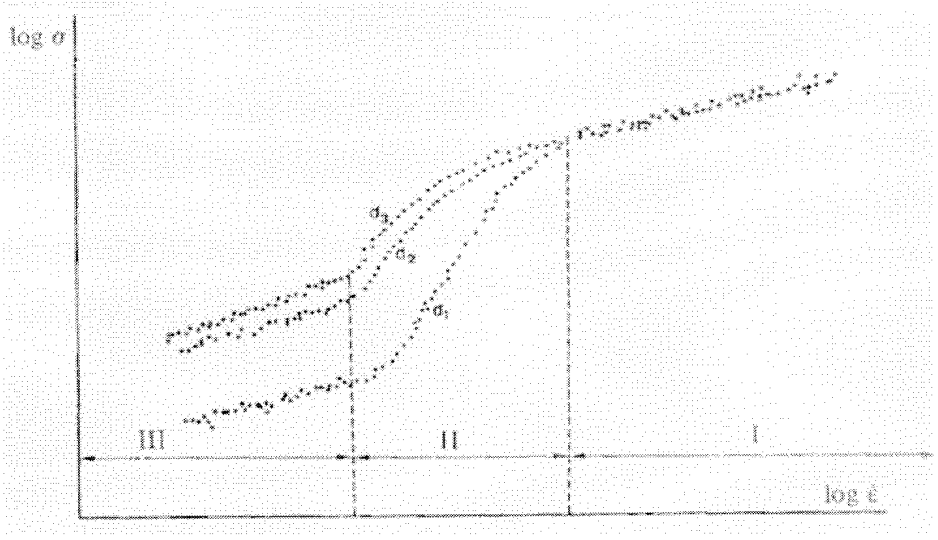

Figure 1.9 Experimental representation of high temperature behavior of materials at a temperature T1 with the following zones: I – Hot forming, II – Superplasticity and III – Creep. Grain size d: $d_3 > d_2 > d_1$ [7; 44]

Considering this law, the experimental representation (Figure 1.9) of $\log \sigma$ as a function of $\log d\varepsilon/dt$ of superplastic materials falls into the region II. The slope m of the curve is:

$$m = \frac{\log(\sigma_1/\sigma_2)}{\log(\dot{\varepsilon}_1/\dot{\varepsilon}_2)} \quad [1.8]$$

and is similar for both hot deformation and creep. On the other hand, superplastic materials with very small grain sizes (d) present a higher m, due to the dependence of superplasticity to grain size. However, at equal grain size, the m coefficient can change while modifying the strain rate ($\dot{\varepsilon}$) [7].

The most realistic models of superplasticity include the GBS as the most important characteristic phenomenon happening in the material at the grain boundaries. Nevertheless, the GBS must happen as a unit process and as such, it requires repeated accommodation. However, the models can be divided into three groups, as follows [26]:

1. Combination of grain boundary sliding and diffusion creep.
2. Combination of grain boundary sliding and grain boundary migration.
3. Combination of grain boundary sliding, grain boundary migration and localized dislocation motion by glide and/or climb.

Morrison gives more importance to the diffusion in the grain boundaries because when adding alloying elements that improve the diffusion, the superplasticity is also improved [26; 45].

Ashby and Verrall proposed a theory (Grain Boundary Sliding, Diffusion Accommodated Flow Rate Controlling) to describe superplasticity in two steps (see Section 1.5.3.1): the first included GBS along with material transport through grain boundary and bulk diffusion to maintain grain continuity and the second included dislocation creep but with less contribution than the first step [38; 46].

This model also considered the $\ln\sigma/\ln\dot{\varepsilon}$ curve (Figure 1.9) as sigmoidal, in which regions I and most of region II disregarded large grain elongations or considerable amount of dislocation motion, but took into account the large amount of GBS and grain rotation. At the high strain rate zone of region II, there is important dislocation motion that derives in total strain, accommodation, small quantities of GBS and grain rotation. At region II,

dislocation creep is dominant and the grains elongate. A disadvantage of this model is the unavailability of input data for the equations for most materials [38; 46].

Baudelet, in turn, proposed the deformation behavior shown in Figure 1.9 as a sequence of controlling mechanisms divided in three regions or zones, but emphasizing that not all materials present all three zones. Some materials only show regions I and II [26; 28; 47]:

- *Region I.* There is very little amount of experimental data in this region. The intergranular creep that takes place provokes deformation in the composite (ferrite-bainite or ferrite-martensite) boundary. Also, some other phenomena take place (a lesser amount of GBS compared to region II, striations at transverse grain boundaries, grain elongation and Herring-Nabarro creep).
- *Transition from region I into region II.* The dominant mechanism starts to be the behavior of the grain boundary (GBS). The shear bands in the grains start to widen.
- *Region II.* The main mechanism at this zone is overall creep. This is the zone where superplasticity occurs.
- *Region III.* Ruled by dislocation creep, which in turn can be controlled by grain-boundary diffusion. However, Kashyap and Mukherjee (48) disagree with this assumption, as they consider that the dislocation creep is controlled by volume diffusion. It is generally agreed that the deformation in this region is ruled by slip and recovery creep, as the materials deformed at this region present slip lines on their surface and the grains present a high density of dislocations.

A high value of m (between 0.3 and 0.9) implies a superplastic behavior of the material at the temperature the material is being tested [7; 46].

Another law that can predict the high temperature tension stress of a material is the Ludwick-Hollomon law:

$$\sigma = K_1 \cdot \varepsilon^n \cdot \dot{\varepsilon}^m \qquad [1.9]$$

where n and m are not related between them: m is the strain-rate sensitivity exponent (as superplasticity is very sensitive to this factor) and n is the strain hardening coefficient.

Materials with a high m value do not necessarily have a high n value (on the contrary, commonly n has a low value) and at high temperatures, the n value is close to zero [7; 27; 43; 45].

Furthermore, the maximum uniform strain matches up with the n strain hardening coefficient. About this, Morrison demonstrates the effect the grain size has on this coefficient:

$$n = \frac{5}{10+d^{-1/2}} \quad [1.10]$$

where d is the intersected mean length measuring grain size in millimeters. The refinement of grain size can increase the elastic limit (yield stress) and the toughness of the steel (Hall-Petch laws), but can negatively act on the ductility of the material when cold worked. At these temperatures ($T < T_M/4$), conventional metallic materials are practically insensitive to the strain rate. After surpassing the mentioned temperature, ductile metallic materials can be divided into two groups: those that are insensitive to the strain rate (conventional metallic materials) and those that are sensitive to this variable (superplastic metallic materials), which will be explained in Section 1.5.3.2 and Section 1.5.3.3 respectively [45].

In a tension test, after the uniform lengthening in a specific zone, a localized neck starts to form. When the test continues, the $\dot{\varepsilon}$ at that zone will increase and, thusly, the $\dot{\varepsilon}^m$ value will considerably increase taking into account the high value of m in the superplastic material. The value of m determines the speed with which the neck develops after the beginning of localized plastic flow. Consequently, the stress value at that zone will also increase and the neck will not continue at that zone but at its surroundings; this produces diffuse necking and the transverse section of the test specimen will decrease in a uniform way, all along the specimen, until the end of the test. Experimentally, as m increases, the elongation-to-failure also increases: superplastic materials reach elongations up to 2000% when tension tested. The value of m increases with temperature (directly proportional) and decreases with grain size (inversely proportional). Moreover, maximum elongations are usually reached when m is maximum, which implies that some diffusion controlled processes such as nucleation transformation and growth must be linked to the superplastic behavior and altering the grain boundary behavior [26; 27; 46; 44; 49; 50; 51; 52; 53; 54].

When the relation between σ and $\dot{\varepsilon}$ is linear ($m = 1$) the material follows the Newton's Law of Viscosity (i.e. hot glass, tar, etc.). Most superplastic metals, however, have values of m close to 0.5 ($> 400\%$ elongation). Therefore, in order for superplasticity to occur, m must have a high value, but this is not the only requirement, as other materials with high strain-rate sensitivity can present grain boundary separation, cavitation at interphase boundaries and other premature failure modes and never reach superplasticity [27].

In 1968 Morrison obtained fine grained ferritic-pearlitic structures (smaller than $10\ \mu m$, ASTM G grain size 10) through hot rolling, the steel was heated and briefly maintained at temperatures between 750 and $900°C$ in order to have ferritic-austenitic ($\alpha + \gamma$) structures with similar proportions. Afterwards, it was deformed at high temperature with testing speeds between 0.1 and $10\ mm/min$; it resulted in strains between 200 and 350% with an m coefficient ($\sigma = K \cdot \dot{\varepsilon}^m$) between 0.4 and 0.6. His conclusions were that the optimum superplastic behavior temperatures were between 750 and $800°C$ in the dual-phase ($\alpha + \gamma$) region and that [45]:

- Fine or ultrafine grained material (less than $10\ \mu m$) is required to obtain superplasticity in steels microalloyed with Mn manufactured by hot rolling, with thickness reductions of $\sim 90\%$ and finishing temperatures close to (but higher than the starting temperature) the allotropic $\gamma + \alpha$ transformation during cooling. In other words the fine grained structure is a necessary condition for the superplastic behavior, among others.
- Maximum superplastic strains are reached in the biphasic ($\alpha + \gamma$) region at temperatures close to $800°C$. The microstructure remains (fined grained material with $5\ \mu m$ or 12 ASTM G) because of the practically insensitive grain growth during deformation.
- Strain rate sensitivity coefficient at these conditions is approximately 0.5 at slow strain rates of $0.1\ mm/min$.
- Ferritic-pearlitic banded structure disappears or decreases with the deformation. The nucleation of decohesions at the ferrite/austenite/carbide interphases, as well as in the α/α grain boundary, result of intergranular deformation by sliding.
- Empirical relation is proposed, relating elongation to fracture A, the m coefficient and the proportionality constant for the test specimens k (where L_0 is the calibrated length, d_0 the diameter and b a constant with a value close to 100 for steels):

$$A(\%) = bm^2 \frac{d_0}{L} \times 100 \qquad [1.11]$$

Researchers consider three regions on the curve shown in the lower part of Figure 1.10: Region II is the range of strain rates where m has a high value and there is optimum superplasticity, the region where m decreases at lower strain rates is Region I and Region III, where m is also low but at higher strain rates. This figure presents the sigmoidal representation of the relationship between the stress and the strain rate where the three regions are also distinguishable (lower part), as well as the boundary sliding contribution to the deformation process (higher part): as it is maximum in Region II (maximum elongation reached) it is the controlling factor for superplasticity and is also where the ductility (middle part) is maximum [7; 46; 55; 56].

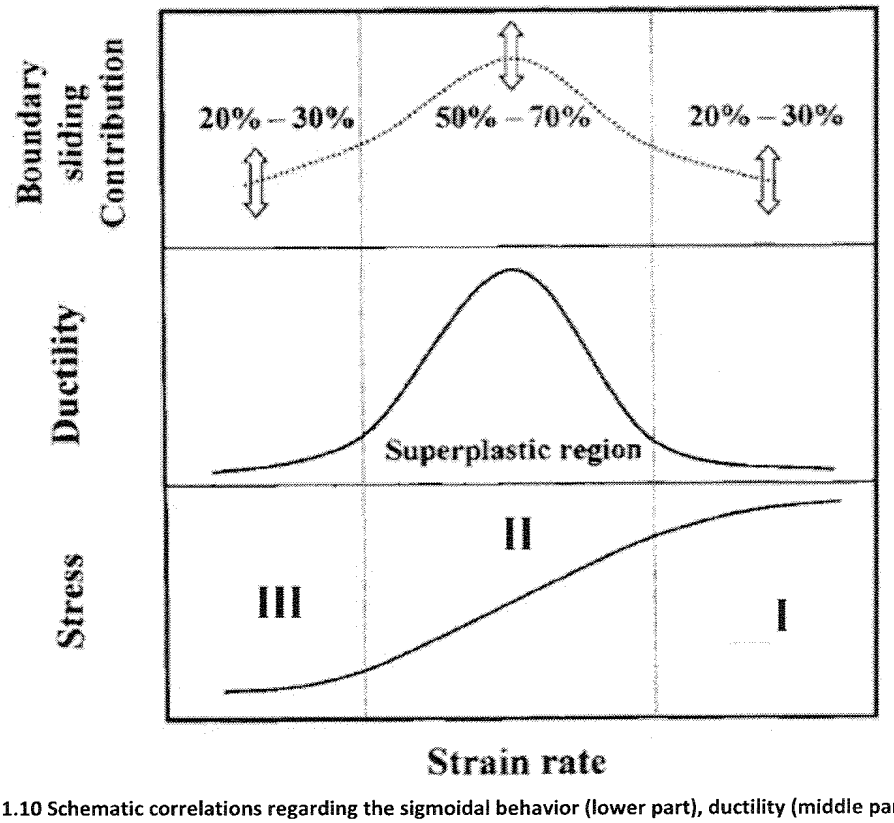

Figure 1.10 Schematic correlations regarding the sigmoidal behavior (lower part), ductility (middle part) and contribution of boundary sliding (upper part) to the total strain of the material. Region I corresponds to hot forming, region II to superplasticity and region III to creep [56]

The creep characteristics of Region III are controlled by the type and amount of impurities, while for Region II are only controlled by the amount of them. Just as it is shown in Figure 1.11, it is believed that region III is defined by the relationship between the impurities and GBS or to its accommodation processes: boundary migration, dislocation motion, diffusional flow or cavitations [56].

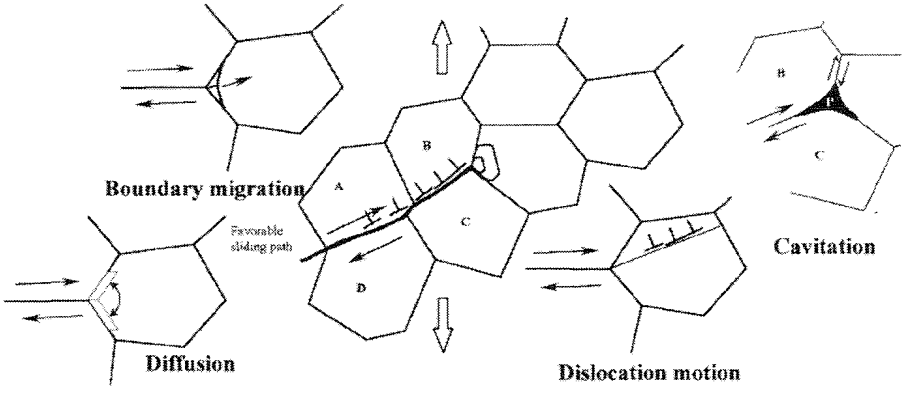

Figure 1.11 Schematic representation of boundary sliding and its accommodation processes [56]

As previously mentioned, superplasticity is a process that requires GBS, but is also ruled by accommodation processes such as (Figure 1.12): diffusion-accommodation proposed by Ashby-Verrall [38], dislocation pile-up accommodation proposed by Ball and Hutchinson [57] and Mukherjee [58].

Sherby, in turn, experimented on ultra-high carbon (UHC) hypereutectoid steels, which became superplastic when thermomechanically deformed at a temperature close to A_{r13} (see shaded region in Figure 1.13). The thermomechanical treatments included: controlled rolling the raw material from the casting process, roughing at $1150°C$ with 10%-passes until a final strain close to $\varepsilon = -2$, finishing between 650 and $600°C$ with 5%-passes with an accumulated strain close to $\varepsilon = -1.5$. Thusly, resulting in ultrafine structures of ferrite grains with sizes between 0.5 and 5 μm and globular precipitates of cementite (volume fraction between 20 and 35%) with a diameter of 0.1 μm, relatively resistant to the coarsening-coalescence in the test temperatures [59].

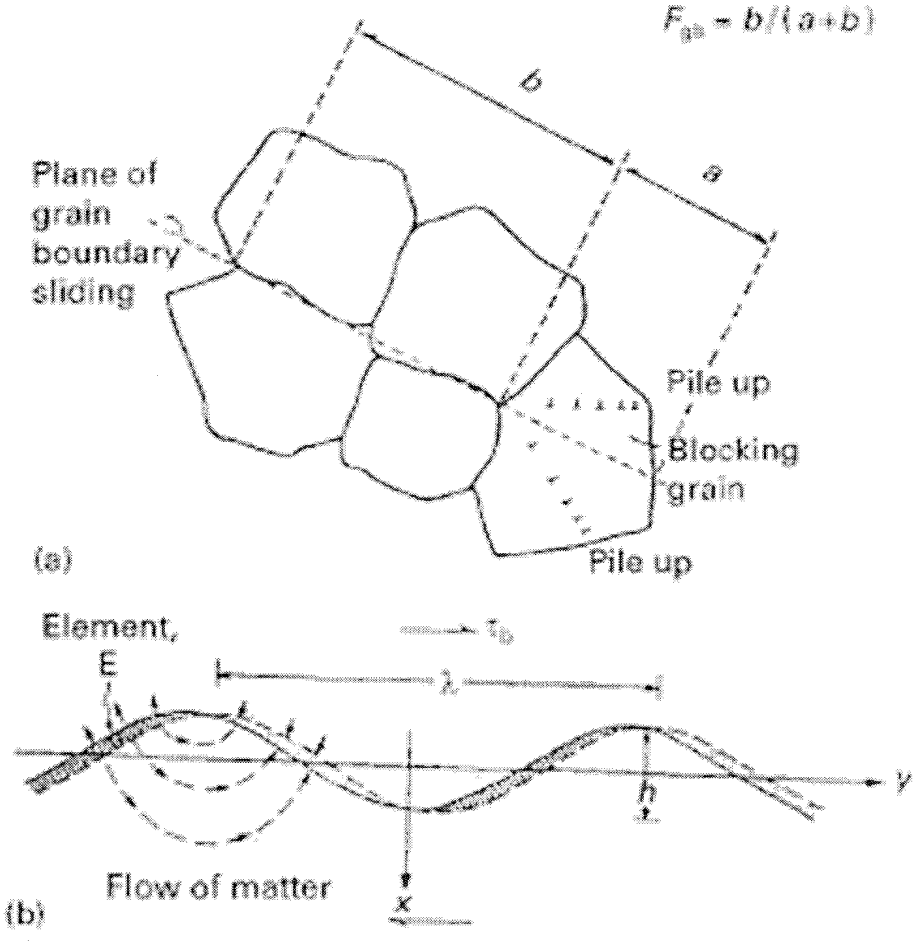

Figure 1.12 a) Schematic illustration of dislocation slip accommodation in the grain-boundary sliding model of Ball and Hutchinson, b) Grain boundary sliding described by Ashby and Verrall [28]

Another conclusion from the UHC experiments is that it would be expected to find structural damage (cavitations and voids) at the ferrite-cementite (subcritical deformations) or in the austenite-cementite (superplastic deformations) interphases due to its a priori different resistance and strain capacity. Moreover, slow strain rates do not facilitate decohesion of the interphases that may be solved by diffusion. Plus, the microstructural factor of grain size is the most important in an environment of adequate temperature and strain rate to achieve superplastic deformations; maintaining the fine grained microstructure stable during deformation is the main obstacle for the industrial applications of this manufacturing process [59].

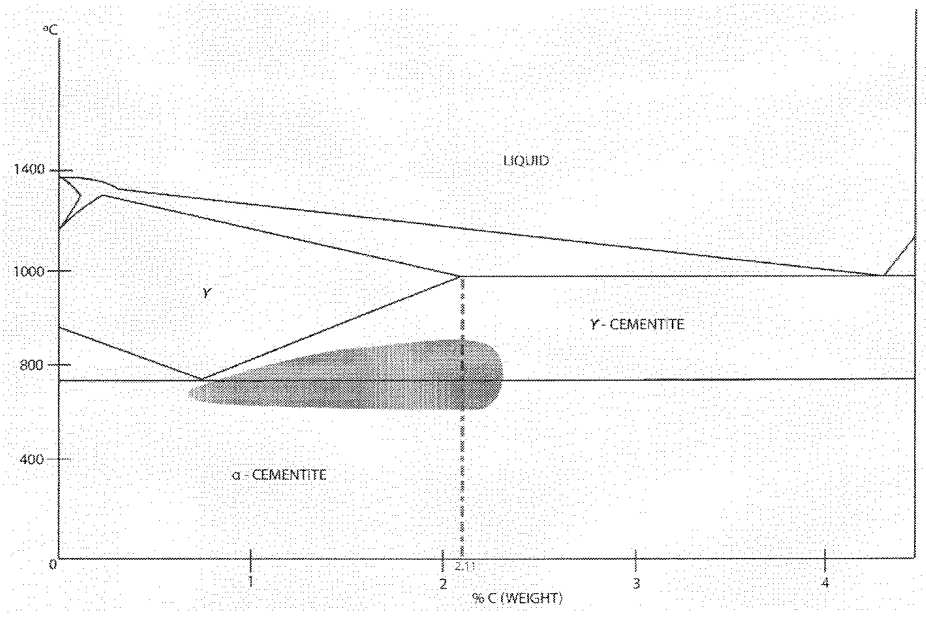

Figure 1.13 Fe-C diagram with shaded area of possible superplasticity. The shaded area indicates where superplastic flow may be expected [59]

1.5.3.1 Ashby-Verrall Model

In the "Grain Boundary Sliding, Diffusion Accommodated Flow Rate Controlling Model" proposed by Ashby and Verrall, the GBS with diffusion is considered in order to achieve the continuity of the material of a group of four grains and size $d = 2l$ (being l the length of a side of the hexagon) through three stages as shown in Figure 1.14. This model is based on three considerations [38]:

- There is matter transport (by diffusion).
- There is a relative movement of the grain boundaries accommodated by diffusion.
- There is rotation of the diffusion-accommodated grains.

The relative movement of the group of four grains shown in Figure 1.14 causes the shape change of the group as a total, meanwhile the grains experiment accommodation

tension stresses that keep them together. These stresses (different from those suffered by the group as a total) are caused by diffusion [38].

In a polycrystalline material, there are different options for diffusion: bulk diffusion (throughout the grains) and grain boundary diffusion. This last type is the most important for intermediate and low temperatures (superplasticity is an example of this type of diffusion). For the accommodation of grains after GBS both types of diffusion are required for low strain stresses. When the stresses increase, the accommodation stresses by diffusion are replaced by a uniform deformation mechanism, which make superplasticity disappear allowing conventional hot deformation mechanisms to take over [38].

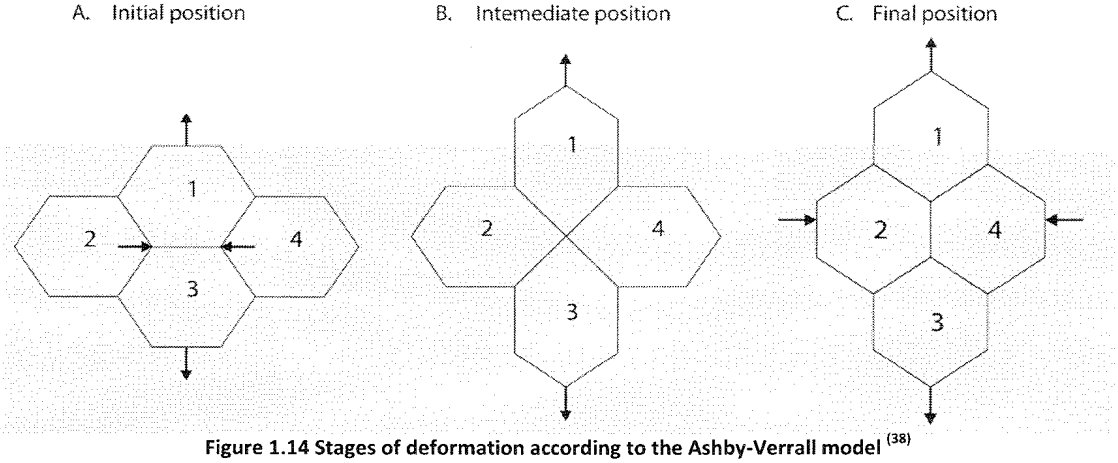

Figure 1.14 Stages of deformation according to the Ashby-Verrall model [38]

1.5.3.1.1 Characteristics of the model

Consider a group of four grains exposed to tension and constant pressure. Each grain has a size of d and a height of d, which produces a volume of $0.65\ d^3$. The initial, intermediate and final stages of the grain group is shown in Figure 1.14: the shape of the individual grains of the initial and final stages is identical but the geometry of the group has changed (real deformation of 0.55). The model consists in four irreversible processes [38]:

- *Diffusion process causing the grains to change shape temporarily experimenting accommodation stresses.*
  From a geometrical point of view, the mean volume of matter that moves per grain in each deformation stage is $0.075\,d^3$ with a mean distance of $0.3\,d$. Grains 1 and 3 experiment perpendicular movement compared to grains 2 and 4. There is a diffusion flow required from a zone at the grain boundary close to another. The value of this diffusion flow is the total number of atoms or vacancies per second flowing from the sources to the sinking or vice versa inside the group of four grains. If there is chemical potential difference between the source and the sinking then the energy required in the process is the multiplication product of this potential difference times the diffusion flow.

- *Reaction in the grain boundary*
  The grains and grain boundaries can be imperfect sources or sinking of punctual defects. An activation barrier appears when a void is eliminated or a grain boundary is added. Theoretically, the activation energy value can be different for sources and sinking, but they will be considered as equal and with a magnitude proportional to the chemical potential difference between the source and the sinking. Therefore, if the flow is originated at the source and then moved to the sinking, the energy dissipated due to the movement of the grain boundary is two times the product of the potential difference times the diffusion flow (voids and atoms).

- *Sliding of the grain boundary*
  Besides the normal displacements caused by diffusion, there are tangent ones at the grain boundaries: they cause a grain to slide with respect to its neighbor. The magnitude of the sliding can be measured by examination of the movement of the grains referred to an origin of coordinates. The energy is used to overcome the "viscosity" of the grain boundary when the sliding is taking place, causing a second irreversible process independent from the previous one: if the shearing stress that appears at the grain boundary is τ, the total area of the grain boundary is A and the relative speed is $\dot{u}$, this stage of the process dissipates an energy equal to $\tau A\dot{u}$. The total displacement due to grain boundary sliding during the process is $u = 0.46\,d$ and the net sliding surface A is $2d^2$.

- *Increase of area of the grain boundary.*
  The area of the grain boundary grows when the group of four grains moves from the initial to the intermediate stage, storing free energy in the system. When the

group of grains moves from the intermediate to the final stage, the grain boundary area diminishes to the initial value, freeing the energy stored previously. It does not seem possible to use this energy for other grain groups in transition from the initial to the intermediate stages; consequently, the energy is dissipated in the form of heat, making the process irreversible.

The total change of area of the grain boundaries ΔA is $0.26\, d^2$ when the "structural unit" moves from the initial to the intermediate stages. If the free energy of the grain boundary is Γ and the area change is ΔA, the energy $\Delta A\Gamma$ is turned into heat.

It can be demonstrated that there is a threshold stress under which there is no flow of matter. The external applied stress and its energy are incapable of modifying, by diffusion, the grain boundary area.

Characteristic	Symbol	Magnitude
Grain volume	$V/4$	$0.65\, d^3$
Intergranular Sliding Strain per unit	ε_0	0.55
Area in which sliding occurs	A	$2\, d^2$
Area change of the 4-grain group in the movement from initial to intermediate position:	ΔA	0.26
In grains 1 and 3		$0.07\, d^2$
In grains 2 and 4		$0.01\, d^2$
According to the Herring-Nabarro mechanism		$0.19\, d^2$
Displacement of a grain from the initial to the final position	u	$0.46\, d$
Volume of matter moved through diffusion (per grain) in the sliding of grains from the initial to the final position:	$M\Omega$	
In grains 1 and 3		$0.07\, d^3$
In grains 2 and 4		$0.01\, d^3$
According to the Herring-Nabarro mechanism		$0.19\, d^3$
Mean distance of diffusion in grains 2 and 4	L	$0.57\, d$

Table 1.1 Geometrical characteristics of the Ashby-Verrall model

The geometrical characteristics of the model are presented in Table 1.1. This model represents the physical processes taking place inside a crystal and calculates the

magnitude of each characteristic in an approximate way through geometry. The calculation of each of these parameters will be explained later on this work [38].

The energy required to plastically deform the material is consumed in [38]:

- Diffusion (matter movement) to facilitate the accommodation (matter continuity) in the grain boundaries.
- Grain boundary sliding, accommodated through the previous diffusion.

Therefore, the Ashby-Verrall equation or law for superplasticity considers two mechanisms, one after the other, of the strain rate as follows [38]:

$$\dot{\varepsilon}_{total} = \dot{\varepsilon}_{D-A\,flow} + \dot{\varepsilon}_{dislocation\,creep} \quad \textbf{[1.12]}$$

where $\dot{\varepsilon}_{D-A\,flow}$ (diffusion accommodated flow) is the strain rate resulting from a grain boundary sliding, accommodated (assuring the continuity of matter) through the diffusion both in bulk and mainly intergranularly, which is similar to the Herring-Nabarro mechanism but with two main differences: the first is that the necessary matter volume to be transported by diffusion is lower than the one for the Herring-Nabarro mechanism; and the second is the threshold stress under which the mechanism would be inoperable. On the other hand, $\dot{\varepsilon}_{dislocation\,creep}$ represents the resulting strain of the plastic flow caused by creep due to the movement and climbing of dislocations, through a mechanism similar to the one proposed by Weertman-Dom [33].

The first mechanism (diffusion accommodated flow) occurs at very low or low strain rates, being very sensitive to the grain size d. The second mechanism occurs at medium or high strain rates, as the ones derived from a hot deformation process. The formulas proposed by the Ashby-Verrall model are:

$$\dot{\varepsilon}_{D-A\,flow} = 98\frac{\Omega\mu}{KTd^2}\left[\frac{\sigma}{\mu} - \frac{0.72\,\Gamma}{\mu d}\right]D_v\left(1 + \frac{\pi\delta}{d}\frac{D_B}{D_v}\right) \quad \textbf{[1.13]}$$

$$\dot{\varepsilon}_{dislocation\,creep} = A_1\frac{\mu b}{kT}\left(\frac{\sigma}{\mu}\right)^n exp\left[-\frac{Q_c}{RT}\right] \quad \textbf{[1.14]}$$

The stresses are included in the shear modulus of the material, σ/μ, with the objective of considering the variation the μ (or shear G) modulus has with temperature, making the material more sensitive to the strain rate (thermal component of the critical shear stress for the dislocation sliding). When plotting the strain rate and the σ/μ parameter the result is a sigmoidal curve (Figure 1.9) considering the grain size as a parameter; three stages are found:

- In stages I and II the sliding and rotation of the grain boundaries would take place and would have the typical properties of a superplastic behavior.
- In stage III, the strain would be mainly intergranular, with sliding and climbing of dislocations associated to the restoration-recrystallization processes depending on the nature of the material.
- The superplastic behavior window can be found in the zone of maximum slope. In other words, where the m coefficient of sensitivity to the strain rate is higher than 0.3. The grain refinement as well as increasing the temperature would improve the superplasticity, provided that the microstructure remains stable with the strain and the grain size does not grow when the temperature rises, which would otherwise produce a change from the dislocation accommodated creep (necessary for superplasticity to occur) to the dislocation creep mechanism (conventional deformation behavior).

1.5.3.2 Conventional Metallic Materials

During tension tests, the strain rate $\dot{\varepsilon}$ exponentially decreases with true strain. If the material is potentially insensitive to the strain rate ($m > 0.1$), then the uniform elongation ε_u would decrease, its neck will be accelerated and the ductility will increase. In reality, cold-worked metallic materials are practically insensitive to the strain rate as previously mentioned ($T < T_M/4$) so the value of the m coefficient will be maximum $m \approx 0.01$ even if the traction test is considered quasi-static; the resistance and ductility of the material are insensitive to the strain rate [45].

1.5.3.3 Superplastic Metallic Materials

These materials are highly sensitive to the strain rate and very poorly to the strain; in other words, the m coefficient has values higher than 0.3, while the n coefficient has values lower than 0.1, which means that the situation of the conventional metallic materials is reverted. Furthermore, the lower the value of the m coefficient, the lower (the rapidly decreasing) transverse area of the test specimen will be. When m has a value close to one, the reduction speed of the transverse area are approximated to a common value; when m equals one, the strain is of the Bingham type (Newton viscous flow or $\sigma \approx \dot{\varepsilon}$) which enables any irregularity in the specimen (incipient neck) to be "stable" during the test [45].

The variation of strain rate with the strain is positive, contrary to conventional materials in which it is negative, producing a "stable" necking condition. Thus, the strain rate varies along the calibrated length of the specimen and is inversely proportional to the transverse section (Backofen criteria). Moreover, superplasticity is a phenomenon linked to necks, which in this case are spread out along all the calibrated length of the specimen in a diffuse way; this is related to the strong influence of the strain rate on the applied tension. When the neck is localized, the adjacent areas stop deforming; the stress equilibrium is maintained due to the different strain rates belonging to different areas from the specimen [43; 45].

1.5.4 Requirements for superplasticity to occur

In order to obtain superplasticity, a fine grained, equiaxed and stable microstructure is required (close to $1\ \mu m$) which will produce intergranular deformation and dislocation climbing. However, the achievement of this ultrafine grained (UFG) structure can sometimes increase the production cost of the material/part, but finer grain size implies increasing the amount of grain boundaries, thus promoting the boundary sliding and reducing the distance for accommodation by diffusion and/or slip [7; 25; 29; 46; 55; 60; 61].

"The fine-structured steel exhibits ideal characteristics in that it is weak and superplastic (~1000% tensile elongation) at warm temperatures and strong and ductile at room temperature, in contrast to the coarse-structured steel which is strong and not very ductile at warm temperatures and relatively weak at room temperature" [27].

A disadvantage of the excessive fine grained structure is the decreasing ductility because of the negative influence on the strain hardening coefficient n (from the expression $\sigma = K\varepsilon^n$) that may block the uniform elongations required in the cold forming operations such as folding or biaxial expansion of low-carbon, high yield stress and weldable steels required in the industry which may present non-homogeneous and unstable deformations (Piobert-Lüders effect) that introduce superficial defects and premature necks in formed products [45].

Another requirement is that the m coefficient has values between 0.3 and 0.7. The latter value is the maximum reached experimentally, which means that it is at least one order of magnitude higher than the one for hot deformation processes and similar to the ones for forming polymers and glasses. The yield stresses are dependent on a small scale on the strains, but are very sensitive to the strain rate and temperature just as shown in Figure 1.15 [43].

Figure 1.16 shows the displacement of the strain rate vs. the elongation to failure to the right (faster strain rates) while decreasing the grain size. It is also noteworthy that the peak elongations will be higher at the faster strain rates as there is less time available for the growth of internal cavities (see section 1.5.5 Microstructure) [60].

Secondly, superplasticity requires forming temperatures higher than $0.5\ T_m$ (50% of its melting temperature), as this process is diffusion-controlled and the deformation of the material must occur under conditions where the diffusive flow is reasonably fast. At these temperatures, the grain size must remain stable and without growth and the corrosion must be avoided (use of inert atmospheres or protective varnishes). After the material's

superplastic forming, it will not behave superplastically at temperatures lower than $0.2\,T_m$. Its room temperature mechanical characteristics will be a function of its nature and the ultrafine grain size: high values of yield stress, tension stress, hardness, tenacity, fatigue stress, among others [7; 25; 29; 60].

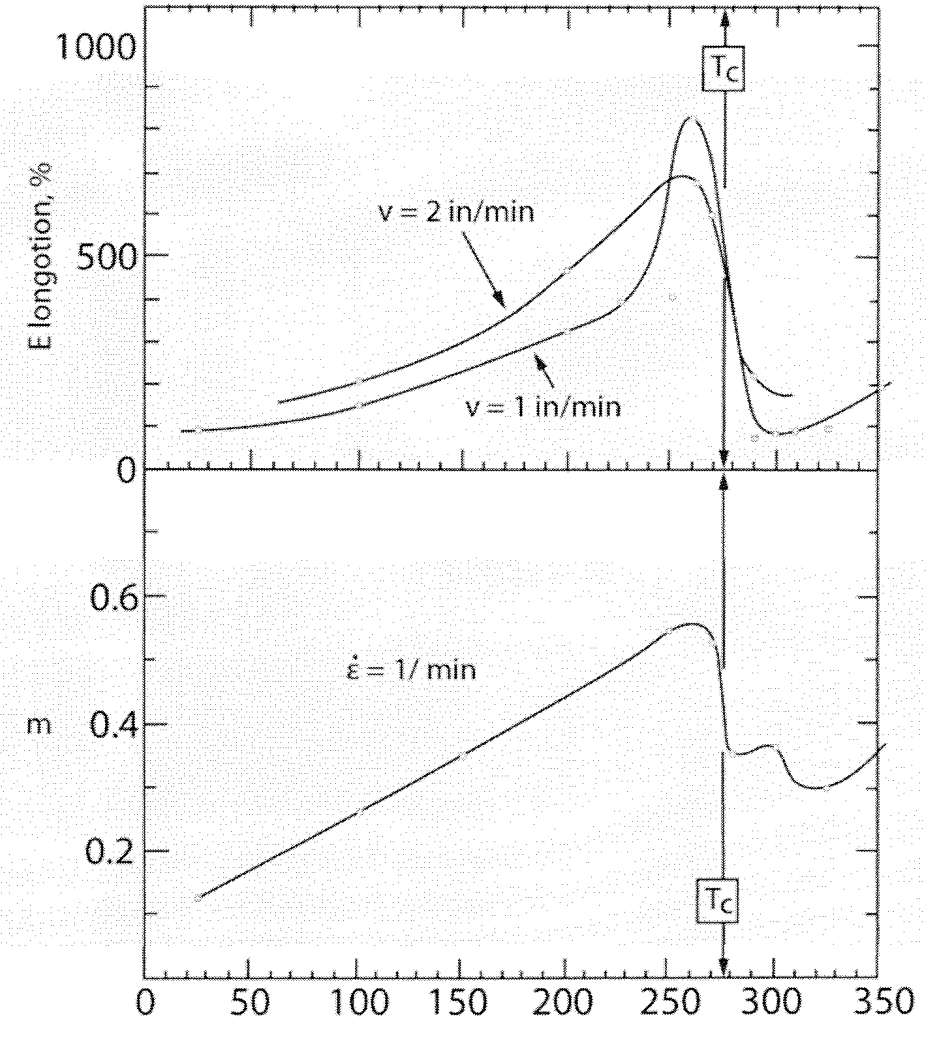

Figure 1.15 Temperature dependence of elongation (upper) and strain rate sensitivity (lower). T_C is the critical temperature [43]

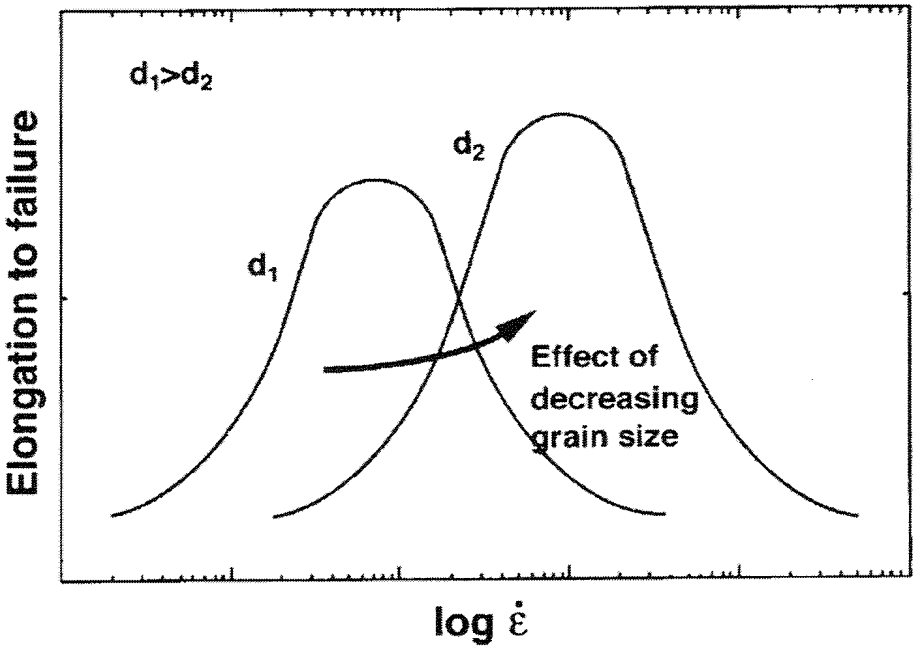

Figure 1.16 Variation of the elongation to failure with strain rate when the grain size is reduced from d_1 to d_2 [60]

Thirdly, it requires slow strain rates (10^{-3} to $10^{-1}s^{-1}$) which are impossible to obtain with conventional forming techniques such as rolling or extruding; when techniques can achieve this, most of the times it's impossible to relate them to productivity. Furthermore, the stress required to deform the material has to be sensitive to the strain rate: if the necking starts, then this area will deform much more quickly and the increase in strain rate will harden the material at this point until it stops and finally the uniform deformation will continue. Also, the high strain rate sensitivity of a material is the origin of the stabilization against localized necking and thus producing high plastic elongation. Nevertheless, the strain rate is related with the grain size in an inversely proportional way as:

$$\dot{\varepsilon} \approx (b/d)^p \qquad [1.15]$$

where $\dot{\varepsilon}$ is the strain rate, b is the Burgers vector, d is the grain size and p can be equal to 2 when the process is related to lattice-diffusion-controlled creep (Nabarro-Herring creep) or equal to 3 when related to grain boundary diffusion-controlled creep (Coble creep). In other words, if the grain size is decreased, a higher strain rate can be used to achieve the same state of superplasticity [7; 25; 29; 62].

Finally, the grain boundaries of the materials have to allow the grain sliding between them and to rotate when stress is applied, due to the movement of dislocations along the grain boundaries. In order for this to happen, it is necessary to apply the right temperature and have a fine grained structure. This requirement is a fundamental characteristic in some superplastic behavior models, such as the one proposed by Ashby and Verrall. The sliding percentage at the superplastic region (II) is very high ($40{\sim}80\%$), which contributes considerably with the maximum superplastic deformation, though this happens for elongations lower than 50%; for higher elongations than this one, the contributing factor is diffusion. The sliding percentage diminishes considerably at regions I and II, as the overall elongations also decrease [29; 38; 55].

On the other hand, Alden lists nine microstructural characteristics required in a material to be deformed superplastically (some of them were previously mentioned) as follows [63]:

1. Strong dependency between stress and strain rate: $\sigma = K\dot{\varepsilon}^m$.
2. Influence of temperature on the diffusional processes related to superplasticity. The activation energies are similar to the grain boundary diffusion and not to the volume diffusion.
3. Creep at a constant load and temperature that does not present primary or transitory phase.
4. Materials, after being superplastically deformed, maintain its initial resistance and ductility at room temperature.
5. Superplastic materials, after deformation, do not show substructures or increase in the dislocation density.
6. Shape factor, length/width, of the crystals is low and unrelated to the superplastic deformations. The number of grains in the transverse section of the samples decreases with deformation.
7. Non-existing texture related to the large superplastic deformations. The grains do not tend to reorient themselves crystallographically speaking in relation to the main material flow directions.
8. Superplasticity is associated to the intergranular sliding and rotation of grains during deformation, meaning they constantly switch their relative positions while accommodating themselves in the matter flow direction.
9. Stable and fine grain size microstructure.

1.5.5 Microstructure

It is agreed that when a material with equiaxed microstructure is deformed under optimum superplastic conditions, the shape of the crystal do not change and they grow very little, without forgetting the GBS that creates precipitate-free zones near grain boundaries [26].

The duplex structure of a material is important in the superplastic behavior as the second phase (30~50% in volume) can inhibit the grain growth of the matrix by stabilizing the microstructure. Therefore, single phase materials will never reach superplasticity by themselves [25; 60; 61; 64].

Superplastic materials can be divided into two groups depending on the type of fracture they present: necks with substantial cross-section area or those whose necks is a very fine point when fractured. However, they all present internal cavitations after fracture but not all present voids (as voids form, their distribution depends on the strain rate). Higher strain rates produce small voids that lay like chains and in a direction almost parallel to the deformation direction (Figure 1.17a), while lower strain rates increase the void size and their distribution appears to be random while their shape is mostly round or spherical (Figure 1.17b) [65; 66].

An explanation of the previous behavior is that with high strain rates, a large number of void nuclei start to form with a chainlike distribution, and as the test time is small enough so neither the voids grow or reach critical radius. On the other hand, with the low strain rates, there is a transition between the small chainlike distributed voids (region III of the superplastic deformation curve) to the large rounded randomly distributed ones (region I) caused by a long test time that influences the void growth on a smaller number of void nuclei formed by stress. This change in void morphology is also backed up by the transition of mechanisms taking place in the deformation of the material: power-law creep at high strain rates to grain boundary diffusion (or vacancy diffusion) process at low strain rates. Furthermore, this also can be analyzed through the critical void radius: it increases while decreasing the strain rate, therefore it also corroborates the transition between processes [65; 66; 67; 68; 69].

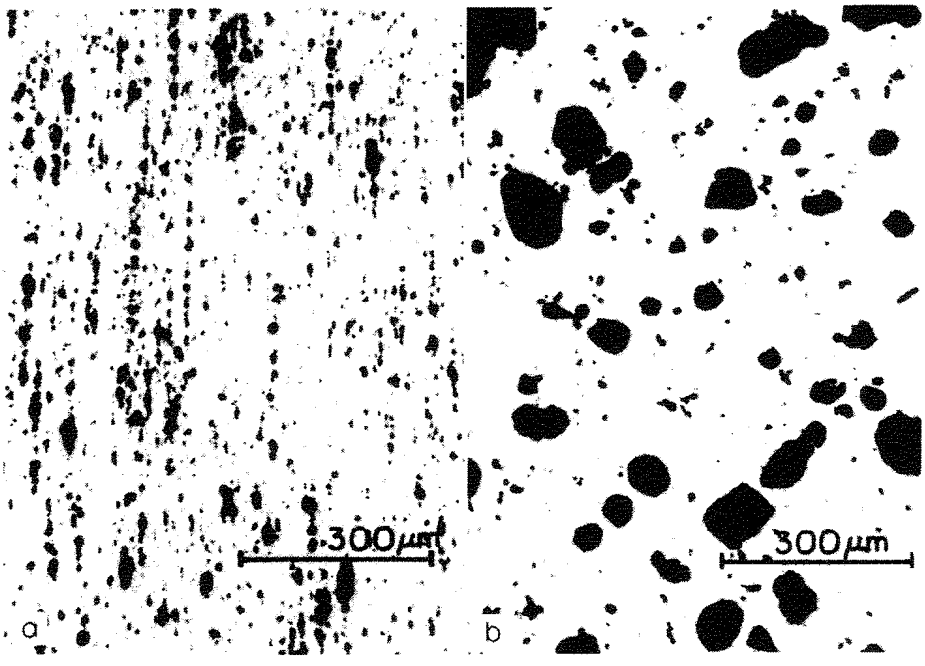

Figure 1.17 Optical micrograph of areas of an Cu alloy behaving superplastically at $823\ \mathrm{K}$ at initial strain rates of a) $3.33 \times 10^{-2}\ \mathrm{s}^{-1}$ and b) $1.67 \times 10^{-5}\ \mathrm{s}^{-1}$; the tensile axis is vertical [65]

Langdon also indicates that sometimes voids interlink themselves and usually in the tensile direction, which is probably due to the high ductility of the material (superplasticity) [65].

Other work establishes that cavities nucleate and grow at the grain boundaries when suffering high temperature creep, and also when the material is behaving superplastically (especially ultrafine grained ones). The reason is that, due to the ultrafine nature of the grains, the voids at the boundaries sometimes involve several grains and it enhances the diffusion process; this is even higher when coalescence of voids also occurs. It is believed that GBS is responsible for the nucleation of voids/cavities in superplasticity, but it requires for the grains to have high angles of disorientation, therefore the processing of the material for obtaining ultrafine grain sizes directly influences the possibility of reaching superplastic behavior. In other words, the more disordered the boundary structure, the better ability of GBS because of the high density of broken bonds across the boundary; the duplex structure in steels suitable for GBS can be formed during the early stage of the deformation [25; 46; 55; 60; 61; 65; 66].

A grain boundary may be of the non-equilibrium type when there are some defects besides their equilibrium content, for example the non-equilibrium grain boundaries produced by the absorption of lattice dislocations. These high-energy defects are unstable and disappear at high temperatures, but they increase both vacancies at boundaries and the diffusion coefficient. In these grain boundaries certain kinetic processes related to diffusion (such as migration and GBS) are accelerated which in turn affect creep, recrystallization and superplasticity, as they are the result of the interaction of the grain boundary with the lattice dislocations, which can occur during the movement of a grain boundary through a strained crystal or when the dislocation enters the grain boundary during plastic deformation. In other words, superplastic flow happens through the GBS as the individual grains of the polycrystalline matrix move over each other in response to the applied stress (Rachinger sliding) and this happens without any elongations of the individual grains. The non-equilibrium grain boundaries are commonly found in ultrafine and hyperfine grained materials. Figure 1.18 shows two non-equilibrium (a) and equilibrium (b) grain boundaries; non-equilibrium GB can be seen as diffuse and with elastic stresses observed within several grains [60; 70; 71].

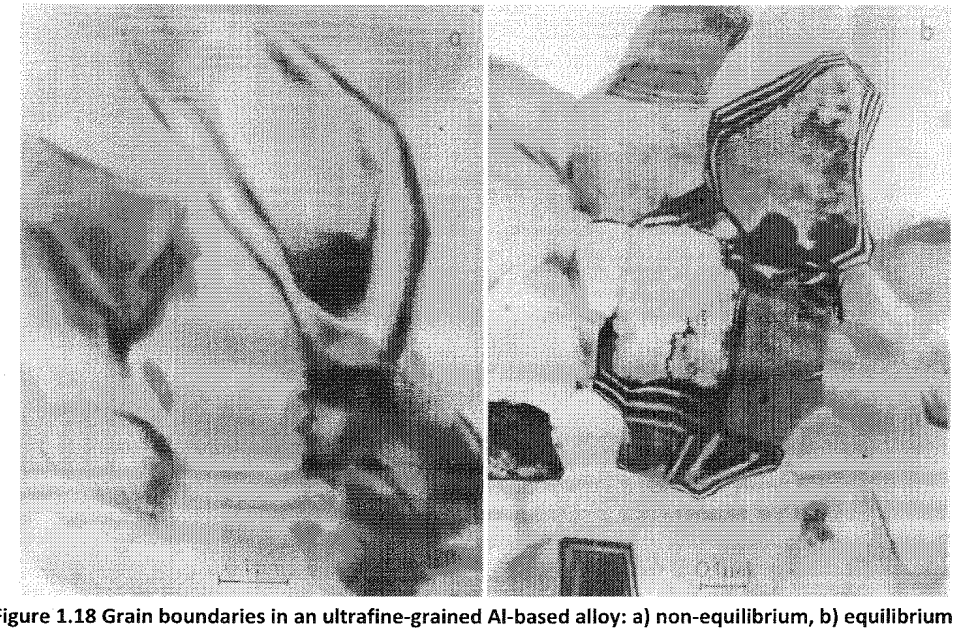

Figure 1.18 Grain boundaries in an ultrafine-grained Al-based alloy: a) non-equilibrium, b) equilibrium [70]

Figure 1.19 shows a representation of the GBS in superplasticity: dislocations move along the grain boundary between two grains and accumulate at the junction of three

grains (A), this concentrates the stress and the slip nucleates in the contiguous grain, the dislocations move across the grain, pile-up at the opposing grain boundary (B) and are then removed by climb into the boundary. Also, the accommodating dislocation can glide through the blocking grain to produce effects on the opposing grain boundary [60].

> *"The degree of the non-equilibrium grain boundary structure is determined by the straining parameters: temperature and strain rate"* [70].

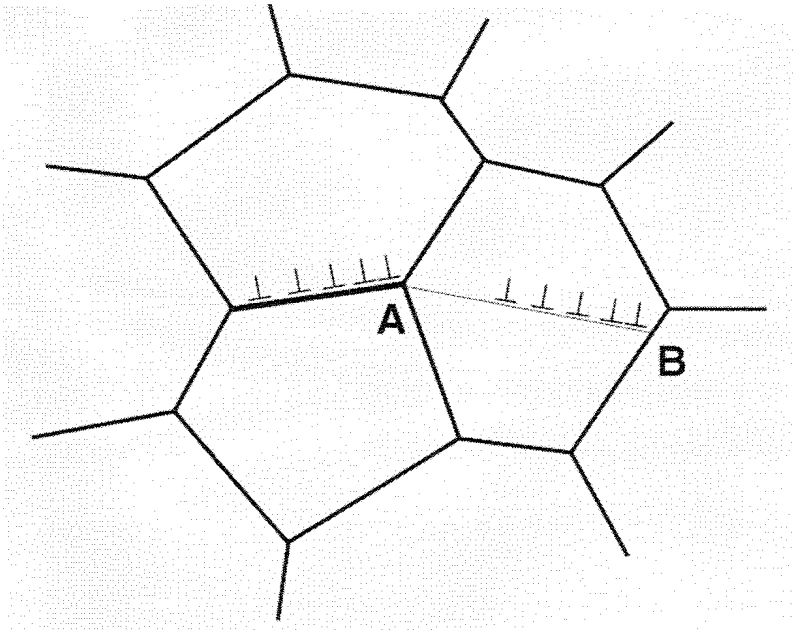

Figure 1.19 Principles of a model for grain boundary sliding in superplasticity: dislocations move along the grain boundary and pile-up at the triple junction A, the stress concentration is removed by the nucleation of slip in the adjacent grain and these intergranular dislocations pile-up at B and climb into the grain boundary [60]

1.5.6 Advantages and Applications

When researchers discovered superplasticity, in the 1970s they proposed some applications such as vacuum forming, drape forming and bottle blowing, some of which nowadays are still impossible [26].

The advantage of superplastic behavior presents itself while manufacturing: the possibility to superplastically form (high deformation) a part with complex geometric shapes in only one operation (i.e. half spheres, curved walled pipes, etc.) for added value, thus increasing the capabilities of the processes/operations. On the other hand, the stress required to manufacture a part is lower (hot deformation) which involves lower tool cost and wear. Also the energy consumption diminishes, while reducing the amounts of both metal used and surfaces machined, resulting in an improvement in the quality of the finished part. Moreover, these materials present high resistance at room temperature and a uniform microstructure after the superplastic deformation [7; 65; 72].

Another characteristic of the superplastic material, that is also an advantage while forming parts, is its high fluidity (ability to fill deep narrow cavities in a die under the influence of relatively low pressure) [72].

Furthermore, there is an increase on the length of time the superplastic material can be manufactured (dozens of times higher than in the plastic state) and reducing the number of processes a part requires (usually to one or two) while eliminating manual tasks (fitting, machining, welding, riveting, embossing, etc.) due to the high quality and tolerance of the parts obtained [62; 72].

Superplastic forming processes can do the following: drawing, forging, extrusion, etc. An example of the drawing process is the hydraulic bulging (Figure 1.20); this process consists in holding the sheet from its ends while applying hydrostatic pressure to it: the maximum height h will increase with m in a directly proportional fashion [72].

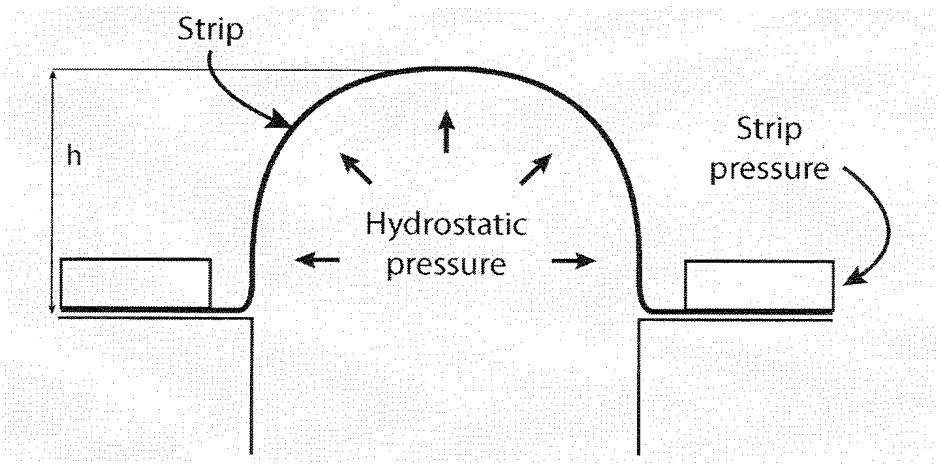

Figure 1.20 Hydraulic bulging process [72]

Sometimes superplastic forming can combine with other manufacturing processes, for example with diffusion welding (used in aerospace and defense industries) to produce large thin-walled structures of complex shape to be used in load-bearing structures, thus replacing heavier, weaker structures assembled from several parts by bolting, riveting, welding, etc. Another example of this combination is forming a structural element of complex shape such as the ones in Figure 1.21 which also includes the joining of elements to one another or to other structural elements. Figure 1.21a shows the formation of a plate with stiffening ribs welded to it (horizontal ribs on the right and vertical ones on the left), Figure 1.21b shows a waffle-shaped part with a finished panel on the top, and Figure 1.21c shows a multi-layered structure that started from three flat-rolled semifinished sheets with an anti-welding material applied between them. These sheets/plates are placed between the heating slabs of a hydraulic press, heated to a specific temperature and welded together by diffusion welding; the middle sheet is formed by injecting an inert gas between the plates, thus obtaining a rigid monolithic structure composed of rolled plates in a single operation [62; 72].

Superplastic deformation can be used to form multilayered structures with complex shapes, since both the structure and the diffusion welds in it are formed while the material is in its superplastic state, also eliminating problems such as aligning the components. Evidently the final shape of the structure is determined by the contour of

the die, but the shape of the filler (inner layer/sheet) depends on the pattern in which the stop-material is applied, resulting in different types of fillers: corrugated, rippled, cellular, waffle-shaped, etc. This process can also include placing structural elements in the die before the operation takes place and through diffusion welding it can be joined to the sheet in the same operation, for example, adding reinforcing plates, fittings, tips, butt straps, fasteners, etc. The accuracy of the finished product is only defined by the accuracy of the tool [72].

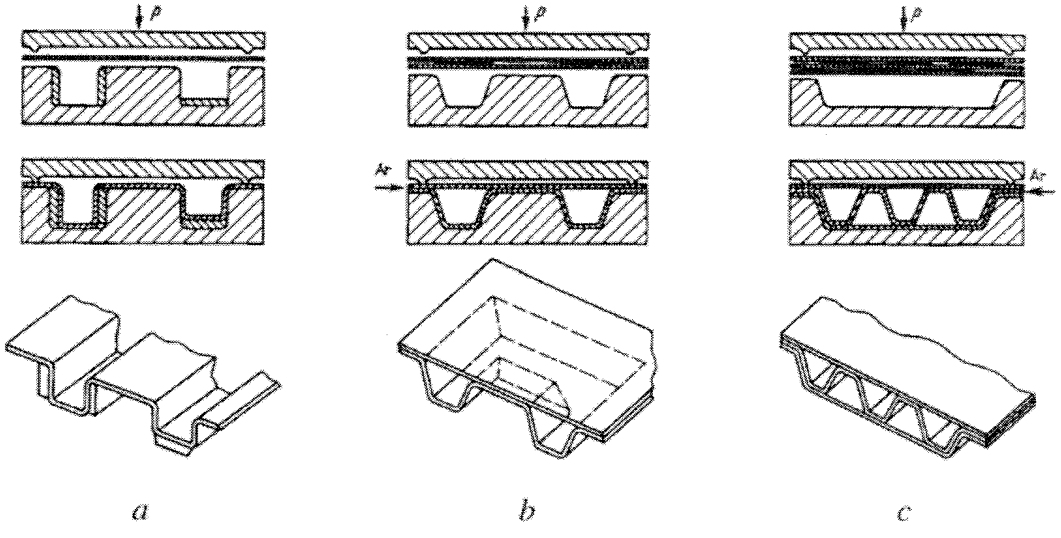

Figure 1.21 Main schemes used in SPD-DW[1]: a) formation of a sheet with the attachment of stiffening ribs by welding, b) fabrication of a ribbed-type structure, c) fabrication of a three layer structure [72]

A disadvantage of superplastic materials is that the parts manufactured this way cannot be used at high service temperatures because they will creep considerably; a solution to this is to thermally treat the parts to increase its grain size. Other disadvantages include [7]:

- The low strain rate required for superplasticity implies high forming times in order to achieve the sliding of grains and subsequent superplastic deformation.
- The high temperature necessary for this process of $\sim 0.5T_m$.
- The previous thermomechanical process to obtain a fine grained structure (hot rolling and/or thermal treatments).

[1] **SPD-DW:** Superplastic Deformation with Diffusion Welding.

- The cavitations formed on certain superplastic alloys during deformation which leads to coalescence and posterior rupture (due to the presence of relatively hard phases in the material).
- The low creep resistance at high temperature which may be solved by thermally treating the material to increase the grain size.

1.5.7 Experimental disadvantages

Superplastic behavior requires maintaining a constant temperature higher than $\sim 0.5T_m$, which implies that the furnace in the traction testing machine has a limit to the elongation of the specimen, otherwise part or parts of the specimen would be outside of its heating areas. Environmental conditions are also important because of the possible oxidation or corrosion of the testing materials which would change the geometrical parameters of the specimen and therefore modifying its final elongation. Finally, the strain rate must be slow enough so the grains deform intergranularly (sliding and rotating) instead of intragranularly, this means that some materials cannot be deformed superplastically in real manufacturing conditions [7; 44].

1.6 References

1. *Grain refinement in Dual-Phase Steels.* **Mukherjee, K., Hazra, S.S. and Militzer, M.** September 2009, Metallurgical and Materials Transactions A, Vol. 40A, pp. 2145-2159.

2. *Effect of Martensite Plasticity on the Deformation Behavior of a Low-Carbon Dual-Phase Steel.* **Mazinani, M. and Poole, W.J.** February 2007, Metallurgical and Materials Transactions A, Vol. 38A, pp. 328-339.

3. *Effect of rolling and epitaxial ferrite on the tensile properties of low alloy steel.* **Ahmad, E., Sarwar, M. and Manzoor, T.** 2006, Journal of Materials Science, Vol. 41, pp. 5417-5423.

4. *The Deformation and Ageing of Mild Steel: III. Discussion of Results.* **Hall, E.O.** 1951, Physical Society of London Proceeding, Vol. 64, pp. 747-753.

5. *The Cleavage Strength of Polycrystals.* **Petch, N.J.** 1953, Iron and Steel Institute Journal, Vol. 174, pp. 25-28.

6. **Pickering, F.B.** *Physical Metallurgy and the Design of Steels.* s.l. : Applied Science Publishers, 1978.

7. **Pero-Sanz Elors, J.A.** *Ciencia e ingeniería de materiales: Estructura, transformaciones, propiedades y selección.* [ed.] CIE Dossat. 5th. 2006. (in spanish).

8. *The Quiet Revolution in Materials Manufacturing and Production.* **Eagar, T.W.** 4, 1998, Journal of Metals, Vol. 50, pp. 19-21.

9. *The relevance of Sir Bessemer's ideas to the Steel Industry in the 21st century.* **Birat, J.P.** 7-8, 2004, Revue de Métallurgie, Vol. 101, p. 587.

10. *Hot strength of creep resistant ferritic steels and relationship to creep rupture data.* **Dimitriu, R.C. and Bhadeshia, H.** 9, 2007, Materials Science and Technology, Vol. 23, pp. 1127-1131.

11. *Changing economics of steel.* **Christmas, I.** 4, 2012, Ironmaking and Steelmaking, Vol. 39, pp. 258-262.

12. *A study on the microstructural changes in hot rolling of dual-phase steels.* **Salehi, A.R., Serajzadeh, S. and Karimi, A.** 2006, Journal of Materials Science, Vol. 41, pp. 1917-1925.

13. *Static Strain Aging Phenomena in Cold-Rolled Dual-Phase Steels.* **Waterschoot, T., De, A.K. and Vandeputte, S.** March 2003, Metallurgical and Materials Transactions A, Vol. 34A, pp. 781-791.

14. *Dual-Phase Ultrafine Grained Steels Produced by Controlled Rolling Processes.* **Quintana, M.J., Gonzalez, R. and Verdeja, L.F.** [ed.] MS&T. Columbus, Ohio : s.n., 2011. MS&T 2011 Proceedings.

15. *Propiedades Mecánicas de Aceros de Fase Dual de Grano Ultrafino.* **Quintana, M.J., González, R. and Verdeja, L.F.** [ed.] SOMIM. Monterrey, Nuevo León : s.n., 2010. Memorias del XVI Congreso Internacional Anual de la SOMIM. (in spanish).

16. *Ultrafine Grained HSLA Steels for Cold Forming.* **González, R., García, J.O. and Barbés, M.A.** 10, 2010, Journal of Iron and Steel Research, International, Vol. 17, pp. 50-56.

17. *The Changing Scene in Steel.* **Paxton, H.W.** 12, 1979, Metallurgical Transactions, Vol. 10A, p. 1815.

18. *Numerical Cooling Strategy Design for Hot Rolled Dual Phase Steel.* **Suwanpinij, P., Togobytska, N. and Prahl, U.** 11, 2010, Steel Research International, Vol. 81, pp. 1001-1009.

19. *Controlled Rolling of Steel Plate and Strip.* **Tanaka, T.** 1981, International Metals Reviews, Vol. 4, pp. 185-191.

20. *Influence of Thermo-Mechanical Processing Parameters and Chemical Composition on Bake Hardening Ability of Hot Rolled Martensitic Steels.* **Asadi, M. and Palkowski, H.** 7, 2009, Steel Research International, Vol. 80, pp. 499-506.

21. *Effect of Composition and Process Variables on Nb (C,N) Precipitation in Niobium Microalloyed Austenite.* **Dutta, B. and Sellars, C.M.** 3, 1987, Materials Science and Technology, Vol. 3, p. 197.

22. *Modelling the Kinetics of Strain Induced Precipitation in Nb Microalloyed Steels.* **Dutta, B., Palmiere, E.J. and Sellars, C.M.** 5, 2001, Acta Materialia, Vol. 49, p. 785.

23. *Nucleation Kinetics of Ti Carbonitride in Microalloyed Austenite.* **Liu, W.J. and Jonas, J.J.** 4, 1989, Metallurgical Transactions, Vol. 20A, p. 689.

24. *Deformation Processing.* **Backofen, W.A.** 12, 1973, Metallurgical Transactions, Vol. 4B, p. 2679.

25. *Structural Superplasticity at Higher Strain Rates of Hypereutectoid Fe-5.5Al-1Sn-1Cr-1.3C Steel.* **Frommeyer, G. and Jiménez, J.A.** February 2005, Metallurgical and Materials Transactions A, Vol. 36A, pp. 295-300.

26. *Superplasticity: A Review.* **Davies, G.J., Edington, J.W. and Cutler, C.P.** 1970, Journal of Materials Science, Vol. 5, pp. 1091-1102.

27. *Superplasticity: Prerequisites and Phenomenology.* **Wadsworth, J., Oyama, T. and Sherby, O.** 1980. InterAmerican Conference on Materials Technology.

28. *A composite model for superplasticity.* **Baudelet, B. and Lian, J.** 1995, Journal of Materials Science, Vol. 30, pp. 1977-1981.

29. **Askeland, D.** *The Science and Engineering of Materials.* 3th. s.l. : PWS Publishing Company, 1998.

30. **Reed-Hill, R.E.** *Creep. Physical Metallurgy Principles.* 2nd. Independence, KY : Cengage Learning, 1994.

31. **Ashby, M.F. and Jones, D.R.H.** *Engineering Materials 1.* s.l. : Pergamon Press, 1986. Vol. 34.

32. **Dieter, G.E.** *Mechanical Metallurgy.* s.l. : McGraw-Hill, 1981.

33. *Theory of Steady-State Creep Based on Dislocation Climb.* **Weertman, J.** 1955, Journal of Applied Physics, Vol. 26, p. 1213.

34. *Some Fundamental Experiments on High Temperature Creep.* **Dorn, J.E.** 1954, Journal of the Mechanics and Physics of Solids, Vol. 3, pp. 85-116.

35. Engineering Archives. [Online] 2008-2012. www.engineeringarchives.com.

36. *Effect of change of scale on sintering phenomena.* **Herring, C.** 1950, Journal of Applied Physics, Vol. 21, pp. 301-303.

37. *Report on a Conference on the strength of materials.* **Nabarro, F.R.N.** 1948, The Physical Society, p. 75.

38. *Diffusion-accomodated flow and superplasticity.* **Ashby, M.F. and Verrall, R.A.** 1973, Acta Metallurgica, Vol. 21, pp. 149-163.

39. *Zinc Alloys with Aluminum and Copper.* **Roseham, W., Haughton, J.L. and Bingham, K.E.** 1920, J. Inst. Metals, Vol. 23, p. 261.

40. *Akad. Nauk SSSR.* **Bochvar, A.A. and Sviderskaia, Z.A.** 1945, Otdel. Tekh. Nauk, Vol. 9, p. 821.

41. *Superductility of Eutectoid Alloys of Aluminum with Zinc.* **Presnyakov, A.A. and Chervyakova, V.V.** 1960, Russian Metallurgy and Fuels (Scientific Information Consultants Translation), Vol. 3, p. 85.

42. *A review of Superplasticity and related phenomena.* **Underwood, E.E.** 1962, Journal of Metals, Vol. 14, p. 914.

43. *Superplasticity in an Al-Zn Alloy.* **Backofen, W.A., Turner, R.I. and Avery, D.H.** 1964, Transactions of the ASM, Vol. 57, p. 980.

44. *Strain-rate sensitivity as a measure of ductility.* **Woodford, D.A.** 1969, Transactions of American Society for Metals, Vol. 62, pp. 291-293.

45. *The Elongation of Superplastic Alloys.* **Morrison, W.B.** 1968, Trans. Metall. Soc. AIME, Vol. 239, p. 710.

46. *Microstructural Aspects of Superplasticity.* **Edington, J.W.** May 1982, Metallurgical and Materials Transactions A, Vol. 13A, pp. 803-715.

47. *A Theory for Flow of Polycrystal.* **Baudelet, B.** 1967, Acta Metall, Vol. 15, p. 1545.

48. **Kashyap, B.P. and Mukherjee, A.K.** *Superplasticity.* [ed.] B. Baudelet and M. Suery. Paris : CNRS, 1985.

49. *A Structural Basis for Superplasticity.* **Avery, D.H. and Backofen, W.A.** 1965, Transactions of American Society for Metals, Vol. 58, pp. 551-562.

50. *Creep-Rupture Characteristics of Al-Mg Solid-Solution Alloys.* **Mullendore, A.W. and Grant, N.J.** 9, 1954, Transactions of Metallurgical Society of AIME, Vol. 200, pp. 973-979.

51. **Conway, J.B. and Flagella, P.N.** *Creep-Rupture Data for the Refractory Metals at High Temperatures.* General Electric Co. Nuclear Systems Programs Technical Report GEMP-685 (R-69-NSP-9).

52. *Creep of Thoriated Nickel Above and Below 0.5 Tm.* **Wilcox, B.A. and Clauer, A.H.** 1966, Transactions of Metallurgical Society of AIME, Vol. 236, pp. 570-580.

53. *Short-Time Creep-Rupture Behavior of Tungsten at 2250°C to 2800°C.* **Green, W.V.** 12, 1959, Transactions of Metallurgical Society of AIME, Vol. 215, pp. 1057-1060.

54. *The Viscous Properties of Exuded Eutectic Alloys of Lead-Tin and Bismusth-Tin.* **Pearson, C.E.** 1934, J. Inst. Metals, Vol. 54, p. 111.

55. *An investigation of grain boundary sliding in superplasticity at high elongations.* **Lin, Z.R., Chokshi, A.H. and Langdon, T.G.** 1988, Journal of Materials Science, Vol. 23, pp. 2712-2722.

56. *The role of boundaries during superplastic deformation.* **Mohamed, F.A.** 2001, Surface and Interface Analysis, Vol. 31, pp. 532-546.

57. *Superplasticity in the Aluminium-Zinc. Eutectoid.* **Ball, A. and Hutchinson, M.M.** 1969, Metal Sci J, Vol. 3, p. 1.

58. *The rate controlling mechanism in superplasticity.* **Mukherjee, A.K.** 1971, Mater Sci Eng, Vol. 8, p. 83.

59. *Superplasticity: Prerequisites and Phenomenology.* **Sherby, O.D., Wadsworth, J. and Oyama, T.** [ed.] U.P. Madrid. Madrid : s.n., 1985. E.T.S.I.C.C.P.

60. *Principles of superplasticity in ultrafine-grained materials.* **Kawasaki, M. and Langdon, T.G.** 2007, J Mater Sci, Vol. 42, pp. 1782-1796.

61. *Grain boundary engineering for superplasticity in steels.* **Furuhara, T. and Maki, T.** 2005, Journal of Materials Science, Vol. 40, pp. 919-926.

62. *Superplasticity: Mechanisms and Applications.* **Vetrano, J.S.** March 2001, JOM, p. 22.

63. **Alden, T.H.** *Review topics in Superplasticity, Plastic deformation of materials.* [ed.] R.J. Arsenault. New York : Academic Press, 1975. pp. 225-266.

64. *Superplasticity of a Stainless Steel Clad Ultrahigh Carbon Steel.* **Daehn, G.S., Kum, D.W. and Sherby, O.D.** December 1986, Metallurgical and Materials Transactions A, Vol. 17A, pp. 2295-2298.

65. *A microscopic examination of void formation in superplastic materials.* **Langdon, T.G.** May 1979, Journal of Microscopy, Vol. 116, pp. 47-54.

66. *An Analysis of Cavity Growth During Superplasticity.* **Miller, D.A. and Langdon, T.G.** December 1979, Metallurgical Transactions A, Vol. 10A, pp. 1869-1874.

67. *Creep cavitation without a vacancy flux.* **Hancock, J.W.** 1976, Metal Sci, Vol. 10, p. 319.

68. *Vacancy potential and void growth on grain boundaries.* **Speight, M.V. and Beeré, W.** 1975, Metal Sci., Vol. 9, p. 190.

69. *Diffusional growth of creep voids.* **Harris, J.E.** 1978, Metal Sci., Vol. 12, p. 321.

70. *Diffusion along Grain Boundaries with Non-Equilibrium Structure.* **Valiev, R.Z., Razumovskii, I.M. and Sergeev, V.I.** 1993, phys. stat. sol., Vol. 139, pp. 321-335.

71. *Grain Boundaries during Superplastic Deformation.* **Valiev, R.Z., Kaibyshev, O.A. and Khannanov, S.K.** 1979, phys. stat. sol., Vol. 52, pp. 447-453.

72. *Promising Processes for Shaping Superplastic Materials.* **Smirnov, O.M.** 7-8, 2010, Metallurgist, Vol. 54, pp. 491-497.

2 Experimental Procedure and Results

2.1 Advanced Thermomechanical Controlled Rolling Processes

The mechanical properties of the final product as a function of its microstructure depend on a single microstructural parameter: grain size. Thus, the evolution of the crystals along the manufacturing processes is of major importance, as well as the possible introduction of variations in order for the product to acquire the necessary values of resistance, ductility and toughness.

This work includes the rolling protocols of four steels (obtained from the Arcelor-Mittal factories in Asturias, Spain). The grain size evolution of them has been simulated during the roughing and finishing passes. The materials are:

- One C-Mn steel with final thickness of 27 mm. Not microalloyed.
- One C-Mn steel with final thickness of 27 mm. Microalloyed with Nb.
- Two C-Mn steels with and without Nb with final thickness of 5 mm. The finishing pass was made in the hot rolling mills followed by a rapid cooling and coiling.

The parameters that influence the microstructural evolution are: strain, strain rate, Zener-Hollomon coefficient, 50% and 95% recrystallization times and grain growth between passes. The data for C-Mn and C-Mn-Nb steels was extracted from the references [1; 2; 3; 4; 5; 6].

2.1.1 Execution phases in the case of a steel with C-Mn

Firstly, the equivalent strain by rolling is calculated using the expression:

$$\varepsilon = \frac{2}{\sqrt{3}} \ln \frac{h_0}{h_f} \quad [2.1]$$

where h_0 is the initial thickness and h_f is the final thickness.

It is important to point out that if recrystallization does not occur, the strain would start to accumulate. Afterwards, the strain rate is calculated, knowing the speed of the rolls (v) and their radius (R), then:

$$\dot{\varepsilon} = \frac{v}{[R(h_0 - h_f)]^{1/2}} \cdot \varepsilon \quad [2.2]$$

being R the ideal gas constant.

Once the strain rate is calculated, the Zener-Hollomon (Z) parameter is obtained which considers the temperature drop (T) and the strain rate increase ($\dot{\varepsilon}$):

$$Z = \dot{\varepsilon} \cdot e^{\left(\frac{37440}{T}\right)} \quad [2.3]$$

where T is the temperature in Kelvin.

Later on, the time required to recrystallize 95% of the material is calculated:

$$t_{x=95\%} = 3.53 \times 10^{-21} \cdot Z^{-0.375} \cdot \varepsilon^{-4} \cdot D_0^2 \cdot e^{\left(\frac{57400}{T}\right)} \quad [2.4]$$

which is activated (exponentially) with temperature; also, it can decrease with the fourth power of the strain and increase with the second power of the initial grain size (D_0 expressed in meters).

Applying the Avrami equation, the recrystallized fraction can be determined when knowing the time between passes (t) and the time required to recrystallize 95% of the material ($t_{x=95\%}$) as follows:

$$X = 1 - \exp\left[\ln(0.05) \cdot \left(\frac{t}{t_{x=95\%}}\right)^2\right] \quad [2.5]$$

The recrystallized grain size, valid for both the roughing and finishing, is calculated through:

$$D_{rex} = 25^{0.67} \cdot \left[\frac{1}{0.067} \cdot \ln\left(\frac{Z}{8.5\times10^9}\right)\right]^{0.67} \cdot \varepsilon^{-1} \cdot D_0^{1/2} \quad [2.6]$$

which depends directly on the initial grain size and is inversely proportional to the strain.

In the same way, the recrystallized grain growth, for both roughing and finishing is:

$$D^{10} = \left[3.87 \times 10^{32} \cdot e^{\left(\frac{-400000}{RT}\right)}\right] \cdot t + D_{rex}^{10} \quad [2.7]$$

which is exponentially activated with temperature and the $1/10$ power of itself. This term can be important in the roughing phase as well as in the waiting times before the finishing pass.

2.1.2 Execution phases in the case of a steel with C-Mn microalloyed with Nb

For this steel in particular, the equivalent strain by rolling as well as the strain rate and the Zener-Hollomon parameters can also be calculated using equations: [2.1], [2.2] and [2.2].

Afterwards, the time required to recrystallize the 50% of the material is calculated for the roughing passes:

$$t_{x=50\%} = 2.52 \times 10^{-19} \cdot \varepsilon^{-4} \cdot D_0^2 \cdot e^{\left(\frac{325000}{RT}\right)} \quad [2.8]$$

and for the finishing pass:

$$t_{x=50\%} = 9.24 \times 10^{-9} \cdot \varepsilon^{-4} \cdot D_0^2 \cdot e^{\left(\frac{130000}{RT}\right)} \quad [2.9]$$

These expressions are similar to the previous case except that for microalloyed steels the expressions do not involve the Zener-Hollomon parameter and the numerator of the exponential term is considerably lower for the finishing process which leads to higher recrystallization times.

From equations [2.8] and [2.9] the time required to recrystallize 95% of the material can be obtained:

$$t_{x=95\%} = \left(\sqrt{\frac{\ln(0.05)}{\ln(0.5)}}\right) \cdot t_{x=50\%} \quad [2.10]$$

In the same way as the previous case and using the Avrami equation, the recrystallized fraction can be determined knowing the time between passes (t) and the time required to recrystallize 50% of the material ($t_{x=50\%}$) as follows:

$$X = 1 - \exp\left[\ln(0.5) \cdot \left(\frac{t}{t_{x=50\%}}\right)^2\right] \quad [2.11]$$

As a general rule, it is considered that recrystallization happens when it is equal or higher than 50%.

For both the roughing and finishing passes, the recrystallized grain size is:

$$D_{rex} = 0.9 \cdot \left(\frac{D_0}{\varepsilon}\right)^{-0.67} \quad [2.12]$$

And the recrystallized grain growth, for both roughing and finishing is:

$$D^{10} = \left[2.15 \times 10^{65} \cdot e^{\left(\frac{-1330000}{RT}\right)}\right] \cdot t + D_{rex}^{10} \qquad [2.13]$$

When comparing these last two formulas with equations [2.6] and [2.7], the grain growth is much lower in steels with Nb.

2.1.3 Example of a ATMCRP to obtain a strip with 27 mm in thickness

The microstructural evolution of the controlled rolling of weldable ferritic-pearlitic steels with C-Mn and C-Mn-Nb in the shape of a strip (27 mm in thickness) consists of the following: the roughing begins from a slab with 230 mm in thickness until 60 mm in seven passes, then is the waiting time and finally the finishing to obtain a thickness of 27 mm in six passes. In both steels the starting microstructure is austenite with a grain size of 300 μm. Table 2.1 shows the approximate protocol of the roughing passes of the rolling process, including the waiting time which is made at temperatures between 1075 and 829°C in 406 seconds. Table 2.2 shows the same for the finishing passes.

Pass	Thickness (mm)	Strain (mm/mm)	Temperature (°C)	Time of pass (s)
0	230.00			
1	189.84	0.21	1083	11
2	156.70	0.21	1081	11
3	128.34	0.22	1079	11
4	106.75	0.20	1078	11
5	88.12	0.21	1077	11
6	72.73	0.21	1076	11
7	60.00	0.21	1075	11

Table 2.1 Roughing passes for a strip with 27 mm in thickness

Pass	Thickness (mm)	Strain (mm/mm)	Temperature (°C)	Time of pass (s)
0	60.00			
1	52.24	0.16	829	12
2	45.47	0.16	823	12
3	39.59	0.16	817	12
4	34.47	0.16	811	12
5	30.00	0.16	805	12
6	27.00	0.12	799	12

Table 2.2 Finishing passes for a strip with 27 mm in thickness

Figure 2.1 compares the evolution of the grain size for both steels: microalloyed and non-microalloyed with Nb. From the figure it is evident that the microalloyed steel reaches a finer grain size at the end of the roughing passes. Moreover, the rate of the reduction of grain size is lower in the microalloyed steel as a consequence of the microalloying elements; this effect is more evident during the last passes of roughing and during the waiting times.

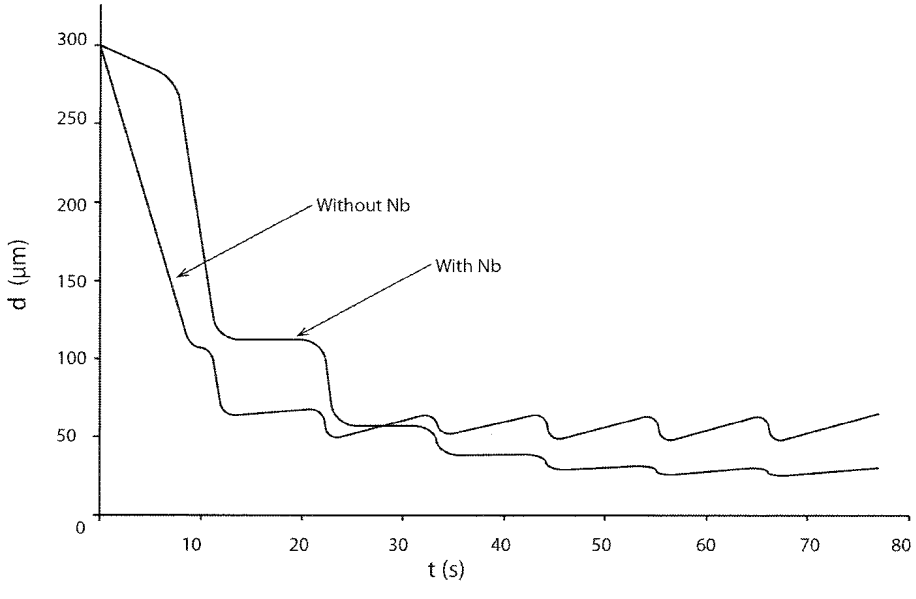

Figure 2.1 Grain size evolution during the roughing passes for steels with and without Nb

On the other hand, Figure 2.2 compares the evolution of the grain size during the last pass of the roughing process in the supposition that the starting microstructure is a 30 μm recrystallized grain size. Also, it is important to point out the almost null grain growth in the microalloyed steel due to the "pinning" effect of the precipitates on the grain boundaries.

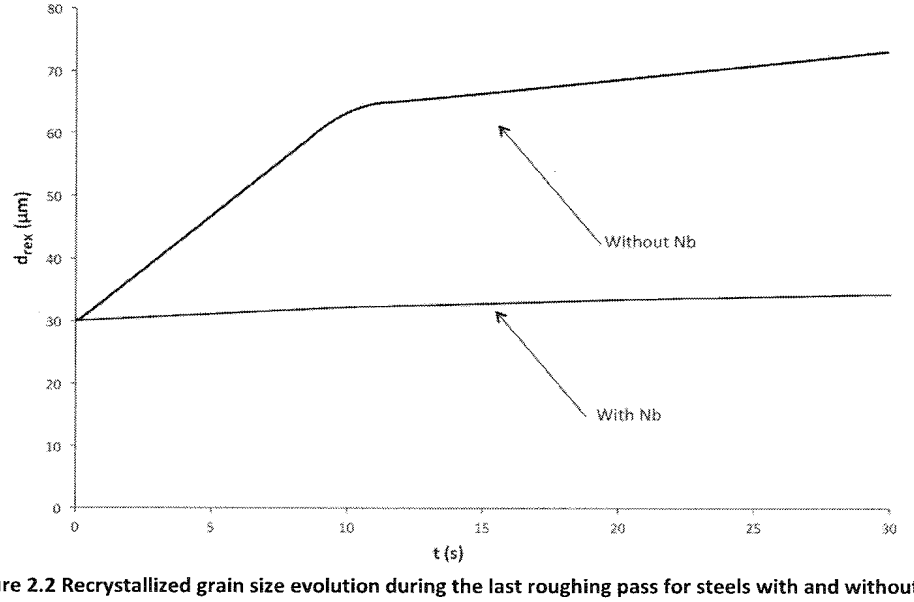

Figure 2.2 Recrystallized grain size evolution during the last roughing pass for steels with and without Nb

A C-Mn steel accumulates deformation and statically recrystallizes during the finishing passes obtaining a final austenitic grain size of ~27 μm, and after the allotropic transformation takes place (coiling) the ferrite has a grain size of ~10 μm. On the other hand, in a C-Mn-Nb steel, the austenite also accumulates deformation but does not recrystallize and after the allotropic transformation the ferritic grain size is ~4 μm.

The recrystallization kinetics of the finishing passes for both steels is shown in Figure 2.3: the Nb considerably delays the recrystallization kinetics of the austenite.

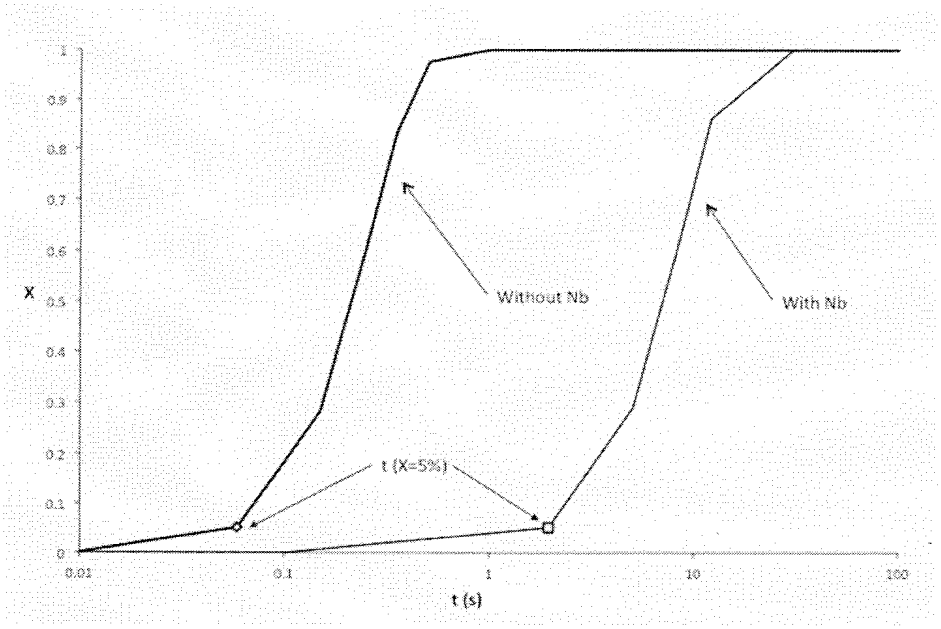

Figure 2.3 Recrystallization kinetics for steels with and without Nb in the finishing passes

2.1.4 Example of a ATMCRP to obtain a strip with 5 mm in thickness

In this case the strip ends up as a strip with a thickness of 5 mm starting from a slab of 230 mm and roughing processes until reaching 40 mm in seven passes and a finishing process, once the waiting is over, until the 5 mm thickness is reached in six passes. For both materials, weldable ferritic-pearlitic C-Mn and C-Mn-Nb steels, the starting microstructure is austenitic with a grain size of 300 μm. Table 2.3 presents the approximate rolling roughing process protocol, while Table 2.4 does the same but for the finishing process.

For this example, Figure 2.4 presents the changes in grain size during the roughing process for a steel microalloyed with Nb and one not-microalloyed with Nb (5 mm band). Similar to the case of the 27 mm strip, the grain size is smaller for the microalloyed steel at the end of the roughing process, as well as a reduction in the rate of growth between passes.

Pass	Thickness (mm)	Strain (mm/mm)	Rolling speed (rev/min)	Temperature (°C)	Time of pass (s)
0	230.00				
1	197	0.222	41.30	1187	11.8
2	164	0.222	44.40	1180	9.6
3	131	0.231	47.60	1174	10
4	98	0.213	51.50	1165	9.2
5	71	0.222	56.30	1156	9.2
6	52	0.222	60.50	1138	6.6
7	40	0.222	65.00	1119	10.2

Table 2.3 Roughing passes for a strip with 5 mm in thickness

Pass	Thickness (mm)	Strain (mm/mm)	Rolling speed (rev/min)	Temperature (°C)	Time of pass (s)
0	40.00			1070	
1	25.00	0.529	50.40	928	6.55
2	15.82	0.478	79.60	925	4.15
3	10.46	0.326	120.40	928	2.74
4	7.89	0.253	159.70	927	2.07
5	6.34	0.247	198.80	936	1.66
6	5.12	0.152	245.90	930	1.34

Table 2.4 Finishing passes for a strip with 5 mm in thickness

Figure 2.5 shows the changes in grain size during the last pass of the roughing process, supposing that the starting point is a recrystallized microstructure with a grain size of 30 μm. This figure as well as Figure 2.2 demonstrates the "pinning effect" the precipitates have on the grain size (as it grows very little).

Furthermore, Figure 2.6 compares the recrystallization kinetics of both the microalloyed and non-microalloyed steel during the finishing process. Compared to Figure 2.3, the recrystallization happens faster in the strip with a thickness of 5 mm than in the one with 27 mm.

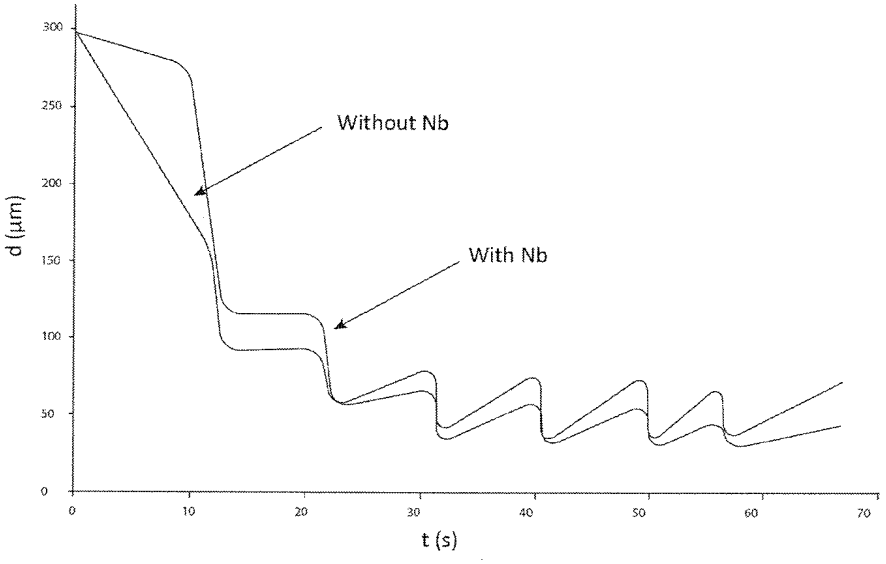

Figure 2.4 Grain size evolution during the roughing passes for steels with and without Nb

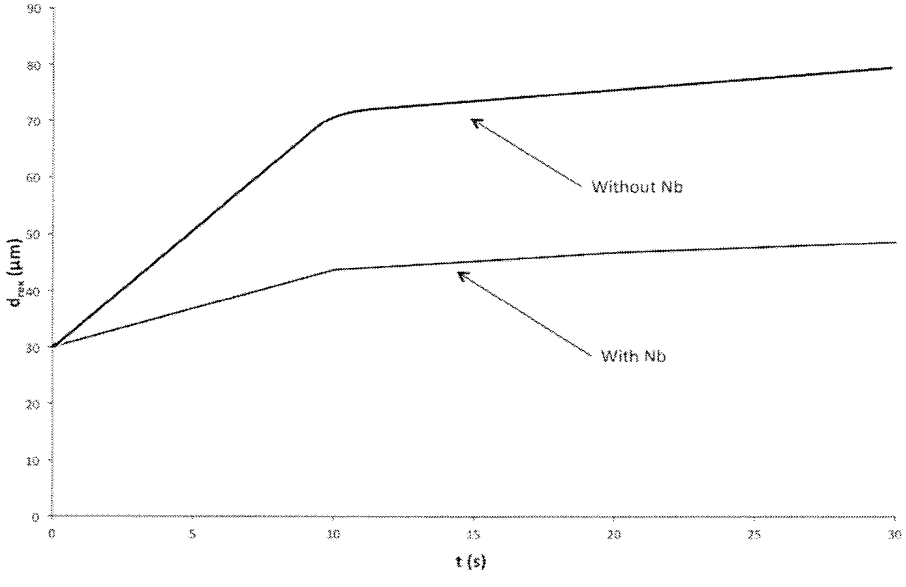

Figure 2.5 Recrystallized grain size evolution during the last roughing pass for steels with and without Nb

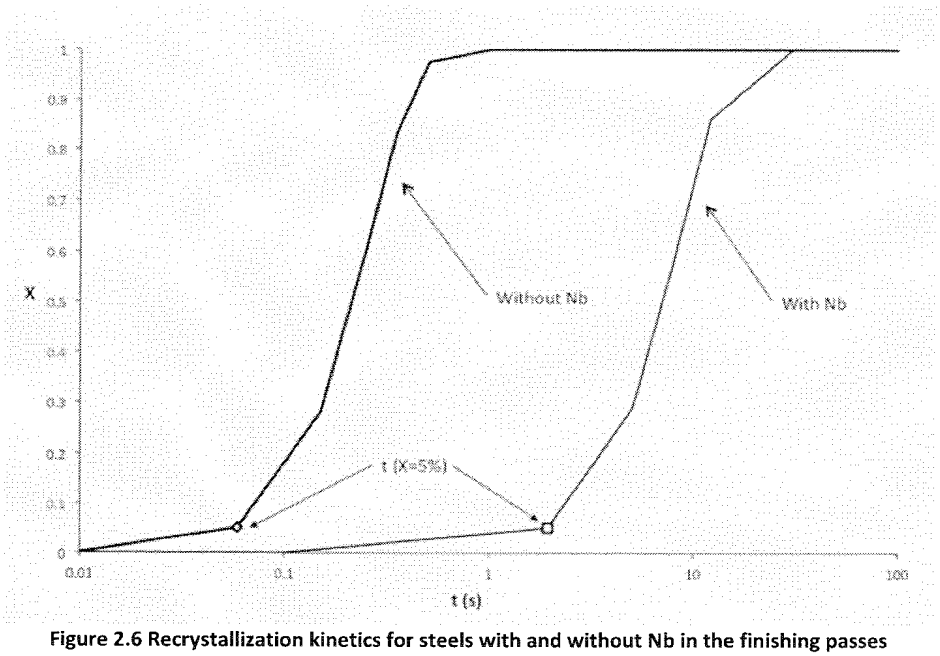

Figure 2.6 Recrystallization kinetics for steels with and without Nb in the finishing passes

2.2 Room Temperature testing of DP steels

For these tests, two dual-phase steels were used: DP600 and DP780, in the shape of strips with a thickness of $1.35\ \mathrm{mm}$ made with the ATMCRP process detailed in the previous subchapter (homogenization, roughing, waiting, finishing, controlled cooling and coiling) in the rolling direction. Their chemical composition is: $0.03 - 0.1\%$ C, $0.04 - 0.4\%$ Si, $1.5 - 2.1\%$ Mn, $< 0.015\%$ P and $< 0.010\%$ S.

To determine their characteristics, tension tests in accordance to the ASTM E8-04 standard were made in an INSTRON 5583-Standard universal testing machine with a calibrated extensometer distance of $50\ \mathrm{mm}$, using a displacement rate of $10\ \mathrm{mm/min}$ until the total fracture of the specimens (Figure 2.7). Two tension tests per material were made to corroborate the repeatability of the mechanical behavior.

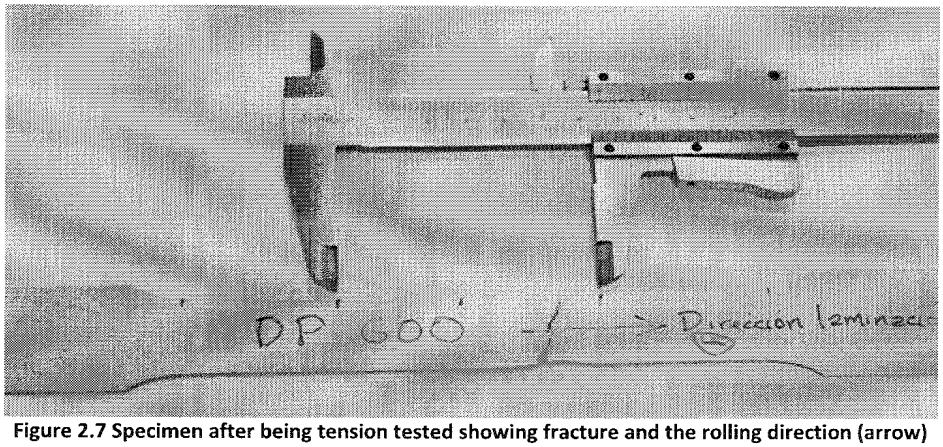

Figure 2.7 Specimen after being tension tested showing fracture and the rolling direction (arrow)

Also, microstructural characterization was made using traditional metallographic techniques: a metallographic cutter to section the specimens (to observe longitudinal sections of them), grinding and polishing (using alumina) and finally chemical etch (Nital-2). Afterwards, quantitative analysis of the grain sizes of the ferrite and martensite was made using a Buehler Omnimet image analyzer.

2.2.1 Traction tests

Figure 2.8 shows the stress-strain engineering curves for the DP600 and DP780 steels tested at room temperature; it is evident that the DP780 presents a higher yield stress than the DP600, with a tension stress close to 800 MPa, while for the DP600 is close to 650 MPa. Also, DP600 has a higher elongation ($\%A$) as shown in Table 2.5. Furthermore, DP600 has an evident yield stress (threshold activation stress for the dislocation movement) contrary to the DP780 where the parallel line at 0.2% was required in order to obtain its yield stress.

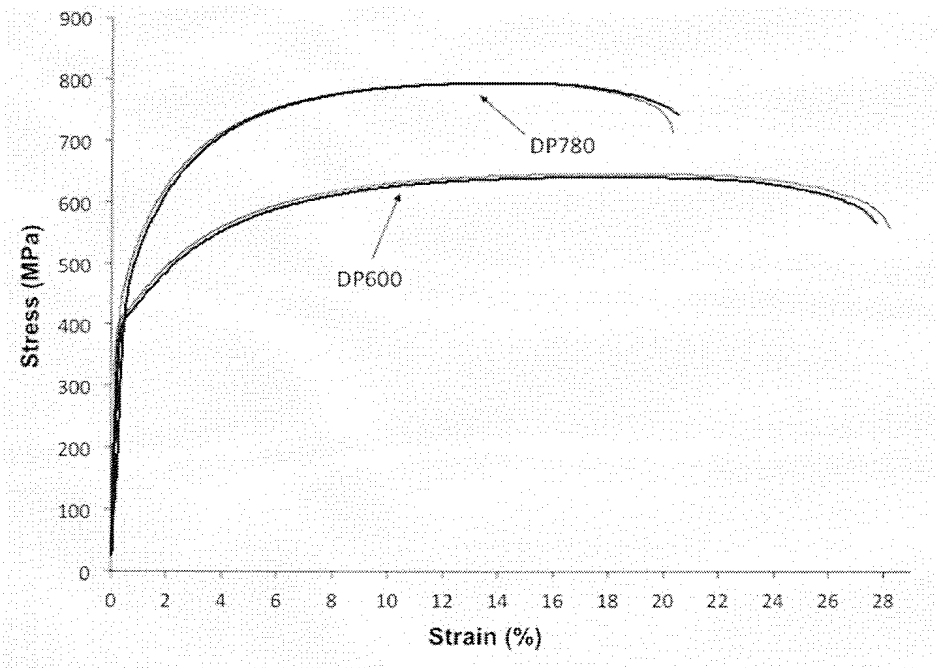

Figure 2.8 Stress-strain engineering curves for both of the steels tested at room temperature

	DP600	DP780
S_y (MPa)	353.6	365.3
S_{max} (MPa)	644.6	794.9
A (%)	27.95	20.41
S_y/S_{max}	0.55	0.46
n	0.2	0.2

Table 2.5 Dual-phase steels mechanical properties

On the other hand, the linear regression curve of the plastic deformation of true yield vs. true maximum stresses (logarithms) was obtained (Figure 2.9) in order to calculate the n strain hardening coefficient taking into account the equation:

$$\log \sigma = n \log \varepsilon + \log K \qquad [2.14]$$

where n is the slope of the straight line obtained by linear regression. Both values (presented in Table 2.5) are higher than 0.15, in other words, high enough for manufacturing processes of bending or drawing, though the DP780 has a higher value due to its higher strength and lower plasticity.

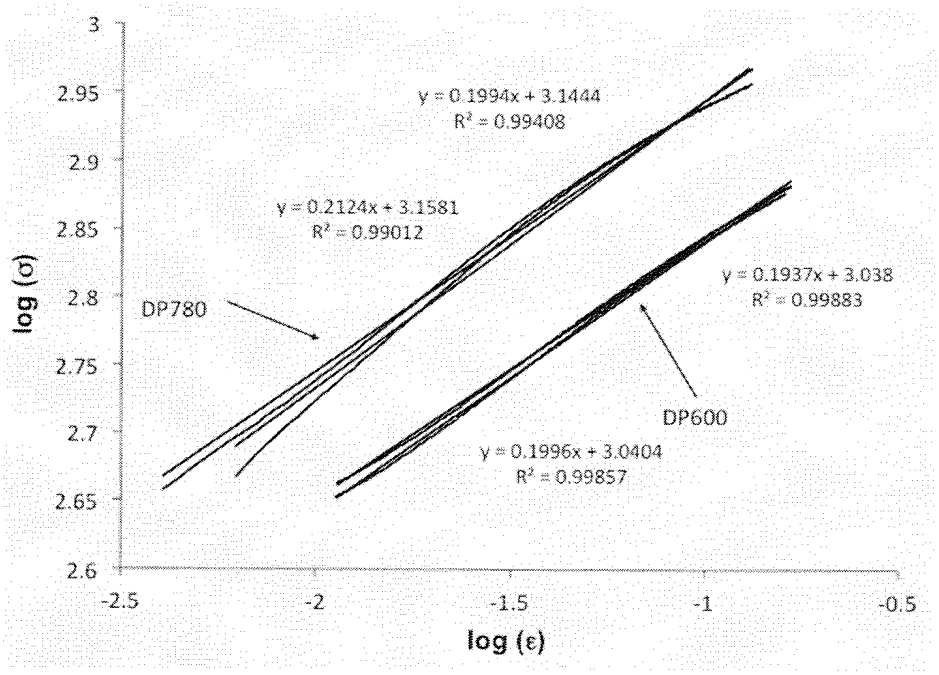

Figure 2.9 Linear regression for the strain hardening coefficient n for DP600 and DP780 steels, including the regression equation and correlation coefficient (R^2)

2.2.2 Micrographs

Quantitative metallography, shown in Figure 2.10 for the DP600 and Figure 2.11 for the DP780, present the microstructure (a), the identification of both ferrite and martensite phases done by the Buehler Omnimet equipment connected to the microscope (b), the ferrite grain size histogram (c) and the martensitic grain size histogram (d). From Figure 2.10a it can be noted that the DP600 steel has a slightly equiaxed microstructure as well as some grains elongated in the rolling direction (horizontal); this effect is evident in the banded structure of the DP780 steel. The distribution of the ferrite grain size indicates that this phase in the DP600 (Figure 2.10c) can be approximated to a normal distribution with mean grain size between 14 and 15 ASTM G; this is contrary to what happens on the DP780 which is a combination of big and small grains, with a mean size between 17 and 18 ASTM G.

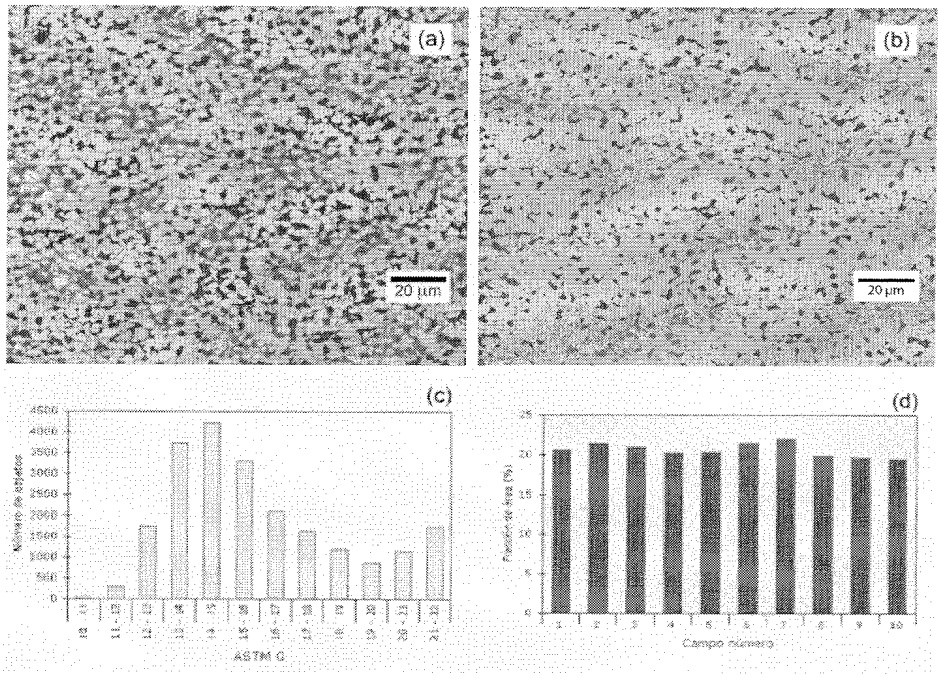

Figure 2.10 Quantitative metallography of the microstructure (a) of the DP600 steel, phases identification (b), ferrite grain size histogram (c) and percentage amount of martensite (d)

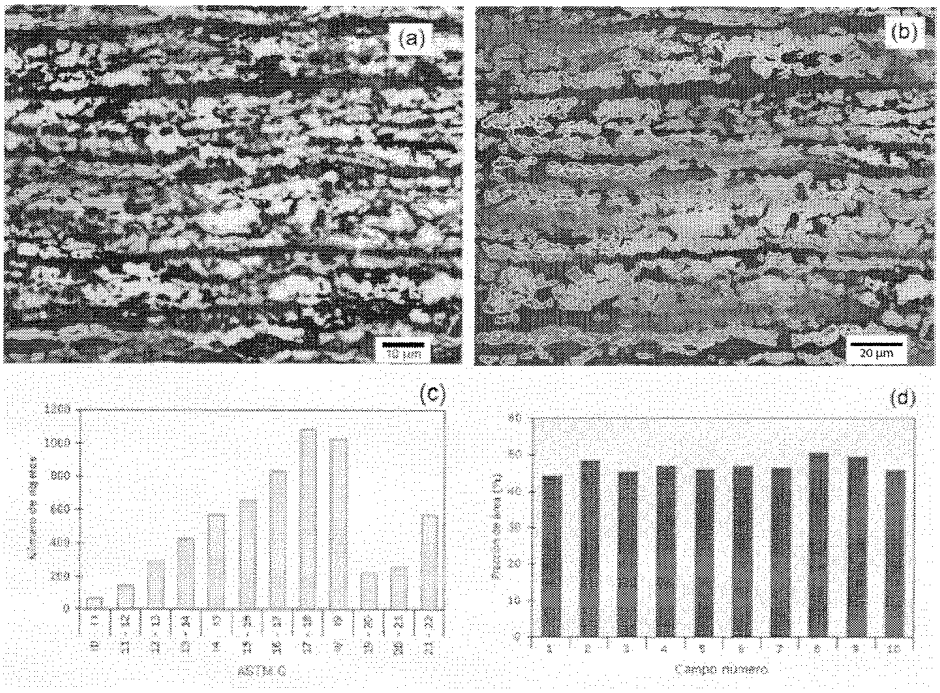

Figure 2.11 Quantitative metallography of the microstructure (a) of the DP780 steel, phases identification (b), ferrite grain size histogram (c) and percentage amount of martensite (d)

In spite of the previous paragraph, the martensite in both steels is a continuous phase, so it does not allow the determination of delimited zones or grains and it is only possible to calculate its volumetric fraction: ~20% for the DP600 and ~45% for the DP780.

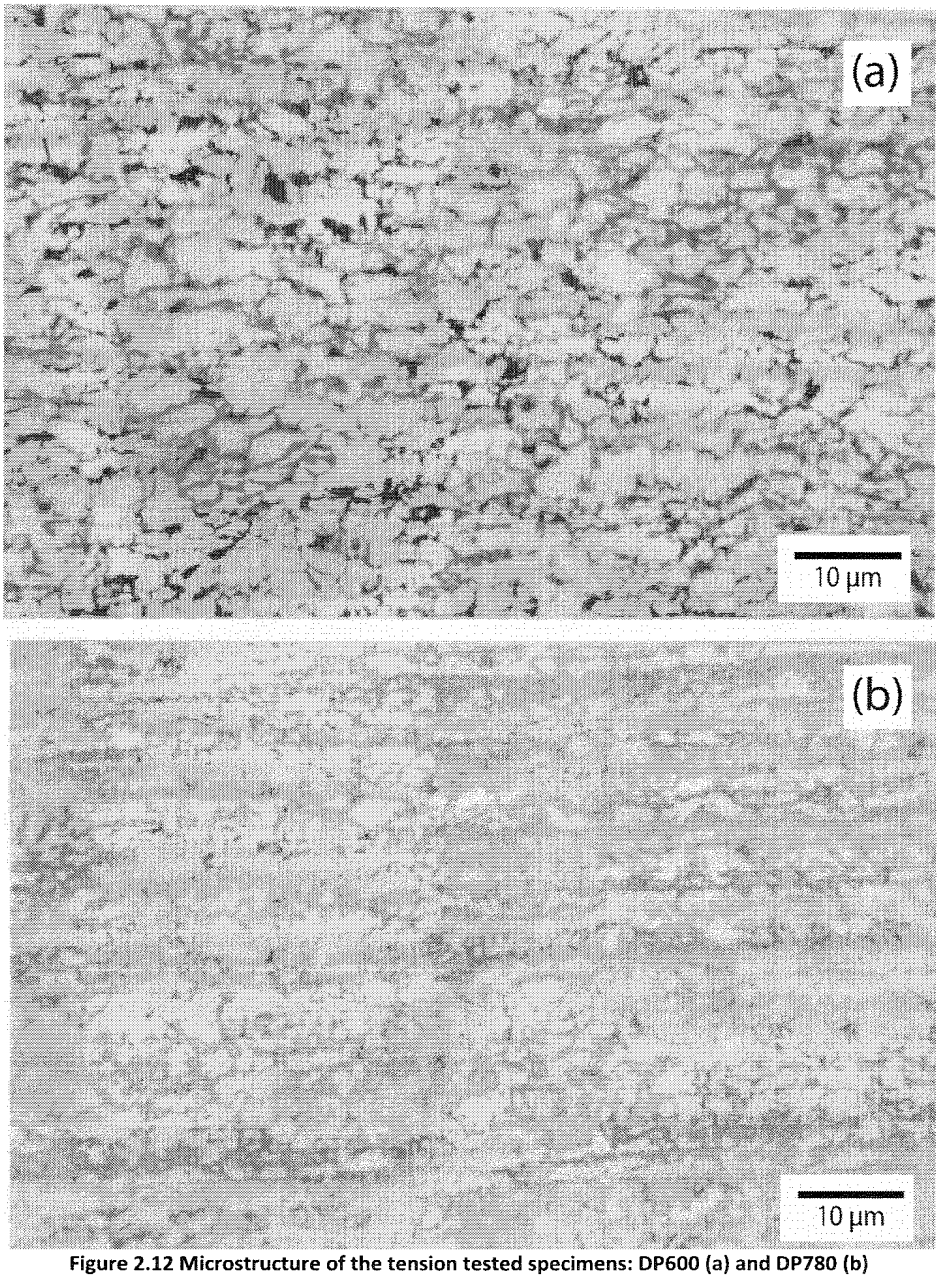

Figure 2.12 Microstructure of the tension tested specimens: DP600 (a) and DP780 (b)

Figure 2.12 compares the microstructure of both steels after the tension test. The ferrite grain size is evidently higher in the DP600 steel (a) and the banded structure DP780 is still present but it is not as noteworthy as before the test.

2.3 High Temperature testing of HSLA steels

2.3.1 Dilatometry test

This test was made in order to determine the A_1 and A_3 temperatures, as in this range the structure is biphasic ($\alpha + \gamma$) and the material can present superplasticity [7].

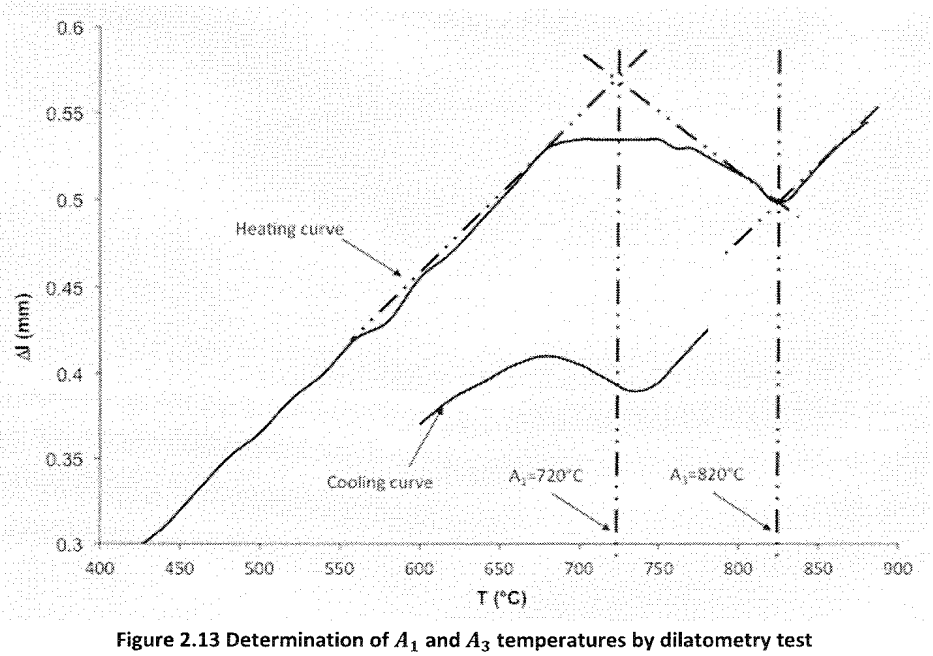

Figure 2.13 Determination of A_1 and A_3 temperatures by dilatometry test

The dilatometry absolute curve of the steel was obtained using specimens of $10\ \mathrm{mm}$ in diameter and $57.2\ \mathrm{mm}$ in length and a Griffin dilatometer with a Sullivan potentiometer and a Chromel-Alumel thermocouple.

The result of the test is presented in Figure 2.13, where it can be observed that A_1 occurs at$720°\mathrm{C}$ and A_3 at $820°\mathrm{C}$, which relatively match the values expected from the Andrews formulas: $A_1 = 726°\mathrm{C}$ and $A_3 = 840°\mathrm{C}$ [8]. This figures shows the heating and cooling curves that have, as expected, different A_1 and A_3 values, but it confirms that at $800°\mathrm{C}$ the material would be in its biphasic $(\alpha + \gamma)$ state.

2.3.2 Superplastic testing

2.3.2.1 Mechanical tests

The steel used in high temperature tests has the following composition: 0.168% C, 1.361% Mn, 0.453% Si, 0.022% P, 0.009% S, 0.026% Cu, 0.003% As, 0.028% Al, 0.035% Cr, 0.026% Ti, 0.002% V, 0.033% Nb, 0.004% Mo, 0.031% Ni, 0.002% Sn, 0.027% Al (soluble), 0.0001% B, 0.0055% N, 0.0000% Zr, 0.0001% Ca, 0.0000% C, 0.0000% B (soluble) and $2.00\ \mathrm{ppm}$ H. This steel is slightly alloyed with Mn and Si and microalloyed with Ti and Nb. The carbon content is practically the same as the peritectic reaction (0.17% C). Furthermore, titanium prevents the austenitic grain size before and during the roughing process, and both Nb and Ti raise the non-recrystallization temperature of the austenite T_{nr} allowing the finishing passes to be made on deformed austenite in an accumulated way, so the allotropic transformation can result in ultrafine ferrite microstructure.

The mechanical properties according to the Euronorms 10149-2 and 10051 are: yield stress of $447\ \mathrm{MPa}$ (the norm requires $360\ \mathrm{MPa}$), rupture stress of $567\ \mathrm{MPa}$, yield

elongation (with L_0 of 50 mm) of 31% and impact resistance at $-20°C$ of 96 J (the norm requires 27 J).

The traction properties of the material in its hot rolled raw state have been corroborated as shown in Figure 2.14 where both the engineering and true tension curves are presented.

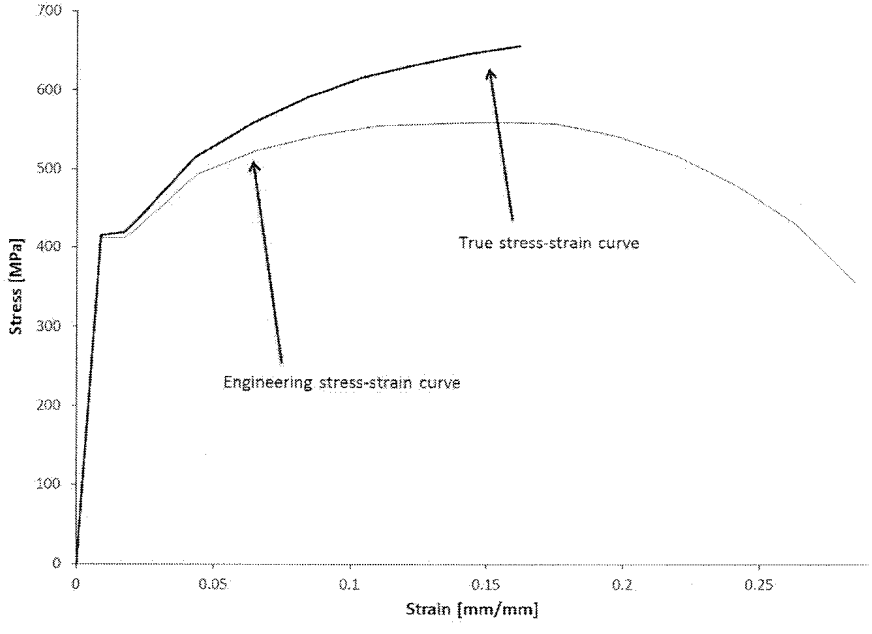

Figure 2.14 Traction curves of the steel in its hot rolled raw state

2.3.2.1.1 Calculus of the $\boldsymbol{n}$ coefficient

There are two graphical methods to calculate the strain hardening n coefficient. The first consists in obtaining the $\log\sigma - \log\varepsilon$ curve, which results in a straight line with slope n. This value can be inferred from linear regression methods of the $\sigma = K\varepsilon^n$ behavior.

From Figure 2.15, the value of the strain hardening coefficient can be approximated to 0.22.

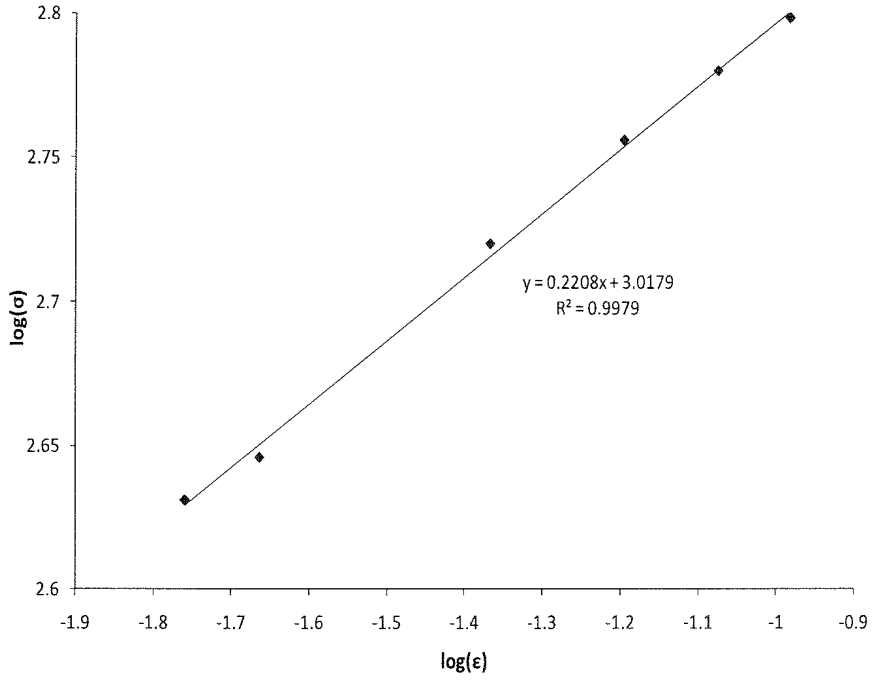

Figure 2.15 Logarithm of stress vs. logarithm of strain curve to determine the strain hardening coefficient

The second method considers the intersection of the true stress – true strain curve with the $\frac{d\sigma}{d\varepsilon}/\varepsilon$ curve. The intersection is the value of the strain hardening coefficient as shown in Figure 2.16 where n has a value of 0.208 which means that both methods result in very similar values for the strain hardening coefficient and that both of them are valid.

The samples for the tests were obtained from a steel sheet in an axis parallel to the rolling direction and machined in cylindrical shape: $10\ \mathrm{mm}$ in diameter and calibrated gage length (L_0) of either 57 or $30\ \mathrm{mm}$ according to the ASTM E21-05 standard.

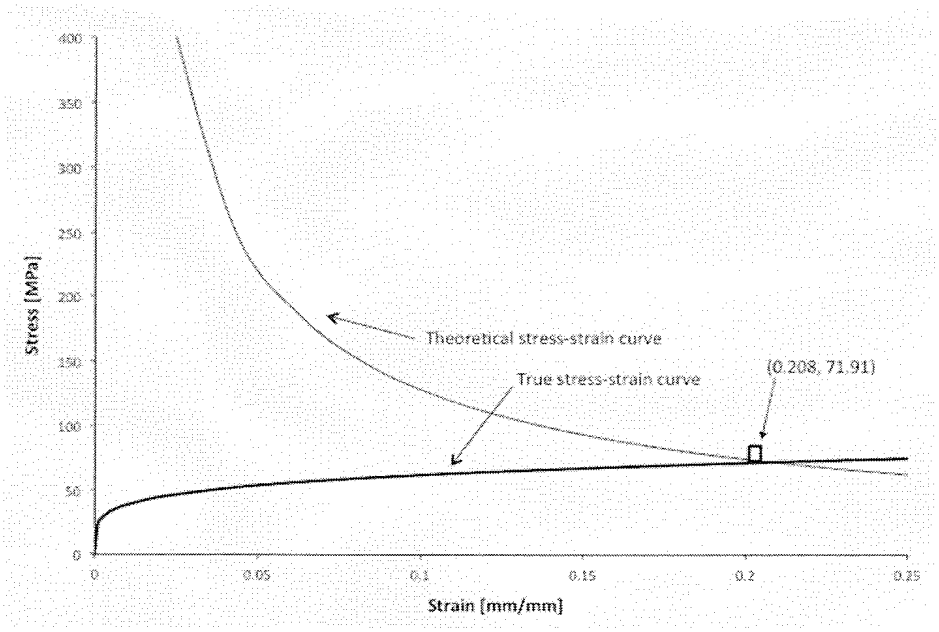

Figure 2.16 True stress – true strain curve and $\frac{d\sigma}{d\varepsilon}/\varepsilon$ curve to determine the strain hardening coefficient

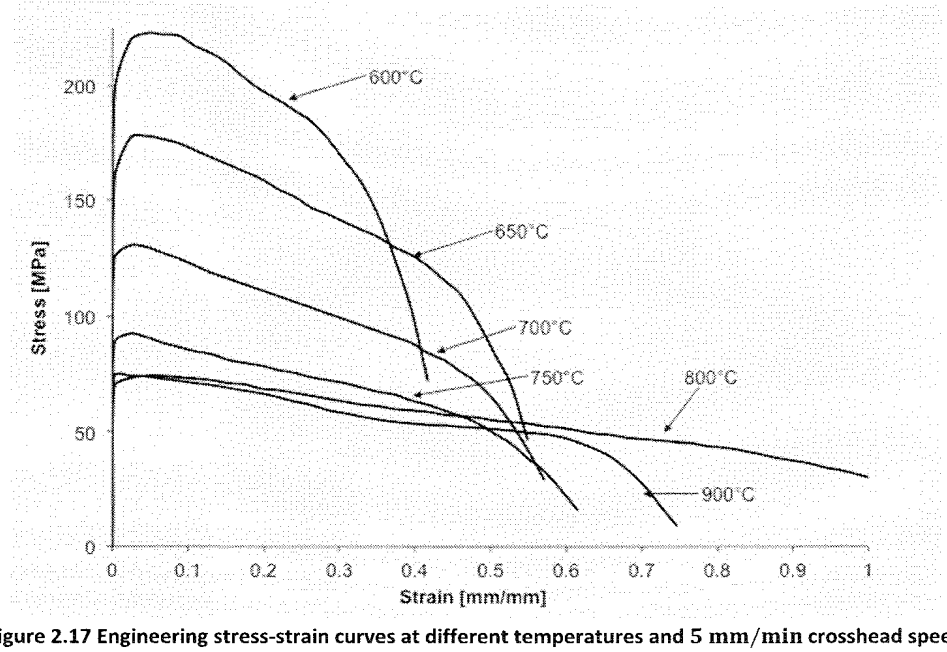

Figure 2.17 Engineering stress-strain curves at different temperatures and $5\ \mathbf{mm/min}$ crosshead speed

High temperature tests were made at different temperatures between 600 and 900°C at 50°C intervals and different crosshead speeds in order to define the

temperature interval at which the steel would present superplasticity in an INSTRON 5583-Standard universal testing machine. Figure 2.17 shows the engineering traction curves for samples tested at 5 mm/min, as expected, the higher the temperature the lower the maximum stress the material may withstand, which for 600°C is above 200 MPa and for 900°C is below 80 MPa. It is noteworthy that at 800°C the elongation of the sample is higher than 100%. On the other hand, Figure 2.18 corresponds to tests made 10 times slower than Figure 2.17. The steel show lower maximum stresses and specifically for test temperatures of 600, 650 and 750°C, there is evidence of the formation of more than one neck resulting in descending and ascending zones in the curve; once again, at 800°C the elongation surpasses 100%. Finally, Figure 2.19 was obtained from tests made at an even lower crosshead speed where the low strain rate promotes at 650 and 700°C the formation of multiples necks (ripples in the curves) and similar to the previous cases, at temperatures above 750 and below 850°C the result is smooth deformation and very high elongations which would indicate superplasticity.

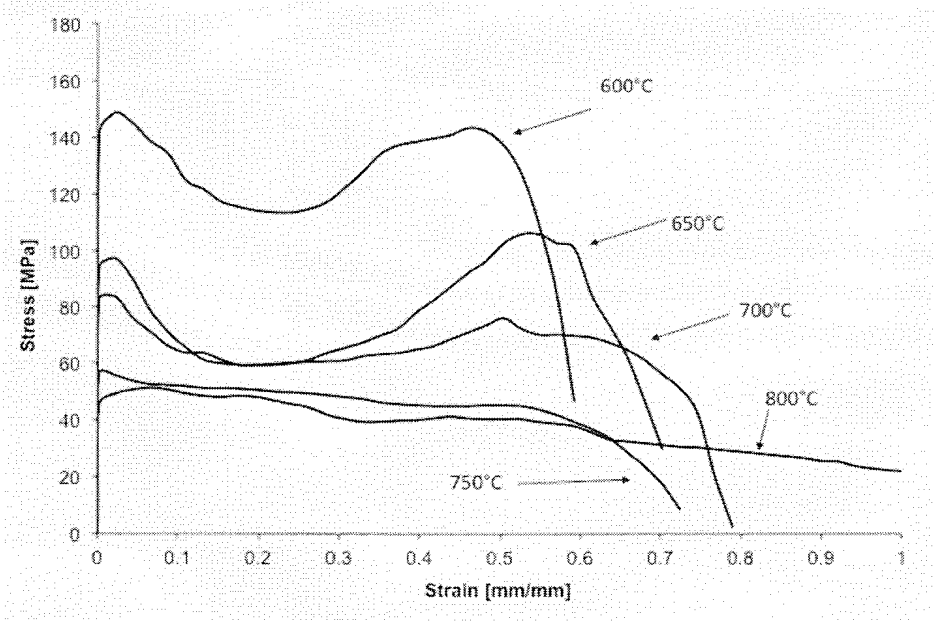

Figure 2.18 Engineering stress-strain curves at different temperatures and 0.5 mm/min crosshead speed

After all these tests (crosshead speeds of 0.2, 0.5 and 5 mm/min) were made, three behaviors can be defined:

- At subcritic temperatures, lower than $720°C$, elongations are smaller than 100%. The steel can be considered as non-superplastic.
- At intercritic temperatures, between 720 and $820°C$, elongations are higher. At $750°C$ there is an increase of the elongation when decreasing the crosshead speed. At $800°C$, the steel has more than 100% in elongation and the traction curves show the ripples typical of superplastic behavior.
- At supercritic temperatures, in austenitic phase and temperatures higher than $820°C$, the specimens rupture with very clear localized necks (ductile fracture).

After analyzing these last three figures, the temperature of $800°C$ was determined as the temperature at which the steel may present superplastic behavior. Once this temperature was defined, more tests were made varying the crosshead speeds to obtain the optimum strain rate for the superplastic behavior. All the tests were made on an INSTRON 1195 equipment with a load capacity of 100 kN and a furnace INSTRON 3112 capable of reaching $1000°C$. The tests took place without a protective atmosphere at speeds between 0.05 and 10 mm/min with previous uniform heating from room to test temperature lasting 1 hour followed by $5\sim10$ min of stabilization.

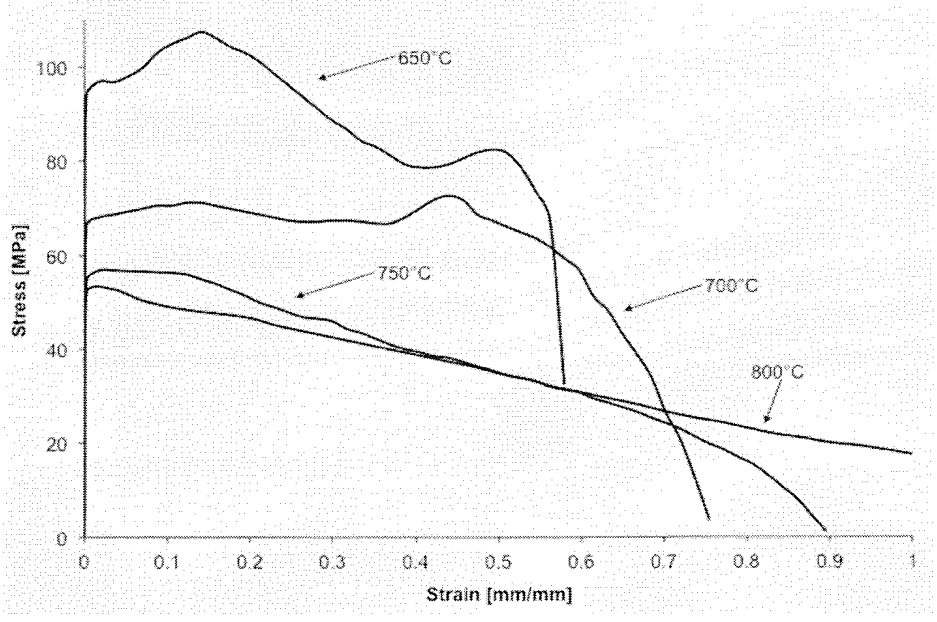

Figure 2.19 Engineering stress-strain curves at different temperatures and 0.2 mm/min crosshead speed

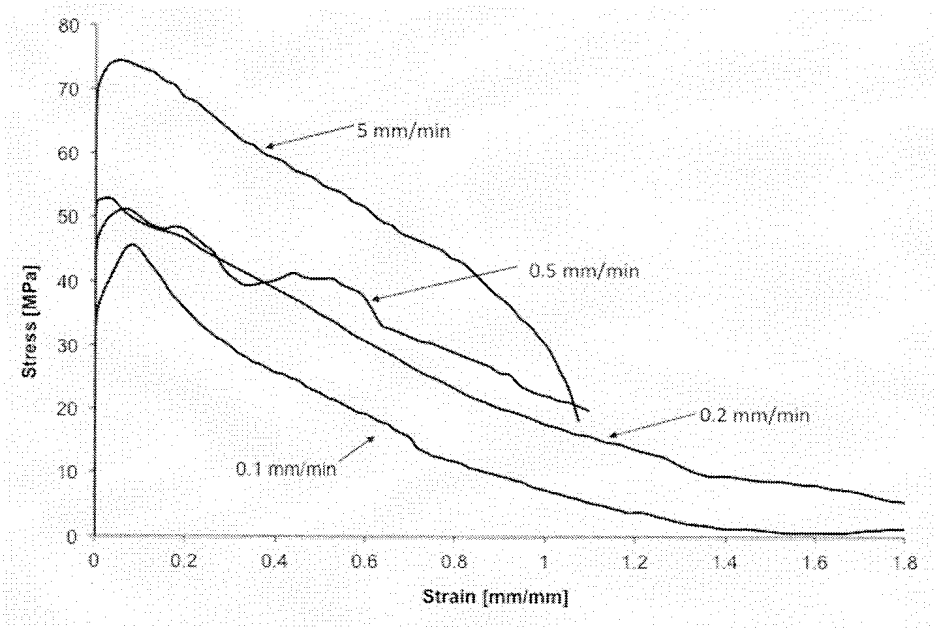

Figure 2.20 Engineering stress-strain curves at $800°C$ and different crosshead speeds

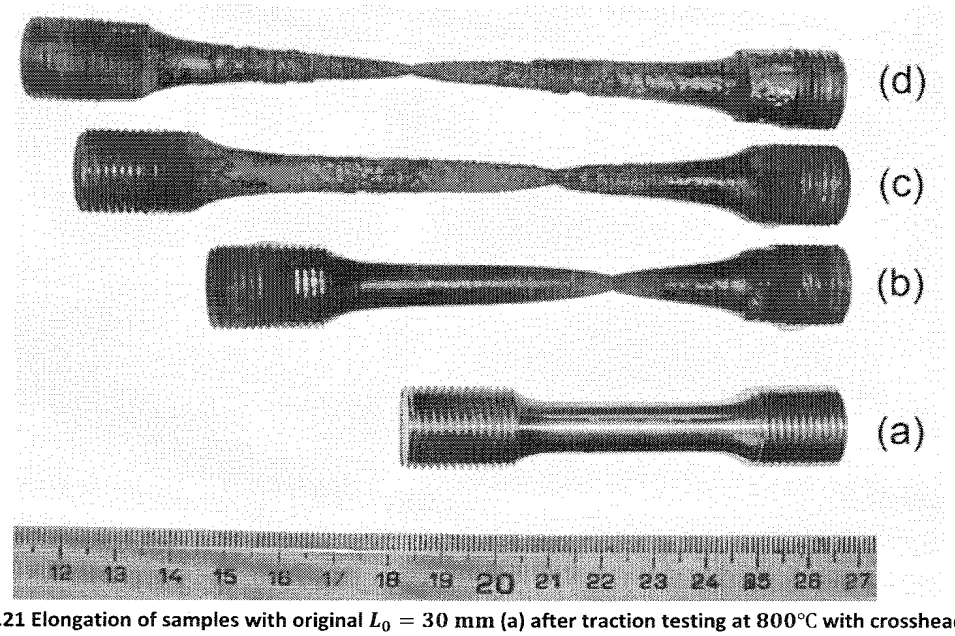

Figure 2.21 Elongation of samples with original $L_0 = 30$ mm (a) after traction testing at $800°C$ with crosshead speeds of 0.5 (b), 0.2 (c) and 0.1 (d) mm/min

The result of these tests is shown in Figure 2.20, where though some ripples are evident during deformation at 5 mm/min, this phenomenon is promoted at 0.5 mm/min.

The smooth deformation of the samples was only achieved when the crosshead speed was lowered to $0.2\ \mathrm{mm/min}$. For 0.2 and $0.1\ \mathrm{mm/min}$, the elongation of the samples is close to 200%, as shown in Figure 2.21 showing also diffuse necking; this figure compares a specimen with $L_0 = 30\ \mathrm{mm}$ (untested) with samples deformed at $800°\mathrm{C}$ and three different crosshead speeds.

Specimen initial length (mm)	Crosshead speed (mm/min)	Strain rate (s^{-1})	Yield stress (MPa)	Elongation (%)
30		$2.83\text{x}10^{-5}$	25 (creep)	Non-determined
30	0.05	$2.78\text{x}10^{-5}$	27.4	137.5
30	0.1	$5.56\text{x}10^{-5}$	34.4	181.7
57	0.2	$5.85\text{x}10^{-5}$	37.6	>110.0
30	0.2	$1.11\text{x}10^{-4}$	52.80	191.3
57	0.5	$1.46\text{x}10^{-4}$	45.8	>110.0
30	0.5	$2.78\text{x}10^{-4}$	57.3	92.7
57	5	$1.46\text{x}10^{-3}$	70	>110.0
57	10	$2.92\text{x}10^{-3}$	82.4	84.2
30	10	$5.56\text{x}10^{-3}$	86.2	105
23	20	$1.45\ \text{x}10^{-2}$	93.68	126.6

Table 2.6 Tension testing results obtained with different strain rates at 800°C

Table 2.6 shows the values of the yield stress (σ_y) and strain rate ($\dot{\varepsilon}$) obtained from the tests at $800°\mathrm{C}$. Furthermore, according to expression:

$$\sigma = K\dot{\varepsilon}^m \qquad [2.15]$$

where K is a function of the temperature, the previous deformation the steel may have suffered and the grain size; coefficient m expresses the sensibility of the applied tension to the strain rate as follows:

$$m = \left(\frac{\log(\sigma_{y_2}/\sigma_{y_1})}{\log(\dot{\varepsilon}_{0_2}/\dot{\varepsilon}_{0_1})}\right)_{T,d,\varepsilon} \qquad [2.16]$$

where σ_y is the yield stress at 0.2% and $\dot{\varepsilon}_0$ the initial strain rate, in tests made at two different strain rates. Thusly the dependence of stress and strain rate is shown in Figure 2.22a where a clear zone II behavior can be seen, also, the transition from zone I (creep) and zone II is not evident as much lower strain rates should be tested in order to observe it. Moreover, at higher strain rates, zone III emerges. The regression lines presented in the figure have slope values of ~ 0.6 for zone II and ~ 0.1 for zone III.

Figure 2.22b shows the m coefficient from equation [2.16] as a function of strain rate using pairs of data obtained from tension tests. When this coefficient has values between 0.3 and 0.7, superplastic behavior is achieved [9], in this case the maximum value of m will be reached at a strain rate close to $2.8 \times 10^{-5}\ s^{-1}$. In other words, at $800°C$ this will be the best deformation rate in order to obtain superplasticity in this steel.

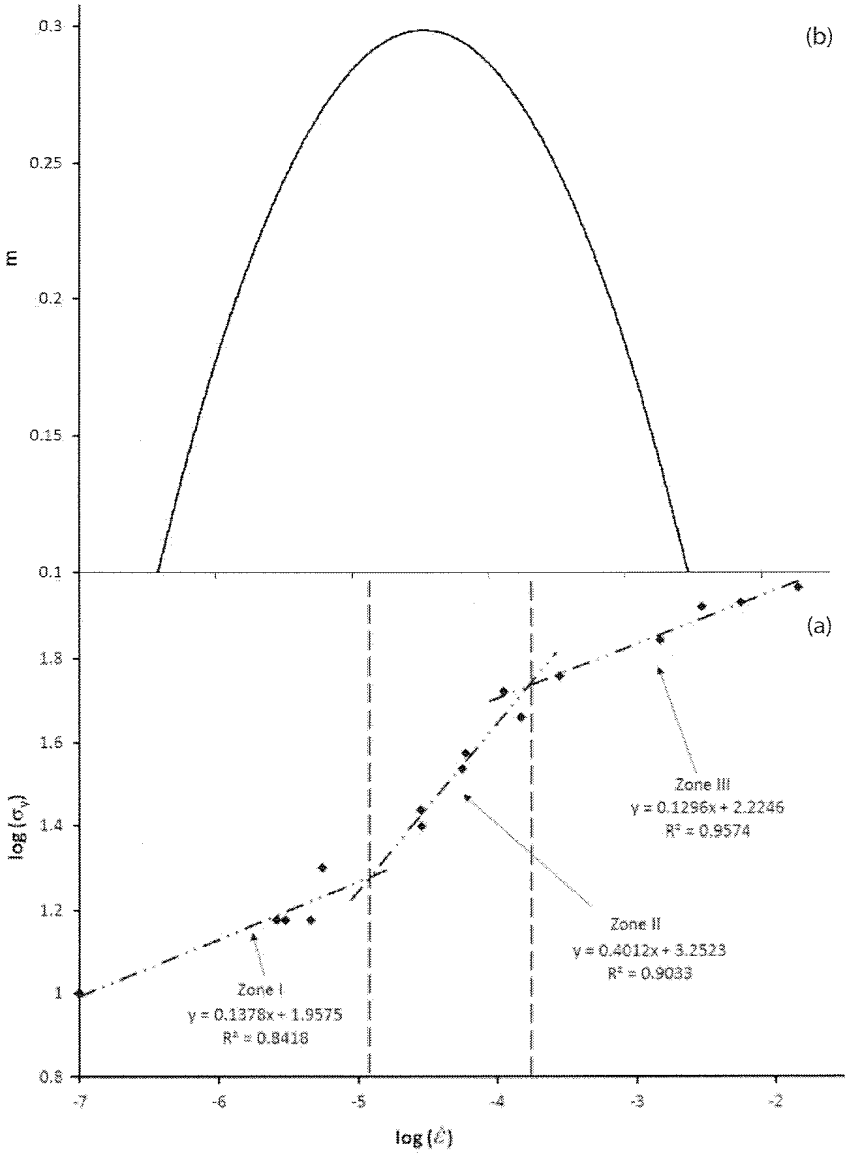

Figure 2.22 Influence of strain rate on yield stress (a) and super-index m (b) of equation [2.16] in superplastic behavior at $800°C$

Other traction tests were made at 750°C, to corroborate that the material does not behave superplastically at this temperature; the results are shown in Table 2.7.

Also, creep tests were made on the same INSTRON universal testing machine as well as the EUROTHERM furnace. The calibrated length is 30 mm (the same as for the superplasticity tests).

Specimen initial length (mm)	Crosshead speed (mm/min)	Strain rate (s^{-1})	Yield stress (MPa)	Elongation (%)
57	5	$1.46x10^{-3}$	87.41	63.2
57	0.2	$5.85x10^{-5}$	54.35	90.2
57	0.1	$2.92x10^{-5}$	32.47	92.3

Table 2.7 Tension testing results obtained with different strain rates at 750°C

Strain rate (s^{-1})	Yield stress (MPa)	Logarithm of strain rate	Logarithm of yield stress / shear modulus
$4.2x10^{-6}$	20	-5.38	-3.54
$4.5x10^{-6}$	15	-5.35	-3.67
$3.0x10^{-6}$	15	-5.52	-3.67
$2.6x10^{-6}$	15	-5.59	-3.67
$1.0x10^{-7}$	10	-7.00	-3.84

Table 2.8 Creep tension testing results at 800°C

On the other hand, in Figure 2.23 three stages or different behaviors can be distinguished:

1. *Stage I*, of the superplastic nature: ferrite deforms intergranularly, the grains rotate and the decohesions formed are filled by diffusion. The m coefficient has values between 0.4 and 0.5.
2. *Stage II*, for strain rates $10^{-4} < \dot{\varepsilon}_0 < 10^{-3}\ s^{-1}$. Ferrite deforms and dislocations accumulate as this phase slides intergranularly. Another mechanisms acting in parallel are volume diffusion and grain boundary diffusion.
3. *Stage III*, for strain rates higher than $10^{-3}\ s^{-1}$. Dynamic recovery of the ferrite is the dominant mechanism.

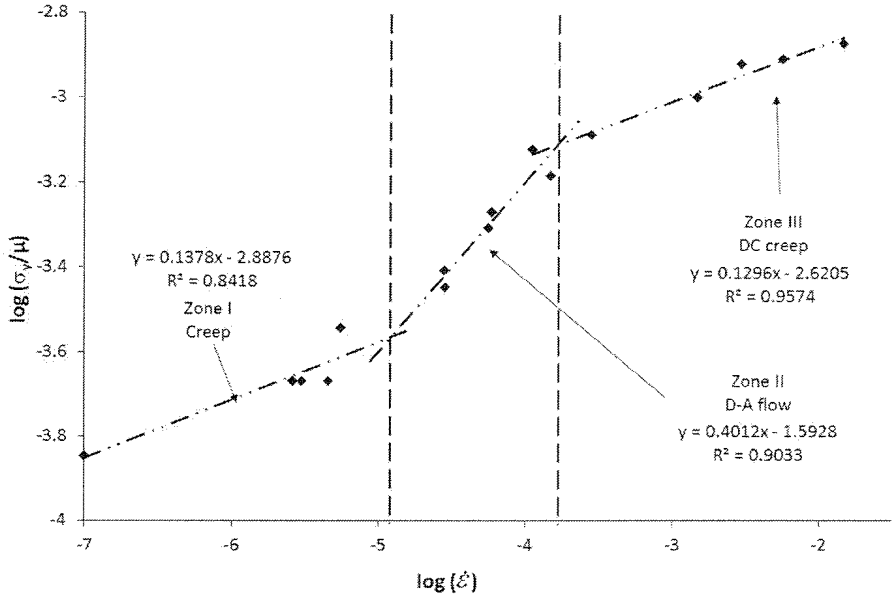

Figure 2.23 Experimental curve of logarithm of yield stress/shear modulus vs. logarithm of strain rate

2.3.2.2 Metallography

Metallographic observations were carried out, before and after the high temperature tests, at transverse sections of the samples in an axis parallel to the rolling direction. Traditional techniques (grinding, polishing and Nital-2 etching) were used. A Nikon Epiphot metallographic equipment connected to a Buehler Omnimet image analyzer was used to determine the ASTM grain size and the distribution of phases. To obtain the ferritic mean size or the pearlite fraction, micrographs at 400 and 6000x were taken, using at least five in order to obtain a 95% confidence level of the results.

Figure 2.24 shows the microstructure of the steel, used to study its superplastic properties, in its hot rolled raw state. It is evident that the material has a ferritic – pearlitic banded structure in the same direction as the rolling one.

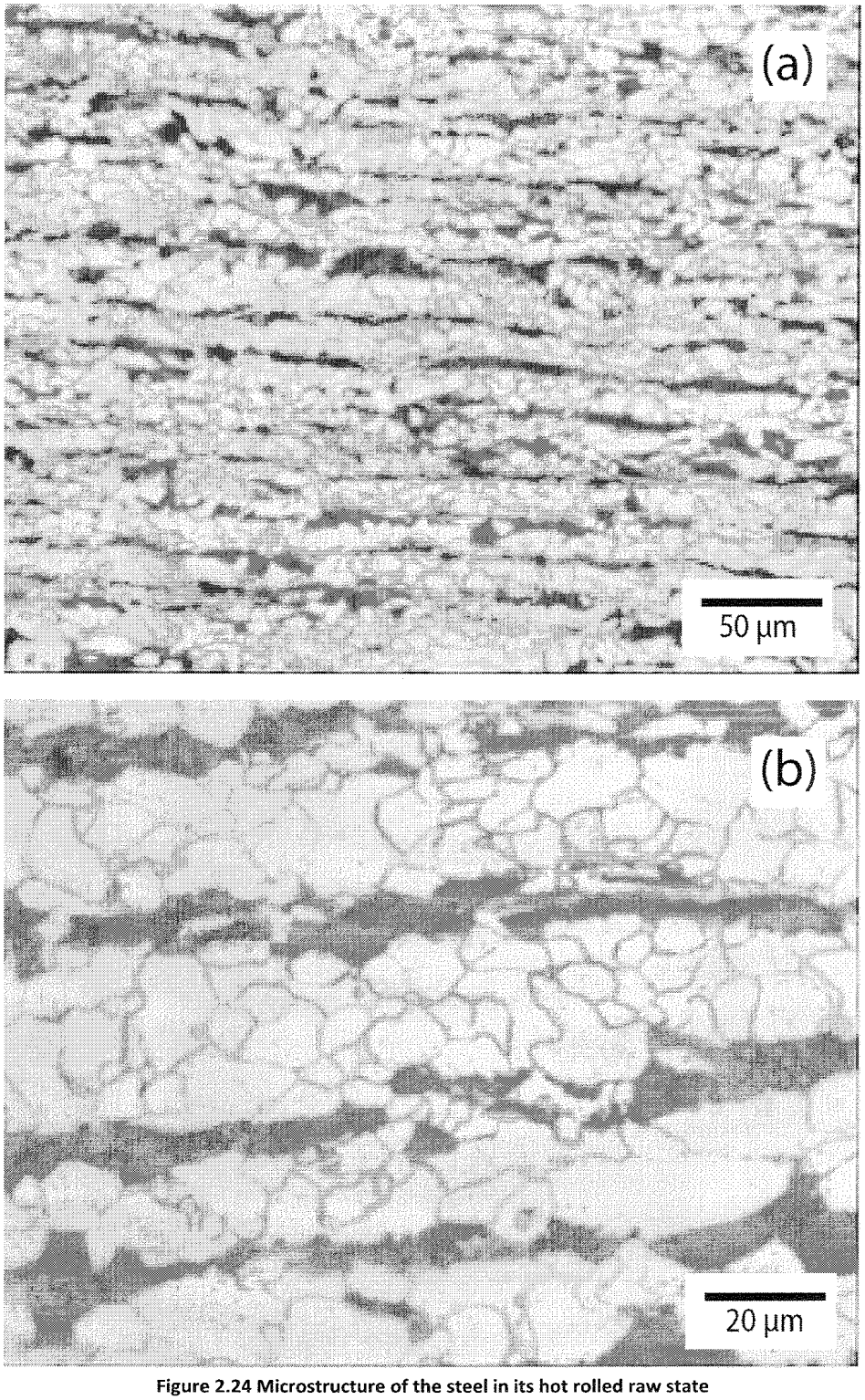

Figure 2.24 Microstructure of the steel in its hot rolled raw state

After it solidifies, the steel experiences a peritectic reaction $\delta(0.09\%C) + L(0.53\%) \leftrightarrow \gamma(0.17\%C)$, with approximately 75% of δ phase and 25% of liquid. The peritectic reaction is not carried out completely because the γ phase (product of the reaction) acts as barrier to the reacting phases (δ and liquid), until the end of the solidification process, where there is a γ constituent with strong segregation of C, alloying elements, microalloying element and impurities that surrounds the δ ferrite dendrites transformed into γ during cooling. Table 2.1 shows some partition coefficients (proportion in liquid/concentration in solid) in the δ and γ phases of the iron in the steels; in other words, at room temperature, the raw state structure would be formed by ferrite crystals surrounded by the pearlite constituent. After the homogenization thermal treatment (or soaking), the only element that has not segregated would be the C and the rest of the elements do not have enough diffusion capacity to distribute themselves uniformly in the austenite crystals; therefore, at the end of the rolling process, zones negatively segregated would transform into ferrite and later, the zones positively segregated would become pearlite.

	Fe- δ	Fe- γ
Oxygen	0.02	0.02
Sulfur	0.02	0.02
Phosphorus	0.13	0.06
Carbon	0.13	0.36
Nitrogen	0.28	0.54
Copper	0.56	0.88
Silicon	0.66	0.95
Molybdenum	0.80	0.60
Nickel	0.80	0.95
Manganese	0.84	0.95
Cobalt	0.90	0.95
Wolfram	0.95	0.50
Chromium	0.95	0.85

Table 2.9 Proportion coefficients of some elements in iron [10]

Moreover, the banded structure in construction C/Mn steels in their hot rolled raw state derives from the non-equilibrium solidification that involves: a peritectic reaction, the proportion coefficients of the alloying elements and impurities lower than one and the allotropic transformation $\delta \rightarrow \gamma \rightarrow \alpha$.

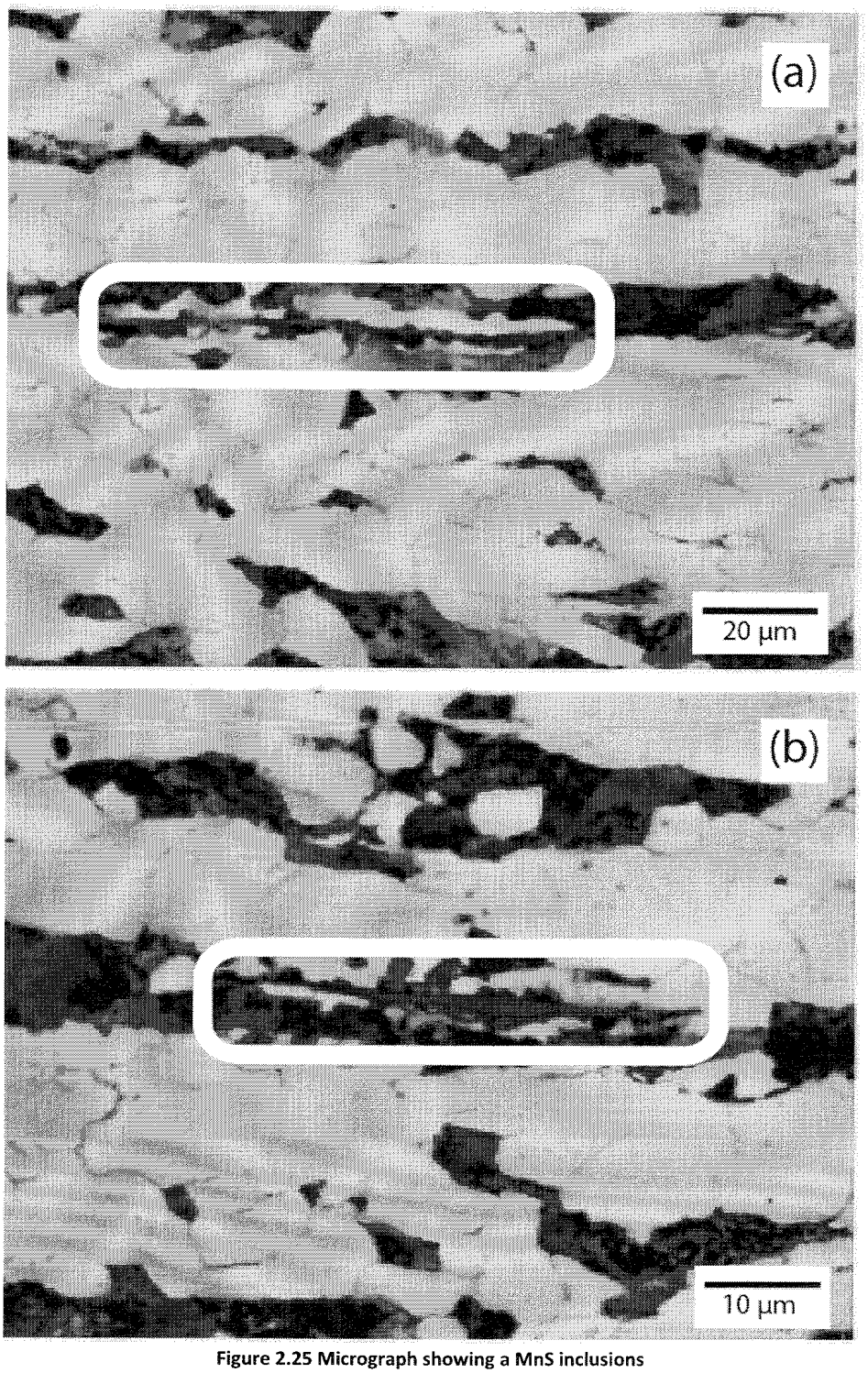

Figure 2.25 Micrograph showing a MnS inclusions

Furthermore, Figure 2.25 shows MnS inclusions, that are deformed longitudinally (in the rolling direction) that are inside or close to pearlite bands; this is evidence of the internal segregation of the steel.

Figure 2.26 shows the distribution histogram of both phases present in the steel: there is slightly more than 70% of ferrite and the rest is pearlite. The ferrite grain size has a mean value of 12 ASTM G, though the micrographs show that this phase is mostly recrystallized. The pearlite bands are mostly continuous with an approximate distance of 50 μm between one band and the other; these bands are alternated with ferrite bands. The proportion of pearlite is similar to the one obtained by the lever rule in the phase diagram for a steel with 0.17 %C, with an eutectic point at 0.65 %C, slightly moved to the left because of the alloying elements Mn (austenite-former element) and Si (ferrite-former element).

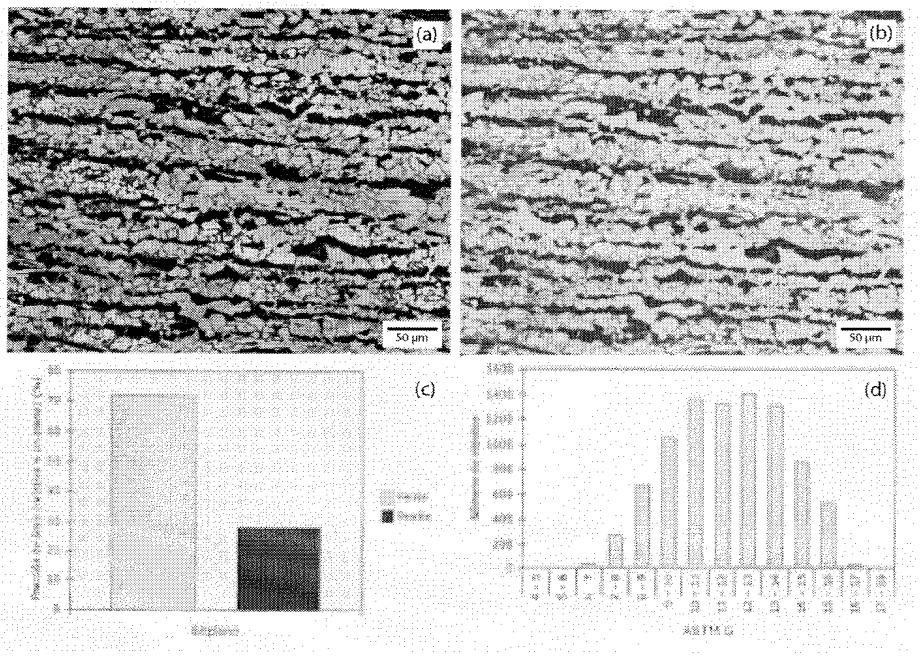

Figure 2.26 Quantitative metallography of the microstructure (a) of the hot rolled raw state steel, phases identification (b), ferrite and pearlite percentage amount histogram (c) and ferrite ASTM G grain size histogram (d)

An attempt to measure the austenitic grain size existing after the hot rolling of the steel was made using a reactive proposed by Vandervoort [11] known as PYGBs (Prior

Austenite Grain Boundaries) which is effective when there is phosphorus segregated in the original austenitic grain boundaries; this etch involves: chemical etch with a watery solution of picric acid and adding a few drops of HCl and a moisturizing agent (detergent). Figure 2.27 shows one of four the micrographs where manual counting was made, the austenitic mean grain size is 4~5 μm; this value corresponds to the one obtained by the model of the hot rolling of the plate. Also, the austenite in the micrographs appears as recrystallized.

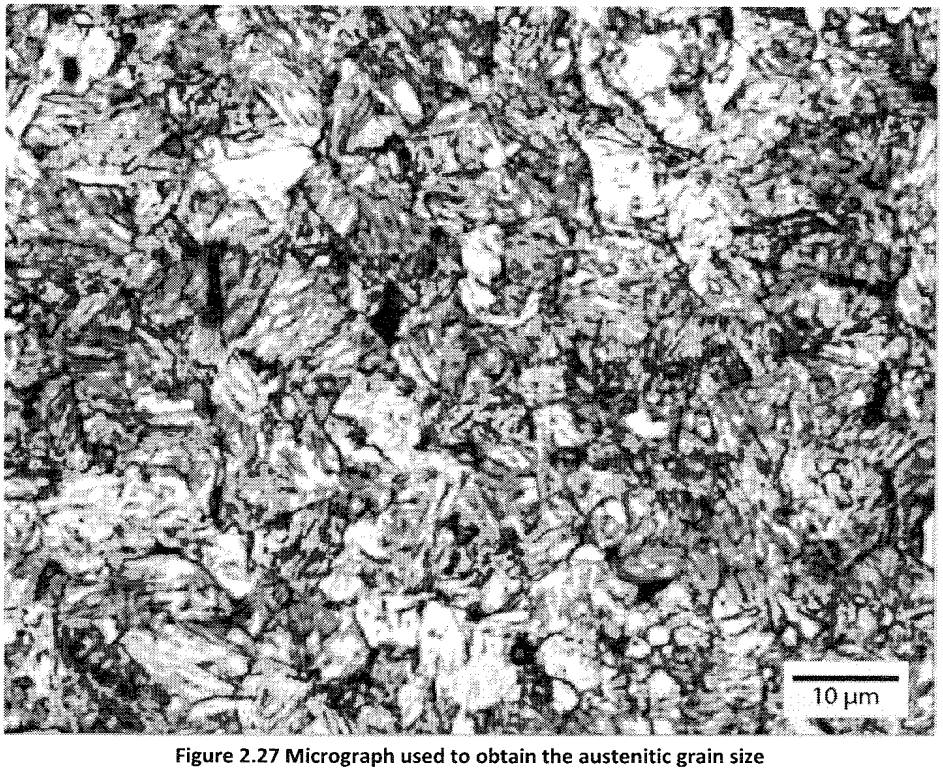

Figure 2.27 Micrograph used to obtain the austenitic grain size

The microstructure of the steel tested at 800°C is shown in Figure 2.28 where the bands that existed before the tests are no longer evident, but there are zones with larger amount of ferrite and little of pearlite and vice versa. Furthermore, the amount of pearlite has dropped slightly and the ferritic grain size has almost stayed the same (approximately 14 ASTM G).

The banded structure of the steel may influence its superplastic behavior; the separation existing between the soft constituent (ferrite) and the hard one (pearlite) can change its mechanical response. Therefore, it may be desirable a homogenous or even mix of both phases in order to reach superplasticity.

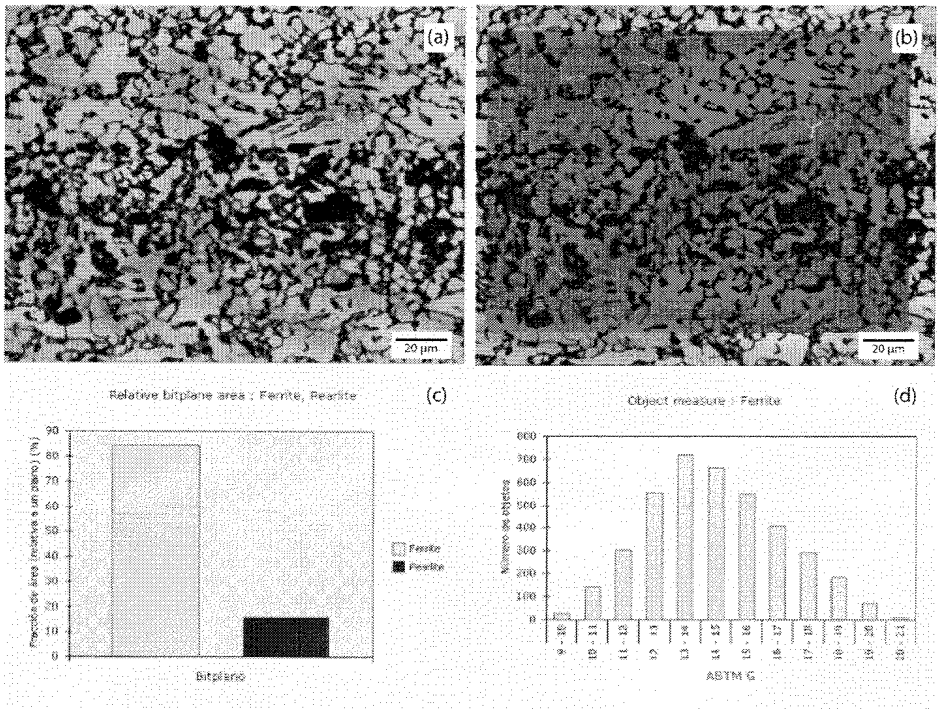

Figure 2.28 Quantitative metallography of the microstructure (a) of the steel tested at 800°C, phases identification (b), ferrite and pearlite percentage amount histogram (c) and ferrite ASTM G grain size histogram (d)

In the following subchapters (2.3.2.2.2 and 2.3.2.2.1) the microstructure of two specimens, one tested at 800°C and one at 750°C, is compared. Both were tested with the same crosshead speed (0.1 mm/min).

2.3.2.2.1 Structural damage at **800**°C

After an $\sim 280\%$ elongation, the microstructure of a specimen tested at $800°C$ presents the following characteristics (Figure 2.29):

- The banded structure has practically disappeared; ferrite and pearlite are homogeneously distributed in both the old ferrite and pearlite bands. The microstructure is equiaxed. The difference is that the pearlite in the old ferrite bands was austenite and the one in the old pearlite bands was austenite transformed by the hot rolling.
- The grain size distribution is similar to the one of the hot rolled raw state. Though the grain size is slightly finer and more common to the mean value.
- The structural damage accumulated by straining is of the same type as the one experimented by materials tested in creep and superplastic conditions. This damage is made by intergranular sliding and decohesions.

Figure 2.30 presents the decohesions detected by optic microscope. Five types of decohesions can be identified: r-shaped decohesion between ferrite, ferrite and pearlite, w-shaped decohesion between ferrite, ferrite and pearlite (carbides), double r-shaped decohesion between ferrite and pearlite, ferrite and pearlite decohesion and finally ferrite and ferrite or pearlite and pearlite decohesion.

After the observation of the decohesions on the optic microscope micrographs, a scanning electron microscope JEOL JSM-5600 with an electroprobe analyzer OXFORD model 6587, was used to observe the same decohesions (Figure 2.31). In Figure 2.32 an r-shaped decohesion can be observed, as Figure 2.33 shows a double r-shaped decohesion or Figure 2.34 presents a w-shaped decohesion. Finally Figure 2.35 shows a decohesion between the matrix (ferrite) and pearlite (precipitates) which would lead to a ductile fracture, very pronounced and practically in the shape of a pencil point (rupture sections measured in mm^2). The intergranular straining of the ferrite (soft/superplastic constituent) and its intrusion in the austenite (hard constituent) maintaining the grain size of the steel appear to be necessary conditions for the deformation of the steel sheet. Higher proportions of ferrite (lower straining temperatures), by limiting the austenite proportion and increasing its instability, eliminate completely the superplastic behavior.

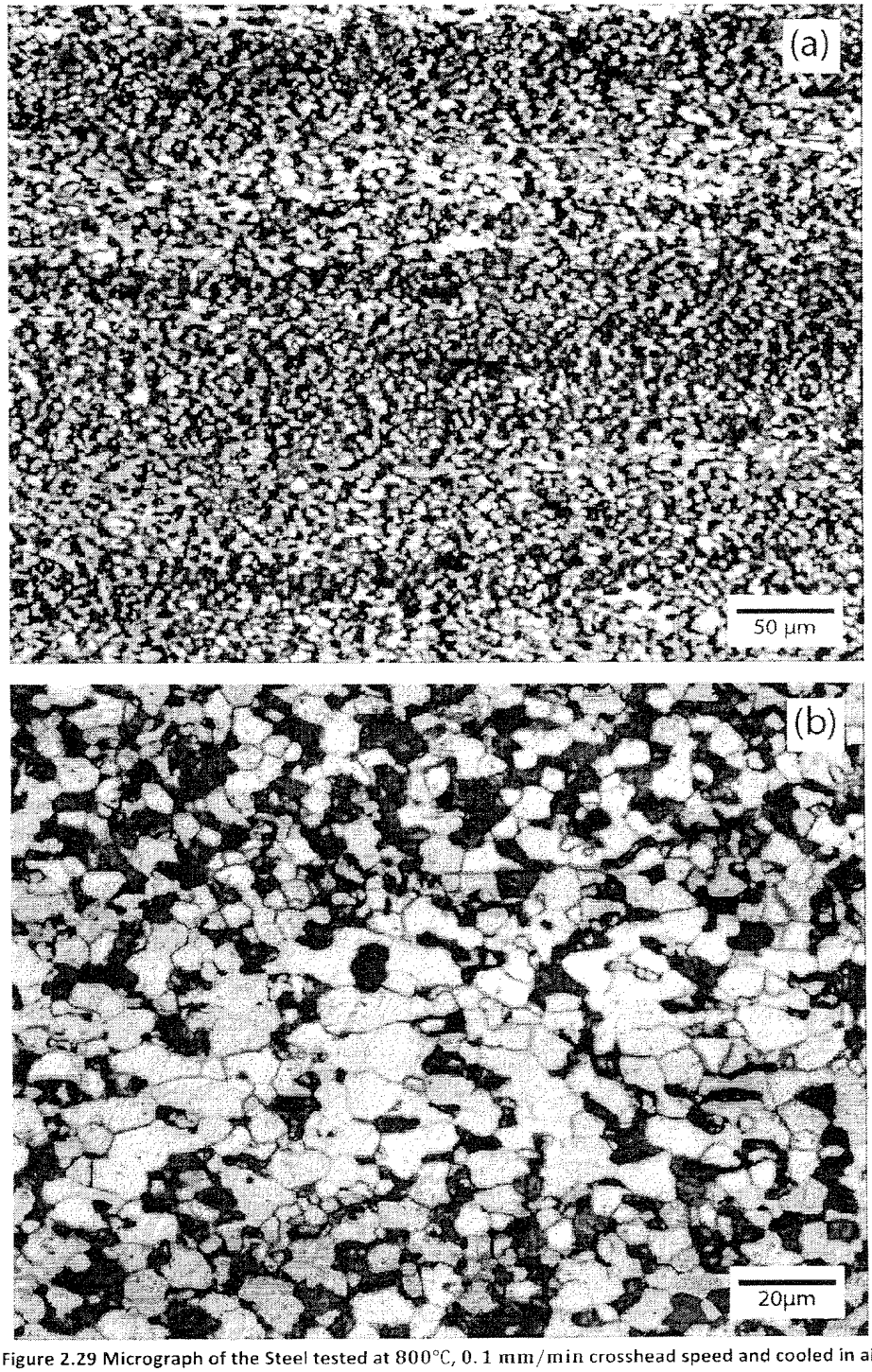

Figure 2.29 Micrograph of the Steel tested at $800°C$, $0.1\ mm/min$ crosshead speed and cooled in air

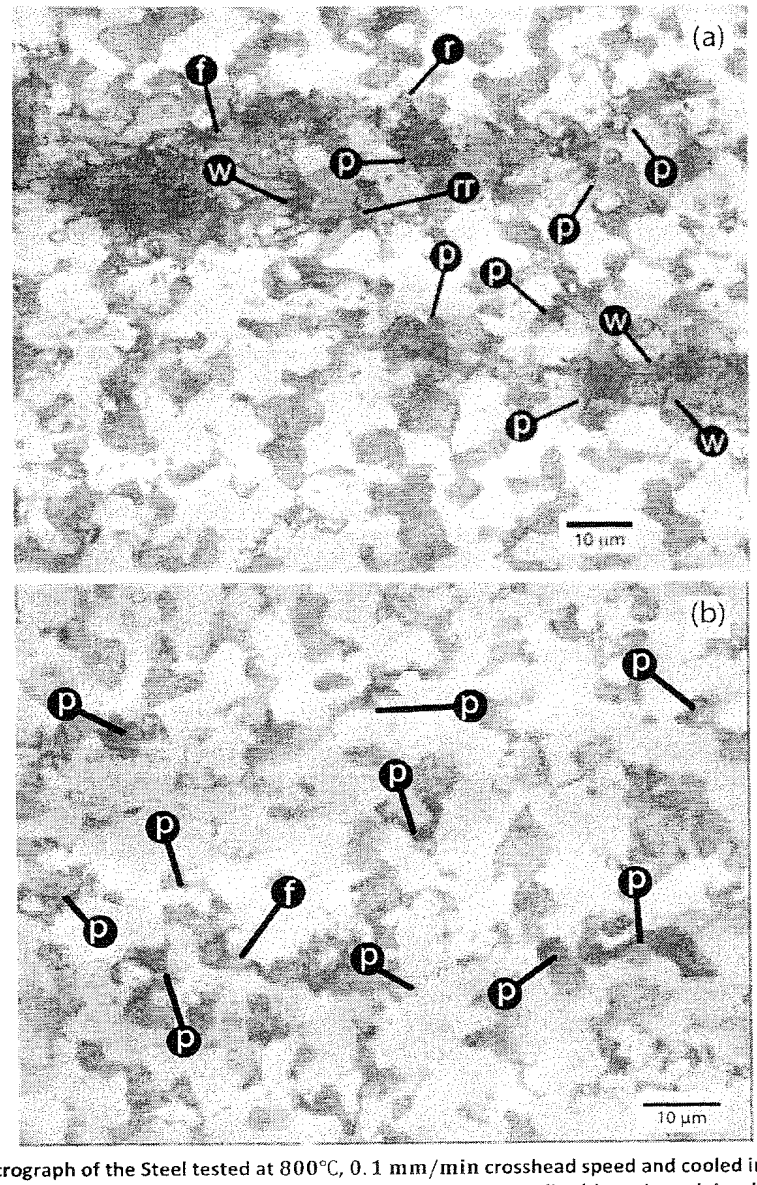

Figure 2.30 Micrograph of the Steel tested at $800°C$, $0.1\ mm/min$ crosshead speed and cooled in air showing the following decohesions: r-shaped decohesion between ferrite-ferrite-pearlite (r), w-shaped decohesion between ferrite-ferrite-pearlite/carbides (w), rr-shaped decohesion between ferrite-pearlite (rr), ferrite-ferrite decohesion (f) and pearlite-pearlite decohesion (p)

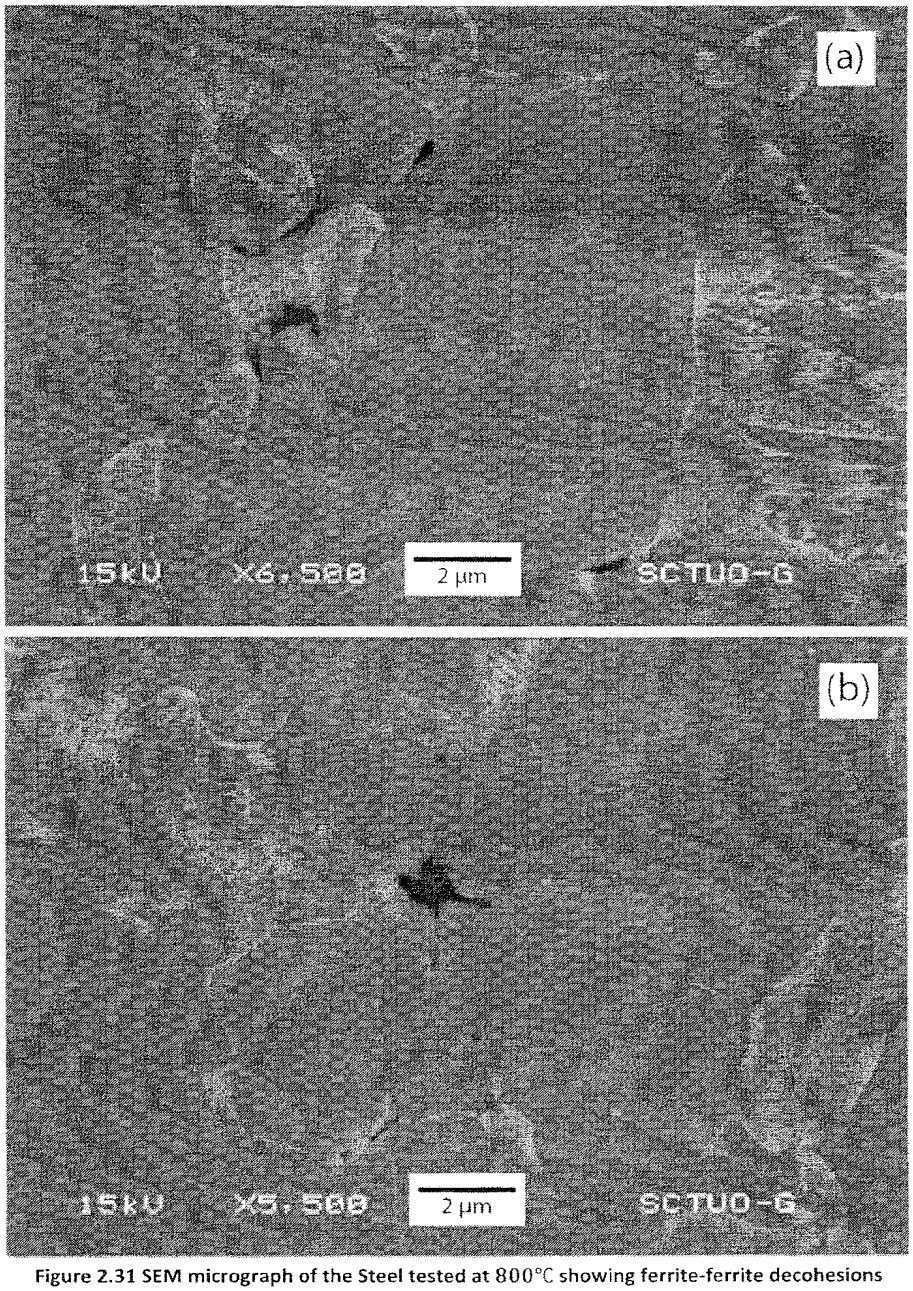

Figure 2.31 SEM micrograph of the Steel tested at 800°C showing ferrite-ferrite decohesions

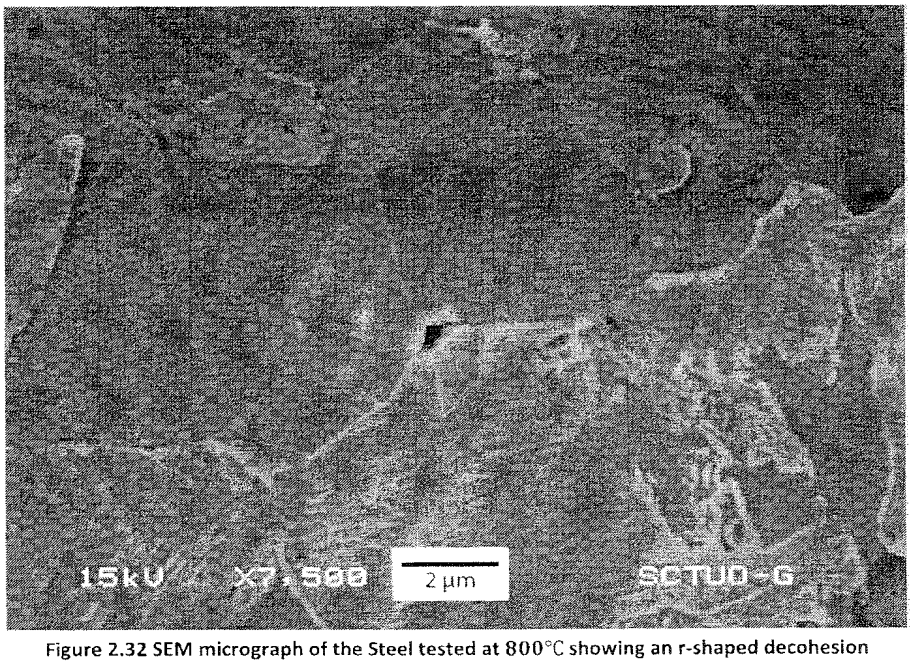

Figure 2.32 SEM micrograph of the Steel tested at 800°C showing an r-shaped decohesion

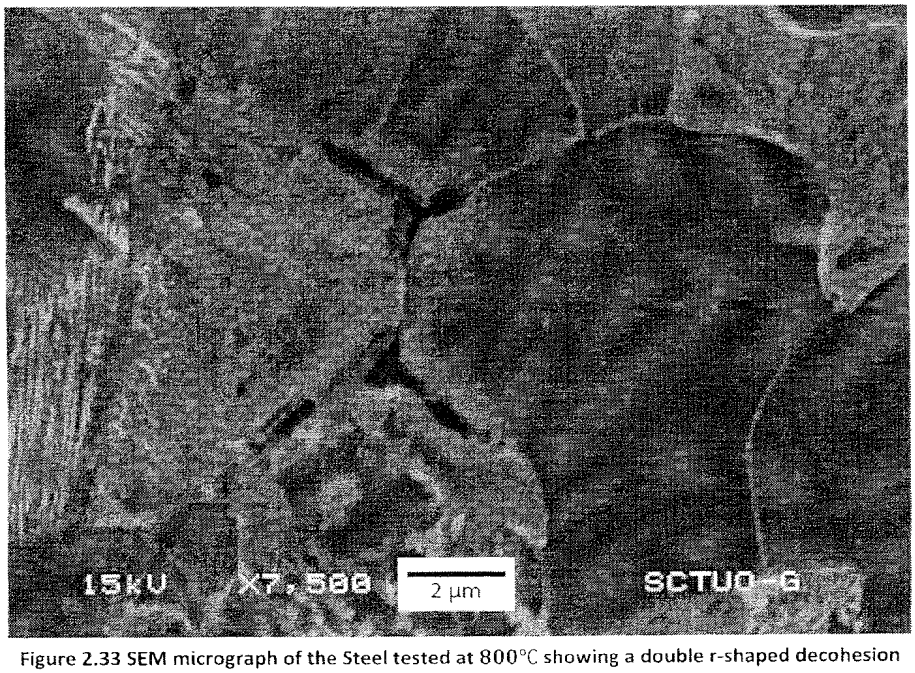

Figure 2.33 SEM micrograph of the Steel tested at 800°C showing a double r-shaped decohesion

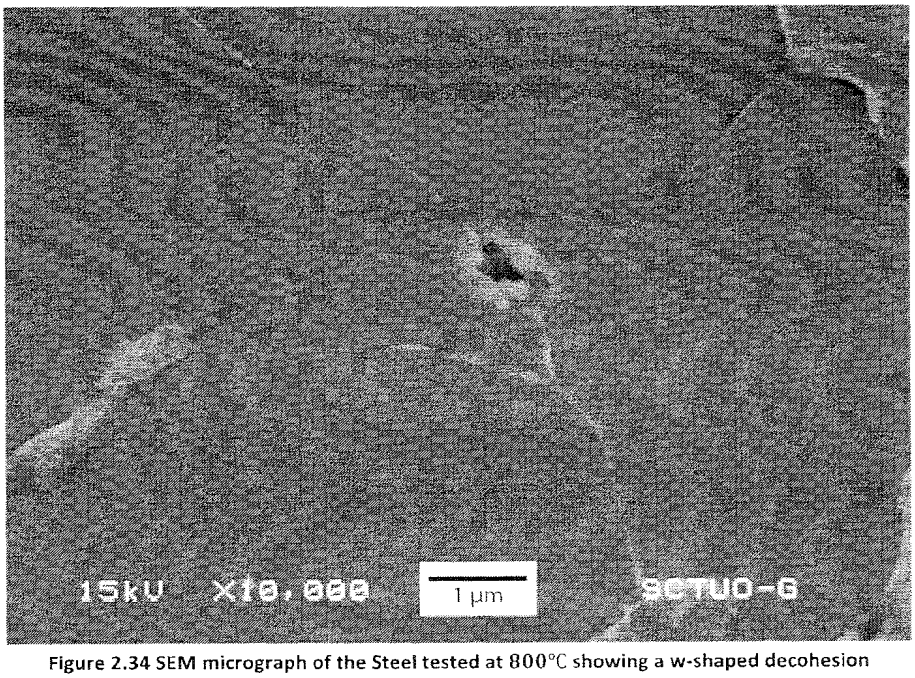

Figure 2.34 SEM micrograph of the Steel tested at 800°C showing a w-shaped decohesion

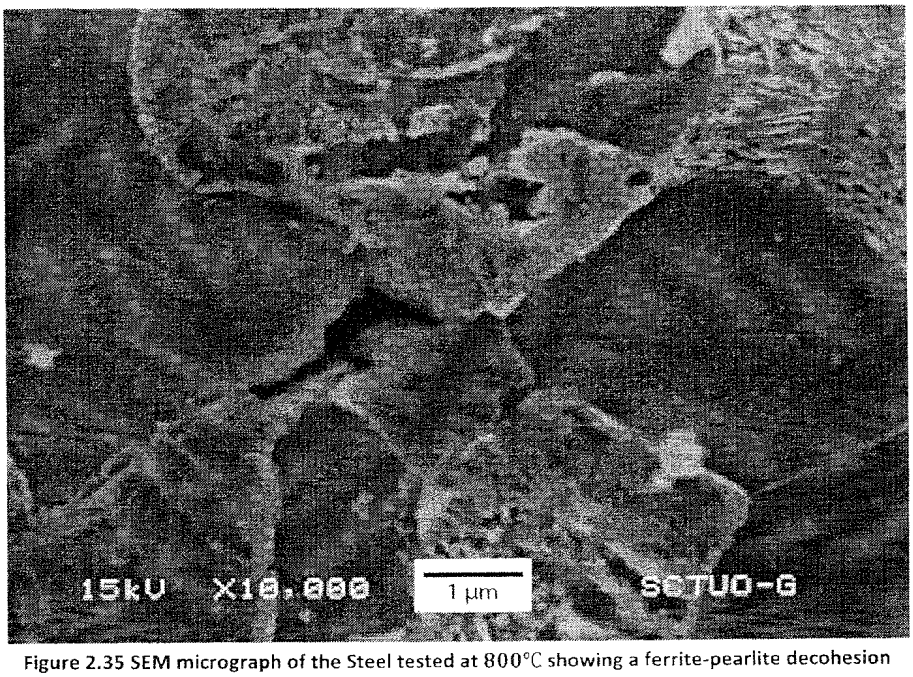

Figure 2.35 SEM micrograph of the Steel tested at 800°C showing a ferrite-pearlite decohesion

2.3.2.2.2 Structural damage at $\mathbf{750}$°C

The traction test resulted in an 125% elongation for this specimen tested ~30°C higher than the eutectoid temperature. After analyzing the microstructure of the steel, Figure 2.36, the following can be concluded:

- The microstructure is formed by ferrite and carbides (cementite, TiC and NbC).
- Ferrite, main constituent, is deformed and presents grain growth, possibly leading to the loss of superplastic behavior. There is no evidence of intergranular sliding.
- The inherent instability of the austenite responds to the testing time and to the traction straining by inducing a negative pressure that moves the $\gamma \rightarrow \alpha$ transformation to higher temperatures leading to a positive volume change (Le Chatelier principle).
- The low solubility of carbides and nitrides in the ferrite leads to its precipitation microscopically. Cementite is the finer of the carbides present, compared to the titanium and niobium carbides which made possible, before and after the controlled rolling, the creation of a UFG steel in thick strips. These precipitates appear to be at the surroundings/grain boundaries of the ferrite grains

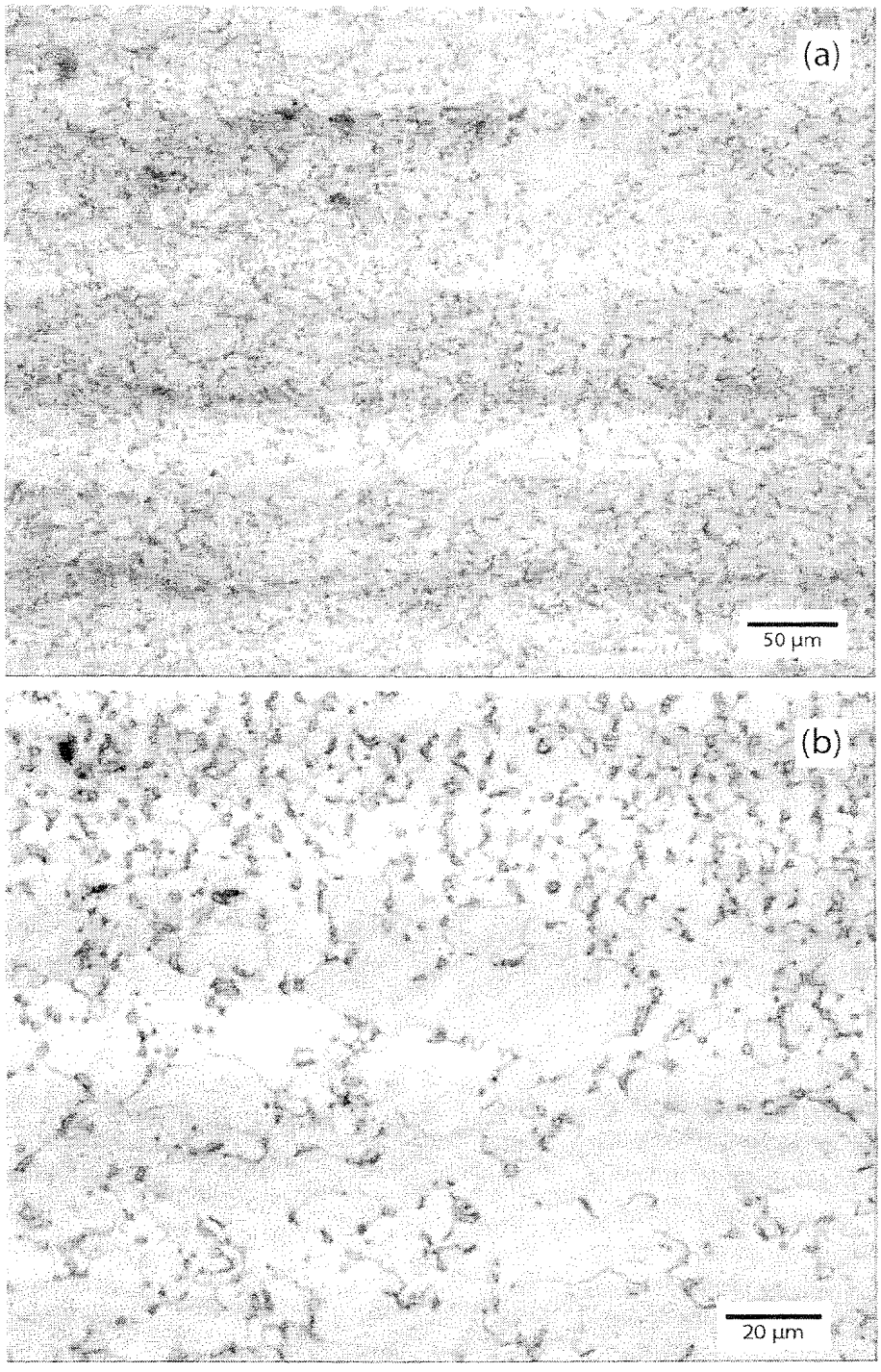

Figure 2.36 Micrograph of the Steel tested at $750°C$, $0.1\ mm/min$ crosshead speed and cooled in air

2.3.2.2.3 Precipitates

Microalloying elements, sometimes present themselves in the form of nitrides or carbides. In the case of the steel studied at high temperatures, the presence of titanium and niobium carbides (or carbonitrides) has a very important function on HSLA steels manufactured by ATMCRP processes, as follows:

- The titanium nitrides are responsible for maintaining the austenitic grain size during the homogenization process before rolling.
- The titanium nitrides and niobium carbonitrides act as an obstacle to the grain growth of the recrystallized austenite in times between passes in the roughing process.
- The massive precipitation of niobium carbonitrides during the waiting time between the roughing and finishing mills, delay the static recrystallization of the austenite in the finishing process, allowing in this process and after the allotropic transformation $\gamma \rightarrow \alpha$ the creation of fine and ultrafine ferrites (UFG steels).
- The niobium and titatium nanoprecipitates are responsible for an increase in the elastic limit, without a negative effect on the stiffness.

The classic Zener formula shown in Figure 2.37, allows, in a semi-quantitative manner, the obtention of equilibrium between the grain size of the matrix D, the volume fraction of the precipitate phase f_v and its grain size d_v according to the expression [12]:

$$D \cong \frac{d_v}{f_v} \qquad [2.17]$$

which brings equilibrium to the tendency of growth with the pinning effect produced by the precipitates. Thus, for precipitate volume fractions of $\sim 10^{-3}$ to 10^{-4} (as in the case of Ti and Nb precipitates) and grain sizes of the matrix (usually ferrite) between 1 and 10 μm, the size of precipitates must be in the nanometric scale (between 1 and 10 nm).

Also, Figure 2.37 shows precipitates that are inhibiting the grain growth. These particles create a traction force (with an approximate value of $\sim 2\gamma/\bar{D}$) at the grain boundary and restricting its movement. However, there is an opposing force (pinning) to

this traction force (pulling). When the mean grain size $\overline{D}$ increases, the pulling force decreases until it becomes insufficient and the grain growth stops.

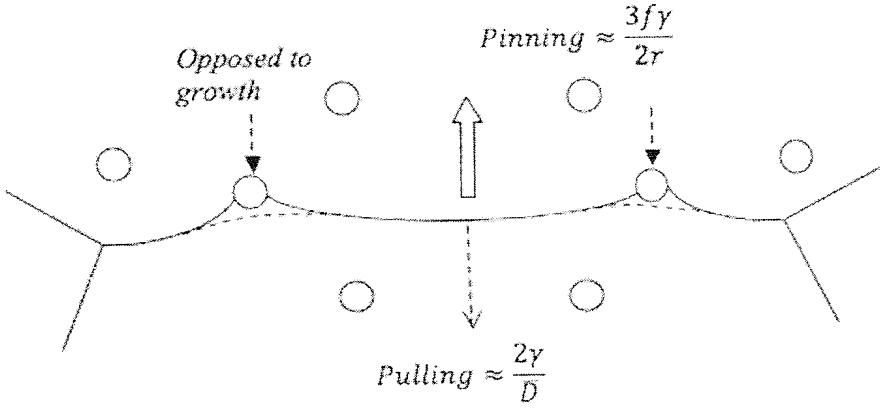

Figure 2.37 Pinning effect: effect of precipitates in the grain boundary migration

Furthermore, it is necessary that at the temperatures at which the precipitates are created (in the case of titanium nitrides, this temperature is 1200°C) the rolling process stops (delay time) in order for the precipitation to take place. Consequently, this type of rolling process in known as controlled rolling.

The solubility formulas for the titanium nitride, titanium carbide, niobium carbide and niobium carbonitride are [8]:

- Titanium nitride

$$\log[\mathrm{N}][\mathrm{Ti}] = \frac{-14400}{T(\mathrm{K})} + 5 \qquad [2.18]$$

- Titanium carbide

$$\log[\mathrm{C}][\mathrm{Ti}] = \frac{-7000}{T(\mathrm{K})} + 2.75 \qquad [2.19]$$

- Niobium carbide

$$\log[\mathrm{C}]^{0.87}[\mathrm{Nb}] = \frac{-7530}{T(\mathrm{K})} + 3.11 \qquad [2.20]$$

- Niobium carbonitride

$$\log[N]^{0.65}\,[C]^{0.24}[Nb] = \frac{-10400}{T(K)} + 4.09 \qquad [2.21]$$

Taking into account the chemical composition of the steel studied at high temperatures (0.168% C, 0.026% Ti, 0.033% Nb and 0.0055% N), the temperatures when the precipitation of nitrides and carbides begin to form can be calculated, and the results are shown in Table 2.10.

Precipitate	T (K)	T (°C)
Titanium nitride	1628	1355
Titanium carbide	1370	1097
Niobium carbide	1430	1157
Niobium carbonitride	1439	1166

Table 2.10 Precipitation temperatures of titanium and niobium

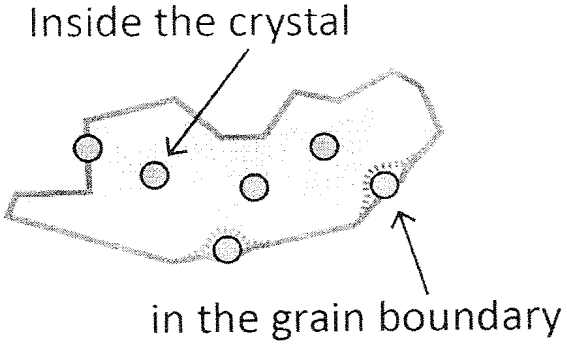

Figure 2.38 Austenite crystal deformed with carbides and nitrides precipitates both inside the crystal and in the grain boundary

The rolling process (ATMCRP) consists in two stages: roughing and finishing; with a delay time between them where the niobium carbonitrides precipitation will take place. The previously mentioned carbides and carbonitrides will begin to precipitate in the austenitic phase therefore delaying both the grain growth as well as the recrystallization of the austenite, in other words, the precipitates form both in the grain boundaries and inside the austenitic crystals favoring the stability of the non-recrystallized microstructure. After the allotropic transformation takes place, the microstructure is formed by very fine

ferrite grains due to the fact that this phase nucleates both in the grain boundaries as well as inside the crystals forming subgrains, deformation bands or structural defects (Figure 2.38).

Titanium Nitrides

The starting temperature for the precipitation of titanium nitrides (Table 2.10) is 1355°C or 1628 K. Figure 2.39 shows the graphic evolution of the titanium and nitrogen content at different temperatures: at 1628 K (precipitation temperature) and two other inferior ones (1373 K and 1273 K). This figure shows the amount of N and Ti dissolved in the material, in other words, it has not precipitated yet. The line obtained by linear regression represents the evolution of the N and Ti content of the steel studied as a function of precipitation. Furthermore, almost all nitrogen precipitates forming TiN at 1373 K (1100°C); at the delay time, the temperatures changes from 1075°C to 829°C, and almost all the N has already precipitated and little is left behind to form other precipitates.

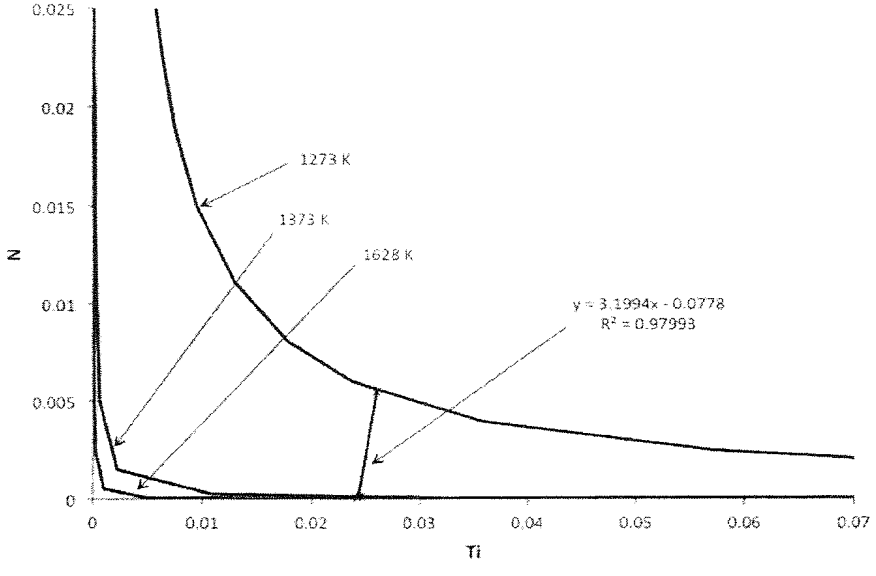

Figure 2.39 Evolution of the content of titanium and nitrogen at different temperatures

Niobium carbides

The starting temperature for the precipitation of niobium carbides (Table 2.10) is 1157°C or 1430 K. Figure 2.40 shows the graphic evolution of the niobium and carbon content at different temperatures: at 1430 K (precipitation temperature) and two other inferior ones (1373 K and 1073 K). It also shows the amount of Nb and C dissolved in the material, in other words, it has not precipitated yet. The line obtained by linear regression represents the evolution of the C and Nb content of the steel studied as a function of precipitation. Moreover, at a temperature of 1073 K, relatively all the Nb has precipitated during the delay time (1075~829°C); this explains the role of this microalloying element: inhibit the grain growth during the waiting time and strongly delaying the static recrystallization of the austenite in the finishing stage, stimulating the fine ferrite grain size after the allotropic transformation and a slight structural hardening of it as a result of the nanometric size of the precipitates.

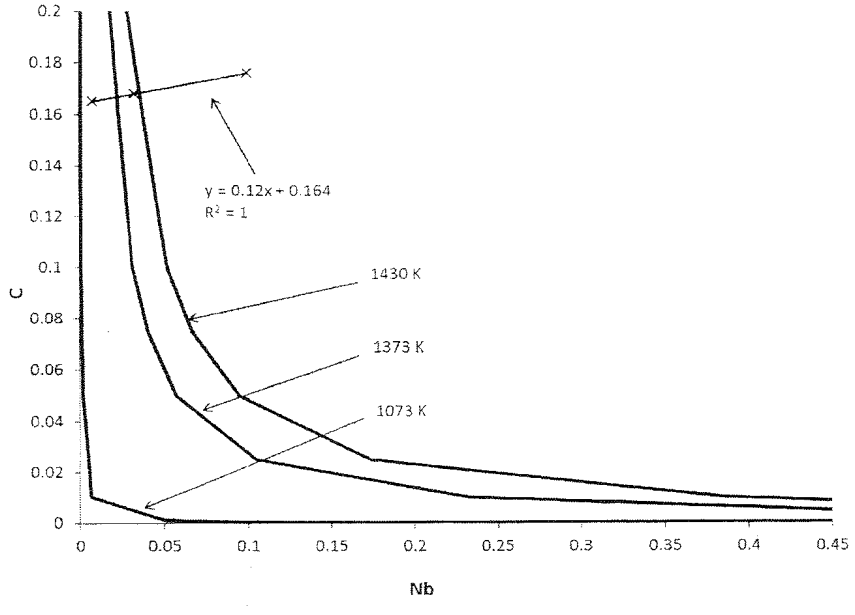

Figure 2.40 Evolution of the content of niobium and carbon at different temperatures

To confirm both behaviors and to identify different types of carbides, SEM microscopy was made. Figure 2.41 shows a titanium carbonitride, identified by the shape

of almost a rectangle; also, element mapping confirms that niobium precipitates form using the titanium as a base because the titanium carbonitrides have formed at higher temperatures. And Figure 2.42 presents a series of titanium carbonitrides together with niobium carbides (grown over the TiCN) that precipitated on the pearlitic band.

Figure 2.43 shows another type of precipitates, in this case a vanadium carbide formed in the grain boundary of a ferrite and Figure 2.44 shows a titanium carbonitrade that acted a substrate to the growth of not only a niobium carbide but also a vanadium carbide.

Figure 2.45 shows two carbides identified in the steel, a vanadium carbide and a very small molybdenum carbide.

Figure 2.41 SEM micrograph showing a titanium carbonitride and niobium carbide (a), dot mapping of titanium (b) and dot mapping of niobium (c) in the sample

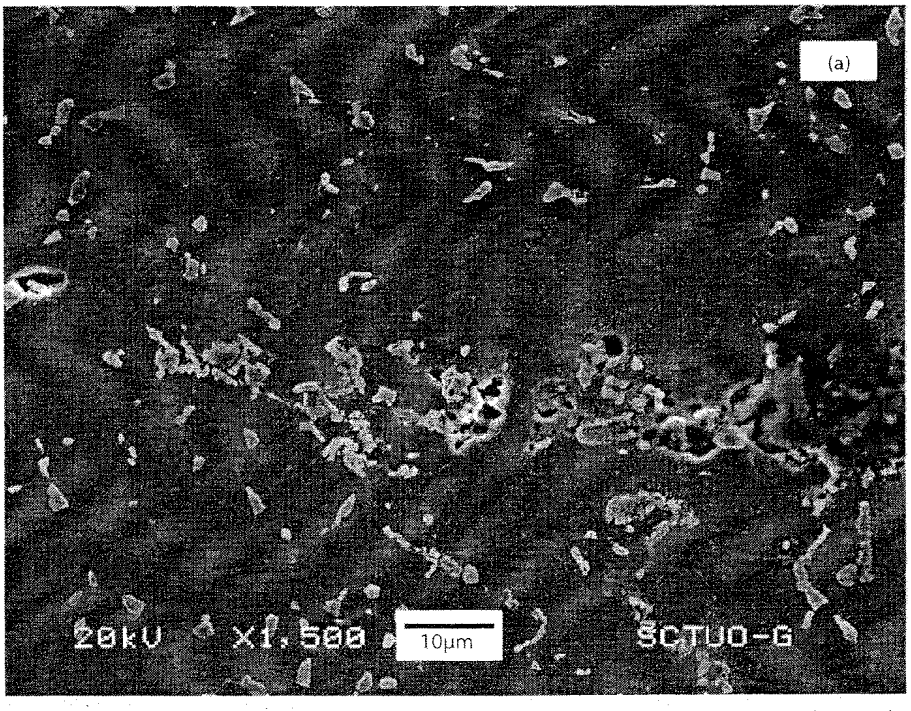

(b) (c)

Figure 2.42 SEM micrograph showing a string of titanium carbonitrides and niobium carbides (a), dot mapping of titanium (b) and dot mapping of niobium (c) in the sample

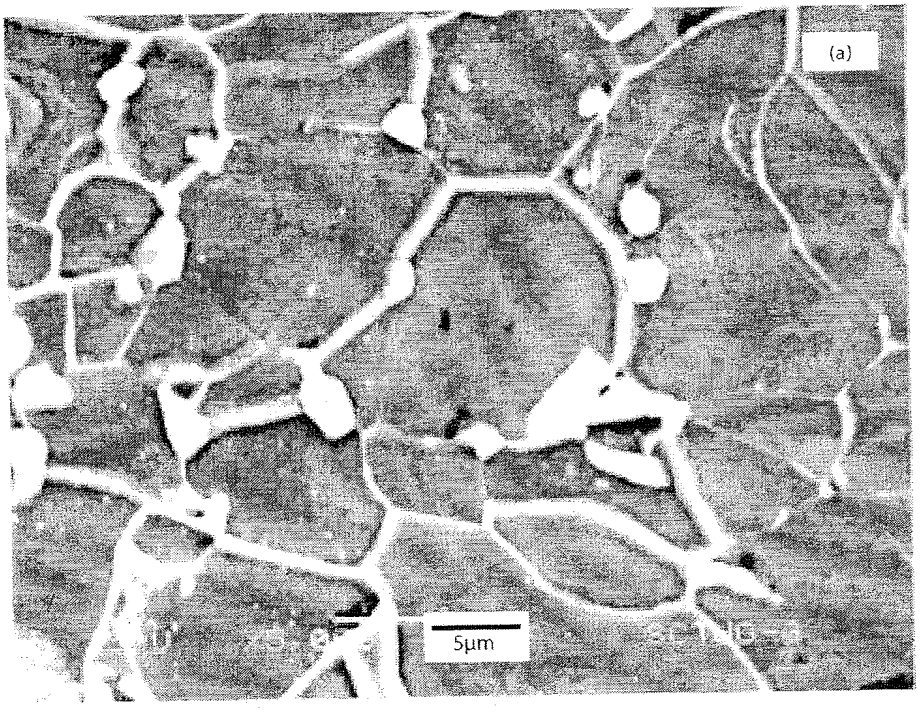

Figure 2.43 SEM micrograph showing a vanadium carbide (a), dot mapping of vanadium (b) in the sample

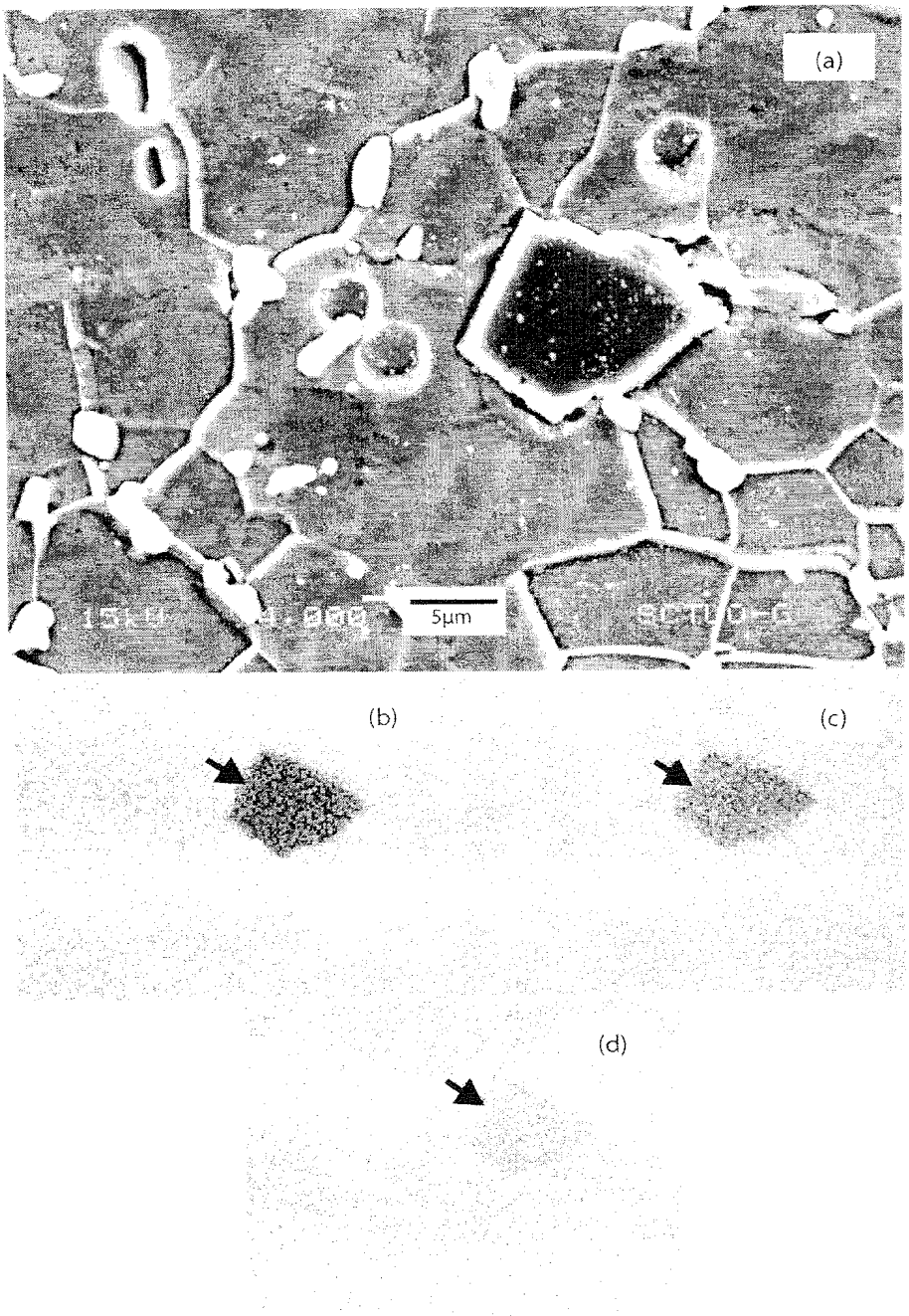

Figure 2.44 SEM micrograph showing a titanium carbonitride, a niobium carbide and vanadium carbide (a), dot mapping of titanium (b), dot mapping of niobium (c) and dot mapping of vanadium (d) in the sample

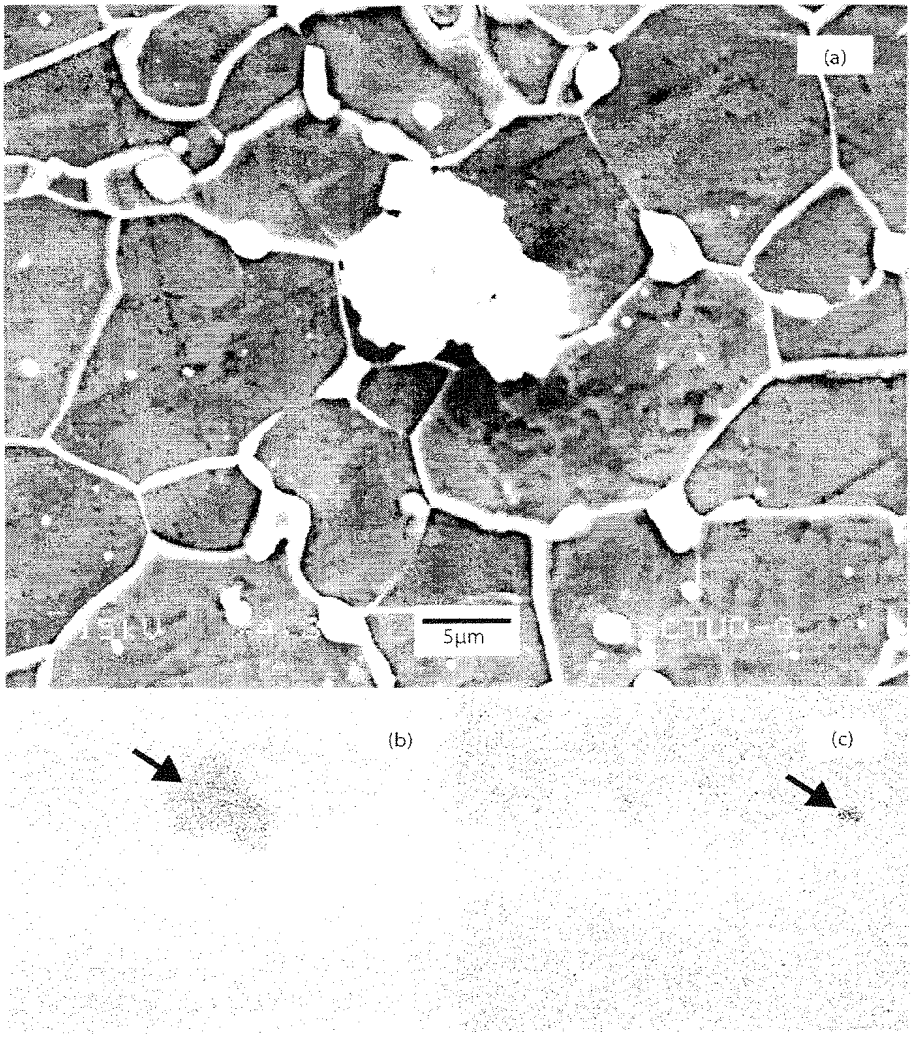

Figure 2.45 SEM micrograph showing a vanadium carbide and a molybdenum carbide (a), dot mapping of vanadium (b) and dot mapping of molybdenum (c) in the sample

2.3.2.2.4 Subgrains

As previously mentioned with the precipitation and the possible defects that can be caused by precipitates in the grain boundary, subgrains are formed in the ferrite grains.

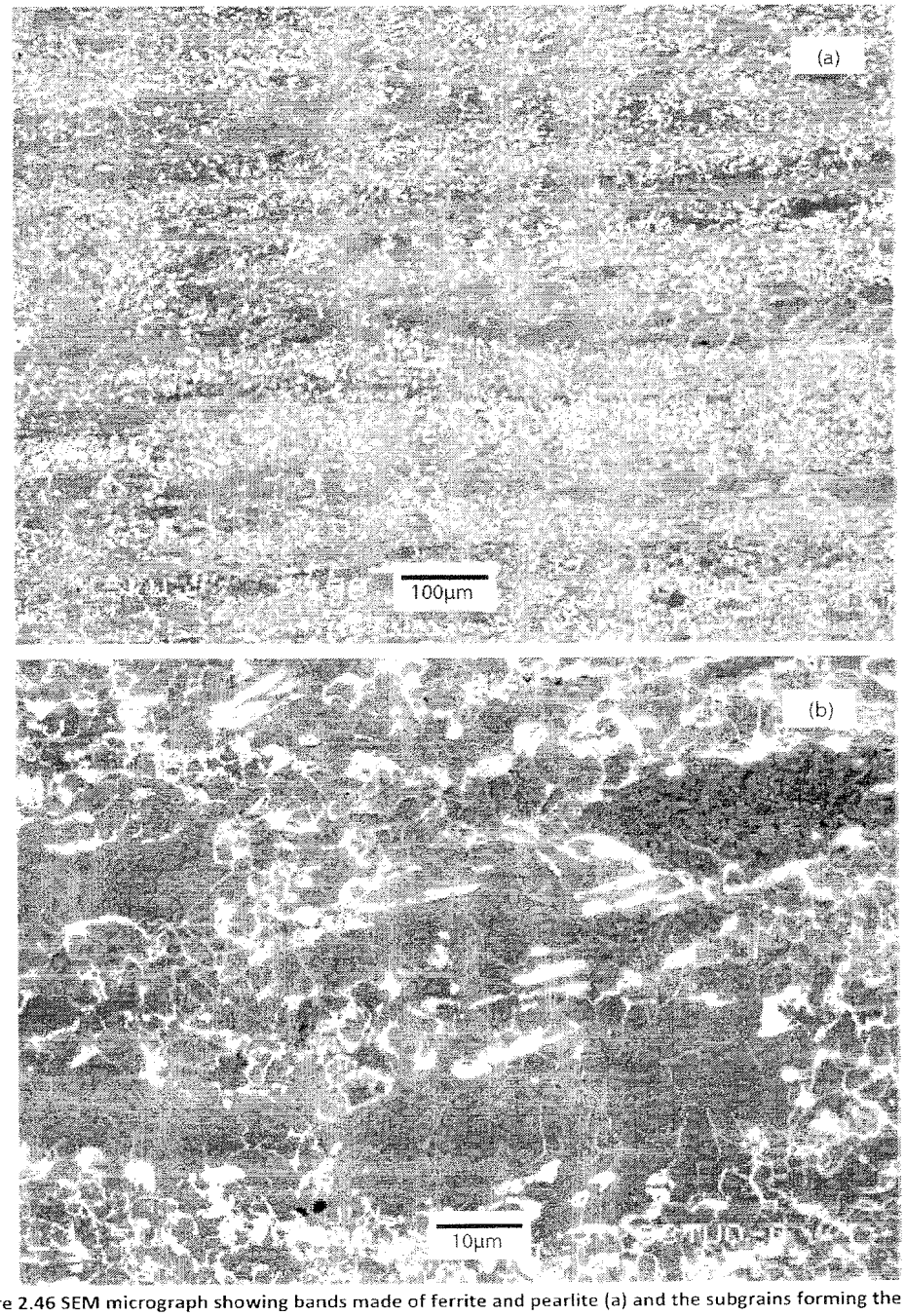

Figure 2.46 SEM micrograph showing bands made of ferrite and pearlite (a) and the subgrains forming the ferrite grains (b)

Figure 2.46a shows the microstructure of the steel superplastically deformed at 800°C, with bands of ferrite and pearlite, but at a close up (Figure 2.46b and Figure 2.47)

each ferritic grain is formed by subgrains; the ferritic grain boundary can be identified by the presence of cementite precipitates, while the subgrain boundary does not show these structures.

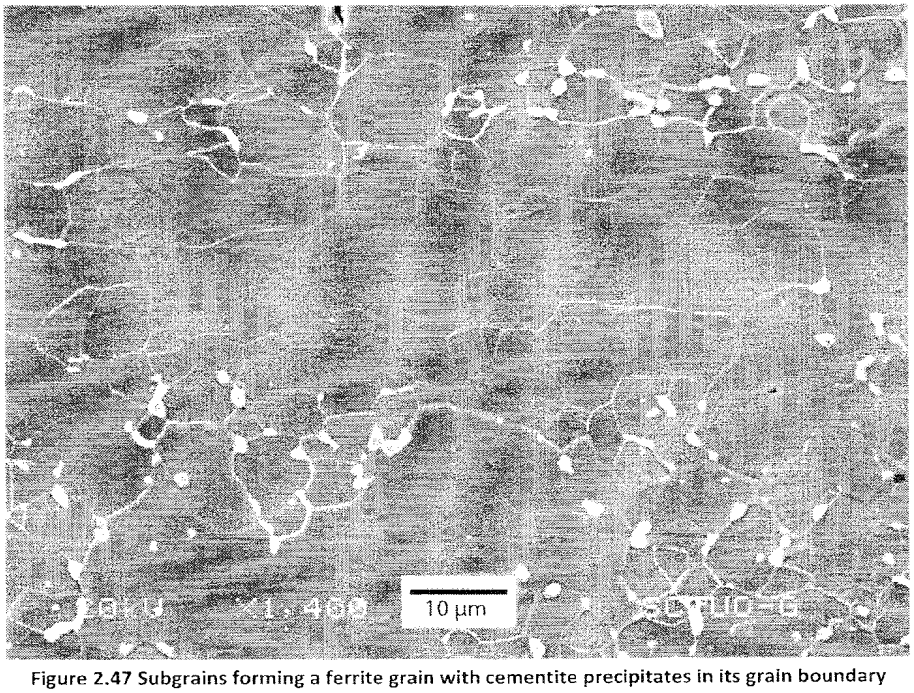

Figure 2.47 Subgrains forming a ferrite grain with cementite precipitates in its grain boundary

2.3.3 Ashby-Verrall model of superplasticity

This model supposes that the grains are hexagonal prisms with size parameters d as shown in Figure 2.48. The rest of the parameters of the model mentioned in Chapter 1 will be calculated in the following paragraphs:

1. Grain volume

$$Volume = Area \times height$$

$$Grain\ area = \frac{Perimeter \times apothem}{2} = \frac{6l \cdot \frac{l\sqrt{3}}{2}}{2} = \frac{3\sqrt{3}}{2} l^2 = 2.5980\, l^2$$

and knowing that $d = 2l$, then:

$$V = Grain\ area\ \times d = 2.5980 \left(\frac{d}{2}\right)^2 \cdot d = 0.65\ d^3$$

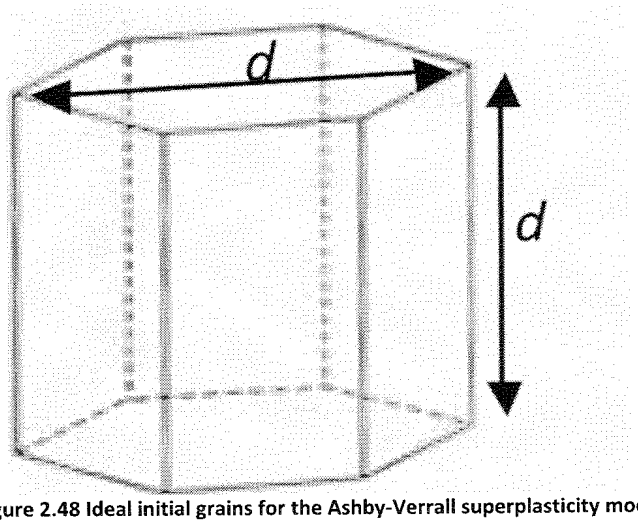

Figure 2.48 Ideal initial grains for the Ashby-Verrall superplasticity model

2. Strain per unit caused by intergranular sliding
   From Figure 2.49 it can be inferred that:

$$L_0 = 2 \cdot \frac{l\sqrt{3}}{2} = l\sqrt{3}$$

While for the intermediate position (Figure 2.50) the distance changes to:

$$L_0 = 3l$$

The engineering strain that occurs in the grains caused by the change from the initial to the final position is:

$$e = \frac{L_f - L_0}{L_0} = \frac{3l - l\sqrt{3}}{l\sqrt{3}} = 0.734$$

Thus, the true strain associated to the sliding and rotation of grains will be:

$$\varepsilon = \ln(1 + e) = ln(1 + 0.734) = 0.55$$

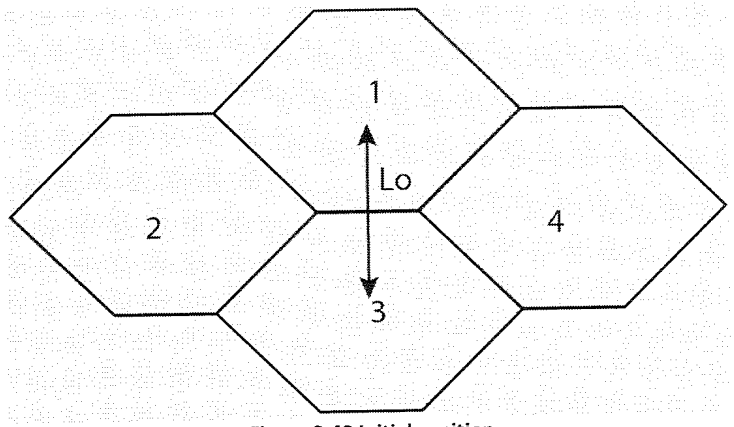

Figure 2.49 Initial position

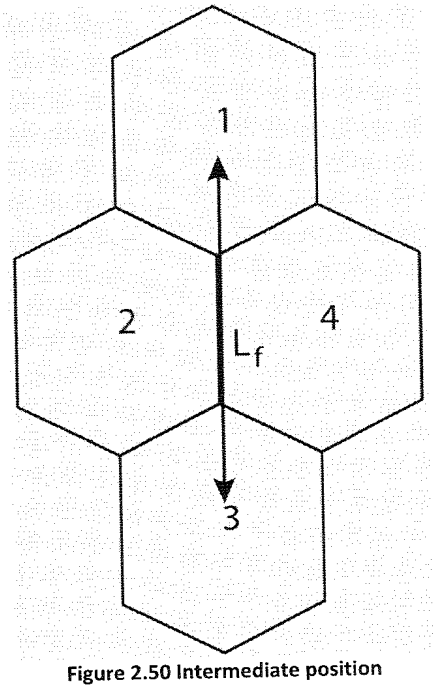

Figure 2.50 Intermediate position

3. Area where the sliding occur

   The sliding takes place at four areas (each a side of a hexagon) as shown in Figure 2.51. Knowing that each side equals $d/2$, then the area will be:

$$Sliding\ area = 4l \cdot d = 2d^2$$

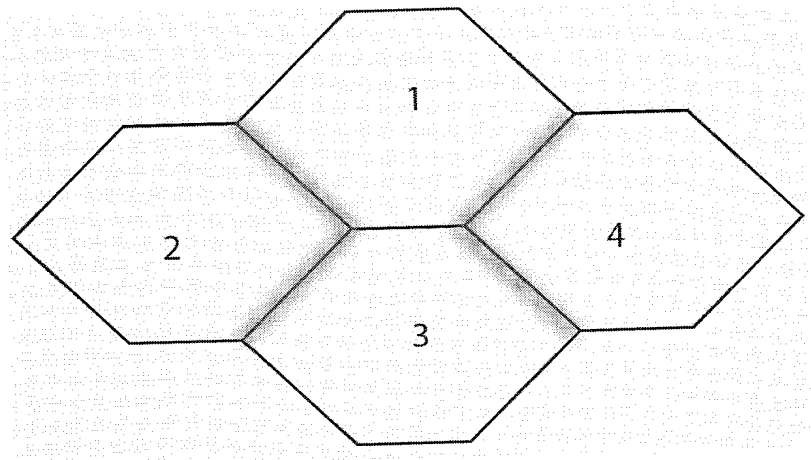

Figure 2.51 Sliding area

4. Area change of the group of four grains when moving from the initial to the intermediate position
   a. Grains 1 and 3

      For this calculation, a CAD software was used. Starting from the initial position and moving to the intermediate one (shown in Figure 2.52), the area change for these two grains is:

$$\Delta A_{total_{1-3}} = 0.07d^2$$

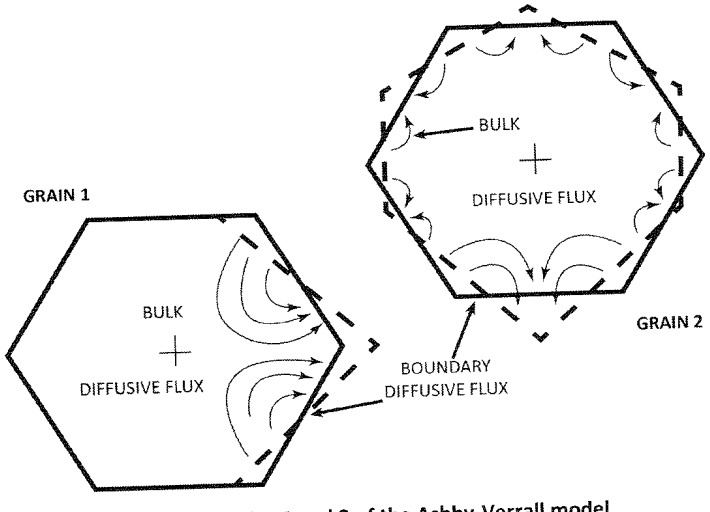

Figure 2.52 Grains 1 and 3 of the Ashby-Verrall model

b. Grains 2 and 4

Likewise using CAD and supposing a conservation of areas (Figure 2.53):

$$l' = h = \sqrt{\left(\frac{l\sqrt{3}}{2}\right)^2 + \left(\frac{l\sqrt{3}}{2}\right)^2} = l\sqrt{\frac{3}{2}}$$

The calculation of the side x of the triangle shown in Figure 2.54 is based on the consideration that the areas of the dashed pentagon and the triangle are the same which lead to the following expression:

$$l\sqrt{3}x + \frac{l^2\sqrt{3}\,sin\,30°}{2} = \frac{l(3-\sqrt{3})}{4\sqrt{3}}$$

and solving for x:

$$x = 0.183l$$

which is shown in Figure 2.55. Concluding that, the total area change for grains 2 and 4 equals:

$$\Delta A_{total_{2-4}} = \frac{0.183l}{2} \cdot \frac{l\sqrt{3}}{4} = 0.039l^2 \cong 0.01d^2$$

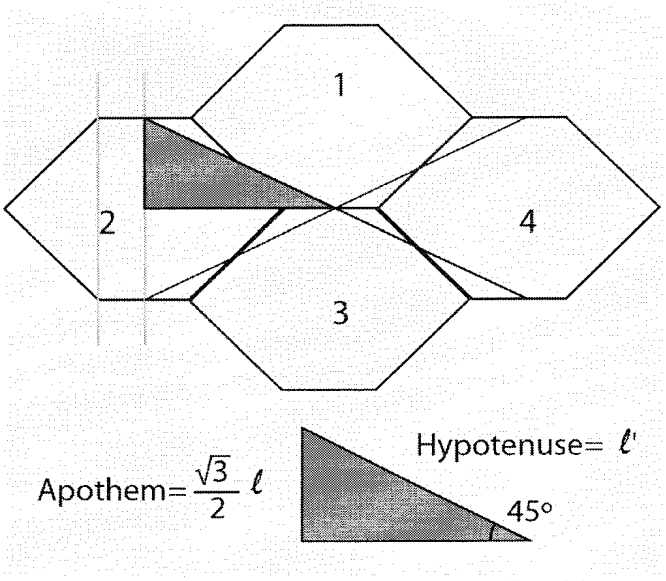

Figure 2.53 Grains 2 and 4 of the Ashby-Verrall model

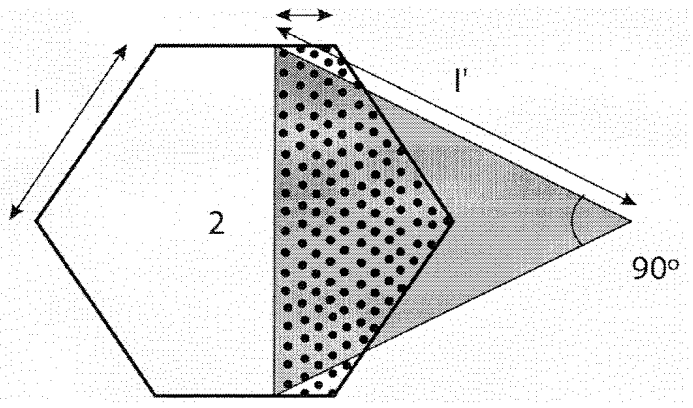

Figure 2.54 Area change in grain 2

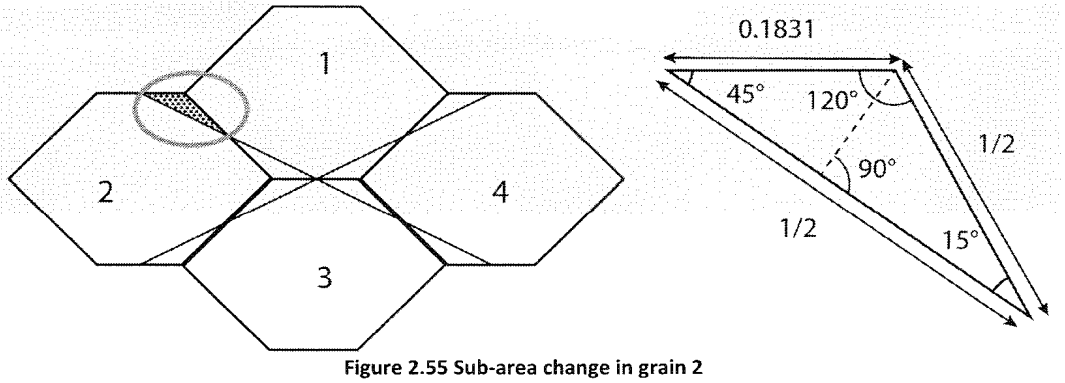

Figure 2.55 Sub-area change in grain 2

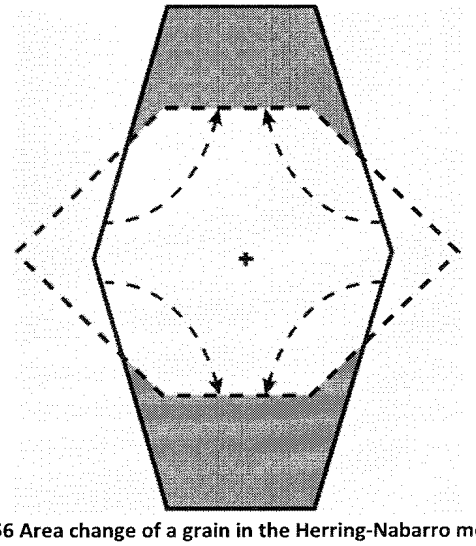

Figure 2.56 Area change of a grain in the Herring-Nabarro mechanism

c. Herring-Nabarro mechanism

Once again, CAD assisted and using Figure 2.56, the change of area for the group of four grains moving from the initial to the intermediate position according to the Herring-Nabarro mechanism is:

$$\Delta A_{total_{H-N}} = 0.19d^2$$

5. Displacement suffered by a grain from the initial to the intermediate position

Using Figure 2.57 as a starting point and knowing that $15°$ is the angle a grain rotates when it moves from the starting to the final position, then:

$$u = 0.5l \cdot \cos 15° = 0.48l$$

This value of displacement is similar to that reported by Ashby-Verrall ($u \approx 0.46l$) which validates the calculation of this parameter in a geometrical manner [13].

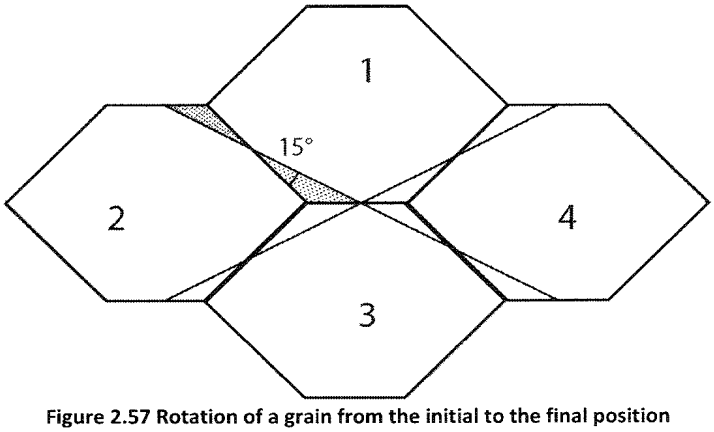

Figure 2.57 Rotation of a grain from the initial to the final position

6. Volume of matter moved by diffusion per grain during the sliding of grains from the initial to the final position

a. In grains 1 and 3

The volume of matter moved by diffusion in grains 1 and 3 is:

$$Volume_{total_{1-3}} = \Delta A_{total_{1-3}} \cdot d = M\Omega = 0.07d^2 \cdot d = 0.07d^3$$

b. In grains 2 and 4

Geometrically calculating the volume of matter moved in grains 1 and 3 as:

$$Volume_{total_{2-4}} = \Delta A_{total_{2-4}} \cdot d = M\Omega = 0.01d^3$$

c. Herring-Nabarro mechanism
According to the Herring-Nabarro mechanism, the volume of matter moved by diffusion will be:

$$Volume_{total_{H-N}} = \Delta Volume_{total_{H-N}} \cdot d = M\Omega = 0.19d^3$$

7. Mean distance of diffusion
Using CAD software, the mean distance of diffusion is calculated:

$$Distance_{mean_{2-4}} = 0.57d$$

2.3.3.1 Application of the model on lead

Once the Ashby-Verrall model was corroborated, it was confirmed with lead at a temperature of 300 K (equivalent to 50% of the melting point) and grain sizes of 1, 3 and 5 μm. The remaining data is shown in Table 2.1.

Parameter	Value	Parameter	Value
A_1 (*)	6×10^6	Ω (atomic volume) (cm^3)	3.023×10^{-23}
b (cm)	4×10^{-8}	k (erg/cm^2)	1.38×10^{-16}
Q_c (cal/mol)	26100	τ (superficial energy) (erg/cm^2)	250
n (*)	6.2	T (K)	300
μ (dyn/cm^2)	5×10^{10}	d (cm)	0.0001
D_v (cm^2/s)	1.75756×10^{-19}	Δ (cm)	7×10^{-8}
D_b (cm^2/s)	6.9196×10^{-12}		

Table 2.11 Ashby-Verrall model parameters for lead. (*) A_1 is an adimensional constant and n is an adimensional exponent

All the units are in the CGS system with energy in cal as it was the system used by Ashby-Verrall, and not the SI system universally accepted. These result are, representatives and easy to compare to the empirical ones, as the experiments are easy to make at room temperature. Figure 2.58b presents the $\log\sigma - \log\dot{\varepsilon}$ curve for lead with the three regions: the first two are dominated by the Herring-Nabarro mechanisms (modified by Ashby) and the third corresponds to the hot deformation. There is a window where the data $(\sigma, \dot{\varepsilon})$ under which $\dot{\varepsilon}_{AD} > \dot{\varepsilon}_{DC}$ and over than $\dot{\varepsilon}_{AD} < \dot{\varepsilon}_{DC}$ translating to superplastic behavior (Figure 2.58a) where $0.3 < m < 0.7$; for lead the window is $10^{-6} < \dot{\varepsilon} < 10^{-5}\mathrm{s}^{-1}$ and $2 \times 10^{-5} < \sigma/\mu < 2 \times 10^{-4}$ for the grain size and temperature determined. The m coefficient of Figure 2.58c was calculated through the Backofen approximation:

$$m = \frac{d\,log\,\sigma}{d\,log\,\dot{\varepsilon}}$$

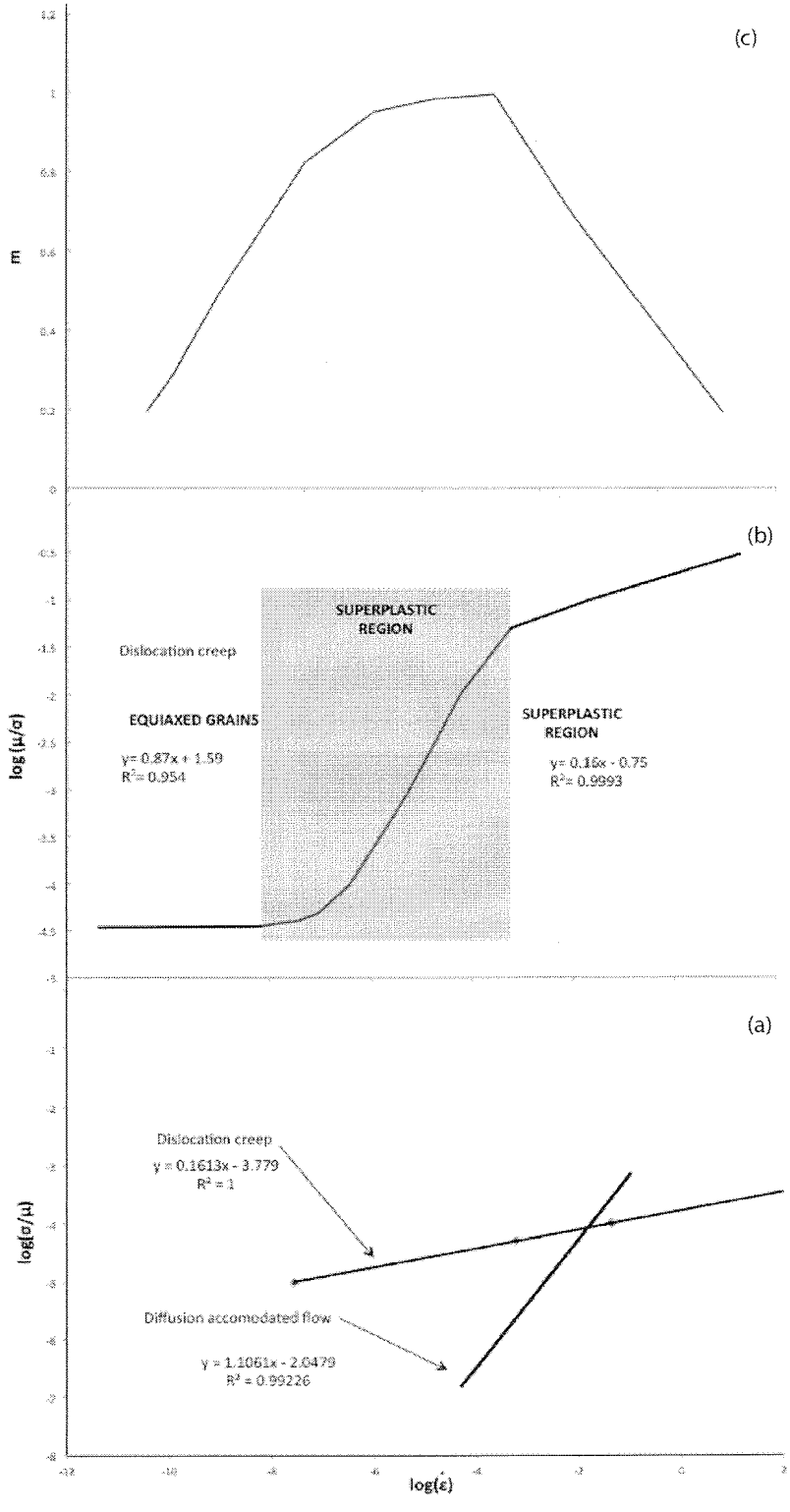

Figure 2.58 a) Mechanisms acting on the behavior of lead, b) Sum of both mechanisms showing the superplastic region and c) m coefficient for lead

2.3.3.2 Application of the model on zinc

In a similar way the Ashby-Verrall model for lead, in zinc at a temperature of 300 K (equivalent to 43% of the melting point) and grain sizes of 1, 3 and 5 μm with data from Table 2.12 the model was corroborated.

Parameter	Value	Parameter	Value
A_1 (*)	1.47×10^{11}	Ω (atomic volume) (cm^3)	1.52×10^{-23}
b (cm)	2.67×10^{-8}	k (erg/cm^2)	1.38×10^{-16}
Q_c (cal/mol)	21900	τ (superficial energy) (erg/cm^2)	100
n (*)	6.1	T (K)	300
μ (dyn/cm^2)	3.6×10^{11}	d (cm)	0.0001
D_v (cm^2/s)	1.82892×10^{-17}	Δ (cm)	5.34×10^{-8}
D_b (cm^2/s)	69.03056×10^{-12}		

Table 2.12 Ashby-Verrall model parameters for zinc. (*) A_1 is an adimensional constant and n is an adimensional exponent

Figure 2.59b shows the $\log\sigma - \log\dot{\varepsilon}$ curve for zinc also with the three regions as well as a window where the data $(\sigma, \dot{\varepsilon})$ under which $\dot{\varepsilon}_{AD} > \dot{\varepsilon}_{DC}$ (superplastic creep) and over than $\dot{\varepsilon}_{AD} < \dot{\varepsilon}_{DC}$ (hot deformation) presented in Figure 2.59a.

The superplastic window (Figure 2.59c) moves to higher $\dot{\varepsilon} = 10^{-4}s^{-1}$ (with grain size of 0.5 μm) compared to that for larger grain sizes ($10^{-8}s^{-1}$ and grain size 8 μm), this displacement has potential for industrial applications for superplastic forming. In a similar way, the stresses are higher for the 0.5 μm grain size (6×10^{-5}) than for 8 μm (10^{-5}). In a general way (Figure 2.59c) the superplastic window lies in $10^{-8} < \dot{\varepsilon} < 10^{-5}s^{-1}$ and $10^{-4} < \sigma/\mu < 10^{-3}$ for the determined grain size.

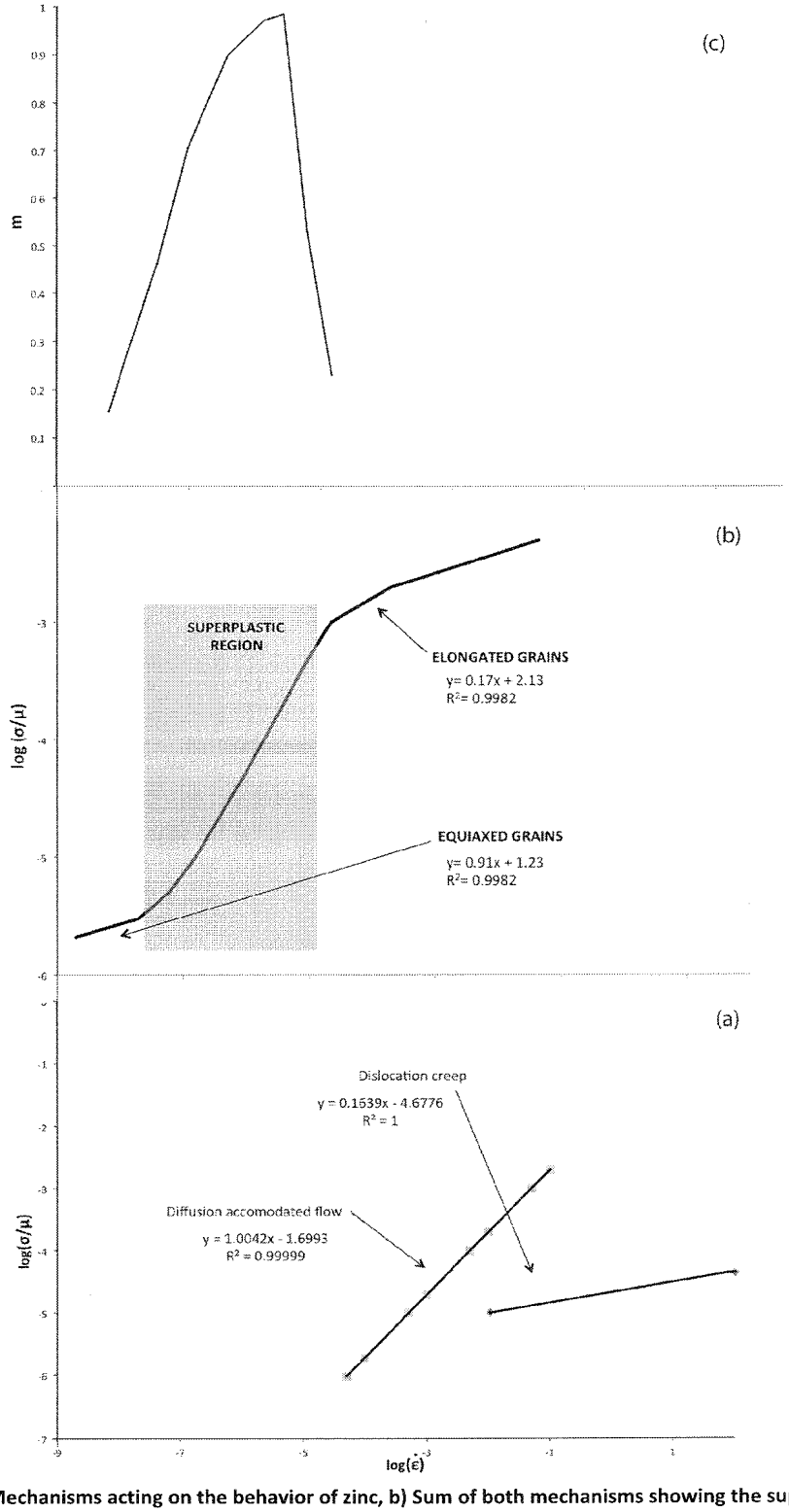

Figure 2.59 a) Mechanisms acting on the behavior of zinc, b) Sum of both mechanisms showing the superplastic region and c) m coefficient for zinc

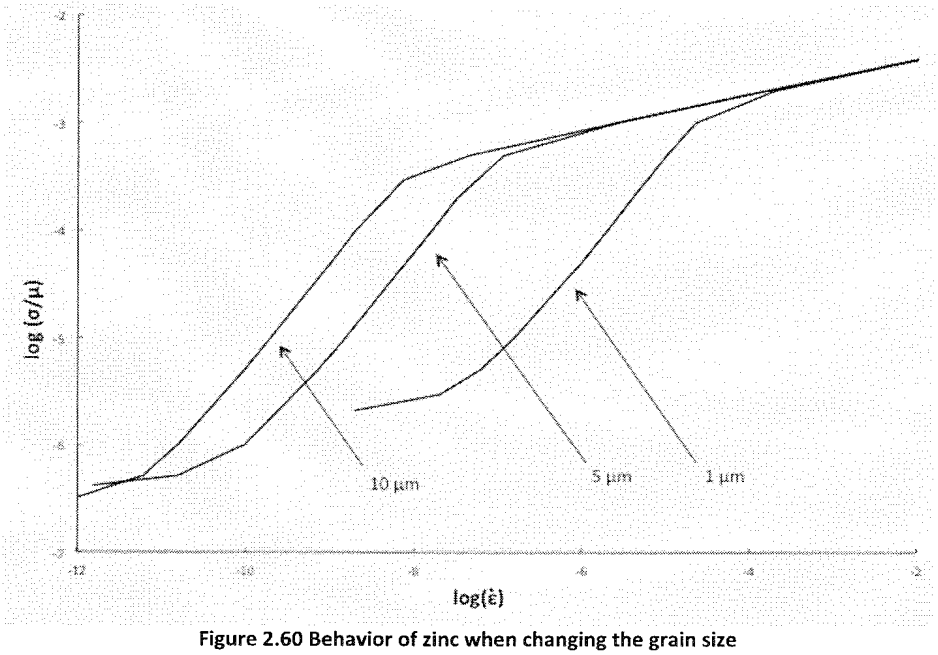

Figure 2.60 Behavior of zinc when changing the grain size

2.3.3.3 Application of the model on the steel tested

The results of the steel tested at 800°C can be compared to the Ashby-Verrall model which is:

$$\dot{\varepsilon}_{total} = \dot{\varepsilon}_{D-A\ flow} + \dot{\varepsilon}_{dislocation\ creep} \quad [2.22]$$

The mechanisms of intergranular sliding accommodated by diffusion ($\dot{\varepsilon}_{D-A\ flow}$) and of creep (sliding and climbing of dislocations, $\dot{\varepsilon}_{dislocation\ creep}$) act simultaneously (in parallel). The parameters of the steel tested are shown in Table 2.13 in the CGS unit system (to compare to the metals proposed by Ashby-Verrall).

Parameter	Value	Parameter	Value
A_1 (*)	2.88×10^{38}	Ω (atomic volume) (cm^3)	1.2195×10^{-23}
b (cm)	2.51×10^{-8}	k (erg/cm^2)	1.38×10^{-16}
Q_c (cal/mol)	57300	τ (superficial energy) (erg/cm^2)	600
n (*)	6	T (K)	1073
μ (dyn/cm^2)	7×10^{11}	d (cm)	0.0005
D_v (cm^2/s)	4×10^{-12}	Δ (cm)	5.0229×10^{-8}
D_b (cm^2/s)	6.28×10^{-9}		

Table 2.13 Ashby-Verrall model parameters for the Steel tested. (*) A_1 is an adimensional constant and n is an adimensional exponent

The calculus of the D_V and D_B coefficients that influence the creep, superplasticity and hot work laws was made in the following way [12]:

- The D_V coefficient matches the one for auto-diffusion in the ferrite, and is responsible for the volume diffusion, the creep by sliding and the dislocation climbing, also partly, of the superplasticity. Its value is:

$$D_V = 2\ exp\left(\frac{-\frac{57{,}300cal}{mol}}{RT}\right)\left[\frac{cm^2}{s}\right]$$

  which at $800°C$ takes the approximate value of 5×10^{-12} cm^2/s.
- The D_B coefficient calculus is based on the superplastic behavior of the steel at 750 and 800°C when slowly deformed by traction (results are shown in Table 2.14).

  Applying the general law $\sigma = K\dot{\varepsilon}^m$, it may be deduced that:

$$m_{800°C} = \frac{log\left(\frac{5.73}{3.44}\right)}{log(5)} = 0.32$$

  and

$$m_{750°C} = \frac{log\left(\frac{5.73}{3.31}\right)}{log(5)} = 0.34$$

  Leading to a "slightly superplastic" behavior with a value of $m \approx 0.33$. Comparing the results of the traction tests and using the general law for creep:

$$\dot{\varepsilon} = K{\varepsilon_1}^m \exp\left(\frac{-Q}{RT}\right)$$

then:

$$\frac{\dot{\varepsilon}_{800}}{\dot{\varepsilon}_{750}} = \frac{5.56 \times 10^{-5}}{9.92 \times 10^{-5}} = \left(\frac{3.44}{3.31}\right)^{\frac{1}{m}} \exp\left[\frac{-Q}{R}\left(\frac{1}{1073} - \frac{1}{1023}\right)\right]$$

where

$$\exp\left[\frac{-Q}{R}\left(\frac{1}{1073} - \frac{1}{1023}\right)\right] = \frac{1.904}{1.123} = 1.695$$

and solving for the activation energy:

$$Q = \frac{2 \cdot 0.528 \cdot 1073 \cdot 1023}{50} \approx 23{,}180 \text{ cal/mol}$$

In other words, a value of activation energy at half the one required for the volume diffusion ($Q_V = 57{,}300$ cal/mol), can be identified with the activation energy for the grain boundary diffusion (Q_B). Therefore, the value of D_B will be:

$$D_B \approx \exp\left(\frac{-23{,}180}{2 \cdot 1073}\right) = 2 \times 10^{-5} \text{cm}^2/\text{s}$$

which is seven orders of magnitude higher than D_V. Using the general formula:

$$D_{app} = D_V\left[1 + \frac{\pi\delta}{d}\frac{D_B}{D_V}\right]$$

$$D_{app} = 5 \times 10^{-12}\left[1 + \frac{\pi\, 5 \times 10^{-8}}{5 \times 10^{-4}}\frac{2 \times 10^{-5}}{5 \times 10^{-12}}\right] \approx \frac{\pi\, 5 \times 10^{-8}\, 2 \times 10^{-5}}{5 \times 10^{-4}}$$

$$\approx 6.28 \times 10^{-9} \text{ cm}^2/\text{s}$$

In other words, the global diffusion coefficient (D_{app}) is three orders of magnitude higher than the volume diffusion, this shows the importance of the grain boundary diffusion coefficient, the matter transport through the grain boundaries to accommodate and fill the sliding of the grain boundaries in the superplastic behavior.

Temperature	L_0	v_T	$\dot{\varepsilon}_0$	Yield stress (kg/mm^2)
800	30	0.5	2.78×10^{-4}	5.73
800	30	0.1	5.56×10^{-5}	3.44
750	57	0.5	1.46×10^{-4}	5.73
750	57	0.1	2.92×10^{-5}	3.31

Table 2.14 Results at 750 and 800°C for the calculus of grain boundary diffusion

Figure 2.61b presents the values of the logarithm of yield stress/shear modulus ($\log(\sigma/\mu)$) vs. the values of the logarithm of strain rate ($\log(\dot{\varepsilon})$) for both the strain rate due to diffusion accommodated flow and the strain rate due to dislocation creep mechanisms. From the figure three stages can be deduced:

1. A first stage dominated by $\dot{\varepsilon}_{D-A\,flow}$ for values of $\sigma/\mu \leq 10^{-3}$ and $\dot{\varepsilon} < 10^{-4}\ s^{-1}$.
2. A second stage where both $\dot{\varepsilon}_{D-A\,flow}$ and $\dot{\varepsilon}_{dislocation\,creep}$ act together for values of $10^{-3} < \sigma/\mu < 10^{-2}$ and $10^{-4} < \dot{\varepsilon} < 10^{-2}\ s^{-1}$.
3. And a third stage where $\dot{\varepsilon}_{\text{dislocation creep}}$ is the main mechanisms for values of $10^{-2} < \sigma/\mu < 1$ and $\dot{\varepsilon} > 10^{-2}\ s^{-1}$.

Furthermore, Figure 2.61a takes into account both components of the strain rate to graph the integrated curve of the Ashby-Verrall model (behavior law) of the steel investigated at $800°C$ and a grain size of $5\ \mu m$.

Moreover and taking into account the data from Figure 2.61b, in particular its slope, coefficient m can be calculated, the results are shown in Figure 2.61c where the superplastic window can be determined, in other words, the interval of stresses and strain rates where the steel behaves superplastically. This figure can be compared to Figure 2.22a which shows the experimental curve of this coefficient.

The curve of Figure 2.61c has an approximate center at strain rates close to $10^{-5}\ s^{-1}$ and creep stresses of $30{\sim}40\ MPa$. The value of the m coefficient supposes that the structure of the steel is 100% ferritic, which is not the case for the steel investigated.

Finally, Figure 2.62 compares the "ideal" superplastic behavior for grain sizes of 1, 5 and $10\ \mu m$ respectively, along with the experimental values. They are closer to the theoretical curve of a $5\ \mu m$ grain size steel.

The theoretical behavior is that in stage I, creep stresses diminish with the increase in grain size, which means that with low strain rates, the intergranular straining mechanism would stop being dominant (creep stresses lower than $1\ MPa$) at least initially.

The sliding and climbing of dislocations would be energetically favorable compared to the intergranular one. This is contrary to what happens in stage III (characterized by creep straining or creep by cavitations) which is linked to intergranular straining and decohesions.

Also, Figure 2.62 shows the equation that describes the sigmoidal curve of the behavior of the steel; which is:

$$y = -0.0206x^3 - 0.2812x^2 - 0.968x - 3.9098$$

that has a correlation of 0.9846, a value close to 1 means the equation closely has the same tendency as the experimental data.

A possible explanation why the experimental curve crosses the 1, 5 and $10\ \mu m$ curves is the grain size distribution present in the steel: there are grains with sizes of $10\ \mu m$ and grains with sizes of $1\ \mu m$. Also, the presence of precipitates (Ti, Nb) C influence the mechanical behavior of the steel by the anchoring effect previously mentioned.

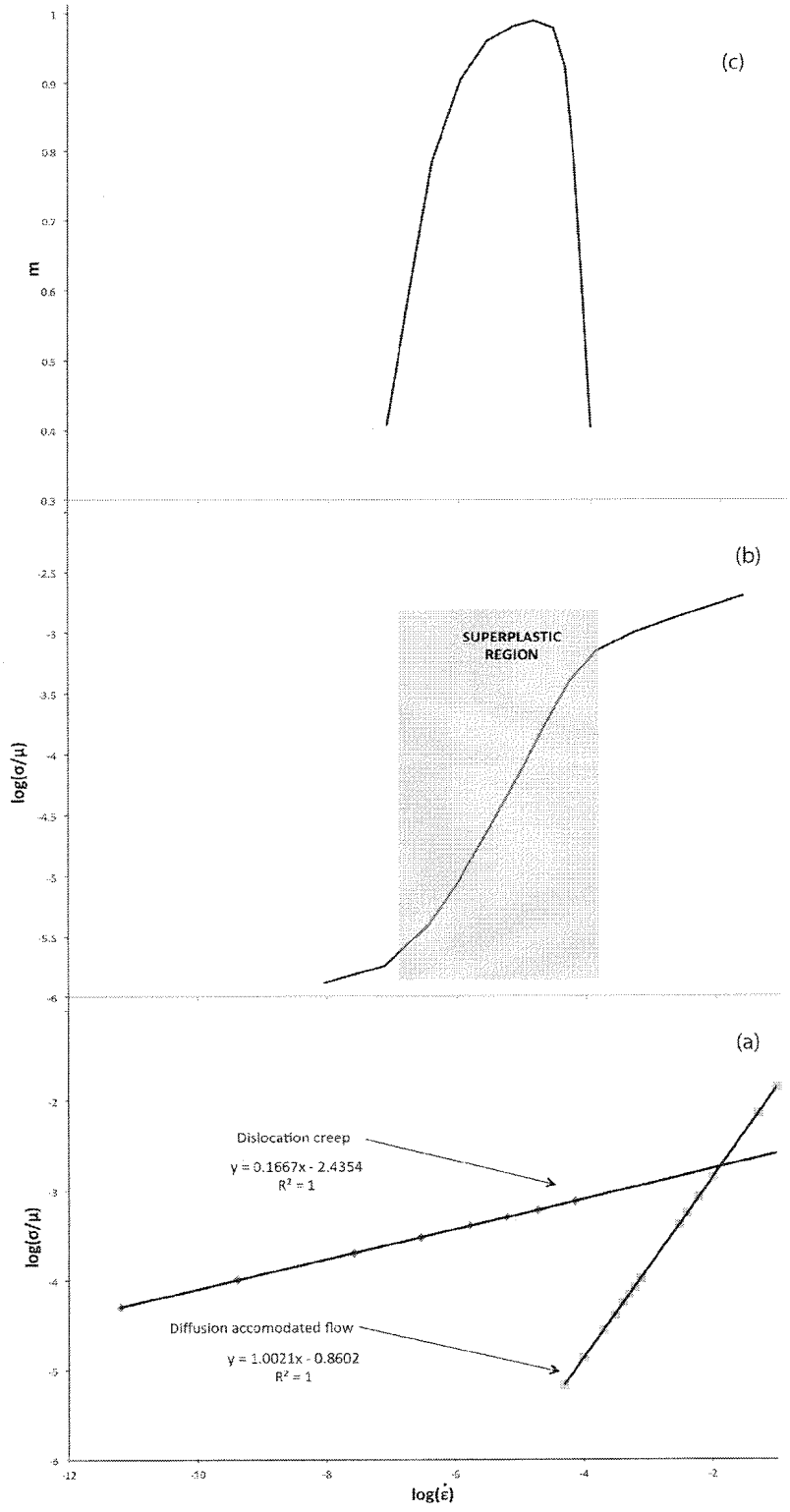

Figure 2.61 a) Mechanisms acting on the behavior of the steel tested, b) Sum of both mechanisms showing the superplastic region and c) m coefficient for the steel tested

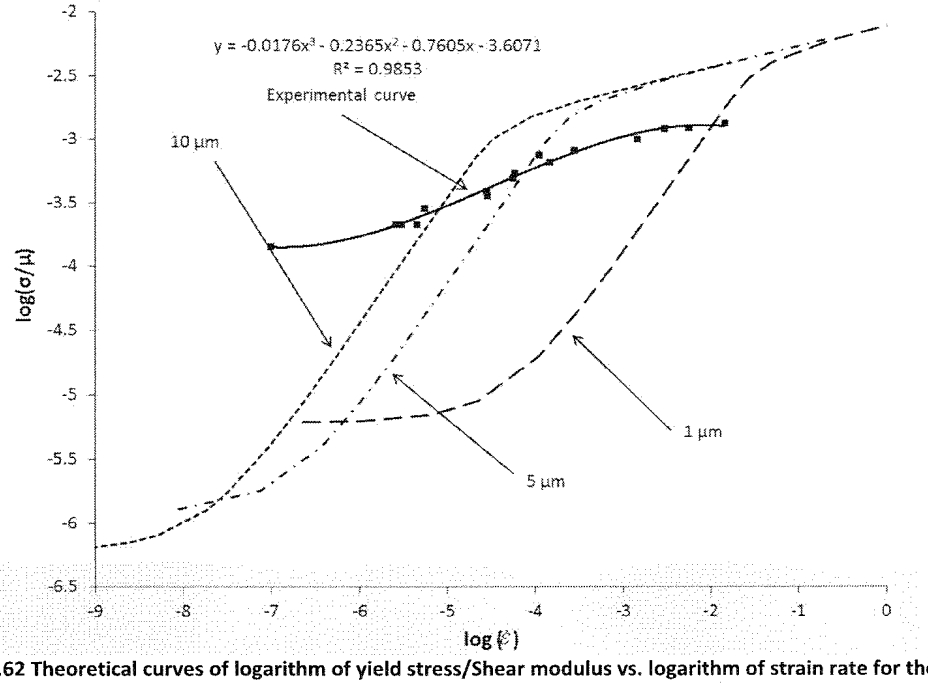

Figure 2.62 Theoretical curves of logarithm of yield stress/Shear modulus vs. logarithm of strain rate for the steel investigated considering different grain sizes

2.4 Statistical confidence level evaluation for experimental procedures in metallography and mechanical testing of the investigated steels

For the quantitative metallographic analysis of grain size, phase distribution and volume fraction of minority constituents, measurements were made in an automatic digital image analysis equipment coupled to a metallographic optical microscope, considering the ASTM E-112 and E-1181-02 standards.

Counting contemplated as many micrographs as necessary to obtain main values of grain size G and mean linear intercept $\bar{L}$ with a confidence level interval of 95% and a deviation lower than 10%. The relation between G and $\bar{L}$ was obtained using the formula:

$$G = -3.356 - 6.644 \log \bar{L}\,(\mathrm{mm})$$

In the case of DP steels, magnifications higher than 100 were used (as these are ultrafine steels) and qualitative determination of the ASTM G number was made using the formula:

$$\text{ASTM } G = G' + 6.64 \log \frac{M}{100}$$

where G' is the ASTM grain size measured as if the micrograph was taken at $100x$ and M is the actual magnification of the micrograph.

The measurement of the mean linear intercept is automatically performed by the equipment on lines traced on the micrograph at 0, 45, 90 and 135° from the rolling direction. The volume fraction f_v, for example for the pearlite, is measured by point counting analysis on the micrographs using a mesh of dots with an optimal gap in order to avoid that two consecutive dots are placed in the same pearlite colony. The number of dots measured was at least 396, which results in $f_v/\sigma_v = 0.05$, where σ_v is the standard deviation in statistical analysis, resulting in a confidence level of 95% for the pearlite volume fraction.

To determine the mechanical properties of the steels, a load cell 2518-111 in a universal testing machine INSTRON model 5583-Standard was used. The manufacturer assures that this cell has an accuracy of $\pm 0.5\%$ of the load measured in Newtons. Figure 2.63 shows an example of a curve stress vs. strain and the higher and lower limits for the measurement of stress in all the curves. On the other hand, for all the mechanical tests, at least two tests were made in order to confirm the repeatability of the data obtained or were repeated for those tests where the data was inconsistent.

In the case of the measurement of strain at high temperatures, the manufacturer assures a variation of $\pm 0.05\%$ to the displacement measured in mm or ± 0.01mm (whichever is greater). This results in the tests of specimens with $L_0 = 30$ mm in an error in the strain of $0.03 \sim 0.05\%$.

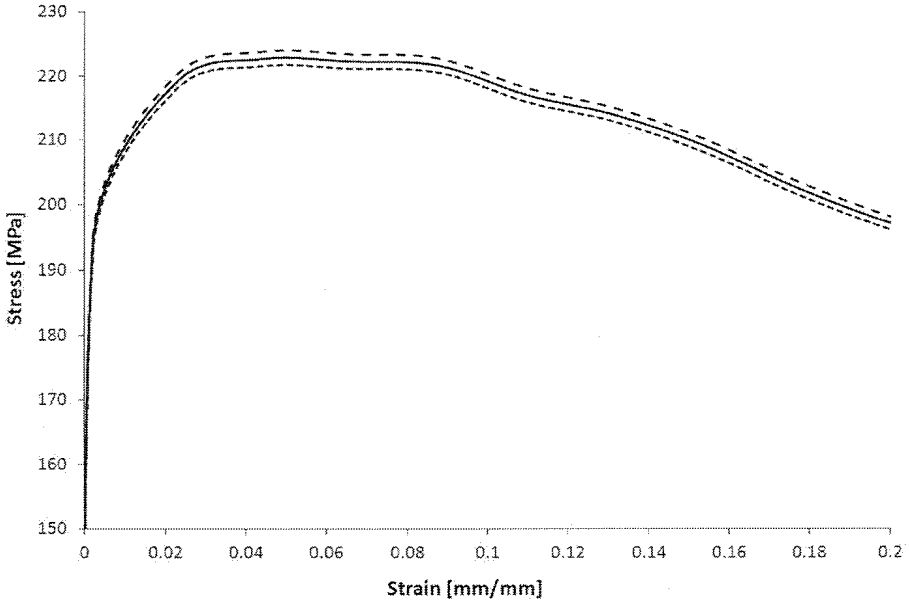

Figure 2.63 Stress vs. Strain curve showing the upper and lower limits due to load measurement accuracy of the testing equipment

On the other hand, tests at high temperature use a furnace with thermocouples that have an accuracy of $\pm 2.2°C$ or $\pm 0.75\%$ (whichever is great); resulting in an error of $\pm 6°C$ for tests at $800°C$. Furthermore, during the tests the maximum variation the furnace control had was $\pm 2°C$, this variation added to the one of the thermocouples results in a total error in the temperature of $\pm 8°C$.

2.5 References

1. **Urcola, J.J. and Fuentes, M.** 5, 1980, Revista de Metalurgia del CENIM, Vol. 16, pp. 263-267.

2. **Urcola, J.J. and Fuentes, M.** 6, 1980, Revista de Metalurgia del CENIM, Vol. 16, pp. 337-342.

3. **Urcola, J.J. and Fuentes, M.** 1, 1981, Revista de Metalurgia del CENIM, Vol. 17, pp. 9-15.

4. *Strengthening of austenite by niobium...* **Dutta, B. and Sellars, C.M.** 1986, Material Science and Technology, Vol. 2, pp. 146-153.

5. *Recrystallization and grain growth in hot rolling.* **Sellars, C.M. and Whiteman, J.A.** 1979, Metal Science, pp. 187-194.

6. *Effect of composition and process variables...* **Dutta, B. and Sellars, C.M.** 1987, Material Science and Technology, Vol. 3, pp. 197-206.

7. **Baudelet, B.** 1971, Mémoires scientifiques de la Revue de Métallurgie, Vol. 68, p. 479.

8. **Pero-Sanz, J.A.** *Ciencia e Ingeniería de Materiales.* Madrid : CIE-Dossat 2000, 2006.

9. *Superplasticity: A Review.* **Davies, G.J., Edington, J.W. and Cutler, C.P.** 8, 1970, Journal of Materials Science, Vol. 5, pp. 1091-1102.

10. *Controlled Rolling of Steel Plate and Strip.* **Tanaka, T.** 1981, International Metals Reviews, Vol. 4, pp. 185-212.

11. **Vander Voort, G.F.** *Metallography Principles and Practice.* s.l. : ASM International, 1999.

12. **Porter, D.A., Easterling, K.E. and Sherif, M.Y.** Phase Transformations in Metals and Alloys. 2009, 2, pp. 63-110.

13. *Diffusion-accomodated flow and superplasticity.* **Ashby, M.F. and Verrall, R.A.** 1973, Acta Metallurgica, Vol. 21, pp. 149-163.

3 Discussion

3.1 Iron-Carbon phase diagram

Figure 3.1 shows the iron - cementite phase diagram. It is important to point out the two fundamental transformations that take place on the left hand side of the diagram:

1. Peritectic reaction ($L + \delta \rightarrow \gamma$) happening at $1495°C$ and at 0.17% C.
2. Eutectoid reaction ($\gamma \rightarrow \alpha + Fe_3C$) occurring at $727°C$ and at 0.77% C.

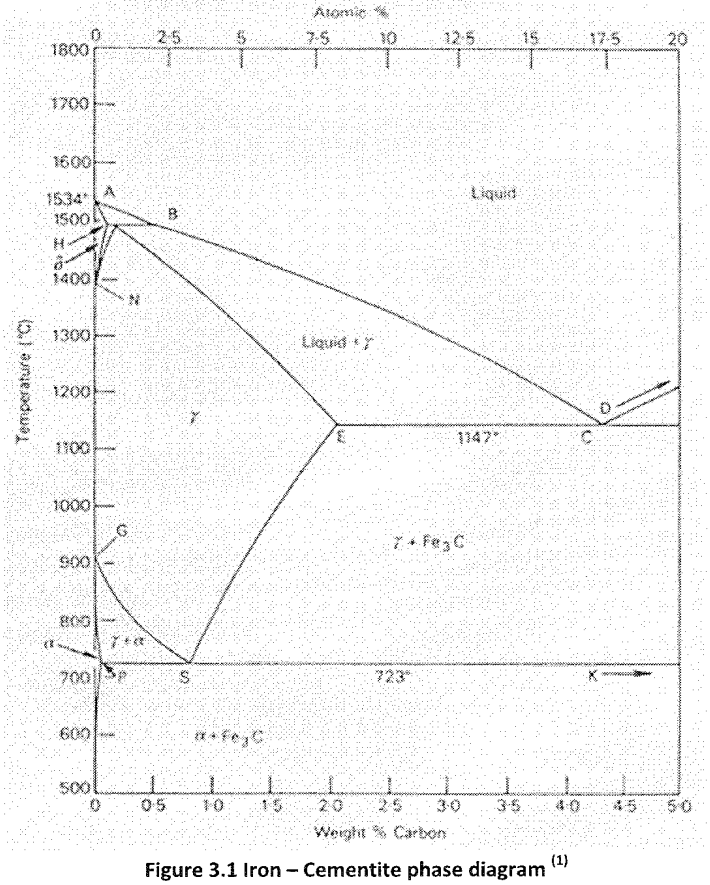

Figure 3.1 Iron – Cementite phase diagram [1]

It is noteworthy that the peritectic reaction and the segregation of manganese, silicon, chromium and molybdenum during solidification are responsible for the banded and anisotropic microstructure obtained in both DP and HSLA steels. In other words, the manganese reduces the activity of carbon in the austenite, thus the carbon segregates with the manganese and during hot rolling processes the pearlite forms on the regions with concentrations of carbon and manganese [2].

Furthermore, the role of alloying elements in a phase diagram is changing the solid state transformation curves, in other words the A_3 and A_1 temperatures. Consequently, two types of alloying elements can be distinguished: ferrite-former elements and austenite-former elements.

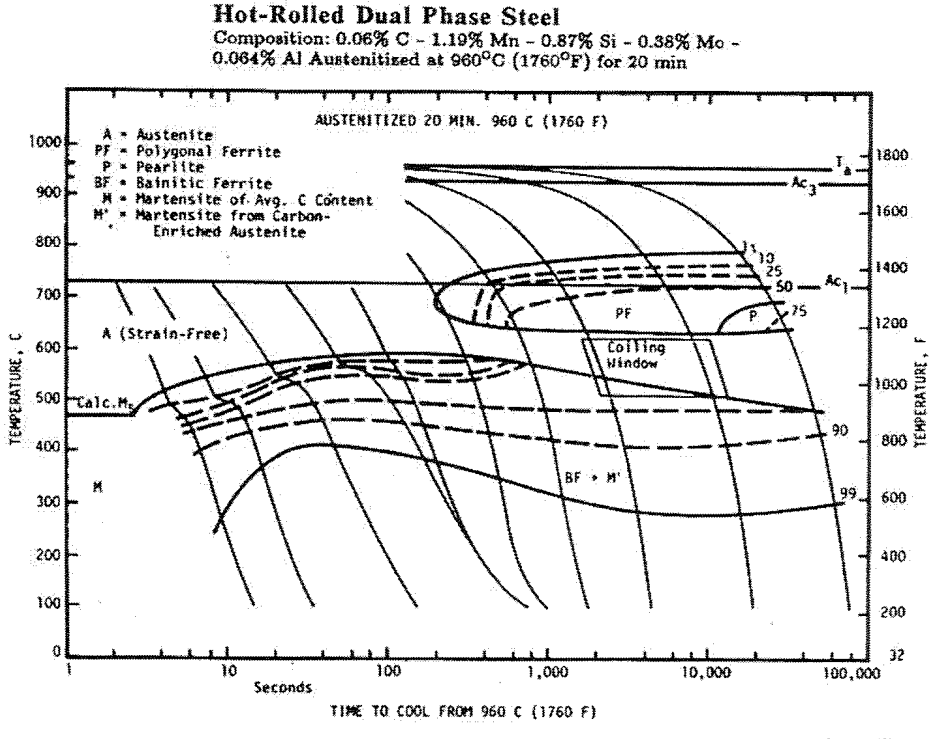

Figure 3.2 Time-Temperature-Transformation diagram of a hot rolled dual phase steel showing the coiling window [3]

The austenite-former alloying elements present in the steels tested include carbon, silicon, chromium and manganese which tend to separate the ferritic-pearlitic transformation from the bainitic-martensitic one in order to obtain a coiling window

(Figure 3.2) and as a result the DP steels; while the ferrite-former alloying elements include chromium, molybdenum, titanium, niobium and vanadium. Titanium and niobium usually avoid the ferritic grain growth by the means of precipitation, particularly the titanium precipitates in the roughing process as shown in the previous chapter while niobium tends to grow on titanium carbonitrides already formed. On the other hand, vanadium is normally used to harden the ferrite.

Moreover, when the controlled rolling process ends, the microstructure is formed by austenite, and it must be quenched (sometimes using pulverized water, as in the case of DP steels) in order to obtain the requirements, thusly changing the cooling rate of the material and producing a banded structure of ferrite and bainite/martensite.

3.2 Advanced Thermomechanical Controlled Rolling Processes

A result of the controlled rolling, the steels acquire a very fine ferritic grain size (UFF or Ultrafine Ferrite), through three sequential processes:

1. The precipitation of titanium carbonitrides (in the thermal homogenization process) and niobium carbonitrides (in the delay and finishing processes).
2. The mentioned precipitation delays the austenitic static and dynamic recrystallization, increases the non-recrystallization temperature and accumulates straining in the non-recrystallized austenite.
3. The allotropic transformation of austenite into ferrite over a fine or very deformed recrystallized austenite. This must occur at the end of the controlled rolling process.

The fine grain size is the goal of every hot rolled material obtained by controlled rolling processes. The titanium precipitates start to have an effect in the roughing process, avoiding high grain growth of the austenite between passes through the pinning effect on the grain boundary and obtaining at the end of the roughing, an austenitic grain size of 30~40 μm. Afterwards, in the delay time, the temperature is ideal for the niobium to precipitate which also avoids the grain growth and increases the time required for the austenite to recrystallize; the result is that at the end of the finishing process the

microstructure is formed by non-recrystallized austenite and niobium precipitates in both its grain boundaries as well as inside the crystals. After this, two routes were to be taken, fast cooling (pulverized water) to obtain ferrite and martensite-bainite bands (DP steels) or slow cooling to obtain ferrite and pearlite bands (HSLA steels).

Therefore, the microalloying elements play a fundamental role in order to achieve a ferritic grain size as small/fine and homogeneous as possible; this, as shown in the previous chapters, is a fundamental condition for the creation of HSLA steels and a necessary condition for a material to present superplastic behavior along with other requirements.

3.3 Room temperature behavior of DP steels

The ATMCRP creates double-phase ferritic-martensitic microstructures and, depending on the chemical composition of the steel, different amounts of martensite (20 to 45%) and ferritic grain size (14 to 18 ASTM G).

Comparing Figure 2.8, Figure 2.10d and Figure 2.11d, it can be concluded that the DP780 steel has a higher resistance than the DP600 because of its higher amount of martensite in the microstructure as this phase (geometry) is an effective barrier to dislocations when the material is being deformed. Furthermore, the higher plasticity of the DP600 can be explained through the higher amount and larger grain size of ferrite (Figure 2.10c and Figure 2.11c).

Moreover, when looking closer at the stress-strain curve of Figure 2.8 into the zone close to the yield stress, the DP600 presents instability (564 MPa) which means that the material's plastic deformation process is mainly controlled by the deformation of grains or zones of ferrite (as shown in Figure 2.12a). On the other hand, the smoothness of the DP780 curves is evidence of the interaction between the martensitic (hard) and ferritic

(soft) phases; the martensite crystals act as stress concentrators and their adjacent ferritic grains must suffer plastic deformation and furthermore there are ferrite grains with internal stresses generated during the volume change of austenite into martensite, resulting in a plastic deformation with a n coefficient of 0.2. This strain hardening coefficient in both steels (DP600 and DP780) is high enough to allow subsequent manufacturing processes (drawing or bending) of parts [4].

In other references it has been observed that a n coefficient lower than 0.1 results in instabilities during the rolling processes and/or manufacture of the finished products (particularly for automotive applications). Thusly, the ATMCRP are attractive to obtain steels with tension stresses between 650 and 800 MPa and plastic deformations between 12 and 20%, for low-weight applications and/or high mechanical reliability [5; 6; 7; 8].

From Figure 2.10c and Figure 2.11c there is evidence of a second ferrite mean grain size in the right hand size of the histograms. This result can be explained when looking at the microstructure with higher magnifications; the martensite bands are not only formed of martensitic grains, trapped between these grains are very fine grains of ferrite (grain sizes of ~ 0.01 μm).

Furthermore, Speich [9] and Bucher and Hamburg [10] proposed two equations to calculate both the yield and the tension stresses in DP steels:

$$\sigma_y = f_\alpha\left(54 + 17 d_\alpha^{-1/2}\right) + f_\mu \frac{\sigma_{y\mu}}{3} \quad [3.1]$$

$$\sigma_{max} = 354 + 10.5(\%\mu + \%B) + 7.84 d_\alpha^{-1/2} \quad [3.2]$$

where σ_y is the yield stress [MPa], σ_{max} is the tension stress [MPa], f_α is the ferrite fraction, f_μ is the martensite fraction, $(\%\mu + \%B)$ is the amount of bainite and martensite, d_α is the ferritic grain size [mm] and $\sigma_{y\mu}$ is the yield stress of the martensite calculated through:

$$\sigma_{y\mu} = 620 + 2585 c_\mu \quad [3.3]$$

where c_μ is the carbon content of the martensite obtained by:

$$c_\mu = 100\frac{c_0}{f_\alpha} \qquad [3.4]$$

being c_0 the initial carbon content of the steel.

Figure 3.3 shows the graphic representation of equations [3.1] and [3.2] for the DP600 steel, the intersection of both stresses is at $0.2\ \mu m$, which means that if this material has a grain size of this value or a smaller one, the ductility will be lost; also, in order for the material to be effective in the drawing and bending processes (strain hardening coefficient n higher than 0.2) the grain size must be higher than $2.4\ \mu m$.

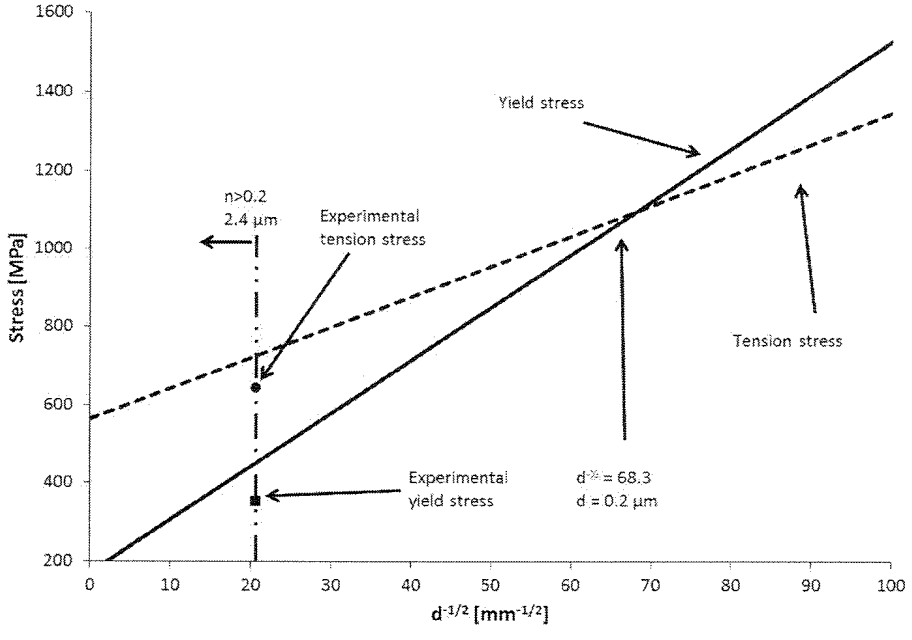

Figure 3.3 Relationship between stress and grain size of DP600 steel

Figure 3.4 shows the same graph but for the DP780 steel, the intersection of both stresses is at $0.02\ \mu m$ (which means the ferrite has a grain size in the nanometric scale), meaning that the steel will lose its ductility if the grain size is of this value or lower; also, in order for the material to be effective in the drawing and bending processes, the grain size must be higher than $0.8\ \mu m$.

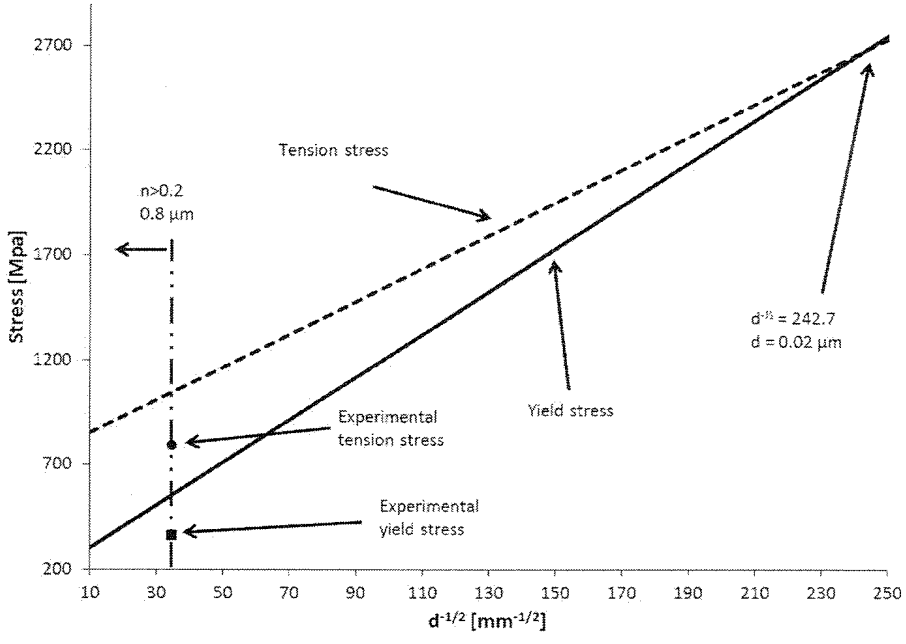

Figure 3.4 Relationship between stress and grain size of DP780 steel

3.4 High temperature behavior of HSLA steels and superplasticity

When hot deformed or traction tested, the behavior of a material can be described in three stages as [11]:

1. Initial or microstrain deformation: the plastic strain rate in the sample goes from zero to the value of the test. The stress increases fast, though slower than in tests made at usual temperatures.
2. Strain/work hardening: the slope of the curve is reduced in about one order of magnitude and is sensitive to both temperature and strain rate. The work hardening diminishes gradually until the third stage begins.
3. Steady state region: the strain hardening is zero and the three variables (stress, temperature and strain rate) remain constant, meaning this part of the curve is a horizontal straight line. This horizontal only happens in those cases where the only mechanism acting is the dynamic recovery. But in the cases of dynamic recrystallization, adiabatic heating, precipitate coarsening or superplastic flow

acting together with the dynamic recovery, this part of the curve has a descending slope as is the case of most of the curves of Figure 3.5.

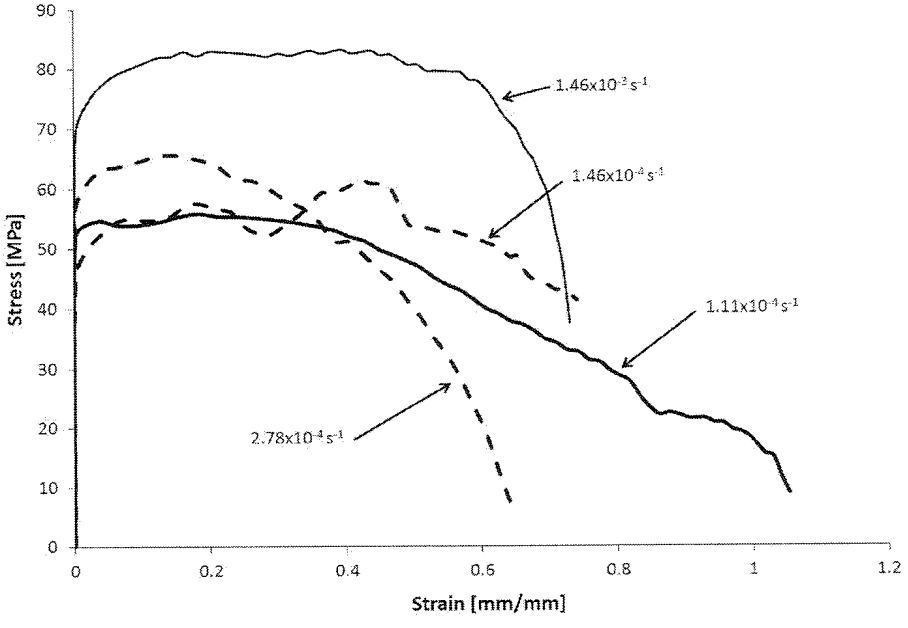

Figure 3.5 True stress vs. true strain of samples tested at 800°C

Superplastic behavior as described in chapter one is a necking phenomenon when a material is traction tested, in particular a diffuse neck will form on the specimen as shown in Figure 3.6. Furthermore, the flow stress is highly dependent on the strain rate, though this last condition varies along the section of the specimen and is inversely proportional to its cross-section area. However, the dynamic equilibrium is maintained by the difference in strain rates at the locations with the largest and smallest cross-sections [12].

The results of tension tests made at high temperatures on the steel show that both the temperature of the test as well as the strain rate must be adequate in order to obtain superplasticity (close to 200% in elongation). Though the curves of Figure 2.17 have the usual shape obtained in a high temperature tension test, when the strain rate is lowered (Figure 2.18) unusual behavior, such as the formation of more than one necking zones during plastic deformation, starts to show. From Figure 2.17, Figure 2.18 and Figure 2.19,

it is evident that the material presents elongations much higher than at any other temperature.

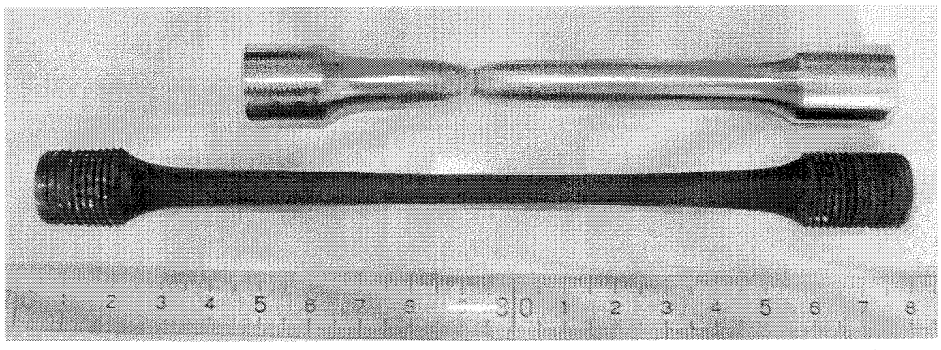

Figure 3.6 Specimens with a localized neck (upper part) and a diffuse neck (lower part)

The behavior of the steel tested at high temperatures (Figure 3.5) presents three strain mechanisms related to the traction speed (time elapsed in the test):

1. A first one associated to the deformed ferrite, dynamically restored ($5\ \mathrm{mm/min}$ curve).
2. A second one initially superplastic, but with non-stable microstructure, continued by grain growth that induces hardening (ferrite restoration) and concluded by localized necking (conventional) ($0.5\ \mathrm{mm/min}$ curve).
3. A third one, also superplastic, that applies to stable or nearly stable structures that do not stop the intergranular straining associated to superplasticity. The mechanisms of straining by sliding and climbing of dislocations, as well as intergranular sliding accommodate by diffusion mainly at the grain boundaries (Ashby-Verrall model) are the dominating ones ($0.2\ \mathrm{mm/min}$ curve).

The microstructure of the steel of Figure 2.24 is formed by bands of pearlite and ferrite, which is typical in construction steels that suffered a peritectic reaction and solidification under non-equilibrium conditions. As the proportion coefficient for carbon, alloying elements (Mn, Si, Cr and Mo) and impurities (P and S) in this steel is lower than one, the microstructure cannot be regenerated through soaking treatments before hot rolling processes [(1)].

The microstructure after high temperature superplastic deformation is a homogeneous one formed by ferrite grains that are slightly elongated in the rolling

direction with evidence (subgrains) of having suffered dynamic recovery during deformation along with very fine ferrite grains close to pearlite grains (Figure 2.32 and Figure 2.33). Furthermore, the following can also be seen:

- The banding has nearly disappeared but there still are zones with large amount of ferritic grains and zones with large amounts of pearlite.
- Decohesions shaped as w and r, mainly located in the ferrite/pearlite interphase, are unequivocal proof of intergranular sliding during the deformation process.
- Small cavities in the α-pearlite (previous austenite grains) interphase, which shows different deformation capacity for each of these phases.
- Null evidence of generalized grain growth during deformation, as grain size is very similar to the original one.
- Grain (or grain clusters) sliding and rotating, as a consequence of superplastic deformation.

At $750°C$ the material does not behave superplastically, the banded microstructure from the hot rolled raw state disappears and only ferrite grains that have suffered dynamic recovery along with carbides in their grain boundaries remain (Figure 2.41 and Figure 2.42). Furthermore, the theoretical Iron-Cementite Phase Diagram (Figure 3.1) shows that at both 800 and $750°C$, the microstructure should be the same. A possible explanation is that these tests imply a negative pressure on the sample (typical phase diagrams consider a pressure of $1\ \mathrm{atm}$) which could induce a change in the eutectoid temperature and its movements upwards in the diagram (Figure 3.7) which would result that at $750°C$ the material would be on a different zone than at $800°C$. In an invariant phase transformation, the temperature variation caused by a pressure change equals enthalpy change divided by the product of temperature and volume change which is known as the Clausius-Clapeyron equation; since austenite has a smaller molar volume than pearlite, then the volume change is less than zero, while the enthalpy change is also less than zero, therefore the temperature variation caused by a pressure change is negative. Furthermore, an increase in pressure lowers the equilibrium transition temperature and viceversa [13].

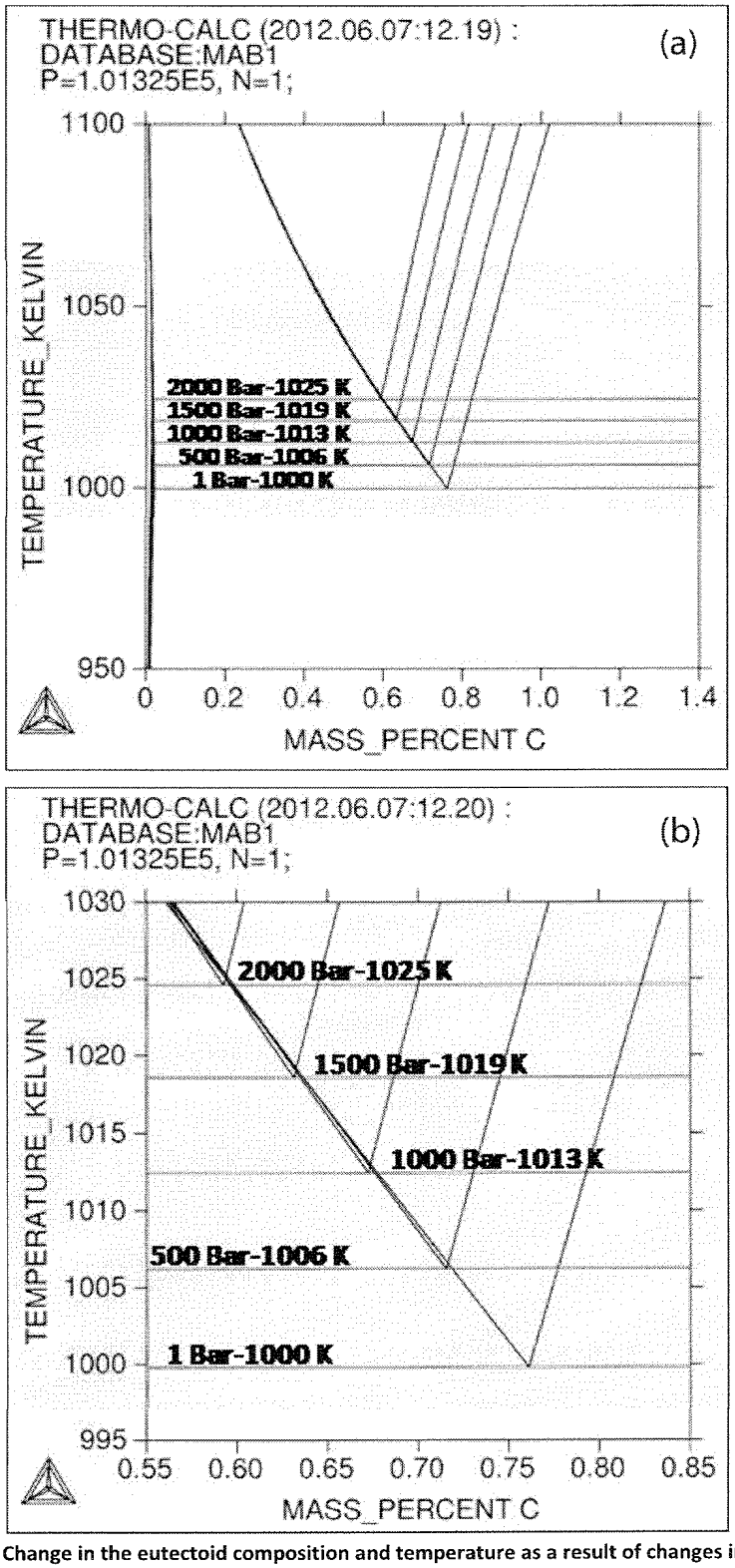

Figure 3.7 Change in the eutectoid composition and temperature as a result of changes in pressure

The free energy curve as a function of the concentration of a phase in a system can be calculated for each temperature. The tangent line to this curve would allow the calculation of the chemical potential of each of the phase's constituents. In the case of equilibrium between phases, there will be a common tangent line to the curve and thusly defining the equilibrium as the chemical potentials must be equal in all of them (thermodynamical equilibrium); the use of all this information can result in the creation of phase diagrams using thermodynamics.

The term PV (being P the pressure and V the molar volume of a phase) is normally ignored when creating phase diagrams because: first, the processes usually happen at atmospheric pressure and second, the necessary pressures for the resulting energy change to be high enough for it to be a factor in the system are very high, which means they can be ignored. However, in some systems (in the case of the HSLA steel tested at high temperatures) there may be a significant increase or decrease in the pressure and therefore in its PV term that could result in changes in the equilibrium conditions and thusly in its phase diagrams. In the case of the HSLA steel tested at high temperature, at the eutectoid point ($1000\ \mathrm{K}$) there are austenite, ferrite and cementite in equilibrium with molar volumes of:

$$\mathrm{Fe_3C}\text{: } \bar{V} = 23.675 \times 10^{-6}\ \mathrm{m^3/mol}$$

$$\mathrm{Fe_\alpha}\text{: } \bar{V} = 7.302 \times 10^{-6}\ \mathrm{m^3/mol}$$

$$\mathrm{Fe_\gamma}\text{: } \bar{V} = 7.164 \times 10^{-6}\ \mathrm{m^3/mol}$$

From these last three values, the molar volume for cementite is more than three times higher than for the other two phases which at high pressures could modify the phase diagram. Using Thermocalc software (PBIN database), the term PV has been introduced, taking into account that the pressure in this case is negative.

From Figure 3.7a it can be observed that a negative pressure of $2000\ \mathrm{bar}$ would move the eutectoid point upwards by $25\ \mathrm{K}$. And from a temperature of 1000 to $1023\ \mathrm{K}$ ($750°\mathrm{C}$) the negative pressure required would be $1825\ \mathrm{bar}$ ($\sim 183\ \mathrm{MPa}$), which is a pressure value similar in magnitude to the negative hydrostatic pressure created by intergranular and ductile decohesions as a result of the traction test.

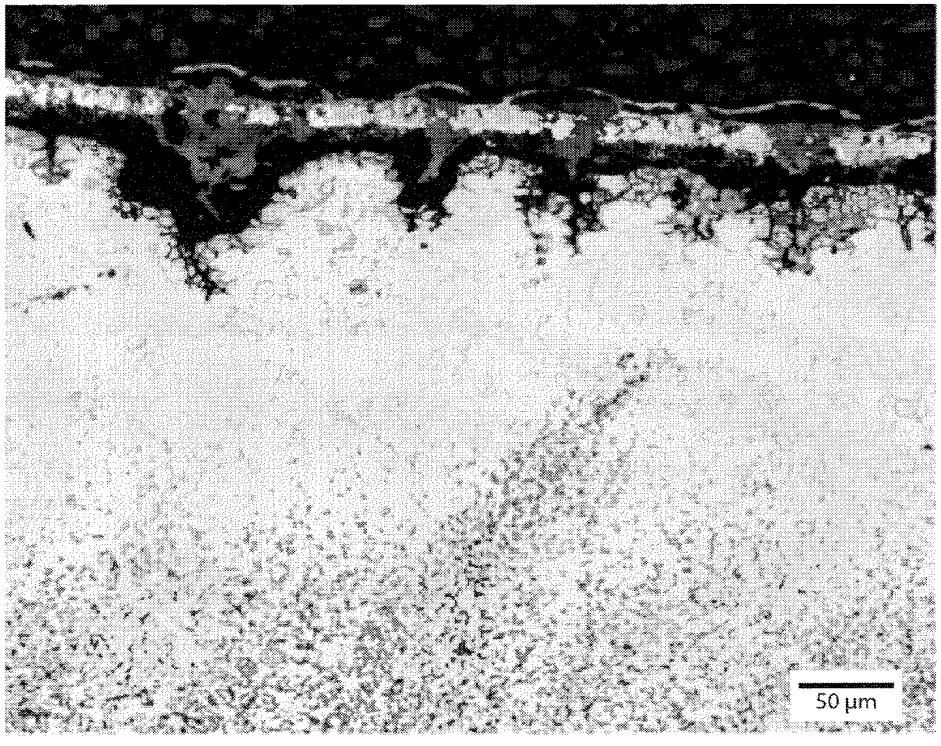

Figure 3.8 Micrograph showing the oxide layer on the surface of the sample

The oxidation suffered by the material also plays a role in its possible superplastic behavior (Figure 2.21 and Figure 3.8) as it changes the relationship between the transverse section of the specimen and its length. Particularly, oxidizing environments can induce a loss of $\sim 50\%$ of material, thusly the grains loose the capacity of rotating and sliding and they behave as typical steels deformed at high temperatures. Specimens tested without protective atmosphere can form scabs on its surface as evidence of the superficial oxidation process and consequently decreasing the possible final elongation of the material.

Furthermore, the oxidation of a particular metal in air is limited by the outward diffusion of metallic ions through an unbroken film of one type of oxide. The kinetics of oxidation of construction steels at high temperature are [14]:

$$\Delta m^2 = K_p t \qquad [3.5]$$

where

$$K_p = 37 \exp\left(\frac{-138\ kJ\ mol^{-1}}{RT}\right)\ \left[\frac{kg^2}{m^4 s}\right] \quad [3.6]$$

At $800°C$ and for the reaction $Fe + O = FeO$ (wustite), the loss in thickness (oxide layer thickness) per hour is approximately $\sim 0.1\ mm/hour$. For an intergranular corrosion process, just as the one observed in traction tests at low strain rates (crosshead speeds of $0.2\ mm/min$) the oxide film acts as an obstacle to the intergranular straining and eliminates the possibility of superplastic behavior on the material.

3.4.1 Ashby-Verrall model for the steel

When analyzing Equation [2.22], the apparent diffusivity is three orders of magnitude higher than the bulk diffusivity. Therefore, the diffusion through grain boundaries is the one ruling the process of intergranular sliding in superplasticity; this diffusion has been widely studied [15].

Any polycrystalline material can deform following the mechanism proposed by the Ashby-Verrall model, described as [16]:

$$\dot{\varepsilon} = \dot{\varepsilon}_{D-A\ flow} + \dot{\varepsilon}_{dislocation\ creep} \quad [3.7]$$

where

$$\dot{\varepsilon}_{D-A\ flow} = 98\frac{\Omega\mu}{KTd^2}\left[\frac{\sigma}{\mu} - \frac{0.72\,\Gamma}{\mu d}\right] D_v\left(1 + \frac{\pi\delta}{d}\frac{D_B}{D_v}\right) \quad [3.8]$$

$$\dot{\varepsilon}_{dislocation\ creep} = A_1\frac{\mu b}{kT}\left(\frac{\sigma}{\mu}\right)^n exp\left[-\frac{Q_c}{RT}\right] \quad [3.9]$$

The overall flow rate (Equation [3.7]) is approximated when adding:

- the model for diffusion-accomodated flow, which is very similar to the Herring-Nabarro-Coble creep model from a mechanical point of view (Equation [3.8]), and
- the model for dislocation creep, which is the most obvious competing mechanism, described by Weertman [17] or Dorn [18], shown in Equation [3.9] leading to a sigmoidal curve as shown in Figure 2.71 where for low strain rates the diffusion accommodated flow (non-uniform deformation) is dominant and for high strain rates the dislocation creep (uniform deformation) is the ruling mechanism, and at superplastic behavior both mechanisms act [16].

Moreover, Figure 3.9 shows evidence of grains that have rotated together (not only one grain but a cluster of grains), even to the point of making the bands vertical instead of horizontal (rolling direction) as they were before the test.

Later on, Vasin et al. [19] described the superplastic behavior in terms of the mechanical response of various combinations of non-linear viscous elements where the main objective would be finding the best combination of both variation of the stress flow (σ) and the strain rate ($\dot{\varepsilon}$) in order to obtain the optimum sigmoidal behavior which seem to be the typical feature of a superplasticity curve. These authors, similar to what Ashby and Verrall [16] did nearly three decades ago, propose a combination of two electrical elements in a parallel configuration (with strain rates corresponding to grain boundary sliding and diffusion creep) and a third element in series with the other two (corresponding to intergranular slip and dislocation creep), also achieving a sigmoidal curve with reasonable accuracy. In other words, a superplastic behavior curve has a sigmoidal shape just as the ones obtained, for the steel tested at $800°C$, in the previous chapter.

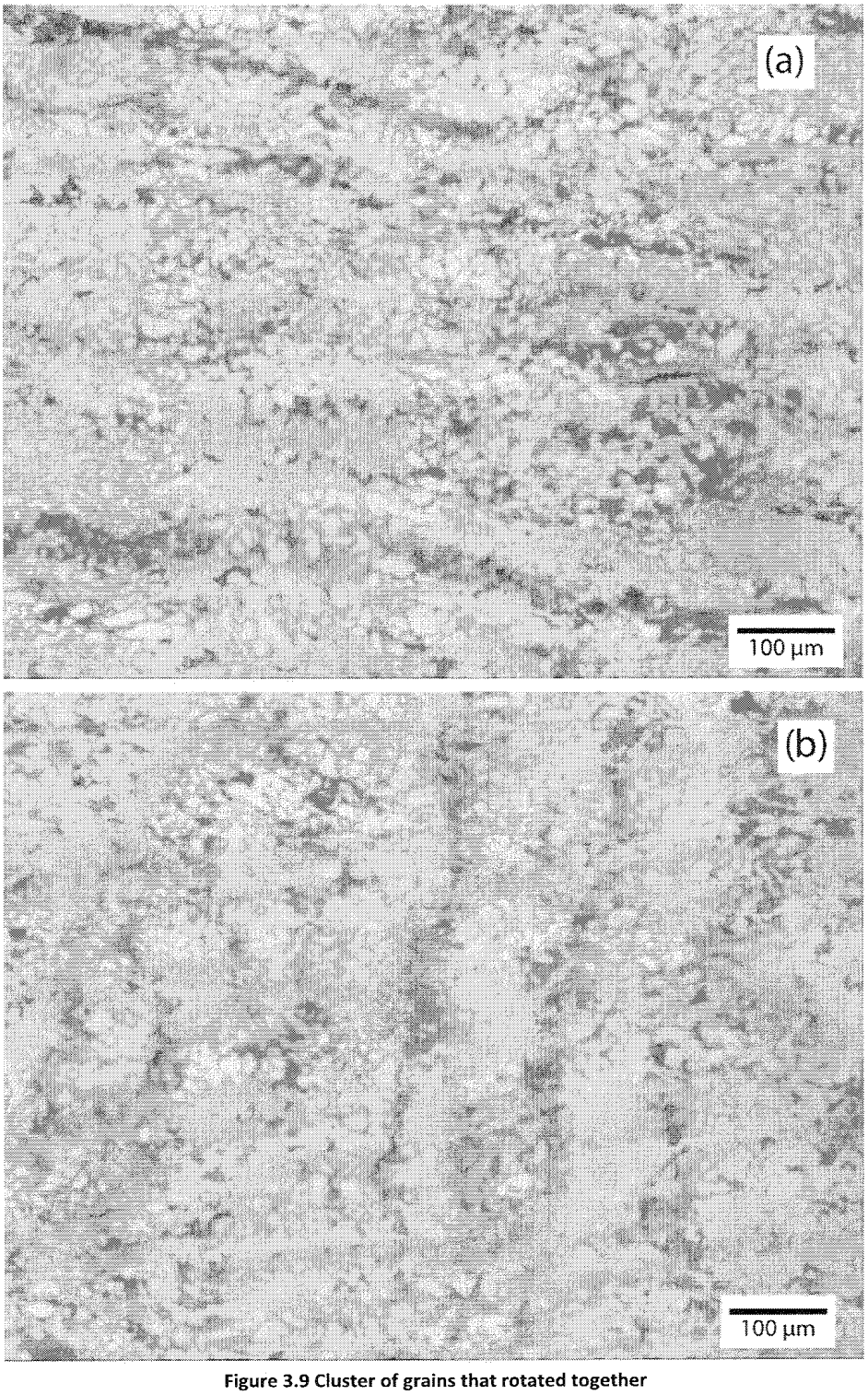

Figure 3.9 Cluster of grains that rotated together

3.5 References

1. **Pero-Sanz, J.A.** *Ciencia e Ingeniería de Materiales.* Madrid : CIE-Dossat 2000, 2006.

2. **Leslie, W.C.** *The Physical Metallurgy of Steels.* Tokyo : McGraw-Hill, 1982.

3. **Vander Voort, G.F.** *Atlas of Time-Temperature Diagrams for Irons and Steels.* s.l. : ASM International, 1991.

4. *Tempering of Ferrite-Martensite Steels.* **Speich, G.R. and Miller, R.L.** [ed.] R.A. Kot and B.L. Bramfitt. Chicago, Illinois : The Metallurgical Society of AIME, 1981. Fundamentals of Dual-Phase Steels. pp. 279-304.

5. *Strength and ductility of ultrafine grained aluminum...* **Tsuji, N., Ito, I. and Saito, Y.** 2002, Scripta Materialia, Vol. 47, pp. 893-899.

6. *Ultrafine grained structure formation in steels using dynamic strain induced transformation processing.* **Beladi, H., Kelly, G.L. and Hodgson, P.D.** 2007, Int. Mater. Rev., Vol. 52, pp. 14-28.

7. *Special Issue on Ultrafine Grained Steels.* **Furuhara, T.** 2008, ISIJ International, Vol. 48, pp. 1037-1157.

8. *A new route to fabricate ultrafine-grained structures in carbon steels without severe plastic deformation.* **Okitsu, Y., Takata, N. and Tsuji, Y.** 2009, Scripta Materialia, Vol. 60, pp. 76-79.

9. *Physical Metallurgy of Dual-Phase Steels.* **Speich, G.R.** [ed.] R.A. Kot and B.L. Bramfitt. Chicago, Illinois : The Metallurgical Society of AIME, 1981. Fundamentals of Dual-Phase Steels. pp. 3-46.

10. **Bucher, J.H. and Hamburg, E.G.** *High Strength Formable Sheet Steel.* s.l. : SAE Reprint 770164, 1977.

11. **Jonas, J.J. and McQueen, H.J.** Recovery and Recrystallization during High Temperature Deformation. *Mise en forme des métaux et alliages.* Paris : Editions du Centre National de la Recherche Scientifique, 1976, pp. 99-143.

12. **Reed-Hill, R.E.** *Creep. Physical Metallurgy Principles.* 2nd. Independence, KY : Cengage Learning, 1994.

13. **Porter, D.A. and Easterling, K.E.** *Phase Transformations in Metals and Alloys.* s.l. : Van Nostrand Reinhold, 1988.

14. **Ashby, M.F. and Jones, D.R.H.** *Engineering Materials 1.* s.l. : Pergamon Press, 1986. Vol. 34.

15. *Structural Superplasticity at Higher Strain Rates of Hypereutectoid...* **Frommeyer, G. and Jiménez, J.A.** 2005, Metallurgical and Materials Transactions A, Vol. 36A, p. 295.

16. *Diffusion-accomodated flow and superplasticity.* **Ashby, M.F. and Verrall, R.A.** 1973, Acta Metallurgica, Vol. 21, pp. 149-163.

17. *Theory of Steady-State Creep Based on Dislocation Climb.* **Weertman, J.** 1955, Journal of Applied Physics, Vol. 26, p. 1213.

18. *Some Fundamental Experiments on High Temperature Creep.* **Dorn, J.E.** 1954, Journal of the Mechanics and Physics of Solids, Vol. 3, pp. 85-116.

19. *Mechanical modelling of the universal superplastic curve.* **Vasin, R.A., Enikeev, F.U. and Mazurski, M.I.** 2000, Journal of Materials Science, Vol. 35, pp. 2455-2466.

4 Conclusions

4.1 Advanced Thermomechanical Controlled Rolling Processes

ATMCRP allow, especially through direct quenching of the steel sheets, modifications in the amount of martensite present in the double-phase steels, as well as the size and distribution of the soft ferrite grains.

HSLA steels microalloyed with Ti – Nb and obtained by ATMCRP are usually ultrafine grained steels with grain sizes lower than $5\ \mu m$.

4.2 Room temperature behavior of DP steels

Thanks to the microstructure (phases present, amount of each phase and its distribution) induced by the ATMCRP, the products made with these steels have mechanical properties such as yield stresses up to $600\ MPa$ and tension stresses close to $800\ MPa$, which is only possible for a low alloy steel if the formed microstructure is of the ultrafine grained type (> 14 ASTM G) along with precipitates of Ti, Nb and V.

On the other hand, it is also very important that the strain hardening coefficient n is higher than 0.15 to avoid instabilities and defects during the drawing and/or bending processes used in the manufacture of products from the automotive industry among others. Otherwise, the steel may have very limited or non-practical applications, and the data obtained for similar microstructures produced at laboratory scale is not relevant for its industrial uses.

The compromise between an UFG microstructure (grain sizes close to or smaller than $1\ \mu m$) and high values of n, is possible because of the internal stresses suffered by the ferrite caused by the transformation of austenite into martensite during cooling.

4.3 High temperature behavior of HSLA steels and Superplasticity

The construction steel microalloyed with Ti/Nb (in the form of carbonitrides of Ti, Nb and V) as a sheet with a thickness of $27\ mm$ and manufactured by hot controlled rolling techniques has an ultrafine grain size (12 ASTM G, $5\ \mu m$). A few of its mechanical properties are: a yield stress of $447\ MPa$, high sub-zero tenacity, low cost and easy to weld. Its production in the Arcelor Mittal factory in Veriña (Gijón, Spain) is higher than $150{,}000$ metric tons per year. HSLA steels obtained by ATMCRP deformed at high temperatures ($750 - 800°C$) in the intercritic region ($\alpha + \gamma$), present superplastic behavior in tension with elongations higher than 100%.

The modeling of the grain size evolution during the roughing process, waiting time and finishing in construction steels microalloyed with Ti/Nb according to the Sellars – Urcola [1; 2] model, lead to the creation, both in plate ($\sim 25mm$) as in strip ($\sim 5mm$), of austenite partially or totally deformed at the end of the ATMCRP. This will result, after the allotropic transformation, in ultrafine ferrite steels (ferrite grain size equal or higher than 12 ASTM G). The banded structure (ferrite-pearlite) phenomenon is directly proportional to the carbon content (between 0.06 and 0.17% C).

The mechanism described by Ashby-Verrall [3] seems to be the most appropriate model to describe this superplastic behavior: rotation and sliding of grains activated by diffusion processes at the grain boundaries. At low strain rates ($\sim 10^{-4} s^{-1}$) the dominating phenomena are rotation and intergranular sliding of the ferrite, diminishing the defects (cavities, pores, decohesions) produced by grain boundary diffusion. At higher strain rates, the mechanism that rules is the dynamic recovery of the ferrite by sliding and climbing of the dislocations (intergranular mechanism) common on conventional hot deformation processes. At the temperature proposed ($800°C$), inside the intercritic stable

ferrite and austenite interval, the construction steels with UFG/UFF microstructure and bands created by hot rolling, with thicknesses lower than 5 mm would be superplastic at strain rates that would make its conventional manufacturing processes competitive.

This steel presents superplastic properties which allow high deformations when traction tested (higher than 100%) when both the temperature and strain rate are adequate. For the steel tested, the strain rate at which the material presents the best superplastic behavior at 800°C is $\sim 10^{-4} s^{-1}$, with yield stresses lower than 60 MPa and elongations higher than 200%. The steel maintains its fine grain size during the straining; the austenite present (transformed to pearlite during cooling) prevents the growth of the superplastic ferritic grains. The original ferritic-pearlitic banded structure evolves into a more homogeneous structure formed by ferrite and pearlite during straining: the bands blur or disappear because of the non-homogeneous deformation of ferritic grain clusters (sliding and rotating). Though these steels may show superplastic deformation at high temperature, this type of deformation does not imply a generalized grain coarsening of the microstructure even when the strain rate is very low ($10^{-5} s^{-1}$).

Finally, at temperatures lower than 800°C (for example at 750°C) steels with mainly ferritic structure behave differently than at this temperature. The austenite becomes thermodynamically unstable in tension, transforming into ferrite and carbides (mainly cementite); during cooling the ferritic grains grow and the steel would, at least partially, lose its superplastic behavior during slow straining deformation. It is important to point out that after testing at 800°C the microstructure is formed by pearlite, ferrite and precipitates, while after 750°C tests, the room temperature microstructure is only formed by ferrite and precipitates.

Therefore the selection of the adequate temperature for straining is critical in UFG construction steels, just as it occurs in conventional superplastic metallic alloys.

4.4 References

1. *Recrystallization and grain growth in hot rolling.* **Sellars, C.M. and Whiteman, J.A.** 1979, Metal Science, pp. 187-194.

2. **Urcola, J.J. and Fuentes, M.** 6, 1980, Revista de Metalurgia del CENIM, Vol. 16, pp. 337-342.

3. *Diffusion-accomodated flow and superplasticity.* **Ashby, M.F. and Verrall, R.A.** 1973, Acta Metallurgica, Vol. 21, pp. 149-163.

4 Conclusiones

4.1 Método Avanzado de Control Termomecánico para Laminación

El método avanzado de control termomecánico para laminación (ATMCRP) permite, a través del templado de las placas de acero, manipular la cantidad de martensita presente en los aceros de doble fase (DP) y también el tamaño y la distribución de los granos suaves de ferrita.

Los aceros HSLA microaleados con Ti y Nb y manufacturados por el mismo método son generalmente aceros de grano ultrafino y con tamaños de grano menores a $5\ \mu m$.

4.2 Comportamiento en frío de aceros DP

La microestructura (fases presentes, cantidad de cada fase y su distribución) resultado de los métodos ATMCRP, se ve reflejada en las propiedades mecánicas de las piezas fabricadas con estos aceros. Estas propiedades incluyen esfuerzos de cedencia de hasta $600\ MPa$ y esfuerzos de tension cercanos a los $800\ MPa$; esto solo es posible si el acero de baja aleación tiene microestructura de grano ultrafino (> 14 ASTM G) y precipitados de Ti, Nb y V.

Por otra parte, es muy importante que el coeficiente de endurecimiento por deformación n sea mayor a 0.15, para evitar zonas de deformación inestable y defectos durante los procesos de estirado y doblado usados en la manufactura de productos para las industrias automotriz y de manufactura en general. Si esto no se cumple, las

aplicaciones prácticas de estos aceros serán muy limitadas o nulas, y los datos obtenidos de materiales con microestructuras similares producidos a nivel de laboratorio no son relevantes para las industrias que pueden utilizarlos.

El balance entre la microestructura UFG (tamaños de grano cercanos a o más pequeños que $1\ \mu m$) y los altos valores de n, existe debido a los esfuerzos internos sufridos por la ferrita generados por la transformación de austenita a martensita durante el enfriamiento.

4.3 Comportamiento en caliente de aceros HSLA y Superplasticidad

El acero de construcción microaleado con Ti y Nb (formando carbonitruros de Ti, Nb y V) en forma de placa de $27\ mm$ de espesor y manufacturado por técnicas de laminación controlada en caliente, tiene tamaño de grano ultrafino (12 ASTM G, $5\ \mu m$). Algunas de sus propiedades mecánicas son: esfuerzo de cedencia de $447\ MPa$, alta tenacidad por debajo del cero absoluto, bajo costo y fácil de soldar. Su producción en la planta de Arcelor Mittal en Veriña (Gijón, España) es mayor a las $150{,}000$ toneladas métricas al año. Los aceros HSLA manufacturados por ATMCRP y deformados a altas temperaturas ($750 - 800°C$) en la región intercrítica ($\alpha + \gamma$), presentan comportamiento superplástico a tensión con elongaciones mayores al 100%.

El modelado de la evolución del tamaño de grano durante los procesos de desbaste, tiempo de espera y acabado en aceros de construcción microaleados con Ti/Nb de acuerdo al modelo de Sellars – Urcola [1; 2], lleva a la obtención, tanto en placas ($\sim 25mm$) como en láminas ($\sim 5mm$), de austenita parcial o totalmente deformada al final del proceso de ATMCRP. Esto resulta, después de la transformación alotrópica, en aceros con ferrita de tamaño ultrafino (tamaño de grano ferrítico igual o mayor a 12 ASTM G). El fenómeno de la estructura bandeada (ferrita – perlita) es directamente proporcional al contenido de carbono (entre 0.06 y 0.17% C).

El mecanismo descrito por Ashby-Verrall [3] es el modelo más adecuado para describir este comportamiento superplástico: rotación y deslizamiento de granos, activado por procesos de difusión en las fronteras de grano. A velocidades de deformación bajas ($\sim 10^{-4} s^{-1}$) el mecanismo dominante activado por la difusión en fronteras de grano es la rotación y deslizamiento intergranular de la ferrita, reduciendo los defectos (cavidades, poros y descohesiones). A velocidades de deformación más altas es la recuperación dinámica de la ferrita debido al deslizamiento y apilamiento de dislocaciones (mecanismo intergranular) común en procesos convencionales de deformación en caliente. A la temperatura propuesta ($800°C$), en el intervalo intercrítico de ferrita y austenita estables, los aceros de construcción con microestructura UFG/UFF y bandas manufacturados por laminación en caliente, con espesores menores a $5\ mm$, serían superplásticos a velocidades de deformación que harían competitiva su producción por métodos de manufactura convencionales.

Este acero presenta propiedades superplásticas que permiten alcanzar altas deformaciones al ensayarlo a tracción (mayor al 100%) y cuando la temperatura y la velocidad de deformación son adecuados. Para el acero ensayado, la velocidad de deformación a la que el material presenta el comportamiento superplástico óptimo a $800°C$ es $\sim 10^{-4}\ s^{-1}$, con esfuerzos de cedencia menores a $60\ MPa$ y elongaciones mayores a 200%. El acero mantiene su tamaño de grano durante la deformación: la austenita presente (transformada a perlita durante el enfriamiento) evita el crecimiento de los granos ferríticos superplásticos. La estructura bandeada ferrita – perlita original se convierte en una estructura más homogénea formada por ferrita y perlita en la deformación: las bandas se difuminan o desaparecen debido a la deformación no homogénea de grupos de granos ferríticos (deslizamiento y rotación). A pesar de que estos aceros pueden presentar deformación superplástica a alta temperatura, este tipo de deformación a temperaturas elevadas no implica un crecimiento generalizado del tamaño de grano inclusive cuando la velocidad de deformación es muy baja ($10^{-5} s^{-1}$).

Finalmente, a temperaturas menores a $800°C$ (por ejemplo a $750°C$), los aceros con microestructura principalmente ferrítica se comportan diferente que a esta temperatura. La austenita se vuelve termodinámicamente inestable a tensión, transformándose en ferrita y carburos (principalmente cementita); durante el enfriamiento los granos ferríticos crecen y el acero, por lo menos parcialmente, perdería su comportamiento superplástico durante la deformación a velocidades bajas. Es importante notar que después de los

ensayos a 800°C la microestructura está formada por perlita, ferrita y precipitados, mientras que, tras ensayarlos a 750°C, la microestructura a temperatura ambiente sólo está constituida por ferrita y precipitados.

Por lo anterior, la selección de la temperatura adecuada para la deformación es crítica en aceros de construcción UFG, de igual manera que con aleaciones metálicas superplásticas convencionales.

4.4 Referencias

1. *Recrystallization and grain growth in hot rolling.* **Sellars, C.M. y Whiteman, J.A.** 1979, Metal Science, págs. 187-194.

2. **Urcola, J.J. y Fuentes, M.** 6, 1980, Revista de Metalurgia del CENIM, Vol. 16, págs. 337-342.

3. *Diffusion-accomodated flow and superplasticity.* **Ashby, M.F. y Verrall, R.A.** 1973, Acta Metallurgica, Vol. 21, págs. 149-163.

5 References

Ahmad E., Sarwar M. and Manzoor T. Effect of rolling and epitaxial ferrite on the tensile properties of low alloy steel [Journal] // Journal of Materials Science. - 2006. - Vol. 41. - pp. 5417-5423.

Alden T.H. Review topics in Superplasticity, Plastic deformation of materials [Book] / ed. Arsenault R.J.. - New York : Academic Press, 1975. - pp. 225-266.

Asadi M. and Palkowski H. Influence of Thermo-Mechanical Processing Parameters and Chemical Composition on Bake Hardening Ability of Hot Rolled Martensitic Steels [Journal] // Steel Research International. - 2009. - 7 : Vol. 80. - pp. 499-506.

Ashby M.F. and Jones D.R.H. Engineering Materials 1 [Book]. - [s.l.] : Pergamon Press, 1986. - Vol. 34.

Ashby M.F. and Verrall R.A. Diffusion-accomodated flow and superplasticity [Journal] // Acta Metallurgica. - 1973. - Vol. 21. - pp. 149-163.

Askeland D. The Science and Engineering of Materials [Book]. - [s.l.] : PWS Publishing Company, 1998. - 3th.

Avery D.H. and Backofen W.A. A Structural Basis for Superplasticity [Journal] // Transactions of American Society for Metals. - 1965. - Vol. 58. - pp. 551-562.

Backofen W.A. Deformation Processing [Journal] // Metallurgical Transactions. - 1973. - 12 : Vol. 4B. - p. 2679.

Backofen W.A., Turner R.I. and Avery D.H. Superplasticity in an Al-Zn Alloy [Journal] // Transactions of the ASM. - 1964. - Vol. 57. - p. 980.

Ball A. and Hutchinson M.M. Superplasticity in the Aluminium-Zinc. Eutectoid [Journal] // Metal Sci J. - 1969. - Vol. 3. - p. 1.

Baudelet B. [Journal] // Mémoires scientifiques de la Revue de Métallurgie. - 1971. - Vol. 68. - p. 479.

Baudelet B. A Theory for Flow of Polycrystal [Journal] // Acta Metall. - 1967. - Vol. 15. - p. 1545.

Baudelet B. and Lian J. A composite model for superplasticity [Journal] // Journal of Materials Science. - 1995. - Vol. 30. - pp. 1977-1981.

Beladi H., Kelly G.L. and Hodgson P.D. Ultrafine grained structure formation in steels using dynamic strain induced transformation processing [Journal] // Int. Mater. Rev.. - 2007. - Vol. 52. - pp. 14-28.

Birat J.P. The relevance of Sir Bessemer's ideas to the Steel Industry in the 21st century [Journal] // Revue de Métallurgie. - 2004. - 7-8 : Vol. 101. - p. 587.

Bochvar A.A. and Sviderskaia Z.A. Akad. Nauk SSSR [Journal] // Otdel. Tekh. Nauk. - 1945. - Vol. 9. - p. 821.

Bucher J.H. and Hamburg E.G. High Strength Formable Sheet Steel [Report]. - [s.l.] : SAE Reprint 770164, 1977.

Christmas I. Changing economics of steel [Journal] // Ironmaking and Steelmaking. - 2012. - 4 : Vol. 39. - pp. 258-262.

Conway J.B. and Flagella P.N. Creep-Rupture Data for the Refractory Metals at High Temperatures [Report] : Nuclear Systems Programs Technical Report GEMP-685 (R-69-NSP-9) / General Electric Co..

Daehn G.S., Kum D.W. and Sherby O.D. Superplasticity of a Stainless Steel Clad Ultrahigh Carbon Steel [Journal] // Metallurgical and Materials Transactions A. - December 1986. - Vol. 17A. - pp. 2295-2298.

Davies G.J., Edington J.W. and Cutler C.P. Superplasticity: A Review [Journal] // Journal of Materials Science. - 1970. - Vol. 5. - pp. 1091-1102.

Dieter G.E. Mechanical Metallurgy [Book]. - [s.l.] : McGraw-Hill, 1981.

Dimitriu R.C. and Bhadeshia H. Hot strength of creep resistant ferritic steels and relationship to creep rupture data [Journal] // Materials Science and Technology. - 2007. - 9 : Vol. 23. - pp. 1127-1131.

Dorn J.E. Some Fundamental Experiments on High Temperature Creep [Journal] // Journal of the Mechanics and Physics of Solids. - 1954. - Vol. 3. - pp. 85-116.

Dutta B. and Sellars C.M. Effect of Composition and Process Variables on Nb (C,N) Precipitation in Niobium Microalloyed Austenite [Journal] // Materials Science and Technology. - 1987. - 3 : Vol. 3. - p. 197.

Dutta B. and Sellars C.M. Strengthening of austenite by niobium... [Journal] // Material Science and Technology. - 1986. - Vol. 2. - pp. 146-153.

Dutta B., Palmiere E.J. and Sellars C.M. Modelling the Kinetics of Strain Induced Precipitation in Nb Microalloyed Steels [Journal] // Acta Materialia. - 2001. - 5 : Vol. 49. - p. 785.

Eagar T.W. The Quiet Revolution in Materials Manufacturing and Production [Journal] // Journal of Metals. - 1998. - 4 : Vol. 50. - pp. 19-21.

Edington J.W. Microstructural Aspects of Superplasticity [Journal] // Metallurgical and Materials Transactions A. - May 1982. - Vol. 13A. - pp. 803-715.

Engineering Archives [Online]. - 2008-2012. - www.engineeringarchives.com.

Frommeyer G. and Jiménez J.A. Structural Superplasticity at Higher Strain Rates of Hypereutectoid Fe-5.5Al-1Sn-1Cr-1.3C Steel [Journal] // Metallurgical and Materials Transactions A. - February 2005. - Vol. 36A. - pp. 295-300.

Furuhara T. and Maki T. Grain boundary engineering for superplasticity in steels [Journal] // Journal of Materials Science. - 2005. - Vol. 40. - pp. 919-926.

Furuhara T. Special Issue on Ultrafine Grained Steels [Journal] // ISIJ International. - 2008. - Vol. 48. - pp. 1037-1157.

González R., García J.O. and Barbés M.A. Ultrafine Grained HSLA Steels for Cold Forming [Journal] // Journal of Iron and Steel Research, International. - 2010. - 10 : Vol. 17. - pp. 50-56.

Green W.V. Short-Time Creep-Rupture Behavior of Tungsten at 2250°C to 2800°C [Journal] // Transactions of Metallurgical Society of AIME. - 1959. - 12 : Vol. 215. - pp. 1057-1060.

Hall E.O. The Deformation and Ageing of Mild Steel: III. Discussion of Results [Journal] // Physical Society of London Proceeding. - 1951. - Vol. 64. - pp. 747-753.

Hancock J.W. Creep cavitation without a vacancy flux [Journal] // Metal Sci. - 1976. - Vol. 10. - p. 319.

Harris J.E. Diffusional growth of creep voids [Journal] // Metal Sci.. - 1978. - Vol. 12. - p. 321.

Herring C. Effect of change of scale on sintering phenomena [Journal] // Journal of Applied Physics. - 1950. - Vol. 21. - pp. 301-303.

Jonas J.J. and McQueen H.J. Recovery and Recrystallization during High Temperature Deformation [Book Section] // Mise en forme des métaux et alliages. - Paris : Editions du Centre National de la Recherche Scientifique, 1976.

Kashyap B.P. and Mukherjee A.K. Superplasticity [Book] / ed. Baudelet B. and Suery M.. - Paris : CNRS, 1985.

Kawasaki M. and Langdon T.G. Principles of superplasticity in ultrafine-grained materials [Journal] // J Mater Sci. - 2007. - Vol. 42. - pp. 1782-1796.

Langdon T.G. A microscopic examination of void formation in superplastic materials [Journal] // Journal of Microscopy. - May 1979. - Vol. 116. - pp. 47-54.

Leslie W.C. The Physical Metallurgy of Steels [Book]. - Tokyo : McGraw-Hill, 1982.

Lin Z.R., Chokshi A.H. and Langdon T.G. An investigation of grain boundary sliding in superplasticity at high elongations [Journal] // Journal of Materials Science. - 1988. - Vol. 23. - pp. 2712-2722.

Liu W.J. and Jonas J.J. Nucleation Kinetics of Ti Carbonitride in Microalloyed Austenite [Journal] // Metallurgical Transactions. - 1989. - 4 : Vol. 20A. - p. 689.

Mazinani M. and Poole W.J. Effect of Martensite Plasticity on the Deformation Behavior of a Low-Carbon Dual-Phase Steel [Journal] // Metallurgical and Materials Transactions A. - February 2007. - Vol. 38A. - pp. 328-339.

Miller D.A. and Langdon T.G. An Analysis of Cavity Growth During Superplasticity [Journal] // Metallurgical Transactions A. - December 1979. - Vol. 10A. - pp. 1869-1874.

Mohamed F.A. The role of boundaries during superplastic deformation [Journal] // Surface and Interface Analysis. - 2001. - Vol. 31. - pp. 532-546.

Morrison W.B. The Elongation of Superplastic Alloys [Journal] // Trans. Metall. Soc. AIME. - 1968. - Vol. 239. - p. 710.

Mukherjee A.K. The rate controlling mechanism in superplasticity [Journal] // Mater Sci Eng. - 1971. - Vol. 8. - p. 83.

Mukherjee K., Hazra S.S. and Militzer M. Grain refinement in Dual-Phase Steels [Journal] // Metallurgical and Materials Transactions A. - September 2009. - Vol. 40A. - pp. 2145-2159.

Mullendore A.W. and Grant N.J. Creep-Rupture Characteristics of Al-Mg Solid-Solution Alloys [Journal] // Transactions of Metallurgical Society of AIME. - 1954. - 9 : Vol. 200. - pp. 973-979.

Nabarro F.R.N. Report on a Conference on the strength of materials [Journal] // The Physical Society. - 1948. - p. 75.

Okitsu Y., Takata N. and Tsuji Y. A new route to fabricate ultrafine-grained structures in carbon steels without severe plastic deformation [Journal] // Scripta Materialia. - 2009. - Vol. 60. - pp. 76-79.

Paxton H.W. The Changing Scene in Steel [Journal] // Metallurgical Transactions. - 1979. - 12 : Vol. 10A. - p. 1815.

Pearson C.E. The Viscous Properties of Exuded Eutectic Alloys of Lead-Tin and Bismusth-Tin [Journal] // J. Inst. Metals. - 1934. - Vol. 54. - p. 111.

Pero-Sanz Elors J.A. Ciencia e ingeniería de materiales: Estructura, transformaciones, propiedades y selección [Book] / ed. Dossat CIE. - 2006. - 5th. - (in spanish).

Pero-Sanz J.A. Ciencia e Ingeniería de Materiales [Book]. - Madrid : CIE-Dossat 2000, 2006. - (in spanish).

Petch N.J. The Cleavage Strength of Polycrystals [Journal] // Iron and Steel Institute Journal. - 1953. - Vol. 174. - pp. 25-28.

Pickering F.B. Physical Metallurgy and the Design of Steels [Book]. - [s.l.] : Applied Science Publishers, 1978.

Porter D.A. and Easterling K.E. Phase Transformations in Metals and Alloys [Book]. - [s.l.] : Van Nostrand Reinhold, 1988.

Porter D.A., Easterling K.E. and Sherif M.Y. Phase Transformations in Metals and Alloys [Book Section]. - 2009.

Presnyakov A.A. and Chervyakova V.V. Superductility of Eutectoid Alloys of Aluminum with Zinc [Journal] // Russian Metallurgy and Fuels (Scientific Information Consultants Translation). - 1960. - Vol. 3. - p. 85.

Quintana M.J., Gonzalez R. and Verdeja L.F. Dual-Phase Ultrafine Grained Steels Produced by Controlled Rolling Processes [Conference] // MS&T 2011 Proceedings / ed. MS&T. - Columbus, Ohio : [s.n.], 2011.

Quintana M.J., González R. and Verdeja L.F. Propiedades Mecánicas de Aceros de Fase Dual de Grano Ultrafino [Conference] // Memorias del XVI Congreso Internacional Anual de la SOMIM / ed. SOMIM. - Monterrey, Nuevo León : [s.n.], 2010. - (in spanish).

Reed-Hill R.E. Creep. Physical Metallurgy Principles [Book]. - Independence, KY : Cengage Learning, 1994. - 2nd.

Roseham W., Haughton J.L. and Bingham K.E. Zinc Alloys with Aluminum and Copper [Journal] // J. Inst. Metals. - 1920. - Vol. 23. - p. 261.

Salehi A.R., Serajzadeh S. and Karimi A. A study on the microstructural changes in hot rolling of dual-phase steels [Journal] // Journal of Materials Science. - 2006. - Vol. 41. - pp. 1917-1925.

Sellars C.M. and Whiteman J.A. Recrystallization and grain growth in hot rolling [Journal] // Metal Science. - 1979. - pp. 187-194.

Sherby O.D., Wadsworth J. and Oyama T. Superplasticity: Prerequisites and Phenomenology [Conference] // E.T.S.I.C.C.P. / ed. Madrid U.P.. - Madrid : [s.n.], 1985.

Smirnov O.M. Promising Processes for Shaping Superplastic Materials [Journal] // Metallurgist. - 2010. - 7-8 : Vol. 54. - pp. 491-497.

Speich G.R. and Miller R.L. Tempering of Ferrite-Martensite Steels [Conference] // Fundamentals of Dual-Phase Steels / ed. Kot R.A. and Bramfitt B.L.. - Chicago, Illinois : The Metallurgical Society of AIME, 1981. - pp. 279-304.

Speich G.R. Physical Metallurgy of Dual-Phase Steels [Conference] // Fundamentals of Dual-Phase Steels / ed. Kot R.A. and Bramfitt B.L.. - Chicago, Illinois : The Metallurgical Society of AIME, 1981. - pp. 3-46.

Speight M.V. and Beeré W. Vacancy potential and void growth on grain boundaries [Journal] // Metal Sci.. - 1975. - Vol. 9. - p. 190.

Suwanpinij P., Togobytska N. and Prahl U. Numerical Cooling Strategy Design for Hot Rolled Dual Phase Steel [Journal] // Steel Research International. - 2010. - 11 : Vol. 81. - pp. 1001-1009.

Tanaka T. Controlled Rolling of Steel Plate and Strip [Journal] // International Metals Reviews. - 1981. - Vol. 4. - pp. 185-191.

Tsuji N., Ito I. and Saito Y. Strength and ductility of ultrafine grained aluminum... [Journal] // Scripta Materialia. - 2002. - Vol. 47. - pp. 893-899.

Underwood E.E. A review of Superplasticity and related phenomena [Journal] // Journal of Metals. - 1962. - Vol. 14. - p. 914.

Urcola J.J. and Fuentes M. [Journal] // Revista de Metalurgia del CENIM. - 1980. - 6 : Vol. 16. - pp. 337-342.

Urcola J.J. and Fuentes M. [Journal] // Revista de Metalurgia del CENIM. - 1980. - 5 : Vol. 16. - pp. 263-267.

Urcola J.J. and Fuentes M. [Journal] // Revista de Metalurgia del CENIM. - 1981. - 1 : Vol. 17. - pp. 9-15.

Valiev R.Z., Kaibyshev O.A. and Khannanov S.K. Grain Boundaries during Superplastic Deformation [Journal] // phys. stat. sol.. - 1979. - Vol. 52. - pp. 447-453.

Valiev R.Z., Razumovskii I.M. and Sergeev V.I. Diffusion along Grain Boundaries with Non-Equilibrium Structure [Journal] // phys. stat. sol.. - 1993. - Vol. 139. - pp. 321-335.

Vander Voort G.F. Atlas of Time-Temperature Diagrams for Irons and Steels [Book]. - [s.l.] : ASM International, 1991.

Vander Voort G.F. Metallography Principles and Practice [Book]. - [s.l.] : ASM International, 1999.

Vasin R.A., Enikeev F.U. and Mazurski M.I. Mechanical modelling of the universal superplastic curve [Journal] // Journal of Materials Science. - 2000. - Vol. 35. - pp. 2455-2466.

Vetrano J.S. Superplasticity: Mechanisms and Applications [Journal] // JOM. - March 2001. - p. 22.

Wadsworth J., Oyama T. and Sherby O. Superplasticity: Prerequisites and Phenomenology [Conference] // InterAmerican Conference on Materials Technology. - 1980.

Waterschoot T., De A.K. and Vandeputte S. Static Strain Aging Phenomena in Cold-Rolled Dual-Phase Steels [Journal] // Metallurgical and Materials Transactions A. - March 2003. - Vol. 34A. - pp. 781-791.

Weertman J. Theory of Steady-State Creep Based on Dislocation Climb [Journal] // Journal of Applied Physics. - 1955. - Vol. 26. - p. 1213.

Wilcox B.A. and Clauer A.H. Creep of Thoriated Nickel Above and Below 0.5 Tm [Journal] // Transactions of Metallurgical Society of AIME. - 1966. - Vol. 236. - pp. 570-580.

Woodford D.A. Strain-rate sensitivity as a measure of ductility [Journal] // Transactions of American Society for Metals. - 1969. - Vol. 62. - pp. 291-293.

6 Suggestions for future work

In this thesis, the superindex m of the equation $\sigma = K\dot{\varepsilon}^m$ was calculated through the expression:

$$m = \frac{\log(\sigma_{y_2}/\sigma_{y_1})}{\log(\dot{\varepsilon}_{0_2}/\dot{\varepsilon}_{0_1})}$$

where σ_y is the yield stress at 0.2% and $\dot{\varepsilon}_0$ the initial strain rate, in tests made at two different strain rates. Figure 2.22b shows the m coefficient from this equation using pairs of data obtained from tension tests.

But another possibility and a suggestion for future work is to calculate the superplasticity m coefficient through the formula:

$$m = \frac{\log(F_2/F_1)}{\log(\dot{\varepsilon}_{0_2}/\dot{\varepsilon}_{0_1})}$$

where F is the load the specimen suffers under tension. This calculation must be done between data from specimesn under different strain rates and, as a suggestion, every 10% of strain of the specimen.

Considering the data (load every 10% of strain) from the universal testing machine INSTRON for two specimens with different strain rates and calculating the superindex m, Figure 6.1 can be obtained. In particular, this curve takes into account data from a specimen with $L_0 = 30$ mm tested at a crosshead speed of 0.2 mm/min (strain rate $\dot{\varepsilon}_0 = 1.11 \times 10^{-4}\ \mathrm{s}^{-1}$) and another specimen with $L_0 = 57$ mm tested at a crosshead speed of 0.2 mm/min (strain rate $\dot{\varepsilon}_0 = 5.85 \times 10^{-5}\ \mathrm{s}^{-1}$). This curve shows that the superindex m is not constant and increases with strain.

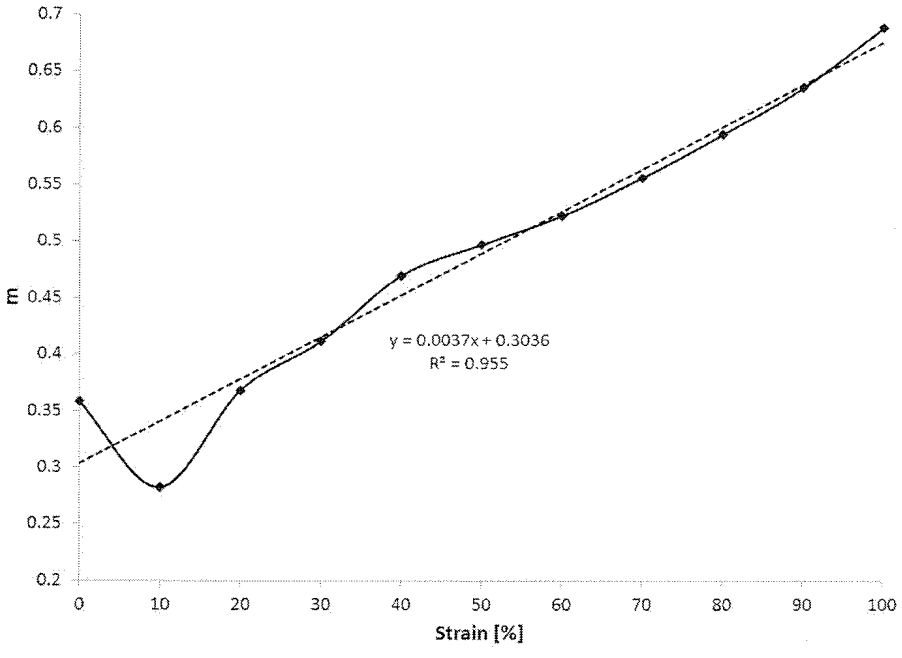

Figure 6.1 Variation of superindex m while changing strain values

The variation of the m values could be interesting as this would mean reaching a higher value than the one calculated through the yield stresses. And a new optimum superplastic window could be found, not just with temperature and strain rate, but also with the percentage of strain suffered by the steel. From a manufacturing point of view, this would mean achieving higher deformations with even less load/stress resulting in even cheaper drawing or bending processes.

On the other hand, it would be interesting to analyze using transmission electron microscopy the presence, distribution and position of precipitates inside or at the boundaries of the ultrafine grains.

7 Appendix

Ultrafine Grained HSLA Steels for Cold Forming. **González, R.; García, J.O.; Barbés, M.A.; Quintana, M.J.; Verdeja, L.F. and Verdeja, J.I..** 10, 2010, Journal of Iron and Steel Research, International, Vol. 17, pp. 50-56.

Ultrafine grained steels and the n coefficient of strain hardening. **González, R.; Quintana, M.J.; Verdeja, L.F. and Verdeja, J.I.** 9, 2011, Memoria de trabajos de difusión científica y técnica, pp. 45-54.

Dual-Phase Ultrafine Grained Steels Produced by Controlled Rolling Processes. **Quintana, M.J.; González, R.; Verdeja L.F. and Verdeja, J.I.** [ed.] MS&T. Columbus, Ohio, 2011. MS&T 2011 Proceedings. Vol. Recent Developments in Steel Processing, pp. 504-511. October 16-20.

Superplasticity of Ultrafine Grained Low-Carbon HSLA Steels. **Verdeja, J.I.; Quintana, M.J.; García, J.O.; Verdeja, L.F.; González, R. and Fernández, S.** [ed.] MS&T. Pittsburgh, Pennsylvania, 2012. MS&T 2012 Proceedings. Vol. Recent Developments in Steel Processing, pp. 945-956. October 7-11.

Superplasticity of ultrafine grained low-alloy steels. **Fernández, S.; Quintana, M.J.; García, J.O.; Verdeja, L.F.; González, R. and Verdeja, J.I.** 10, 2012 Memoria de trabajos de difusión científica y técnica, pp. 45-56.

Superplastic HSLA steels: microstructure and failure. **Fernández, S.; Quintana, M.J.; García, J.O.; Verdeja, L.F.; González, R. and Verdeja, J.I.** 2013, Journal of Failure Analysis and Prevention (accepted, to be published in Vol. 13, issue 4, 2013).

Structural ultrafine grained steels obtained by advanced controlled rolling. **González, R., García, J.O.; Barbés, M.A., Quintana, M.J.; Verdeja, L.F. and Verdeja, J.I.** 2013, Journal of Iron and Steel Research, International (accepted, to be published in 2013).

JOURNAL OF IRON AND STEEL RESEARCH, INTERNATIONAL. 2010, 17(10): 50-56

Ultrafine Grained HSLA Steels for Cold Forming

R González[1], J O García[2], M A Barbés[2], M J Quintana[1], L F Verdeja[2], J I Verdeja[2]
(1. School of Engineering, Panamerican University, Mexico City 03920, Mexico;
2. ETSIMO, Oviedo University, Oviedo 33004, Asturias, Spain)

Abstract: The industrial level production of ultrafine grained (or ultrafine ferrite) ferrous alloys was investigated through three examples of steels that complied with the EN 10149-2 Euronorm and were produced by advanced controlled hot rolling techniques. The steel samples were tension tested and chemically analyzed, and the microstructure was evaluated through quantitative metallographic techniques to determine parameters such as yield stress, amount of microalloying elements, strain hardening coefficient, grain size, and grain size distribution. These steels were microalloyed with Ti, Nb, and Mn with ASTM grain sizes of approximately 13—15. The careful control of chemical composition and deformation during production, giving a specific attention to the deformation sequences, austenite nonrecrystallization temperatures and allotropic transformations during cooling, are indispensable to obtain steels with an adequate strain hardening coefficient that allows cold working operations such as bending, stretching or drawing.
Key words: ultrafine steel; metallography; strain hardening; Euronorm

Though the most important industries for the 21st century are thought to be the development of advanced materials (also known as new materials), information technologies, artificial intelligence, and biotechnology[1], price reductions and improvements in quality and properties in steel have maintained this material as a leader in all industrial applications[2]. More specifically, the use of structural materials in the second half of the 20th century included the competition between Fe-C alloys and other metallic materials, which resulted in advanced steels that respond to large production necessities. The interest in Fe alloys is based upon other things, in its changes during solid state transformations, restoration and recrystallization, and textures[3].

For example, there is an ongoing activity in the steel industry to develop new methods to produce high strength low alloy (HSLA) structural steels with lower cost and improved properties. The use of heat treatments such as normalizing and quenching and tempering, and more recently, thermomechanical controlled rolling processing techniques (TMCRP) and the use of continuous annealing processing lines (CAPL) have been developed to produce fine ferrite grain sizes in final products. These techniques have shown a significant improvement in strength, fracture toughness, and weldability through the refinement of ferrite grain size (up to 12 ASTM G, $d_\alpha \approx 5$ μm), which was the grain size lower limit reachable in the industry 30 years ago[4]. However, the Hall-Petch equation predicts that a reduction from 5 to 1 μm should increase the yield strength of a given steel up to 350 MPa and decrease the impact transition temperature (ITT) up to −100 ℃[5]. In this study, the results of current commercial techniques like TMCRP are presented, which improve properties and allow the replacement of some costly alloy steels with either plain carbon or microalloyed/low alloyed carbon steels, demonstrating that the industrial production of fine, equiaxed ferrite grains with $d \approx 2-3$ μm is possible.

Thermomechanical processing such as controlled rolling, controlled cooling and direct quenching save energy in steel manufacture by minimizing or even eliminating the heat treatment after hot deformation, thereby increasing the productivity for high grade steels. It generally demands a change in alloy design and frequently reduces the productivity of the hot deformation process itself, but makes it possible to reduce the total amount of alloying addi-

Biography: R González(1967—), Male, Doctor; **E-mail**: robglez@up.edu.mx; **Received Date**: October 20, 2009

tions and to improve strength, toughness, and weldability, whilst sometimes producing new and beneficial characteristics in the steel.

A large amount of the rolled steel products currently produced are of the microalloyed type. These steels are usually soaked at high temperatures when roughing deformation is carried out. In the case of conventional controlled rolling (CCR), rough rolling is followed by fast cooling and finishing passes are carried out at temperatures where the austenite remains un-recrystallized. The microalloying elements, which remain in solution (partially or completely) during rough deformation, start to precipitate after finishing deformations at low temperatures. Nb, Ti and V are the most commonly used microalloying elements and during cooling, they combine with C and/or N to form carbide, nitride and/or carbonitride precipitates. These fine precipitates play an effective role by retarding recrystallization (and therefore, increasing the recrystallization-stop temperature) that usually follows deformation and thus, helps to retain the accumulated strain and deformed structures of austenite grains.

1 Experimental

The research was made in three HSLA steels in the form of sheet with different thicknesses, obtained by TMCRP in its raw hot rolled state: S355 (4.5 mm), S460 (5 mm) and S550 (3.5 mm). The chemical composition and mechanical properties established by the EN 10149-2 (1995) Euronorm are presented in Table 1 and Table 2, whereas the chemical analysis of the hot rolled strip in mass percent is given in Table 3. The values for C and S were analyzed in an LECO CS444 system by the combustion method; for the remaining elements, an ARL 4460 optical emission spectrometer was used, and Table 3 indicates the average of three measurements.

To determine hardness, tests were made following the UNE-EN IS06507-1 standard, which specifies the Vickers scale (HV). A GNEHM OM-150 universal model durometer was used with a load of 100 N, and the results, average of five measurements in each sample (in the rolling plane surface), are presented in Table 4.

Tension and resilience properties were evaluated by machining samples from the strip with a calibrated length of 100 mm, a gauge of 50 mm, width of 10 mm and thickness of 3 mm, in accordance to UNE-EN 10002-1 standard. The samples were tested in an INSTRON 1195 universal machine, equipped with a load cell of 100 kN. Engineering yield stress,

Table 1 Chemical composition of thermomechanically rolled steels

Name	Material number	w_C/%	w_{Mn}/%	w_{Si}/%	w_P/%	w_S/%[1]	w_{Alt}/%	w_{Nb}/%[2]	w_V/%[2]	w_{Ti}/%[2]	w_{Mo}/%	w_B/%
S355	1.0976	≤0.12	≤1.50	≤0.50	≤0.025	≤0.020	≥0.015	≤0.09	≤0.20	≤0.15	—	—
S460	1.0982	≤0.12	≤1.60	≤0.50	≤0.025	≤0.015	≥0.015	≤0.09	≤0.20	≤0.15	—	—
S550	1.0986	≤0.12	≤1.80	≤0.50	≤0.025	≤0.015	≥0.015	≤0.09	≤0.20	≤0.15	—	—

Note: 1) If ordered, the sulphur content should be less than 0.01%; 2) The sum of Nb, V and Ti should be less than 0.22%.

Table 2 Mechanical properties for thermomechanically rolled steels

Name	Material number	Minimum yield strength/MPa	Tensile strength/MPa[1]	Minimum percentage elongation at fracture		Minimum mandrel diameter when bending at 180°
				If $t<3$ mm, $L_0=80$ mm[2]	If $t\geq3$ mm, $L_0=5.65\sqrt{S_0}$[3]	
S355	1.0976	355	430—550	19	23	0.5t
S460	1.0982	460	520—670	14	17	1t
S550	1.0986	550	600—760	12	14	1.5t

Note: 1) The values for the tensile and bending tests apply to longitudinal test pieces and transverse test pieces, respectively; For thickness $t>8$ mm, the minimum yield strength can be 20 MPa lower; 2) L_0 is the initial length of the tension test sample; 3) S_0 is the initial width of the tension test sample.

Table 3 Chemical composition of investigated steels (mass percent, %)

Steel	C	Si	Mn	P	S	Al	Ti	Nb	V	Cu	N
S355	0.06	0.01	0.32	0.011	0.009	0.026	0.002	0.023	—	0.015	0.056
S460	0.07	0.01	0.60	0.009	0.013	0.036	0.062	0.043	—	0.016	0.042
S550	0.07	0.19	1.55	0.016	0.004	0.029	0.070	0.048	0.005	—	0.045

Table 4 Mechanical properties of investigated steels

Steel	S355	S460	S550
HV10	160	181	220
Equivalent ultimate tensile strength from hardness/MPa	553	607	710
Yield strength/MPa	405	532	630
Ultimate tensile strength/MPa	549	603	711
Total elongation/%	34	22	21
Yield strength/Ultimate tensile strength	0.74	0.88	0.89
Strain hardening coefficient	0.13	0.12	0.11

engineering ultimate tensile strength and total elongation were measured and the ASTM E-646-78 standard was used to determine the tensile strain hardening coefficient n, from the engineering stress (s) -strain (e) curve (Fig. 1), using the Ludwik-Hollomon power curve mathematical expression $\sigma = K\varepsilon^n$, where σ, ε are the true stress and the true strain, respectively, and K is a constant.

Metallographic characterization was carried out on the transverse section parallel to the rolling direction, after mechanical grinding, 6 and 1 μm diamond paste polishing and final polishing with 0.05 μm γ-alumina solution. The Nital-2 reactive was used to etch the samples, which were observed in a Nikon-Epiphot metallographic optical microscope. Due to the fact that in all cases, magnifications higher than 100 were used (as these are ultrafine ferrite steels-UFF, qualitative determination of the ASTM G number, was made using the formula[6]:

$$G = G' + 6.64 \cdot \lg \frac{M}{100} \quad (1)$$

where, G' is the ASTM grain size measured as if the micrograph was taken at a magnification of 100; and M is the actual magnification of the micrograph.

For quantitative metallographic analysis of grain size (mean linear intercept) and volume fraction of the minority constituents (pearlite), a Buehler Omnimet image analyzer system connected to the Nikon Epiphot microscope was used, in accordance to the ASTM E112 standard and the expanded version E1181-02. The measurement of the mean linear intercept is automatically performed by the equipment on lines traced on the micrograph at 0°, 45°, 90° and 135° from the rolling direction. Volume fraction f_v of the pearlite phase is measured by point counting analysis on the micrographs using a mesh of dots with an optimal gap in order to avoid that two consecutive dots are placed in the same pearlite colony. The number of dots measured was at least 396, which results in $f_v/\sigma_v = 0.05$, where σ_v is the standard deviation in statistical analysis, resulting in a confidence level of 95% for the pearlite volume fraction[7]. The relationship between ASTM G grain size and the mean linear intercept $\overline{L}$, in the case of the ferrite phase, was calculated with the formula:

$$G = -3.356 - 6.644 \lg \overline{L} \quad (2)$$

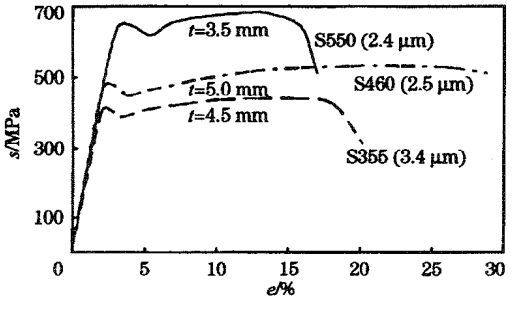

Fig. 1 Engineering stress-strain curves for investigated steels

2 Results and Discussion

The micrographs taken from transverse sections parallel to the rolling direction of S355, S460 and S550 steels show common characteristics (Fig. 2): slight banding of the microstructure in the rolling direction, pancake structure of the ferrite caused by the controlled rolling process with elongated grains in the rolling direction, totally recrystallized structures, and very small volume fraction of pearlite.

The grain morphology in S355 [Fig. 2 (a)] is considerably different from those of samples S460 and S550 [Fig. 2 (b) and (c)], as the latter two steel samples show evidently elongated grains, which also explain their higher yield strength and ultimate tensile strength (Table 4), regardless of the sheet thickness. In Table 4, the estimated ultimate tensile strength values obtained from the hardness are also compared with the tension test ones, resulting in very similar numbers.

Fig. 3 presents the ASTM G grain size frequency histograms for three typical sets of micrographs of the investigated steels, resulting in the data for $\overline{G}$, sd standard deviation and $\overline{L}$ indicated in Table 5. It is clear that these are UFF steels with $\overline{L}$ of approximately 1.9 μm for S460 and S550, and a slightly higher value (approximately 3.1 μm) for the Nb microalloyed S355. The grain size distribution is very similar in samples S460 and S550 [Fig. 3 (b) and (c)], whereas sample S355 shows a more symmetrical and wider distribution [Fig. 3 (a)], which results in a larger amount of small grains in S460 and S550, and

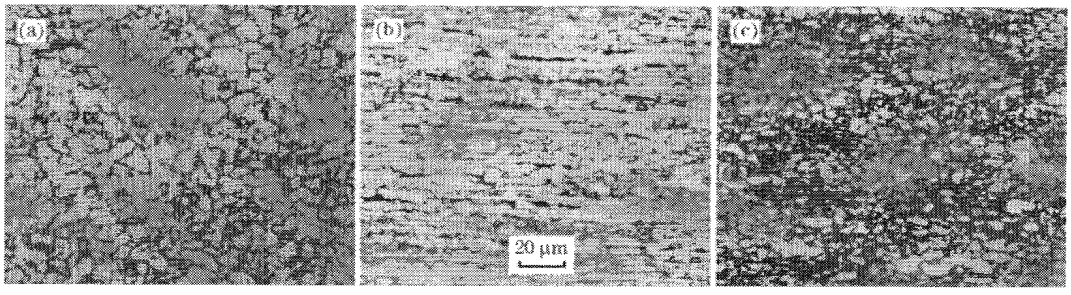

Fig. 2 Captured image of S355 steel (a), S460 steel (b), and S550 steel (c)

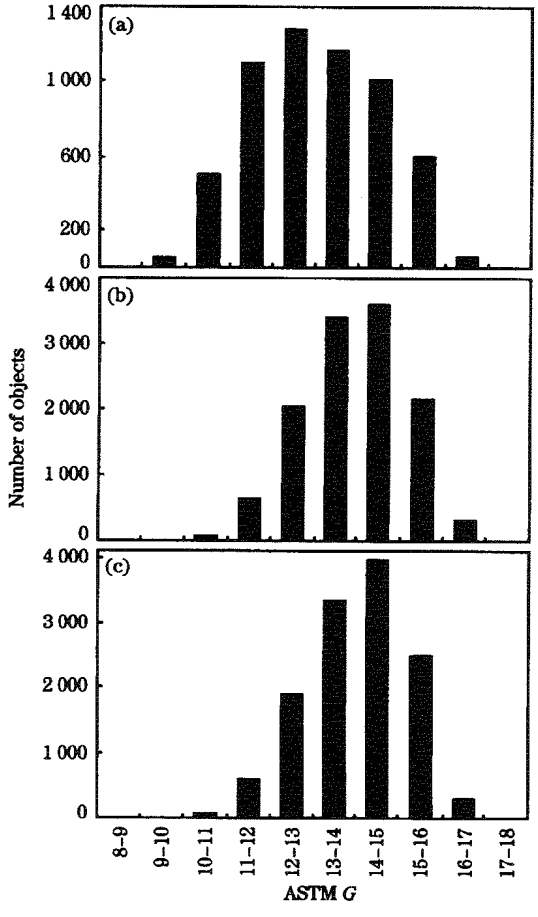

Fig. 3 ASTM grain size distribution in S355 steel (a), S460 steel (b), and S550 steel (c)

therefore a higher yield stress as indicated in Table 4, independently from the amount of second phase particles enhancing resistance.

Table 5 presents the fraction volume of pearlite and the qualitative estimate of the ASTM G grain size obtained by patterns, in accordance to the ASTM E-112 standard, in micrographs with magnification over 600.

In recent years, several reports have been presented for UFF steels, in an attempt to develop high strength along with high fracture toughness materials[8-11]. In a recent work at the Max Planck Institute[2], ultrafine grains of 1—2 μm were achieved in plain carbon steels by combining a hot deformation stage, followed by a heavy warm deformation and final controlled cooling. The carbon content of the steels examined ranged from 0.17% to 0.31% so that a fine cementite dispersion could be achieved in the ferrite matrix which helped to stabilize the ultrafine grains particularly during the long high temperature period while cooling. These materials resulted in yield strength of 590 MPa, ultimate tensile strength of 660 MPa, and elongation of 19%.

Table 5 Microstructural measurements for three investigated steels

Steel	S355	S460	S550
f_v of pearlite/%	3.9	6.9	2.4
ASTM G[1)]	13.0—13.5	14.5—15.0	14.5—15.0
ASTM $\bar{G}$[2)]	13.32	14.70	14.75
sd[2)]	1.67	1.54	1.63
$\bar{L}$[2)]	3.09	1.92	1.88

Note: 1) Qualitatively estimated value; 2) Values measured using the image analyzer system.

The techniques used by the authors just mentioned, ARB (accumulative roll-bonding)[8], DSIT (dynamic strain induced transformation)[9], CRA (cold rolling and annealing)[11], RTA (rapid transformation annealing)[12], are all based on some type SPD (severe plastic deformation) process. This is not the case of steels obtained by TMCRP, where the final thickness reduction (finishing) is only of 50% ($\varepsilon \approx 0.7$). Furthermore, none of these techniques have yet surpassed the laboratory level. As indicated by Howe[13], it may be deduced from all this work that UFF steels have an "Achilles' heel", as they tend to exhibit unstable plasticity upon yielding, restricting its potential industrial applica-

tions: they show uniform elongations (ε_u) and very low strain hardening coefficients ($\varepsilon_u = n < 0.1$), which makes them unviable for forming processes such as bending, stretching, and drawing at room temperature. The tensile curves for many UFF steels obtained in a laboratory scale (grain sizes as small as 0.5 μm have been reported)[12] usually show a local elongation zone normally denominated "Lüders effect" (formation of Lüders bands), which results in fracture. This behavior is typical in effervescent steels not treated with Al/Ti, and in ferrous and non-ferrous alloys with ultrafine grain size[8,14], as shown in Fig. 4 (Morrison and Miller[15], from Leslie[14]).

To explain the low ductility of the UFF steels, the results presented by Morrison and Miller[15] must be considered (Morrison law), in which n is related to the mean grain size d (equivalent to the mean linear intercept, $\bar{L}$) by the equation:

$$n=\frac{5}{10+d^{-1/2}} \tag{3}$$

results in the following: if $d=0.010$ mm, $n=0.25$ and if $d=0.0005$ mm, $n=0.09<0.1$, as shown in Fig. 5 (Morrison and Miller[15], from Leslie[14]), which means that the material has lost its capacity to strain hardening. Moreover, professor Bhadeshia[16] indicates that the apparently insatiable desire for finer microstructure has resulted in mixed outcomes in the field of structural materials: simple grain refinement leads to unacceptable poor ductility because the capacity for work-hardening is lost. Nevertheless, bulk nanostructured steels, microalloyed with Ti, Nb and V, obtained by TMCRP with good properties have been commercialized, based on its success in the $\gamma \rightarrow \alpha$ stress or strain induced transformation to

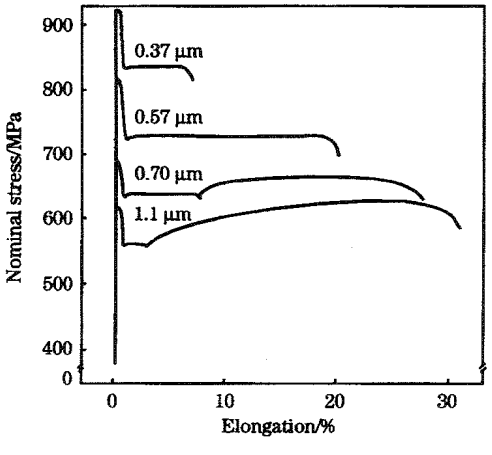

Fig. 4 Effect of grain size on elongation for tension test

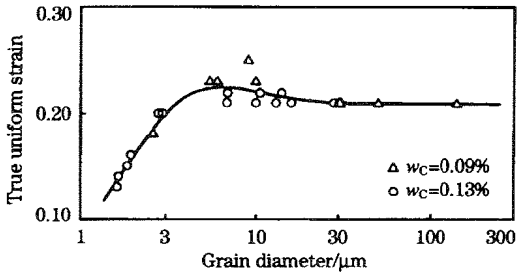

Fig. 5 Variation of uniform elongation with grain size in low-carbon steel

enhance work hardening and anisotropic grains to boost the total amount of interfaces per unit volume. This phenomena must be taken into account, as a normal very small grain size (<1 μm) in its recrystallized state loses its capacity to strain harden and has $\frac{d\sigma}{d\varepsilon}<\sigma$ and thus, if deformed, immediately shows lüdering effect and fracture without any plastic uniform deformation[17].

Fig. 6 schematically illustrates the three stages of the controlled-rolling process and the microstructural change accompanying deformation in each stage. In stage 1, coarse austenite (a) is refined by repeated deformation and recrystallization (b), though the steel transforms to relatively coarse ferrite (b'), except when using "Ti technology" which allows, before rolling is performed, the refinement of homogenized austenite grain size. During stage 2, elongated, unrecrystallized austenite deformation bands are formed (c) and ferrite nucleates on the deformation bands as well as γ-grain boundaries, resulting in fine α grains. In this case, "Nb technology" has to be used in order to accumulate deformation within the austenite when rolling happens at a temperature below the non-recrystallization temperature, T_{nr}, which is a fundamental parameter in the process. In

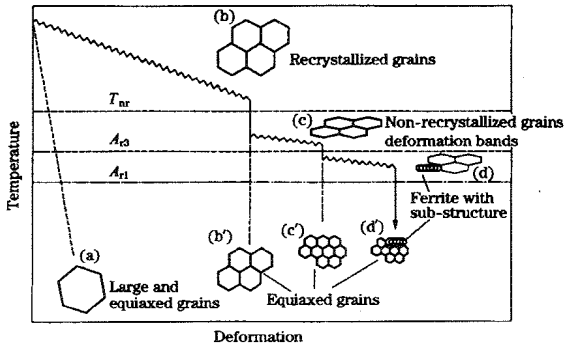

Fig. 6 Schematic diagram of controlled rolling process

the case of stage 3, deformation in the α-γ dual-phase region continues the process started in stage 2, and results in a substructure. If, in a complementary way, "V technology" is used, a structural precipitation hardening of V_4C_3 will occur in the ferrite phase.

Summarizing, controlled rolling procedures include the reduction on the rapid recrystallization region (stage 1), a delay on the rolling between stage 1 and stage 2, and a reduction in the final non-recrystallization region (stage 2). Optionally, deformation below A_{r3} (stage 3) or accelerated cooling may be followed. Accelerated cooling after hot rolling is currently being recognized as a further advanced thermomechanical treatment in the hot rolling process. This cooling process is characterized by accelerated cooling in a γ→α transformation range just after controlled rolling. It has been shown that the accelerated cooling refines the α grain size and thus further improves both the strength and toughness. In industrial practice, when fine recrystallized γ is deformed by 50% ($\varepsilon=0.7$) in the non-recrystallized region, the resulting grain size, under careful cooling conditions and coil design, is higher than 12 ASTM G ($d_\alpha<5$ μm), which compared to common normalized products with a 10 ASTM G ($d_\alpha\approx10$ μm) grain size, at their best, is a considerable improvement[18].

As indicated by Perosanz[19], the solubility products of the mentioned carbonitrides, as well as of other chemical compounds (AlN, MnS, V_4C_3), result in limit solubility temperature of the carbonitrides, non-recrystallization temperature of the austenite and γ→α allotropic transformation temperature during cooling, with values close to ($t<6$ mm):

1) Starting precipitation temperatures T_{ps}

TiN

$$\lg(w_{Ti}w_N)=\frac{-14\,400}{T}+5.0 \tag{4}$$

$$\lg(0.07\times0.005)=\frac{-14\,400}{T}+5.0$$

$T_{ps}=1\,703$ K(1 430 ℃)

Nb(C,N)

$$\lg\left[w_{Nb}\left(w_C+\frac{12w_N}{14}\right)\right]=\frac{-6\,770}{T}+2.26 \tag{5}$$

$$\lg\left[0.04\times\left(0.08+\frac{12\times0.005}{14}\right)\right]=\frac{-6\,770}{T}+2.26$$

$T_{ps}=1\,431$ K(1 158 ℃)

NbC

$$\lg(w_{Nb}^{0.87}w_C)=\frac{-7\,530}{T}+3.11 \tag{6}$$

$$\lg(0.04^{0.87}\times0.08)=\frac{-7\,530}{T}+3.11$$

$T_{ps}=1\,388$ K(1 115 ℃)

TiC

$$\lg(w_{Ti}w_C)=\frac{-7\,000}{T}+2.75 \tag{7}$$

$$\lg(0.07\times0.08)=\frac{-7\,000}{T}+2.75$$

$T_{ps}=1\,399$ K(1 126 ℃)

2) Non-recrystallization temperature (T_{nr})

$$T_{nr}=867+464w_C+(6\,445w_{Nb}-644w_{Nb}^{1/2})+(732w_V-230w_V^{1/2})+890w_{Ti} \tag{8}$$

$$T_{nr}\approx867+37.12+257.8-128.8+62.3=1\,095.4\text{℃}$$

3) γ→α transformation temperature during cooling ($T_{A_{r3}}$) for $t=5$ mm:

$$T_{A_{r3}}=910-310w_C-80w_{Mn}+0.35(t-8) \tag{9}$$

$$T_{A_{r3}}=910-310\times0.08-80\times1.5+0.35\times(5-8)=910-24.8-120-1.05\approx764\text{℃}$$

As mentioned, it is well established that the precipitation of Ti and Nb carbonitrides plays a very important role in controlling austenite grain growth during soaking and roughing operations and the precipitation of Nb carbonitrides retarding recrystallization at temperatures of finished controlled rolling operations[20]. It is well known that in the temperature range of interest, diffusion of carbon and nitrogen is some orders of magnitude faster than the diffusion of titanium and niobium. Therefore, Ti and Nb are expected to be the rate controlling elements[21-23].

3 Conclusions

Recently, the production and commercialization of UFF steels in their raw hot rolled state by TMCRP is a reality. Grain sizes range from 2 to 3 μm (ASTM $\overline{G}$ 14). The yield stresses are up to 700 MPa, and the uniform elongations are higher than 10%. These UFF steels are weldable owing to their low carbon content and they have low impact transition temperatures below 0 ℃. These steels are used in construction and in reinforcement parts for the automotive industry.

The achievement of these properties is the result of a careful control of chemical composition, including microalloying, the know-how acquired in the TMCRP, and giving a specific attention to the deformation sequences, austenite non-recrystallization temperatures, and γ→α allotropic transformation temperature during cooling.

These steels show ductility and forming capacity superior to the ones obtained by other techniques which, even worse, have not yet reached the industrial level, nor the commercial distribution.

The authors wish to thank the Research and Hot Coil Products Department of the ArcelorMittal in Asturias (Spain) Factories (formerly Ensidesa, CSI Planos, Aceralia and Arcelor). They also acknowledge Ms. Teresa Iglesias and Ms. Bertha Mendieta for their invaluable help in experimental work and text and figures revisions.

References:

[1] Eager T W. The Quiet Revolution in Materials Manufacturing and Production [J]. Journal of Metals, 1998, 50(4): 19.

[2] Advances in the Hot Rolling of Steels [J]. Ironmaking and Steelmaking, 2004, 31(1): 8.

[3] Perosanz J A. Steels: Physical Metallurgy. Selection and Design [M]. Madrid: CIE—Dossat, 2000 (in Spanish).

[4] Paxton H W. The Changing Scene in Steel [J]. Metallurgical Transactions, 1979, 10A(12): 1815.

[5] Pickering F B. Physical Metallurgy and the Design of Steels [M]. London: Applied Science Publishers, 1978.

[6] Vander Voort G F. Metallography: Principles and Practice [M]. Ohio: ASM International, 1999.

[7] Sellars C M. Quantitative Metallography for Master Course in Physical Metallurgy [R]. San Sebastián: CEIT de Guipúzcoa, 1981.

[8] Tsuji N, Ito Y, Saito Y, et al. Strength and Ductility of Ultrafine Grained Aluminum and Iron Produced by ARB and Annealing [J]. Scripta Materialia, 2002, 47(12): 893.

[9] Beladi H, Kelly G L, Hodgson P D. Ultrafine Grained Structure Formation in Steels Using Dynamic Strain Induced Transformation Processing [J]. International Materials Reviews, 2007, 52(1): 14.

[10] Furuhara T. Preface to the Special Issue on "Ultrafine Grained Steels" [J]. ISIJ International, 2008, 48(8): 1037.

[11] Okitsu Y, Takata N, Tsuji N. A New Route to Fabricate Ultrafine-Grained Structures in Carbon Steels Without Severe Plastic Deformation [J]. Scripta Materialia, 2009, 60(2): 76.

[12] Lesch C, Alvarez P, Bleck W, et al. Rapid Transformation Annealing: A Novel Method for Grain Refinement of Cold-Rolled Low-Carbon Steels [J]. Metallurgical and Material Transactions, 2007, 38A(9): 1882.

[13] Howe A. Ultrafine Grained Steels: Industrial Prospects [J]. Materials Science and Technology, 2000, 16(11/12): 1264.

[14] Leslie W C. The Physical Metallurgy of Steels [M]. New York: McGraw-Hill, International Book Company, 1981.

[15] Morrison W B, Miller R L. The Ductility of Ultra-Fine-Grain Alloys. Ultrafine-Grain Metals [M]. New York: Syracuse University Press, 1970.

[16] Bhadeshia H K D H. Bessemer Memorial Lecture: The Dimensions of Steel [J]. Ironmaking and Steelmaking, 2007, 34(3): 194.

[17] Backofen W A. Deformation Processing [J]. Metallurgical Transactions, 1973, 4B(12): 2679.

[18] Tamura I, Ouchi C, Tanaka T, Sekine H. Thermomechanical Processing of High Strength Low Alloy Steel [M]. London: Butterworths Ed, 1988.

[19] Perosanz J A. Materials Science and Engineering [M]. Madrid: Cie-Dossat, 2006 (in Spanish).

[20] Porter D A, Easterling K E, Sherif M Y. Phase Transformations in Metals and Alloys [M]. Boca Raton: CRC Press, 2009.

[21] Dutta B, Sellars C M. Effect of Composition and Process Variables on Nb(C, N) Precipitation in Niobium Microalloyed Austenite [J]. Materials Science and Technology, 1987, 3(3): 197.

[22] Dutta B, Palmiere E J, Sellars C M. Modelling the Kinetics of Strain Induced Precipitation in Nb Microalloyed Steels [J]. Acta Materialia, 2001, 49(5): 785.

[23] Liu W J, Jonas J J. Nucleation Kinetics of Ti Carbonitride in Microalloyed Austenite [J]. Metallurgical Transactions, 1989, 20A(4): 689.

Ultrafine grained steels and the *n* coefficient of strain hardening

Aceros de grano ultrafino y el coeficiente n de endurecimiento por deformación

R.González[1], M.J.Quintana[1], L.F.Verdeja[2] and J.I.Verdeja [2]

Recibido: Julio 2011 Aceptado: Agosto 2011

Abstract.- Though many efforts have been made to obtain ultrafine grained steels, the industrial production level has not yet been reached due to the plastic instability during forming. The present work shows, using three examples, that high strength low alloy steels produced by advanced thermomechanical controlled rolling are in fact ultrafine grained steels with grain sizes below 5 μm, establishing also a connection between the coefficient of strain hardening, mechanical strength and admissible thickness tolerances in steel sheets, in order to use these materials in cold work forming (bending and drawing). A minimum value of coefficient *n* must be reached in order to assure commercial use of the steel sheet.

Key words: UFG steels, microstructure, mechanical properties, forming

Resumen.- *Aunque se han hecho muchos esfuerzos para fabricar aceros de grano ultrafino, la producción nunca ha llegado a niveles industriales debido, sobre todo, a la inestabilidad plástica del material durante la deformación. A través de tres ejemplos, el presente trabajo muestra que los aceros de alta resistencia y baja aleación manufacturados por la técnica de rolado avanzado termomecánicamente controlado, son de hecho aceros ultrafinos con tamaños de grano por debajo de 5 μm, estableciendo además conexiones entre el coeficiente de endurecimiento por deformación, resistencia mecánica y tolerancia de los espesores admisibles en placas de acero, de forma que estos materiales puedan ser conformados en frío (plegado y estampado). El coeficiente n debe alcanzar un valor mínimo para asegurar el uso comercial de la placa de acero.*

Palabras clave*: aceros de grano ultrafino, microestructura, propiedades mecánicas, estampado.*

1. Introducción.- Over the last years and in many countries (U.S., Great Britain, Germany, India, Japan and Australia) numerous researches have been carried out to obtain ultrafine grained steels (UGS). These investigations have not yet reached industrial level as the plastic instability during forming ($n \approx 0$) remains an unsolved problem. This work shows, using three examples, how high strength low alloy (HSLA) steels contemplated by Euronorm EN 10149-2 standard and manufactured by advanced thermo-mechanical controlled rolling processes (ATMCRP) are in fact UFG steels and are used primarily in the automotive and construction sectors. Following well established research works and thickness tolerances industrially admitted in hot work

[1] School of Engineering, Universidad Panamericana, Augusto Rodin 498, 03920, México, D.F., Mexico, Tel. (52)55 1251-6859, Fax. (52)55 5482-1600 ext. 6101, robglez@up.edu.mx

[2] E.T.S.I.M.O., Universidad de Oviedo, Independencia 13, Oviedo 33004, Spain, Tel. (34) 985 10-43-03, Fax. (34) 985 10-42-42, lfv@etsimo.uniovi.es

lamination, it is shown that values above n=0.1 are indispensable for UFG steels to be subsequently cold-formed.

In recent years, both the steelmaking industry and laboratories in different parts of the world, have shown an increasing interest in reaching an industrial level production of ultrafine grained steels (ultrafine ferrite – UFF, ultrafine grain – UFG)1, being the most interesting ones those with grain size d (mean linear intercept) lower than 5 μm (grain size G ASTM higher than 12), resulting in an increase in mechanical resistance and fracture toughness expected from these microstructures2. Though, till present time, none of the different techniques that have been set up at a laboratory level, such as severe plastic deformation (SPD)3-5, accumulative roll bonding (ARB)6, dynamic strain induced deformation (DSIT)7,8 and rapid transformation annealing (RTA)9, have achieved to overcome the plastic instability consequence of the low strain hardening n coefficient value that the UFG steels manufactured by these procedures show10.

Only advanced techniques of control rolling such as advanced thermomechanical cold rolling processes (ATMCRP) used by the steelmaking industry in collaboration with research labs such as the Sid-met-mat of ETSIMO (Oviedo University, Spain), have obtained industrial level productions of UFG steels. This is the case of the Arcelor Mittal de Asturias Group (Spain), whose UFF steel productions in raw hot rolled state overpassed the 60,000T level in 2010, in the form of hot rolled sheet (thickness above 1.5 mm). This work tries to establish, in a resumed form, the connection between the n coefficient, grain size, mechanical resistance and thickness tolerances admissible in steel sheets, so that UFG steels may be used in cold work forming operations for bending and drawing.

2. Experimental Work and Results.- Data from 3 UFG steels are presented, with code names S355, S420 and S500, contained in the Euronorm EN10149-2 standard (Specification for hot-rolled flat products made of high yield strength steels for cold forming. Delivery conditions for thermomechanically rolled steels), whose chemical composition and mechanical properties are specified in table I and table II respectively. The steel was delivered in the form of steel sheet with a thickness equal or below 8 mm and were produced by ATMCRP (hot rolled raw state) in the industrial facility of Arcelor Mittal de Avilés (Asturias, Spain). These materials are primarily used in the automotive sector (reinforcements and supports) and in the construction sector (ties, angles and crane arms). Table III shows the chemical analysis, obtained by the average of 3 samples of the steel sheets investigated. Steel S355 and S420 are microalloyed with Nb and low Mn. The S500 steel is microalloyed with Nb-Ti and high Mn, all of them within the specified composition required by the Euronorm.

Name	Material number	C% max	Mn% max	Si% max	P% max	S% max**	Al total % min	Nb% max*	V% max*	Ti% max*	Mo% max	B% max
S315	1.0972	0.12	1.30	0.50	0.025	0.020	0.015	0.09	0.20	0.15	--	--
S355	1.0976	0.12	1.50	0.50	0.025	0.020	0.015	0.09	0.20	0.15	--	--
S420	1.0980	0.12	1.60	0.50	0.025	0.015	0.015	0.09	0.20	0.15	--	--
S460	1.0982	0.12	1.60	0.50	0.025	0.015	0.015	0.09	0.20	0.15	--	--
S500	1.0984	0.12	1.70	0.50	0.025	0.015	0.015	0.09	0.20	0.15	--	--
S550	1.0986	0.12	1.80	0.50	0.025	0.015	0.015	0.09	0.20	0.15	--	--
S600	1.8969	0.12	1.90	0.50	0.025	0.015	0.015	0.09	0.20	0.22	0.50	0.005
S650	1.8976	0.12	2.00	0.60	0.025	0.015	0.015	0.09	0.20	0.22	0.50	0.005
S700	1.8974	0.12	2.10	0.60	0.025	0.015	0.015	0.09	0.20	0.22	0.50	0.005

*Table I: Chemical composition of thermomechanically rolled steels. *The sum of Nb, V and Ti shall be max. 0.22%. **If ordered, the sulphur content shall be max. 0.01%*

ISSN 1510-7450

Name	Material number	Minimum yield strength[MPa]	Tensile strength [MPa]	Min percentage elongation at fracture		Bending at 180° min. mandrel diameter
				t<3 L_0=80 mm	t≥3 L_0=5.65$\sqrt{S_0}$	
S315	1.0972	315	390 – 510	20	24	0t
S355	1.0976	355	430 – 550	19	23	0.5t
S420	1.0980	420	480 – 620	16	19	0.5t
S460	1.0982	460	520 – 670	14	17	1t
S500	1.0984	500	550 – 700	12	14	1t
S550	1.0986	550	600 – 760	12	14	1.5t
S600	1.8969	600	650 – 820	11	13	1.5t
S650	1.8976	650	700 – 880	10	12	2t
S700	1.8974	700	750 - 950	10	12	2t

Table II: Mechanical properties for thermomechanically rolled steels. The values for the tensile test apply to longitudinal test pieces. The values for the bent test apply to transverse test pieces. For t>8 mm the min. yield strength can be 20 MPa lower.

Sample	**S355**	**S420**	**S500**
C	0.09	0.10	0.09
Mn	0.35	0.47	1.41
Si	0.02	0.01	0.02
S	0.008	0.010	0.012
P	0.011	0.016	0.019
Ti	--	--	0.075
Nb	0.021	0.044	0.047
Al	0.038	0.029	0.031

Table III: Chemical analysis of the three steel samples tested.

Table IV presents the mechanical characteristics of the steel sheets tested parallel to the rolling direction, according to EN1002-1. The value of the *n* coefficient was calculated from the engineering curves, as indicated by ASTM E-646-00 (Standard Test Method for Tensile Strain-Hardening Exponents "*n*-Values" of Metallic Sheet Materials) which allows the calculation of the rational tension curve $\sigma = k\varepsilon^n$ (σ true stress; ε true strain; *k* resistance coefficient). Figure 1 shows the engineering stress-strain curve (s-e) of the mentioned steel sheets, adding as a reference the curves of 2 other cold worked steels: an IF steel (free of interstitials and microalloyed with Ti) and a dual-phase DP (Si-Mn-B) steel also produced at Arcelor Mittal in Asturias[11]. Figure 2 presents for the same steels the logarithmic scale of both stress (σ) and strain (ε) which is used to calculate *n* and *k* coefficients by linear regression adjustments of the data.

Sample	S355	S420	S500
t (mm)	3.5	5.2	4.5
R_{eH} (MPa)	401	465	630
R_{eL} (MPa)	390	449	618
e_L (%)	1.6	2.0	2.3
R_m (MPa)	440	534	678
A (%)	33*	27**	26*
R_{eL}/R_m	0.89	0.84	0.91
n	0.12	0.16	0.10
$\overline{G}$ (ASTM)	13.2	13.3	14.2
σ_G (ASTM)	1.40	1.47	1.05
$\overline{L}$ (μm)	3.2	3.1	2.3
%RA	7.6	7.9	5.3

*Table IV: Mechanical properties and parameters of the samples tested, along with quantitative metallographic results. *L0=50 mm. ** L0=55 mm*

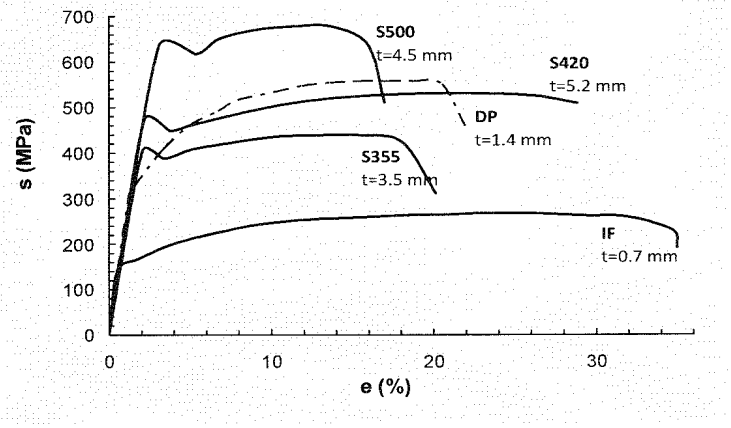

Figure 1: Stress-strain engineering curves of investigated steel sheets and data of DP and IF [11]

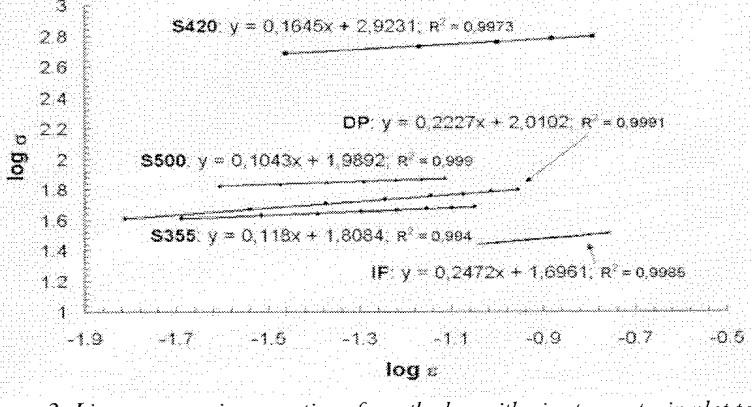

Figure 2: Linear regression equations from the logarithmic stress-strain plot to determine n coefficient

To determine the grain size G and mean linear intercept $\overline{L}$, metallographic samples of the steel sheets were obtained from the transverse section of the orientation parallel to the rolling

ISSN 1510-7450

direction, they were subsequently polished and etched with Nital-2 to reveal the microstructure. Measurements were made in an automatic digital image analysis equipment coupled to a metallographic optical microscope, operated according to ASTM E-112 and ASTM E-1181-02 standards. Counting contemplated as many micrographs as necessary to obtain mean values of G and $\overline{L}$, with a confidence level interval of 95 per cent and a deviation lower than 10 per cent[12]. Table IV also summarizes mean values of G, standard deviation σ, mean linear intercept $\overline{L}$ and mean deviation RA. The relation between G and $\overline{L}$ was obtained using the formula[13]:

$$G = -3.356 - 6.644 \log \overline{L}(mm) \qquad [1]$$

Figures 3, 4 and 5 show micrographs along with counting patterns and histograms of grain number G, that were used to determine the data of table IV of the investigated steels. As expected, these are UFG steels with a structure majorly ferritic and a small amount (less than 10 per cent) of pearlite.

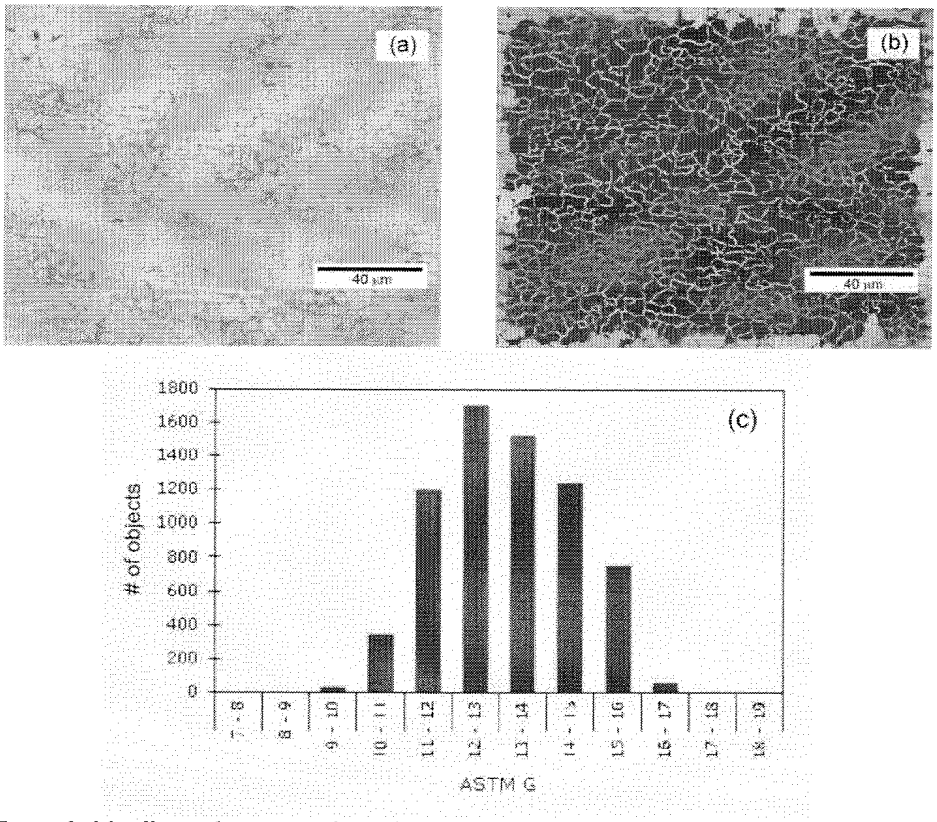

Figure 3: Metallographic image of sample S355 (a), along with detected grain pattern (b) and ASTM G grain size distribution histogram (c)

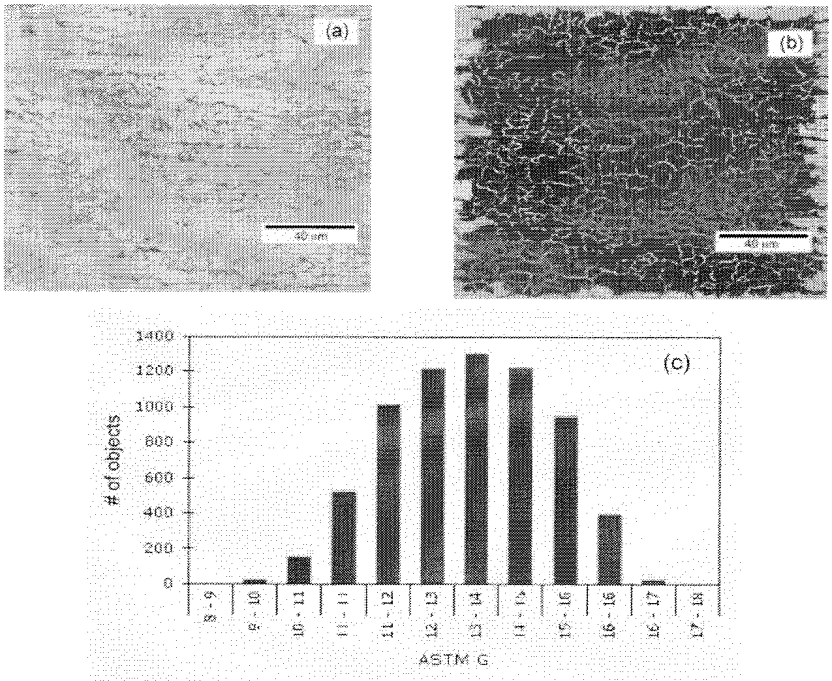

Figure 4: Metallographic image of sample S420 (a), along with detected grain pattern (b) and ASTM G grain size distribution histogram (c)

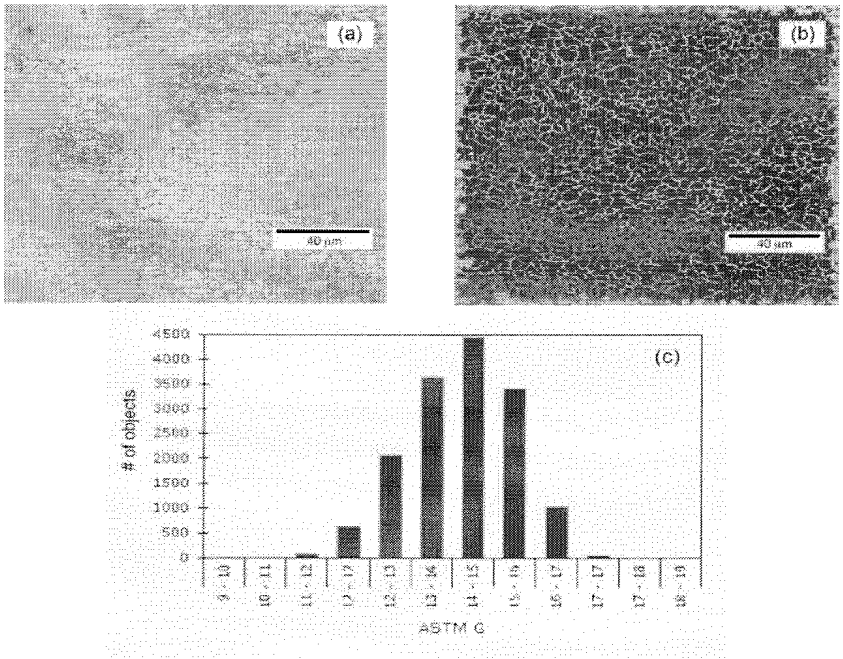

Figure 5: Metallographic image of sample S500 (a), along with detected grain pattern (b) and ASTM G grain size distribution histogram (c)

ISSN 1510-7450

3. Discussion.- It is a well known fact in physical metallurgy, the plastic instability that the UFG steels may present when tension tested[14-20]. In the case of this work, as shown in fig. 1, the yielding instability zones of the steels are between 1.5 and 2.5 per cent, but after that, a uniform plastic strain-hardening deformation is followed. There are three reasons for this:

3.1 Strain-hardening *n* coefficient of these steels diminishes with grain size, in accordance to a Morrison type law [14]:

$$n = 5/\left(10 + d^{-1/2}\right) \qquad [2]$$

where *d* is the mean linear intercept ($\overline{L}$) in mm. Thus, in a steel with grain size d=10μm (0.010 mm), the theoretical *n* value would be n=0.25; for a grain size of d=1μm, the coefficient would be n=0.12, which are calculations that usually exceed the real *n* value.

3.2 The second reason, based on the first one, explains the increasing plastic instability in UFG steels as the grain size becomes smaller. Heterogeneous deformations are generated in the steel, known as Lüders bands, with increasing amplitude ε_L as the capacity of the material for strain-hardening diminishes. When $\varepsilon_L \approx n$ the steel presents necking without showing uniform plastic deformation.

Morrison and Miller[15] quantified the plastic instability limit condition for a steel with a true stress-strain curve that must fit a Ludwik-Hollomon expression of the type $\sigma = k\varepsilon^n$. In other words:

$$\varepsilon_L = n \qquad [3]$$

If s_y is designated as the lower engineering yield stress in tension:

$$\sigma_y = s_y\left(1 + e_L\right) = k\varepsilon_L^n \qquad [4]$$

where σ_y is the true tension yield stress. Combining equations [3] and [4]:

$$k/s_y = \exp[n(1 - \ln\varepsilon_L)] \qquad [5]$$

for which the limit curve ($\varepsilon_L = n$) is represented in figure 6 as k/s_y versus *n*. This last figure highlights that all the steels with traction parameters below the limit curve will not reach uniform plastic deformation levels. The steels presented in this work are above the limit curve but very close to it ($n \approx 0.1$). On the contrary, IF and DP steels, taken as a reference, are well above the limit curve and generate high uniform plastic deformations as they show *n* values above 0.2.

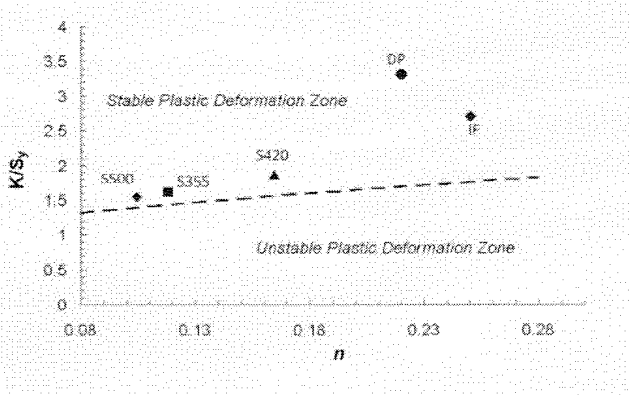

Figure 6: K/Sy ratio plotted vs. n coefficient for the investigated steel sheets

3.3 Cold work in these steels, both from forward deep drawing, as by biaxial expansion is possible when the sheets (mechanically considered as membranes with plane stress states) have strain hardening *n* coefficients and thickness sufficiently high enough. Keeler-Goodwin[21,22],

Backofen[15] and Hosford[19] have shown, among others, that the critical state of deformation in a stamping process is the plane strain state: ε_1 (maximum principal strain in the plane of the sheet) = n; ε_2 (minimum principal strain in the plane of the sheet) = 0; strain according to thickness $\varepsilon_3 = -\varepsilon_1 = n$ [23]. As these formulas show, the n coefficient is a critical factor. Furthermore, in biaxial forward stretching, in order for the sheet to access forming in plane-stress conditions without necking (deformation is located in the thickness direction), it is only possible if the sheet has weaker zones or less thick ones, that allow the plastic collapse. Because of that, Marciniak and Kuczynski[24] defined a defect factor $f = t_{0B}/t_{0A}$ (figure 7) which would make the necking possible in trajectories $\sigma_2/\sigma_1 > 0$ (where σ_2 and σ_1 are respectively the minimum and maximum biaxial tensions at the plane of the sheet). In these conditions the maximum load the sheet can withstand is reached when the deformation at the defect equals the n value. Therefore:

$$\varepsilon_1 > 0\,;\ \varepsilon_2 = 0\,;\ \varepsilon_3 = -\varepsilon_1 \text{ (plane strain)} \qquad [6]$$

$$\ln(t/t_0) = -\ln(l_1/l_0) = -n \text{ (at the limit)};\ t = t_0 \exp(-n) \qquad [7]$$

$$\sigma_{1A} t_A = \sigma_{1B} t_B \text{ (stress compatibility)} \qquad [8]$$

$$k\varepsilon_A^n t_{0A} \exp(-\varepsilon_A) = k\varepsilon_B^n t_{0B} \exp(-n) = kn^n t_{0B} \exp(-n) \qquad [9]$$

$$\varepsilon_A^n \exp(-\varepsilon_A) = (t_{0B}/t_{0A}) n^n \exp(-n) = f n^n \exp(-n) \qquad [10]$$

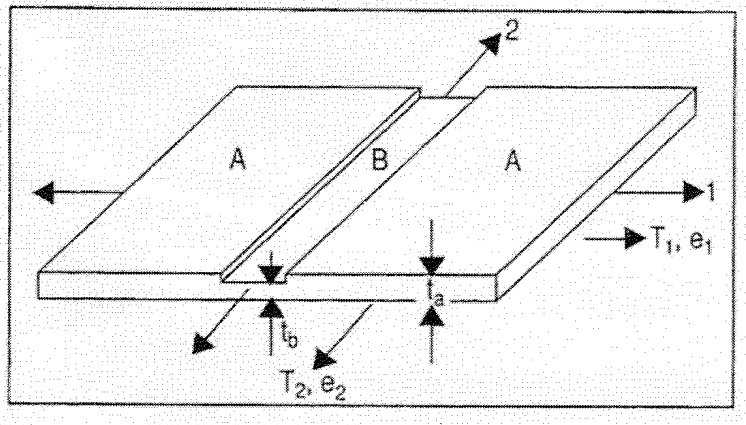

Figure 7: Schematic representation of a steel sheet with preexisting defect. Plane strain conditions

An approximate solution to equation [8] is the following:

$$\varepsilon_A = \varepsilon_u = n - \sqrt{n(1-f)} \qquad [11]$$

Figure 8 presents the variation of ε_A (limit deformation) as a function of the defect factor *1-f* for values of n = 0.05, 0.15 and 0.25 respectively. It may be observed that for thickness tolerances of $f \approx 0.990$, inferior to the ones admitted in the Euronorm EN 10051:199 (Continuously hot-rolled uncoated plate, sheet and strip of non-alloy and alloy steels. Tolerances on dimensions and shape) in hot rolled products ($f \approx 0.975$), and superior to cold ones ($f \approx 0.995$), with values of $n \approx 0.1$ the sheet may present necking, as if it were cold-worked rolled before withstanding substantial homogeneous deformations. Thus, if the *f* factor and thickness tolerances of the sheet

are added to the decrease in the n value as the grain size diminishes (UFG steels), cold work forming in biaxial expansion will not withstand homogeneous deformations as required by the manufacturing process.

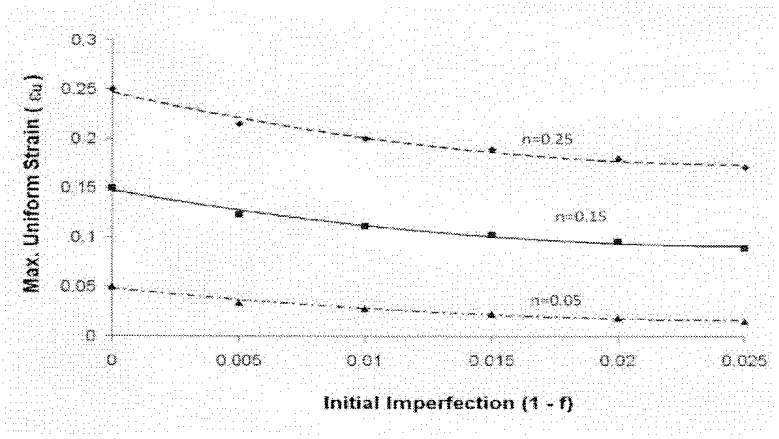

Figure 8: Maximum uniform strain as a function of initial imperfection 1-f in the steel sheet for n coefficient values of 0.05, 0.15 and 0.25

4. Conclusions.- Steels standardized by Euronorm EN-10149-2 in its raw state of hot rolling are in fact UFF (UFG) steels, showing yield stresses in the interval of 315 to 700 MPa and strain hardening coefficients that decrease with yield stress but superior to 0.1.

There are two factors that result in the extinction of the n coefficient, that disable cold-work operations. The first one is an excessively small grain size close to 1μm (16-17 ASTM), which makes uniform deformation processes and strain hardening impossible.

The second one is that thickness tolerances, necessarily admitted in hot and cold rolled products ($0.975<f<0.995$) have an impact in the form of defects in products manufactured by biaxial drawing, so for values of n lower than 0.1 (which means that maximum homogeneous deformations ε_u reaches 0) the steel may not be cold formed.

5. Acknowledgments.- The Sid-met-mat group authors from ETSIMO (Oviedo University, Spain) wish to thank the Central Laboratories and the Hot Coil installation of Arcelor Mittal de Asturias (Spain) factory for their selfless and efficient collaboration. Also to Mr. J.O. García, Ms. T. Iglesias and Ms. B. Mendieta for their valuable contribution in the experimental work and revision of text and figures.

6. References

[1] González, R., García, J.O., Barbés, M.A., Quintana, M.J., Verdeja, L.F., Verdeja, J.I. Ultrafine Grained HSLA Steels for Cold Forming. Journal of Iron and Steel Research International, 2010, vol. 17, num. 10, pp. 50-56.

[2] Special Issue on Ultrafine Grained Steels, ISIJ Int., 2008, vol. 48, num. 8.

[3] Advances in the hot rolling of steels, Conference Report, Ironmaking and Steelmaking, 2004, vol. 31, num. 1, pp. 8–13.

[4] Sakai, T., Belyakov, A., Miura, H. Ultrafine Grain Formation in Ferritic Stainless Steel during Severe Plastic Deformation. Met. and Mat. Trans. A, 2008, vol. 39A, pp. 2206–2214.

[5] Okitsu, Y., Takata, N., Tsuji N. A New Route to Fabricate Ultrafine Grained Structures in Carbon Steels without Severe Plastic Deformation, *Scripta Mat.*, 2009, vol. 60, pp.76–79.

[6] Tsuji, N., Ito, I., Saito, Y., Minamino, Y., Strength and ductility of ultrafine grained aluminum and iron produced by ARB and annealing, *Scripta Mat.,* 2002, vol. 47, pp. 893–899.

[7] Beladi, H., Kelly, G. L., Hodgson, P. D. The Effect of Multiple Deformations on the Formation of Ultrafine Grained Steels, *Met. and Mat. Trans. A,* 2007, vol. 38A, pp. 450–463.

[8] Beladi, H., Kelly, G. L., Hodgson, P. D. Ultrafine grained structure formation in steels using dynamic strain induced transformation processing, *Int. Mat. Rev.,* 2007, vol. 52, num. 1, pp. 14–28.

[9] Lesch, C., Alvarez, P., Bleck, W., Gil-Sevillano, J. Rapid Transformation Annealing: A Novel Method for Grain Refinement of Cold-Rolled Low-Carbon Steels, *Met. and Mat. Trans. A,* 2007, vol. 38A, pp. 1882–1890.

[10] Howe, A. A. Ultrafine grained steels: industrial prospects, *Mat. Sci. and Tech.,* 2000, vol. 16, pp. 1264–1266.

[11] Pero-Sanz, J. A. *Steels: Physical Metallurgy. Selection and Design*, CIE–Dossat 2000, Madrid, Spain, 2004, pp. 257–270. (in Spanish)

[12] Sellars, C. M. *Quantitative Metallography* Presented for the "Master en Metalurgia Física" course at CEIT de Guipúzcoa, Universidad de Navarra, San Sebastián, Spain, 1981.

[13] VanderVoort, G. F. *Metallography. Principles and Practice*, ASM International, Ohio, U.S., 1999, pp. 216–217.

[14] Morrison, W. B. The effect of grain size on the stress-strain relationship in low-carbon steel, *Trans. of the ASM*, 1966, vol. 59, pp. 824–846.

[15] Morrison, W. B., Miller, R.L. *The ductility of ultra-fine-grain alloys. Ultrafine–grain Metals*, Syracuse University Press, New York, U.S., 1970, pp. 183–211.

[16] Backofen, W. A. Deformation processing, *Met. Trans.,* 1973, vol. 4, pp. 2679–2699.

[17] Leslie, W. C. *The Physical Metallurgy of Steels*, McGraw–Hill. International Book Company, U.S., 1981, pp. 1–67.

[18] Dieter, G. E. *Mechanical Metallurgy*, McGraw–Hill Series in Materials Science and Engineering, U.S., 1981, pp. 187-208, 329–377.

[19] Hosford, W. F., Duncan, J. L. Sheet Metal Forming: A Review, *J. of Met.,* 1999, pp. 39 – 44.

[20] Hosford, W. F. *Physical Metallurgy*, CRC Press, London, U.K., 2005, pp. 349–361.

[21] Keeler, S.P. Determination of Forming Limits in Automotive Stampings, SAE Mid – Year Meeting, Chicago, U.S., 1965.

[22] Goodwin, G.M.. Application of Strain Analysis to Sheet Metal Forming. Problems in the Press Shop, SAE Congress, Detroit, U.S., 1968.

[23] Dinda, S., James, K.F., Keeler, S.P., Stine, P. A. How to use circle grid analysis for die tryout, ASM Ed., U.S., 1981.

[24] Marciniak, Z., Kuczynski, K. Limit strains in the processes of stretch forming sheet metal, *Int. J. Mech. Sci.*, 1967, vol. 9, pp. 609 – 620.

Materials Science and Technology (MS&T) 2011
October 16-20, 2011, Columbus, Ohio · Copyright © 2011 MS&T'11®
Recent Developments in Steel Processing

Dual-Phase Ultrafine Grained Steels Produced by Controlled Rolling Processes

M.J. Quintana, R. Gonzalez
School of Engineering, Universidad Panamericana, Mexico City, Mexico

L.F. Verdeja, J.I. Verdeja
E.T.S.I.M.O., Oviedo University, Oviedo, Spain

Keywords: dual-phase steels, ultrafine grained, strain hardening

Abstract

Double-phase steels are an excellent alternative in the production of automotive parts that require high mechanical resistance, high impact strength and elevated elongation. These materials are produced using low-alloy steels as a basis, reducing costs and resulting in a combination of martensite and ferrite structures with ultrafine grain sizes. These characteristics are accomplished through a strict control of rolling conditions: strain rate, cooling rate and direct quenching. This work presents the results of tension testing of two types of double phased steels, along with microstructural characterization, in order to understand the effect of the advanced thermomechanical controlled rolling processes on the formation of the microstructure and the resulting mechanical properties.

Introduction

As structural materials, double-phase steels (DP) show excellent mechanical properties, which also allow weight reduction in the design of mechanical parts, particularly in the automotive industry, due to a high strength – elongation ratio, excellent impact response and consequently, the possibility of using thinner sections [1].

The microstructure of these steels is usually a soft phase (normally ferrite) combined with the dispersion of a hard phase (almost always martensite with traces of bainite). This microstructure results, mechanically, in a soft yield behavior, low yield stress / tension stress ratio and elevated formability [2].

The production of these steels is achieved by the use of thermomechanical hot rolled processes at temperatures close to A_{r3}, where the strict control of the rolling parameters and the cooling rate allow finished products that present grain sizes close to 1 μm, also known as ultrafine grained steels (UFG) [3,4].

The strength of the DP steels is related with the amount of plastic deformation applied during the thermomechanical processes in the intercritic region, due to the formation of substructures in the ferrite. The epitaxial ferrite (phase that grows with thermomechanical processes) is the reason why the tension stress improves while increasing the reduction in the transverse area during rolling. This is achieved without a significant reduction in the ductility of the material [5].

In this type of steels, the reduction in grain size has a very important effect in the strain hardening coefficient n from the plastic behavior equation: $\sigma = K\varepsilon^n$. The n parameter must have a value higher than 0.1 in order to allow forming of final parts [6,7].

Although the use of microalloying elements (like Cr or Ni) may result in an increase in strength, it also has a detrimental effect in the material's formability during manufacturing, that makes the low alloy steels (C, Si and Mn) ideal candidates in order to obtain ultrafine grained microstructures, as well as the geometry of final products (drawing, bending, etc.) [8].

In this research, two double-phase steels with ultrafine grain sizes are investigated analyzing their phase percentage (martensite and ferrite), as well as their low-alloy chemical composition, and linking these parameters with their mechanical properties, which result in very good options for the manufacture of automotive parts with high strength/weight ratio.

Experimental Procedure

The present work used steel strips with 1.35 mm in thickness (t), of two types of double-phase steels (DP600 and DP780). These steels have a chemical composition with the following ranges: 0.03-0.1 %C, 0.04-0.6 %Si, 1.5-2.1 %Mn, <0.015 %P and <0.010 %S.

The strips were made with advanced thermomechanical controlled rolling processes (ATMCRP) from its raw rolled state in the ArcelorMittal de Avilés facilities in Oviedo, Spain. This process consists in the control of the speed and amount of deformation of sheets at adequate times and temperatures to achieve the dual microstructure, in the following steps:

1. *Homogenization.* The slabs obtained by continuous casting with 200~250 mm in thickness, are maintained at temperatures of 1200~1250 °C to start with a recrystallized structure.
2. *Roughing.* In reversible rolling trains (husk tool and roughing tool), approximately 10 passes are made to reduce the thickness to ~20 mm and maintaining a temperature of 1200~1100 °C.
3. *Waiting.* Before the finishing train, the material is cooled to 1100~1000°C.
4. *Finishing.* Consists in a train of hot or semicontinuous bands (7 boxes). The temperature drops to 850 °C, obtaining a thickness of ~1.5 mm.
5. *Controlled cooling.* Atomized water is used as a cooling method until it reaches coiling temperature (~600 °C). During this cooling the partial transformation $\gamma \rightarrow \alpha$ takes place (if the cooling rate increases, the ferrite percentage diminishes).
6. *Coiling.* The sheet is coiled at a temperature of ~600 °C, so that below this temperature the untransformed austenite becomes bainite-martensite. It is very important that the coiling window between the ferritic-pearlitic zone (upper) an the bainitic-martensitic one (lower) matches the mentioned temperature. Below this, with the steel already coiled, the untransformed austenite will become bainite-martensite.

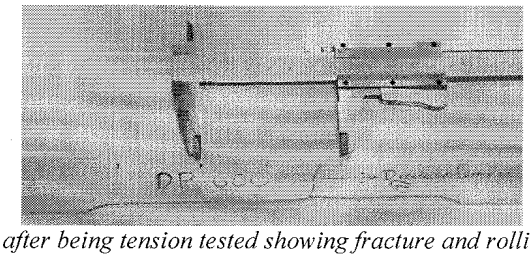

Figure 1 Specimen after being tension tested showing fracture and rolling direction (arrow)

To manufacture steel specimens and determine its mechanical characteristics, the ASTM E8-04 (Standard Tension Testing of Metallic Materials) [9] standard was followed. The samples were tested in an INSTRON 5583-Standard universal machine with a calibrated extensometer distance of 50 mm, using a displacement rate of 10 mm/min until the total fracture of the specimens (figure 1). For each of the steel compositions (DP600 and DP780), two tension tests were made to corroborate the repeatability of the mechanical behavior. The strain hardening coefficient was obtained following the ASTM E646-78 standard [10], for each of the specimens tested.

In order to microstructurally characterize the samples, a metallographic cutter was used to cut the specimens and observe longitudinal sections of them. Traditional grinding and polishing techniques were used to obtain mirror finish, and they were etched in a nitric acid 2% solution (nital-2). Metallographic characterization was made through optical microscopy with a Nikon Epiphot equipment with 10x, 20x and 40x lenses. Quantitative analysis of the grain sizes of the ferrite and the martensite, was made using a Buehler Omnimet image analyzer connected to the optic microscope.

Results

Figure 2 presents the stress-strain (engineering) curves for both the DP600 and the DP780 steels. From the figure, it is evident that the 780 presents a higher yield and tension stresses close to 800 MPa, while the DP600, with tension stress close to 650 MPa has a higher total deformation (A %) before fracture (table 1).

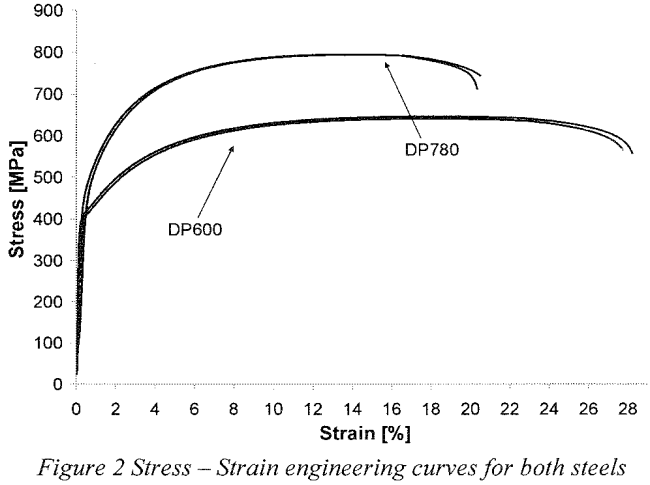

Figure 2 Stress – Strain engineering curves for both steels

Also, in the DP600 steel, the yield stress is clearly marked (threshold activation stress for the dislocation movement), in comparison to the DP780 where it was necessary to calculate the parallel line at a 0.2 % deformation to estimate the yield stress.

Figure 3 presents the linear regression curve of the plastic deformation between the true yield and the true maximum stresses (logarithms) to calculate the coefficient n (strain hardening coefficient), when considering the linearity of the equation:

$$\log \sigma = n \log \varepsilon + \log K \quad (1)$$

where n is the slope of the straight line obtained by linear regression, these values are presented in table 1. Both are higher than 0.1 which means that it is high enough for manufacturing processes such as bending or drawing, though the DP780 has a higher value due to its higher strength and lower plasticity.

Table 1 Dual-phase steels mechanical properties

	DP600	DP780
S_Y (MPa)	353.6	365.3
S_{max} (MPa)	644.6	794.9
A (%)	27.95	20.41
S_Y/S_{max}	0.55	0.46
n	0.2	0.2

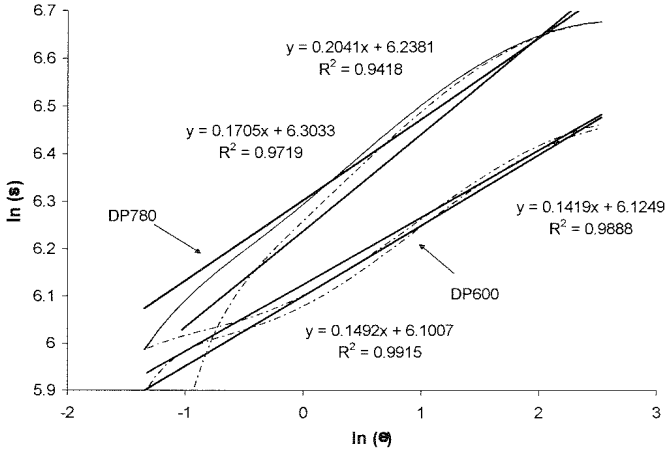

Figure 3 Linear regression for the strain hardening coefficient n for both steels, including the regression equation and correlation coefficient (R^2)

Figures 4 and 5 present the microstructure (a), the identification of the phase by the Buehler Omnimet equipment (b), the ferritic phase grain size histogram (c) and the martensitic phase grain size histogram (d) for both the DP600 and DP780 steels, respectively. It may be observed that the DP600 steel has a slightly equiaxed microstructure and the elongation of some grains in horizontal (rolling) direction is also slightly noted. This same rolling effect is clearly evident in the banded structure of the DP780. The distribution of the ferrite grain sizes indicates that this phase in the DP600 can be approximated to a normal distribution with mean grain size between 14 and 15 ASTM G. On the other hand, the DP780 grains are a combination of big and small ones, with mean grain size of 17-18 ASTM G.

Regardless of the previous, the martensite (figures 4d and 5d) in both steels is presented as a continuous phase, so it does not allow to determine delimited zones or grains and it is only possible to calculate its volumetric fraction: close to 20% for DP600 and close to 45% for DP780.

Figure 6 compares the microstructure of both steels after being tension tested. Independently of the variation of martensite amount and the banded structure in the DP780, the ferrite grain size is considerably higher in the DP600 steel (figure 6a).

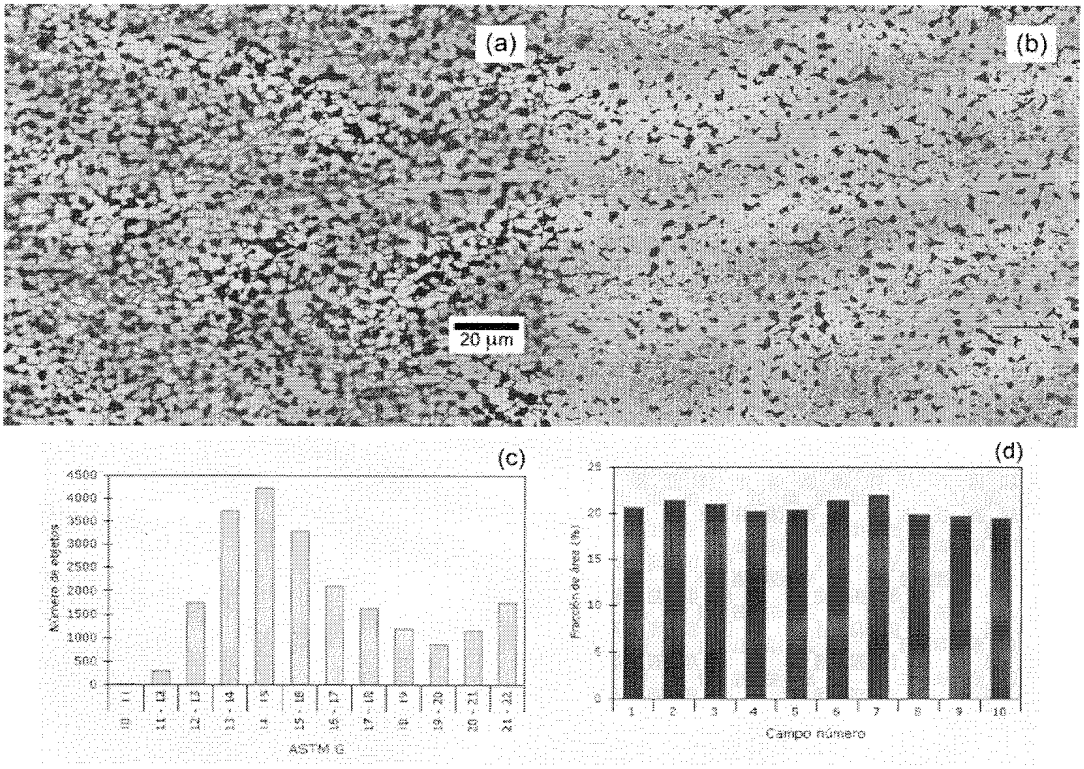

Figure 4 Quantitative metallography of the microstructure (a) of the DP600 steel, phases identification (b), ferrite grain size histogram (c) and percentage amount of martensite (d).

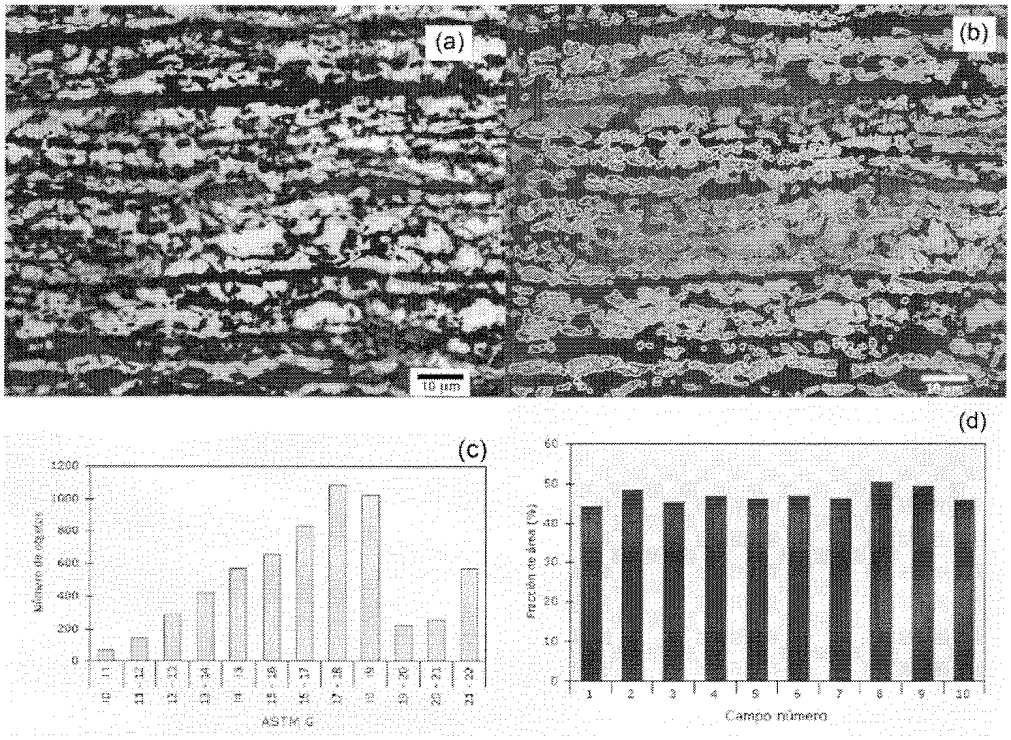

Figure 5 Quantitative metallography of the microstructure (a) of the DP780 steel, phases identification (b), ferrite grain size histogram (c) and percentage amount of martensite (d).

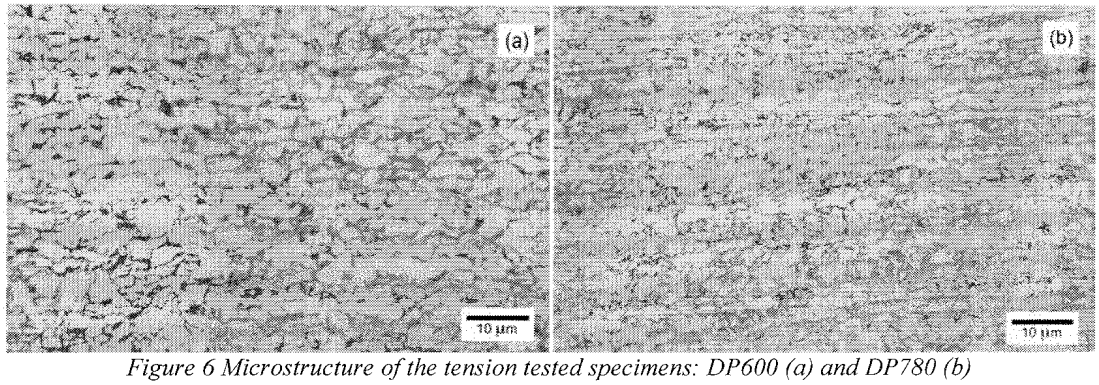

Figure 6 Microstructure of the tension tested specimens: DP600 (a) and DP780 (b)

Discussion

In these low alloy steels, the ATMCRP rolling process achieves, independently of the chemical composition of the steel, double-phase ferritic-martensitic structures with different amounts of martensite (in this case between 20 and 45%) or different ferrite grain sizes (from 14 to 18 ASTM G). Controlled rolling, controlled cooling and direct quenching simultaneously contribute in the modification of the static and dynamic recrystallization mechanisms of the $\gamma \rightarrow \alpha$ transformation, as well as non-diffusive processes of the martensitic formation by accelerated cooling.

Comparing figures 2, 4d and 5d, it is evident that the DP780 steel is more resistant than the DP600 due to its higher martensite amount in its microstructure, because this phase's geometry is an effective barrier to dislocations in deformation, while the higher plasticity in the DP600 can be directly attributed to the higher ferrite amount and a higher grain size (figures 4c and 5c).

When observing the stress-strain curve (figure 2) close to the yield stress, the DP600 steel shows instability at this point (564 MPa), which means that the material plastic deformation process is mainly controlled by the deformation of grains or ferritic zones (as shown in figure 6a). On the other hand, the softness of the DP780 curve indicates that the interaction between the martensitic and ferritic phases (hard and soft) results in a plastic deformation with a *n* coefficient of 0.2. This plastic deformation coefficient in both steels is high enough to allow subsequent processes (drawing and bending) in the manufacture of parts. In other works [11-14], it has been observed that a *n* coefficient lower than 0.1 results in an instability during the rolling process, as well as during the manufacture of finished products (specially automotive ones). Therefore, the controlled rolling processes (ATMCRP) are very attractive in order to obtain products with low S_y/S_{max} ratio (table I), tension stresses between 650 and 800 MPa and plastic deformations between 12 and 20%, specifically designed to fulfill applications of low—weight products and/or high mechanical reliability.

Conclusions

The advanced thermomechanical controlled rolling processes (ATMCRP) allow, specially through direct quenching of the steel sheets, modifications in the amount of martensite present in the double-phase steels, as well as the size and distribution of the soft ferrite grains, which mechanically results in finished products with tension stresses reaching 800 MPa, which is only possible for a low alloy steel if the formed microstructure is of the ultrafine grained type (>15 ASTM G).

It is also very important that the strain hardening coefficient *n* presents a high enough value (>0.1), in order to avoid instabilities and defects during the drawing and bending processes used in the manufacture of products from the automotive industry or others. Otherwise, the steel may have very limited or non practical applications.

Acknowledgments

The present work would not have been possible without the help of the Hot Coiled Products Department of ArcelorMittal de Asturias (Oviedo, Spain), as well as the help of Ms. Bertha Mendieta in the revision of figures and tables.

References

[1] K. Mukherjee, S.S. Hazra and M. Militzer, Grain Refinement in Dual-Phase Steels, *Metall. Mater. Trans. A*, Vol. 40A (September), 2009, p 2145-2159.

[2] M. Mazinani and W.J. Poole, Effect of Martensite Plasticity on the Deformation Behavior of a Low-Carbon Dual-Phase Steel, *Metall. Mater. Trans. A,* Vol. 38A (February), 2007, p 328-339.

[3] A.R. Salehi, S. Serajzadeh, S, A. Karimi Taheri, A study on the microstructural changes in hot rolling of dual-phase steels, *J. Mater. Sci.,* Vol. 41, 2006, p 1917–1925.

[4] T. Waterschoot, A.K. De, S. Vandeputte and B.C. De Cooman, Static Strain Aging Phenomena in Cold-Rolled Dual-Phase Steels, *Metall. Mater. Trans. A*, Vol. 34A (March), 2003, p 781-791.

[5] E. Ahmad, M. Sarwar, T. Manzoor and N. Hussain, Effect of rolling and epitaxial ferrite on the tensile properties of low alloy steel, *J. Mater. Sci.*, Vol. 41, 2006, p 5417-5423.

[6] X. Liu, H. Lan, L. Du and W. Liu, High performance low cost steels with ultrafine grained and multi-phased microstructure, *Sci China Ser E-Tech Sci,* Vol. 52, 2009, p 245-2254.

[7] J.V. Laukonis and R.H. Wagoner, Plastic Behavior of Dual Phase Steel Following Plane-Strain Deformation, *Metall. Mater. Trans. A,* Vol. 16A, 1985, p 421-425.

[8] W.J. Nam and C.M. Bae, Microstructural evolution and its relation to mechanical properties in a drawn dual-phase steel, *J. Mater. Sci.*, Vol. 34, 1999, p 5661 – 5668.

[9] E8-04, Standard Tension Testing for Metallic Materials, ASTM, 2004, USA.

[10] E646-78, Standard Test Method for Tensile Strain-Hardening Exponents (n-values) of Metallic Sheet Materials, ASTM, 1978, USA.

[11] N. Tsuji, I. Ito and Y. Saito, Strength and ductility of ultrafine grained aluminum and iron produced by ARB and annealing, *Scripta Mater.*, Vol. 47, 2002, p 893–899.

[12] H. Beladi, G.L. Kelly and P.D. Hodgson, Ultrafine grained structure formation in steels using dynamic strain induced transformation processing, *Int. Mater. Rev.*, Vol. 52, 2007, p 14–28.

[13] T. Furuhara T, Special Issue on Ultrafine Grained Steels, *ISIJ Int.*, Vol. 48, 2008, p 1037-1157.

[14] Y. Okitsu, N. Takata and Y. Tsuji, A new route to fabricate ultrafine–grained structures in carbon steels without severe plastic deformation, *Scripta Mater.*, Vol. 60, 2009, p 76–79.

Materials Science and Technology (MS&T) 2012
October 7-11, 2012, Pittsburgh, Pennsylvania

Recent Developments in Steel Processing

SUPERPLASTICITY OF ULTRAFINE GRAINED LOW-CARBON HSLA STEELS

José Ignacio Verdeja[1], María José Quintana[2], José Ovidio García[1], Luis Felipe Verdeja[1], Roberto González[2], Sara Fernandez[1]

[1]*E.T.S.I.M.O., Universidad de Oviedo, Oviedo, 33004, Spain*
[2]*School of Engineering, Universidad Panamericana, Mexico City, 03920, Mexico, robglez@up.edu.mx*

Keywords: superplasticity, ultrafine grained, high temperature test, strain rate *m* coefficient, boundary sliding

Abstract

Steels with ultrafine grained structure may present superplastic behavior at specific temperatures and strain rates that allow the grain boundary sliding mechanisms to be activated. The work presents high temperature tension tests in a low carbon, low alloy steel obtained by advanced thermomechanical controlled rolling processes, showing at 800°C elongations as high as 200%. The microstructure of the steel was analyzed in order to identify ferrite and pearlite grain boundaries, and their interaction after the specimens were deformed, showing intergranular decohesions, restored ferrite grains and elimination of banded structure, which are evidence of superplastic mechanisms in this material which is, in fact, ultrafine grained as demonstrated by quantitative metallographic techniques and grain size distribution analysis.

Introduction

Ultrafine grained steels (grain size $\overline{d} \approx 1\sim5\mu m$) are currently intensively studied worldwide, as they offer a solution to finding very high strength materials. They also present high toughness and are produced from standard steel compositions (which reflects in low cost) [1].

Recent works have shown that the ultrafine grained structure may be obtained in a hot rolling mill by Advanced Thermomechanical Control Rolling Processes (ATMCRP) and not only from small scale laboratory tests [2,3]. However, under some circumstances these materials may present an important disadvantage as they exhibit unstable plasticity upon yielding, severely restricting its potential uses [4]. In order to avoid this instability [5] the mechanical behavior of the steel must show a strain hardening coefficient *n* (as measured by tension test with the ASTM standard) higher than 0.1, in its hot rolling raw state. If this is achieved, the steel can be used for cold-work operations such as bending, stretching and drawing and in commercial applications such as automotive and other manufacturing industries [2].

The HSLA steels described in Euronorms 10149-2 and 10051 are examples of these materials, as well as other construction steels or automotive special steels (just as the ones described in the ultralight steel auto body – ULSAB project), resulting in lower cost materials and a step forward in the research for better materials in industry, such as lightweight structures and components with very good weldability and easier to recycle, all of this, reducing the cost of the alloy and meeting

high specifications with steels that have a lower amount of alloying elements and that are considered high-tech [6]. Furthermore, ultrafine grained steels (UFG) may be applied in the future in most of the steel markets and can be used in other industrial applications, such as the ones that require superplastic behavior, just as this work demonstrates.

A large number of non-ferrous alloys show superplasticity behavior during isothermal tensile testing. This behavior is characterized by large elongations, usually higher than 100% and sometimes reaching 1000% or more. Superplasticity, object of numerous research activities that started in the 1960~1970s, has the following properties:

- high strain rate sensitivity to the flow stress as the essential and unique characteristic of superplasticity [7],
- strong variation of properties as a function of grain size and strain rate [8],
- relevance of grain boundary sliding in the deformation mechanism [9],
- vacuum forming of the metal sheet when deformed against the die [10] and
- grain boundary sliding by diffusion and accommodation processes [11].

In other words, in order for the superplastic behavior to show high strain rate sensitivity, high temperature testing (> ½ T_m), a fine microstructure and a relatively low strain rate are required [12-14].

As an example of this, the work presents the high temperature superplastic behavior of an UFG steel microalloyed with Ti-Nb obtained by ATMCRP at the Arcelor Mittal factory in Veriña (Gijón, Spain), as materials of this type can show this behavior when certain conditions are met [15,16]. The characteristics of the steel, delivered in the form of 27.6mm in thickness sheets, are described in the experimental procedure.

Experimental procedure

The specified chemical composition for this steel (in weight %) according to the Euronorm is: C 0.168, Mn 1.361, Si 0.453, P 0.022, S 0.009, Cu 0.026, As 0.003, Al 0.028, Cr 0.035, Ti 0.026, V 0.002, Nb 0.033, Mo 0.004, Ni 0.031, Sn 0.002, Al (soluble) 0.027, B 0.0001, N 0.0055, Zr 0.0000, Ca 0.0001, O 0.0000, H 2.00 ppm, B (soluble) 0.0000. In the same way, the specified mechanical properties are: higher yield stress (σ_y) = 447 MPa, rupture stress (σ_{max}) = 567 MPa, yield elongation with L_0 of 50 mm (El) = 31 % and impact resistance at -20 °C (KCV) = 96 J.

The samples for the tests were obtained from the steel sheet in an axis parallel to rolling direction and were machined in a cylindrical shape: 10 mm in diameter and calibrated gage length of either Lo = 57 or Lo = 30 mm (ASTM E21-05 standard).

High temperature tension tests were made at different temperatures between 600 and 900°C (50°C intervals) and different crosshead speeds in order to define the temperature interval in which the steel would show a superplastic behavior. After defining a temperature in which the material presented this characteristic, more test were made using different crosshead speeds in order to determine the optimum strain rate at which the steel behaves superplastically. An INSTRON 1195 model equipment for traction test with a load capacity of 100 kN was used along with an

INSTRON 3112 model furnace which allows reaching temperatures as high as 1000°C. The tests were made without a protective atmosphere at speeds between 0.05 and 10 mm/min. Before the tests were performed, uniform heating from room to test temperature was made, lasting 1 hour, followed by a 5~10 min of stabilization. Variations of temperature inside the furnace were of maximum ±10°C.

Considering the expression $\sigma = K\dot{\varepsilon}^m$ (where K is a function of the temperature), the previous deformation the steel may have suffered and the grain size, coefficient m expresses the sensitivity of the applied tension to strain rate as follows:

$$m = \left(\frac{\log\left(\sigma_{y_2} / \sigma_{y_1}\right)}{\log\left(\dot{\varepsilon}_{0_2} / \dot{\varepsilon}_{0_1}\right)} \right)_{T,d,\varepsilon} \qquad (1)$$

being σ_y and $\dot{\varepsilon}_0$ the yield stress at 0.2% and the initial strain rate, in tests made at 2 different strain rates.

Taking into account that the steel can present superplastic behavior in the intercritic A_1-A_3 range, when the structure is biphasic ($\alpha + \gamma$) [10], the dilatometry absolute curve of the steel was obtained using specimens of length L_0 = 57.2 mm and diameter D = 10 mm using a Griffin dilatometer with a Sullivan potentiometer and a Chromel-Alumel thermocouple.

Metallographic observations were carried out before and after the high temperature tests were made, analyzing the transverse sections of the samples in an axis parallel to the rolling direction. For most of the samples, normal grinding, polishing and etching with Nital-2 solution procedures were used. A Nikon Epiphot metallographic equipment connected to a Buehler Omnimet image analyzer, which allows the automated counting of features using linear intersection techniques and point counting over a mesh superposed to the microstructure image at 400 and 600x were used in the analysis in order to determine the ASTM grain size and its distribution of either all the grains of the steel or only the ferrite. A sufficient amount of micrographs (a minimum of 5), were used during counting.

The metallographic observation was also used to analyze different types of structural damages produced during superplastic deformation of selected samples.

Results

Figure 1 presents the dilatometry test for the steel where A_1 and A_3 values were registered at 720 and 820°C respectively, and relatively match the values expected from the Andrews formulas [17]: A_1 = 726°C and A_3 = 840°C. The figure shows the heating and the cooling curves which present, as expected, different A_1 and A_3 values, though it confirms that at 800°C the material would be in its $\alpha + \gamma$ state.

Figure 2 presents the engineering traction curves for samples tested at six different temperatures and a crosshead speed of 5 mm/min. As expected, the higher the temperature the lower the

maximum stress the sample may withstand, which for 600°C is above 200 MPa and for 900°C is below 80 MPa. It is noteworthy that at 800°C the elongation of the sample is higher than 100%.

In figure 3, as the crosshead speed is 10 times lower than in figure 2, the steel shows lower maximum stresses and for 600, 650 and 750°C, the evidence of more than 1 necking phenomena which results in descending and ascending zones. Again, at 800°C the elongation surpasses 100%.

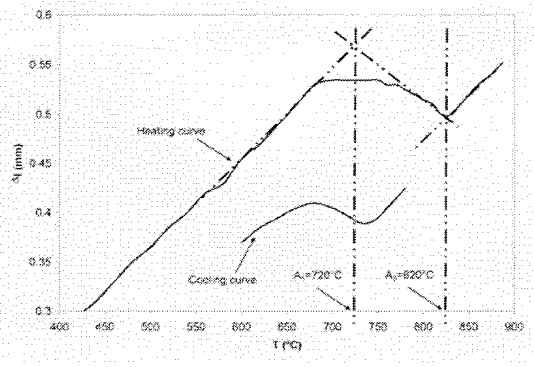

Figure 1. Determination of A_1 and A_3 temperatures by dilatometry test

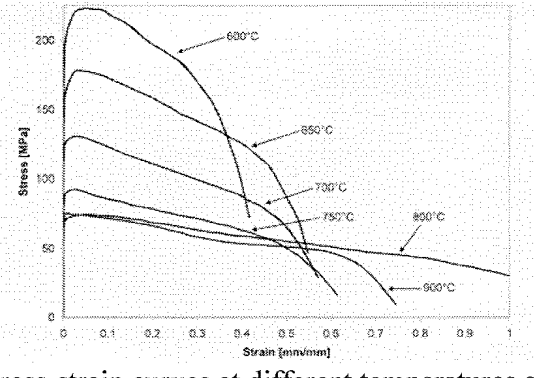

Figure 2. Engineering stress-strain curves at different temperatures and 5 mm/min crosshead speed

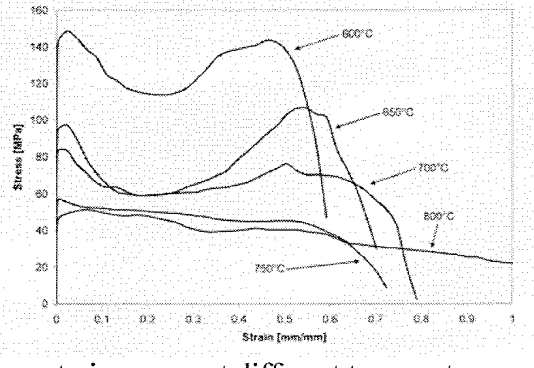

Figure 3. Engineering stress-strain curves at different temperatures and 0.5 mm/min crosshead speed

Considering an even lower crosshead speed (figure 4), the low strain rate promotes at 650 and 700°C the formation of multiple necks shown as ripples in the curves. All these figures indicate that a temperature above 750 and below 850°C results in a smooth deformation and very high elongations of the sample which is an indication of superplasticity.

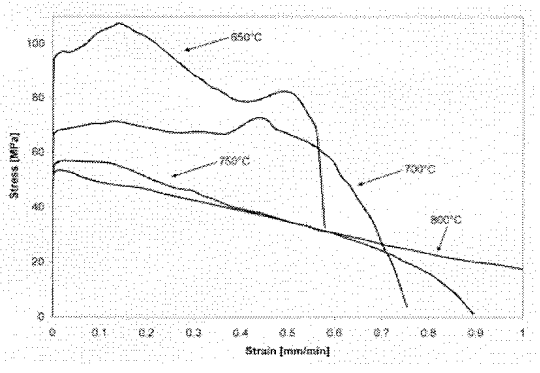

Figure 4. Engineering stress-strain curves at different temperatures and 0.2 mm/min crosshead speed

Once figures 2, 3 and 4 were analyzed and 800°C was determined as a temperature in which the material may present superplastic behavior, traction tests at different crosshead speeds were made with this temperature value (figure 5). Though some ripples are evident during deformation at 5 mm/min, this phenomenon is increased at 0.5 mm/min. The smooth deformation of the samples is only achieved when the crosshead speed is lowered to 0.2 mm/min. For 0.2 and 0.1 mm/min, the elongation of the samples is close to 200%, as shown in figure 6, which compares a specimen with L_0=30 mm with the samples deformed at 800°C and three different crosshead speeds.

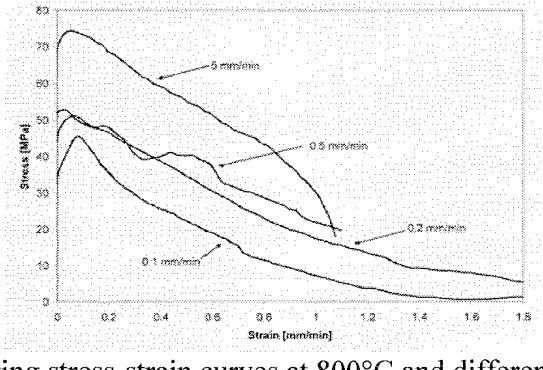

Figure 5. Engineering stress-strain curves at 800°C and different crosshead speeds

The microstructural analysis of the steel in its raw state (figure 7), and analyzing the grain size distribution indicates a 12 ASTM G grain size mean value, which corresponds to approximately 5 μm. This size is small enough for the material to show, under the proper conditions of temperature and strain rate, a superplastic behavior. It is also evident from figure 7 that the hot rolling direction (horizontal axis) produces ferrite and pearlite bands and oriented microstructure.

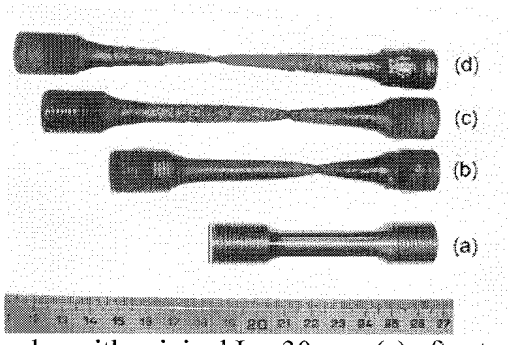

Figure 6. Elongation of samples with original L_0=30 mm (a) after traction testing at 800°C with 0.5 (b), 0.2 (c) and 0.1 (d) mm/min crosshead speeds

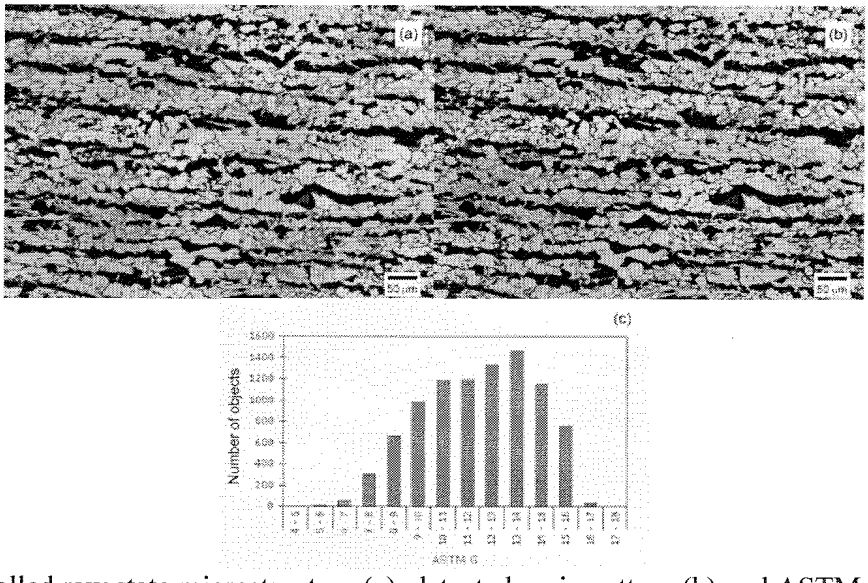

Fig 7. Hot rolled raw state microstructure (a), detected grain pattern (b) and ASTM G grain size distribution histogram (c)

On the other hand, figure 8 presents the same analysis on the hot rolled raw state material, but only measuring the ferrite grains. The mean value of the ferrite grains distribution is closer to 13 ASTM G, which means that the small and soft ferrite grains are responsible for the superplastic behavior.

Figure 9 shows the microstructure of a sample after being superplastically deformed at 800°C (0.1 mm/min crosshead speed) at a zone 15 mm from the rupture of the specimen. The banded oriented structure has almost disappeared and restored ferrite grains are observed. Also, figure 10, shows characteristics of the structure at the same zone with evidence of decohesion between the ferrite and/or the ferrite-pearlite grains of different types. These are evidence of superplastic mechanisms acting during deformation of the sample [18].

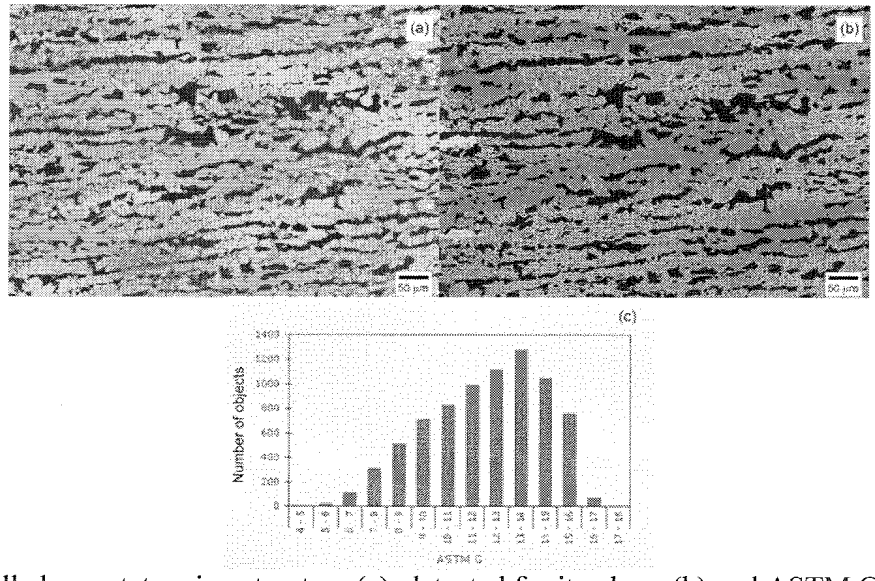

Fig 8. Hot rolled raw state microstructure (a), detected ferrite phase (b) and ASTM G ferrite grain size distribution histogram (c)

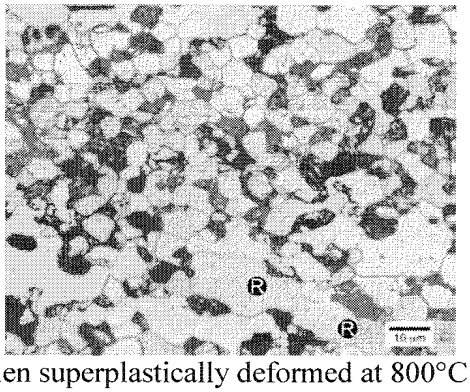

Fig 9. Micrograph of a specimen superplastically deformed at 800°C at a zone close to rupture (15 mm away from it). Restored ferrite (R) is observed.

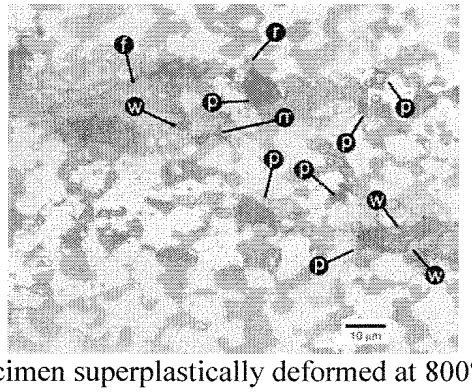

Fig 10. Micrograph of a specimen superplastically deformed at 800°C at a zone close to rupture (15 mm away from it). w-shaped decohesion between ferrite-ferrite-pearlite (w), rr-shaped

decohesion between ferrite and pearlite (rr), ferrite-pearlite decohesion (f) and ferrite-ferrite (r) or pearlite-pearlite decohesion (p) are observed.

Discussion

The tension testing of the steel at high temperature indicates that both the temperature of the test and the strain rate must be adequate to obtain a superplastic behavior (approximately 200% of elongation). Though the curves shown in figure 2 have the usual shape of a tension test, as strain rate becomes lower (figure 3), uncommon behavior, represented by the formation of more than one neck during plastic deformation, becomes evident. Moreover, it is clear that at 800°C (figures 2, 3 and 4) the material presents elongation much higher than at any other temperature.

The microstructure of the steel shown in figure 7 is formed by ferrite and pearlite bands, typical in construction steels which have suffered a peritectic reaction and solidification under non-equilibrium conditions. As the partition coefficient for carbon, alloying elements (Mn and Si) and impurities (P, S) in this steel, is lower than 1, the microstructure cannot be regenerated during soaking treatment before hot-rolling [17].

Table I presents the values of σ_y and $\dot{\varepsilon}$ at a temperature of 800°C. If, considering the superplastic notation [19], the dependence of stress with strain rate is analyzed (figure 11a), a clear zone II behavior is observed, indicating that the transition from zone I (creep) to zone II is not evident as much lower strain rates should be tested in order to observe it. It is also clear that at higher strain rates, a zone III behavior emerges [11]. The regression lines, also indicated in figure 11a, have slope values of ~0.6 for zone II and ~0.1 for zone III. When the strain rate sensitivity coefficient *m* lies between 0.3 and 0.7, superplasticity is achieved [19].

Table I. Tension testing results obtained with different strain rates at 800°C

Specimen initial length (mm)	**Crosshead speed (mm/min)**	**Strain rate (1/s)**	**Yield stress (MPa)**	**Elongation (%)**
30	0.01	$7.00\text{x}10^{-6}$	9.9081 (creep)	non-determined
30	0.05	$2.78\text{x}10^{-5}$	26.88	137.5
30	0.1	$5.56\text{x}10^{-5}$	33.75	189.0
30	0.2	$1.11\text{x}10^{-4}$	51.80	191.3
57	0.5	$1.46\text{x}10^{-4}$	54.35	111.4
30	0.5	$2.78\text{x}10^{-4}$	56.21	116.7
57	5	$1.46\text{x}10^{-3}$	68.67	109.2

Ashby and Verrall have proposed the following constitutive equation that relates tension, strain rate, grain size and temperature [11]:

$$\dot{\varepsilon} = \frac{98\Omega}{kTd^2}\left[\sigma - \frac{0.72\Gamma}{d}\right] D_v \left[1 + \frac{\pi\delta}{d}\frac{D_B}{D_v}\right] \qquad (2)$$

where $\dot{\varepsilon}$ is strain rate, Ω atomic volume of ferrite, T absolute temperature, k Boltzmann constant, σ applied stress,Γ interfacialα/α energy, d grain size, D_v diffusion coefficient for the ferrite volume, δ grain boundary thickness and D_B diffusion coefficient for the ferrite grain boundary. For ferrite, at 800°C, the values of D_v, Ω, Γ and δ are approximately $4x10^{-16}$ m^2/s, $12.2x10^{-30}$ m^3, 0.6 J/m^2 and $5x10^{-10}$ m respectively.

An approximate value for the diffusion coefficient (equation (2)) can be calculated through data $(\sigma, \dot{\varepsilon})$ of the material deformed in superplastic conditions obtained in tests at 750 and 800°C. An approximation to the previous formula for constant grain size (5μm in this case) is the following:

$$\dot{\varepsilon} \propto \sigma^n \exp\left(-\frac{Q}{RT}\right) \tag{3}$$

where Q is the activation energy for the diffusion, R is the constant for ideal gasses and n is a coefficient approximately equal to $1/m$ [12].

Equation (3) results in:

$$\frac{\dot{\varepsilon}_{800}}{\dot{\varepsilon}_{750}} = \left(\frac{\sigma_{y_{800}}}{\sigma_{y_{750}}}\right)^n \exp\left[-\frac{Q}{R}\left(\frac{1}{1073} - \frac{1}{1023}\right)\right] \tag{4}$$

And using the data: $\dot{\varepsilon}_{800} = 5.56\times10^{-5} s^{-1}$ and $\sigma_{y_{800}} = 33.75 MPa$ at 800°C (1073 K) and $\dot{\varepsilon}_{750} = 2.92\times10^{-5} s^{-1}$ and $\sigma_{y_{750}} = 32.47 MPa$ at 750°C (1023 K) for $m \approx 0.3$ (superplastic behavior threshold), results in a value of $Q \approx 97050.024\, J/mol$. Therefore,

$$D \propto \exp\left(-\frac{97050.024}{8.314\cdot1073}\right) = 1.8851\times10^{-5} = 4\times10^{-16}\left(1 + \frac{\pi\left(5\times10^{-10}\right)}{5\times10^{-6}}\frac{D_B}{D_V}\right) \tag{5}$$

where

$$\frac{\pi\delta D_B}{dD_V} \propto \frac{1.8851\times10^{-5}}{4\times10^{-16}}\frac{\pi\left(5\times10^{-10}\right)}{5\times10^{-6}} \propto 15\times10^6 \text{ (at 800°C)} \tag{6}$$

In other words, the diffusivity in grain boundaries is three orders of magnitude higher than the bulk diffusivity. Therefore, the diffusion through grain boundaries is the one ruling the process of intergranular sliding in superplasticity, which has been extensively studied [20].

If the slope m of the yield stress of figure 11a is calculated between each pair of data from tested specimens, as indicated in equation (1), figure 11b indicates that a maximum value of m will be reached at a strain rate close to $0.8x10^{-4}$ s^{-1}, which, at 800°C will be the best deformation rate in order to obtain superplasticity in this steel.

(b)

(a)

Figure 11. Influence of strain rate on yield stress (a) and superindex *m* (b) of equation (1) in superplastic behavior at 800°C.

Figure 9 presents after deformation, ferrite grains of a larger size which are slightly elongated in the rolling direction with evidence (subgrains) of having suffered dynamic recovery during deformation. Furthermore, figure 10 shows:

- decohesions shaped as w and r, mainly located in the ferrite/pearlite (previous austenite grains) interphase, which is an unequivocal proof of intergranular sliding during the deformation process.
- small cavities in the α-pearlite (previous austenite grains) interphase, which shows different deformation capacity for each of these phases.
- null evidence of generalized grain growth during deformation, as grain size is very similar to the original one.
- grain (or grain groups) sliding and rotating, a consequence of superplastic deformation.

Conclusions

HSLA steels microalloyed with Ti – Nb and obtained by ATMCRP are usually ultrafine grained steels with grain sizes lower than 5 μm. Also, when deformed at high temperatures (750 – 800 °C) in the intercritic region (α + γ), a superplastic behavior is shown with elongations higher than 100 %.

The mechanism described by Ashby-Verrall seems to be the most appropriate to describe this superplastic behavior: rotation and sliding of grains activated by diffusion processes at the grain boundaries.

For this steel, the strain rate at which the material presents the best superplastic behavior at 800°C is of $0.8x10^{-4}$ s^{-1}.

Though these steels may show superplastic deformation at high temperature, this deformation does not imply a generalized grain coarsening of the microstructure even when the strain rate is very low (10^{-5} s^{-1}).

Acknowledgments

The authors participating in the SidMetMat group (www.uniovi.es/sid-met-mat) would like to acknowledge the collaboration with the Department of Metal Sheet and Hot Coil of Mittal Arcelor of Gijón – Avilés (Asturias, Spain) for providing the material for this research. Also to T. Iglesias and B. Mendieta for the preparation of images and figures.

References

1 K. Mukherjee, S. S. Hazra and M. Militzer, "Grain refinement in dual-phase steels", *Metallurgical and Materials Transactions A*, 40A (2009), 2145-2159.
2 R. Gonzalez, J. O. García, M. A. Barbes, M. J. Quintana, L. F. Verdeja and J. I. Verdeja, "Ultrafine Grained HSLA Steels for Cold Forming", *Journal of Iron and Steel Research, International*, 17 (2010), 50-56.
3 M. J. Quintana, R. Gonzalez, L. F. Verdeja and J. I. Verdeja, "Dual-Phase Ultrafine-Grained Steels Produced by Controlled Rolling Processes", *Materials Science and Technology (MS&T) 2011*, Ohio, USA (2011), 504
4 A. A. Howe, "Ultrafine grained steels: industrial prospects", *Materials Science and Technology*, 16 (2000), 1264-1266.
5 R. Gonzalez, M. J. Quintana, L. F. Verdeja and J. I. Verdeja, "Ultrafine grained steels and the *n* coefficient of strain hardening", *Memoria de Trabajos de Difusion Cientifica y Tecnica*, 9 (2011), 45-54.
6 *Projects: ULSAB,* http://www.ulsab.org/Projects/ULSAB.aspx, (2012).
7 W. A. Backofen, I. R. Turner and H. Avery, "Superplasticity in an Al-Zn Alloy", *Transaction of the ASM*, 57 (1964), 980-990.
8 W. A. Backofen, "Deformation processing", *Metallurgical Transactions*, 4 (1973), 2679-2699.
9 T. H. Alden, *Plastic deformation of materials. Review Topics in Superplasticity* (New York, NY: Academic Press,1975), 225-266.
10 B. Baudelet, "La Superplasticite et la mise en Forme des materiaux", *Memoires Scientifiques Revue Metalurgie*, 68 (1971), 479-487.
11 M. F. Ashby and R. A. Verrall, "Diffusion-accomodated flow and superplasticity", *Acta Metallurgica*, 21 (1973), 149.
12 W. B. Morrison, "Superplasticity of Low-Alloy Steels", *Transactions of the ASM*, 61 (1968), 423-434.
13 R. E. Reed–Hill, *Creep. Physical Metallurgy Principles*, (Independence, KY: Cengage Learning, 2nd ed., 1994), 827–887.
14 J. S. Vetrano, "Superplasticity: Mechanisms and applications", *JOM*, 3 (2001), 22.

15 M. Kawasaki and T. G. Langdon, "Principles of Superplasticity in Ultrafine-Grained Materials", *Journal of Materials Science*, 42 (2007), 1782-1796.
16 F. A. Mohamed, "The role of boundaries during superplastic deformation", *Surface and Interface Analysis in Materials*, 31 (2001), 532-546.
17 J. A. Pero-Sanz, *Science and Materials Engineering*, (Madrid, Spain: CIE-Dossat 2000, 2006).
18 T. Furuhara and T. Maki, "Grain boundary engineering for superplasticity in steels", *Journal of Materials Science*, 40 (2005), 919-926.
19 G. J. Davies, J. W. Edington, C. P. Cutler and K. A. Padmanabhan, "Superplasticity: A Review", *Journal of Materials Science*, 5 (1970), 1091-1102.
20 G. Frommeyer and J. A. Jiménez, "Structural Superplasticity at Higher Strain Rates of Hypereutectoid Fe-5.5Al-1Sn-1Cr-1.3C Steel", *Metallurgical and Materials Transactions A*, 36A (2005), 295-300.

Superplasticity of ultrafine grained low-alloy steels

Superplasticidad de aceros de baja aleación con grano ultrafino

Sara Fernandez*, María José Quintana**, José Ovidio García*, Luis Felipe Verdeja*, Roberto González**, José Ignacio Verdeja*

*E.T.S.I.M.O., Universidad de Oviedo, Independencia 13, Oviedo 33004, Spain, Tel. (34) 985 10-43-03, Fax. (34) 985 10-42-42, lfv@etsimo.uniovi.es

**School of Engineering, Universidad Panamericana, Augusto Rodin 498, 03920, México, D.F., Mexico, Tel. (52)55 1251-6859, Fax. (52)55 5482-1600 ext. 6101, robglez@up.edu.mx

Abstract

Steels with ultrafine grained structure may present superplastic behavior at specific temperatures and strain rates that allow the grain boundary sliding mechanisms to be activated. The superplastic behavior implies deformation to large strains by grain-boundary sliding with diffusional accommodation, as described by the Ashby-Verrall model. The work presents high temperature tension tests in a low carbon, low alloy steel obtained by advanced thermomechanical controlled rolling processes, showing at 800°C elongations as high as 200%. The microstructure of the steel was analyzed in order to identify ferrite and pearlite grain boundaries, and their interaction after the specimens were deformed. Microanalytical techniques (Optical and SEM) show evidence of: damage growth that prevents the development of higher elongations to failure, non-uniform flow (relative movement-rotation of grains in close proximity to each other) and intergranular non-superplastic deformation (quasi-uniform flow); thus leading to premature failure.

Resumen

Los aceros con estructura de grano ultrafino pueden presentar comportamiento superplástico a temperaturas y velocidades de deformación específicas, que faciliten la activación de los mecanismos de deslizamiento de fronteras de grano. El comportamiento superplástico implica deformaciones elevadas por procesos de deslizamiento de fronteras de grano con acomodo de materia por difusión, tal como lo describe el modelo de Ashby-Verrall. El trabajo presenta pruebas de tensión a temperatura elevada en aceros de bajo carbono y baja aleación obtenidos por procesos avanzados de rolado controlados termomecánicamente, mostrando a 800°C elongaciones de hasta el 200%. La microestructura del acero se analizó para poder identificar las fronteras de grano de la ferrita y de la perlita, y su interacción después de que la probeta fue deformada. Las técnicas de microanálisis (óptico y SEM) muestran evidencia de: crecimiento de defectos que impiden alcanzar elongaciones a ruptura mayores, flujo no uniforme (movimiento-rotación relativo de granos próximos entre sí) y deformación intergranular no-superplástica (flujo cuasi-uniforme), resultando todo esto en fractura prematura.

Keywords: superplasticity, ultrafine grained, strain rate m coefficient, boundary sliding, high-strength low alloy steels (HSLA steels)

Palabras clave: superplasticidad, grano ultrafino, coeficiente m de velocidad de deformación, deslizamiento de fronteras, aceros de alta resistencia y baja aleación.

Superplasticity of ultrafine grained low-alloy steels

Superplasticidad de aceros de baja aleación con grano ultrafino

Sara Fernandez*, María José Quintana**, José Ovidio García*, Luis Felipe Verdeja*, Roberto González**, José Ignacio Verdeja*

*E.T.S.I.M.O., Universidad de Oviedo, Independencia 13, Oviedo 33004, Spain, Tel. (34) 985 10-43-03, Fax. (34) 985 10-42-42, lfv@etsimo.uniovi.es

**School of Engineering, Universidad Panamericana, Augusto Rodin 498, 03920, México, D.F., Mexico, Tel. (52)55 1251-6859, Fax. (52)55 5482-1600 ext. 6101, robglez@up.edu.mx

Abstract

Steels with ultrafine grained structure may present superplastic behavior at specific temperatures and strain rates that allow the grain boundary sliding mechanisms to be activated. The superplastic behavior implies deformation to large strains by grain-boundary sliding with diffusional accommodation, as described by the Ashby-Verrall model. The work presents high temperature tension tests in a low carbon, low alloy steel obtained by advanced thermomechanical controlled rolling processes, showing at 800°C elongations as high as 200%. The microstructure of the steel was analyzed in order to identify ferrite and pearlite grain boundaries, and their interaction after the specimens were deformed. Microanalytical techniques (Optical and SEM) show evidence of: damage growth that prevents the development of higher elongations to failure, non-uniform flow (relative movement-rotation of grains in close proximity to each other) and intergranular non-superplastic deformation (quasi-uniform flow); thus leading to premature failure.

Resumen

Los aceros con estructura de grano ultrafino pueden presentar comportamiento superplástico a temperaturas y velocidades de deformación específicas, que faciliten la activación de los mecanismos de deslizamiento de fronteras de grano. El comportamiento superplástico implica deformaciones elevadas por procesos de deslizamiento de fronteras de grano con acomodo de materia por difusión, tal como lo describe el modelo de Ashby-Verrall. El trabajo presenta pruebas de tensión a temperatura elevada en aceros de bajo carbono y baja aleación obtenidos por procesos avanzados de rolado controlados termomecánicamente, mostrando a 800°C elongaciones de hasta el 200%. La microestructura del acero se analizó para poder identificar las fronteras de grano de la ferrita y de la perlita, y su interacción después de que la probeta fue deformada. Las técnicas de microanálisis (óptico y SEM) muestran evidencia de: crecimiento de defectos que impiden alcanzar elongaciones a ruptura mayores, flujo no uniforme (movimiento-rotación relativo de granos próximos entre sí) y deformación intergranular no-superplástica (flujo cuasi-uniforme), resultando todo esto en fractura prematura.

Keywords: superplasticity, ultrafine grained, strain rate m coefficient, boundary sliding, high-strength low alloy steels (HSLA steels)

Palabras clave: superplasticidad, grano ultrafino, coeficiente m de velocidad de deformación, deslizamiento de fronteras, aceros de alta resistencia y baja aleación.

1. Introduction

Superplasticity is the ability of polycrystalline solids (metals) to achieve extremely high and uniform elongations (from 100 to 1000%) when applying tensile stresses. The high dependency between the creep tension stress and the strain rate results in the lack of necking (or a series of diffuse necks) along the test zone of a specimen [1].

From a microstructural point of view, superplasticity is achieved when two mechanisms take place in the material: grain boundary migration and grain boundary shearing/sliding. Theoretical and microstructural models agree that the most important feature of this behavior is the grain boundary sliding (GBS). Nevertheless, dislocations or diffusion in grains or in zones near grain boundaries are necessary in order to maintain the superplasticity of the material [2].

Four essential characteristics [3] are required in a material for it to be considered superplastic: a stable microstructure of fine equiaxed grains [4], m coefficient (strain-rate sensitivity exponent; $\sigma = K \cdot \dot{\varepsilon}^m$) values between 0.3 and 0.7, slow strain rates (10^{-3} to 10^{-5} s^{-1}) and grain boundaries of the material that allow grain sliding and rotation when stress is applied [5].

In addition to the previous requirements, it is necessary to deform the material at the right temperature which is a fundamental characteristic in some superplastic behavior models, such as the one established by Ashby and Verrall [6]. Their model proposes a theory (Grain Boundary Sliding, Diffusion Accommodated Flow Rate Controlling) to describe superplasticity taking into account two mechanisms: (a) the diffusion-accommodated flow (D-A flow), consisting of GBS along with material transport through grain boundary and bulk crystal diffusion [7] to maintain grain continuity (this phenomena dominates in the low stress regime, strain rates less than 10^{-5} s^{-1}) and (b) the ordinary power-low creep (dislocation creep) which is a quasi-uniform flow mechanism that results in grain-elongation as dislocations accumulate as cells, storing energy; this last mechanism dominates at sufficient high stresses (strain rates higher than 10^{-3} s^{-1}). In the intermediate stress range, both mechanisms compete in order to achieve the superplastic behavior.

The work presents the high temperature superplastic behavior of an UFG steel microalloyed with Ti-Nb obtained by Advanced Thermomechanical Control Rolling Processes (ATMCRP) at the Arcelor Mittal factory in Veriña (Gijón, Spain), as materials of this type can show this behavior when certain conditions are met. The characteristics of the steel, delivered in the form of 27.6 mm in thickness sheets (around one inch), are described in the experimental procedure. The HSLA steels described in Euronorms 10149-2 and 10051 are examples of these materials, as well as other construction steels or automotive special steels (just as the ones described in the ultralight steel auto body – ULSAB project), resulting in lower cost materials and a step forward in the research for better materials in industry, such as lightweight structures and components with very good weldability and easier to recycle, all of this, reducing the cost of the alloy and meeting high specifications with steels that have a lower amount of alloying elements and that are considered high-tech [8]. Furthermore, ultrafine grained steels (UFG) may be applied in the future in most of the steel markets and can be used in other industrial applications, such as the ones that require superplastic behavior, just as this work demonstrates.

Ultrafine grained steels (grain size $\bar{d} \approx 1\sim5\mu m$) are currently intensively studied worldwide, as they offer a solution to finding very high strength materials. They also present high toughness and are produced from standard steel compositions (which reflects in low cost) [9]. Recent works have shown that the ultrafine grained structure may be obtained in a hot rolling mill by ATMCRP and not only from small scale laboratory tests [4,10]. However, under some circumstances these materials may present an important disadvantage as they exhibit unstable plasticity upon yielding, severely restricting its potential uses [11]. In order to avoid this instability [12] the mechanical behavior of the steel must show a strain hardening coefficient n (as measured by tension test with the ASTM standard) higher than 0.1, in its hot rolling raw state. If this is achieved, the steel can be used for cold-work operations such as bending, stretching and drawing and in commercial applications such as automotive and other manufacturing industries [4].

A large number of non-ferrous alloys show superplasticity behavior during isothermal tensile testing. This behavior is characterized by large elongations, usually higher than 100% and sometimes reaching 1000% or more. Superplasticity, object of numerous research activities that started in the 1960~1970s, has the following properties:

- high strain rate sensitivity to the flow stress as the essential and unique characteristic of superplasticity [13],
- strong variation of properties as a function of grain size and strain rate [14],
- relevance of grain boundary sliding in the deformation mechanism [3],

- vacuum forming of the metal sheet when deformed against the die [15] and
- grain boundary sliding by diffusion and accommodation processes [6].

In other words, in order for the superplastic behavior to show high strain rate sensitivity, high temperature testing (> ½ T_m), a fine microstructure and a relatively low strain rate are required [16-18].

2. Experimental procedure and Results

The specified chemical composition for this steel (in weight %) according to the Euronorm is: C 0.168, Mn 1.361, Si 0.453, P 0.022, S 0.009, Cu 0.026, As 0.003, Al 0.028, Cr 0.035, Ti 0.026, V 0.002, Nb 0.033, Mo 0.004, Ni 0.031, Sn 0.002, Al (soluble) 0.027, B 0.0001, N 0.0055, Zr 0.0000, Ca 0.0001, O 0.0000, H 2.00 ppm, B (soluble) 0.0000. In the same way, the specified mechanical properties are: higher yield stress (σ_y) = 447 MPa, rupture stress (σ_{max}) = 567 MPa, yield elongation with L_0 of 50 mm (El) = 31 % and impact resistance at -20 °C (KCV) = 96 J.

As an ultrafine grained microstructure is essential to obtain a superplastic behavior, the steel was produced by ATMCRP, which manly consists of three steps:

1. roughing (in order to reduce the thickness of the slab),
2. waiting period (where the material is cooled between 850 and 1000°C) to obtain Ti and Nb carbides and
3. finishing (where the deformation is accumulated in the austenite in order to obtain the finest ferrite possible after the allotropic transformation), in the same fashion as described in previous works [10].

The samples were obtained from the steel plate in an axis parallel to rolling direction and were machined in a cylindrical shape: 10 mm in diameter and calibrated gage length of either Lo = 57 or Lo = 30 mm (ASTM E21-05 standard). High temperature tension tests were made at different temperatures between 600 and 900°C (50°C intervals) and different crosshead speeds in order to define the temperature interval in which the steel would show a superplastic behavior. After defining a temperature in which the material presented this characteristic, more tests were made using different crosshead speeds in order to determine the optimum strain rate at which the steel behaves superplastically. An INSTRON 1195 model equipment for traction test with a load capacity of 100 kN was used along with an INSTRON 3112 model furnace which allows reaching temperatures as high as 1000°C. The tests were made without a protective atmosphere at speeds between 0.05 and 10 mm/min (strain rates in the range of $10^{-3} - 10^{5} s^{-1}$). Before the tests were performed, uniform heating from room to test temperature was made, lasting 1 hour, followed by a 5~10 min of stabilization. Variations of temperature inside the furnace were of maximum ±10°C.

Considering the expression $\sigma = K\dot{\varepsilon}^m$ (where K is a function of the temperature), the previous deformation the steel may have suffered and the grain size, coefficient m expresses the sensitivity of the applied tension to strain rate as follows:

$$m = \left(\frac{\log\left(\sigma_{y_2} / \sigma_{y_1}\right)}{\log\left(\dot{\varepsilon}_{0_2} / \dot{\varepsilon}_{0_1}\right)} \right)_{T,d,\varepsilon} \tag{1}$$

being σ_y and $\dot{\varepsilon}_0$ the yield stress at 0.2% and the initial strain rate, in tests made at two different strain rates.

Metallographic observations were carried out before and after the high temperature tests were made, analyzing the transverse sections of the samples in an axis parallel to the rolling direction. For most of the samples, normal grinding, polishing and etching with Nital-2 solution procedures were used. A Nikon Epiphot metallographic equipment connected to a Buehler Omnimet image analyzer, which allows the automated counting of features using linear intersection techniques and point counting over a mesh superposed to the microstructure image at 400 and 600x were used in the analysis in order to determine the ASTM grain size and its distribution of either all the grains of the steel or only the ferrite. A sufficient amount of micrographs (a minimum of 5), was used during counting. The metallographic observation was also used to analyze

different types of structural damages produced during superplastic deformation of selected samples. A scanning electron microscope (SEM) JEOL JSM-5600 with an electroprobe analyzer OXFORD model 6587 was used to observe characteristics such as decohesions and identify small precipitates.

Figure 1 presents the engineering tensile curves for samples tested at six different temperatures and a crosshead speed of 5 mm/min. As expected, the higher the temperature the lower the maximum stress the sample may withstand, which for 600°C is above 200 MPa and for 900°C is below 80 MPa. It is noteworthy that at 800°C the elongation of the sample is higher than 100%.

In figure 2, as the crosshead speed is 10 times lower than in figure 1, the steel shows lower maximum stresses and for 600, 650 and 750°C, the evidence of more than one necking phenomena results in descending and ascending zones. Again, at 800°C the elongation surpasses 100%.

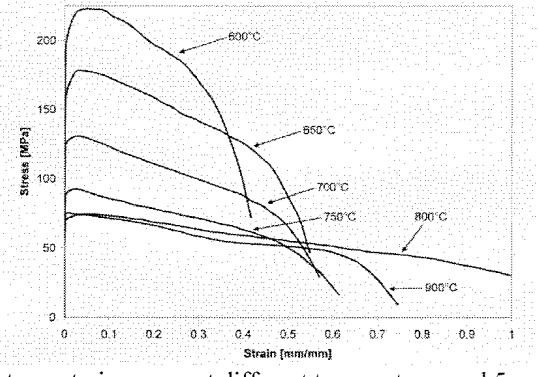

Figure 1: Engineering stress-strain curves at different temperatures and 5 mm/min crosshead speed

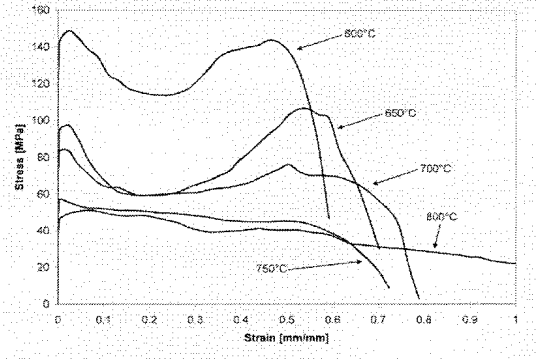

Figure 2: Engineering stress-strain curves at different temperatures and 0.5 mm/min crosshead speed

Considering an even lower crosshead speed (figure 3), the low strain rate promotes at 650 and 700°C the formation of multiple necks shown as ripples in the curves. All these figures indicate that a temperature above 750 and below 850°C results in a smooth deformation and very high elongations of the sample which is an indication of superplasticity.

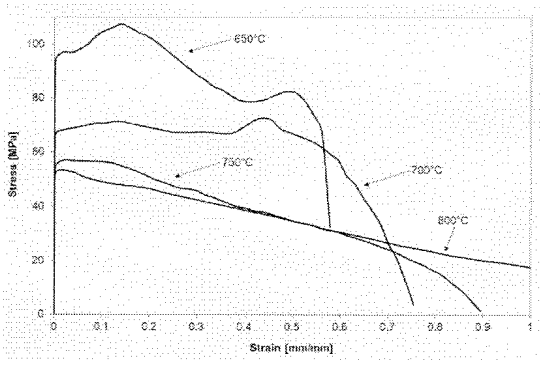

Figure 3: Engineering stress-strain curves at different temperatures and 0.2 mm/min crosshead speed

Once figures 1, 2 and 3 were analyzed and 800°C was determined as a temperature in which the material may present superplastic behavior, tensile tests at different crosshead speeds were made with this temperature value (figure 4). Though some ripples are evident during deformation at 5 mm/min, this phenomenon is increased at 0.5 mm/min. The smooth deformation of the samples is only achieved when the crosshead speed is lowered to 0.2 mm/min. For 0.2 and 0.1 mm/min, the elongation of the samples is close to 200%. Table I presents the results obtained from the tensile tests made at 800°C at different strain rates and different types of tests (tension, superplastic and creep tests).

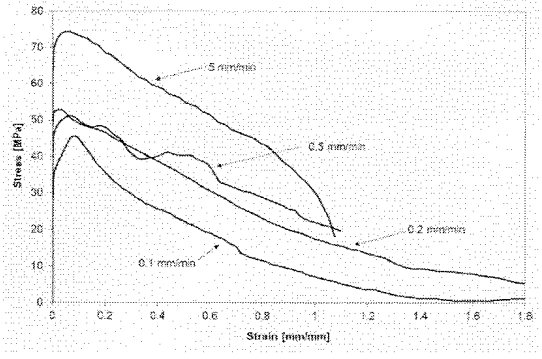

Figure 4: Engineering stress-strain curves at 800°C and different crosshead speeds

	L (mm)	V_t (mm/min)	σ_y (MPa)	A (%)	$\dot{\varepsilon}$	log($\dot{\varepsilon}$)	log(σ_y)
Non Superplastic tests	57	5	70.0	109.2	1.46E-03	-2.84	1.845
	30	0.5	57.3	92.7	2.78E-04	-3.56	1.758
	57	0.5	45.8	111.4	1.46E-04	-3.84	1.660
Superplastic tests	30	0.2	52.8	191.3	1.10E-04	-3.96	1.723
	57	0.2	37.6	>110.0	5.85E-05	-4.23	1.575
	30	**0.1**	**34.4**	**181.7**	**5.56E-05**	**-4.25**	**1.537**
	30	0.05	27.4	137.5	2.78E-05	-4.56	1.438

Table I: Tests made at 800 °C using different strain rates

The microstructural analysis of the steel in its raw state (figure 5), along with the analysis of grain size distribution, shows a 12 ASTM G grain size mean value, which corresponds to approximately 5 μm. This value is small enough for the material to show, under the proper conditions of temperature and strain rate, a superplastic behavior. It is also evident from figure 5 that the hot rolling direction (horizontal axis) produces ferrite and pearlite bands and oriented microstructure.

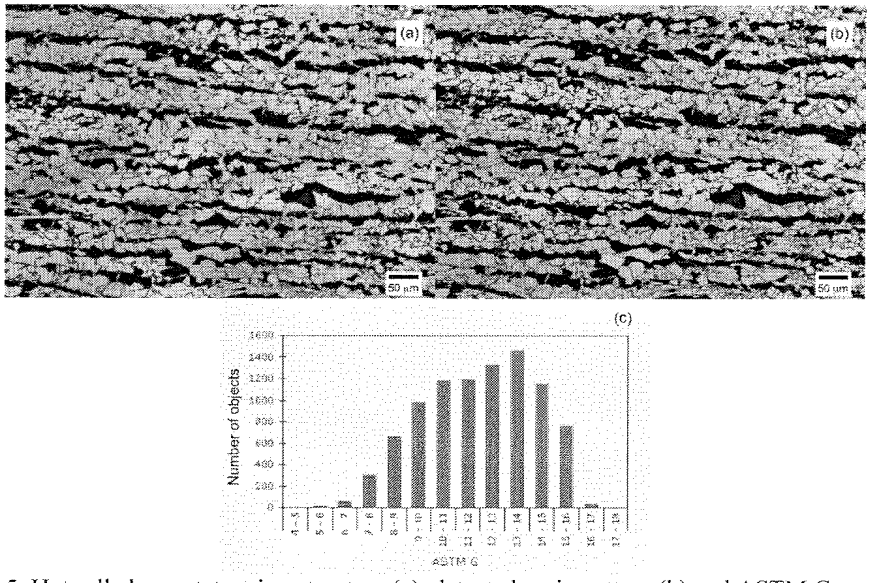

Figure 5: Hot rolled raw state microstructure (a), detected grain pattern (b) and ASTM G grain size distribution histogram (c)

On the other hand, figure 6 presents the same analysis on the hot rolled raw state material, but only measuring the ferrite grains. The mean value of the ferrite grains distribution is closer to 13 ASTM G, which means that the small and soft ferrite grains are responsible for the superplastic behavior.

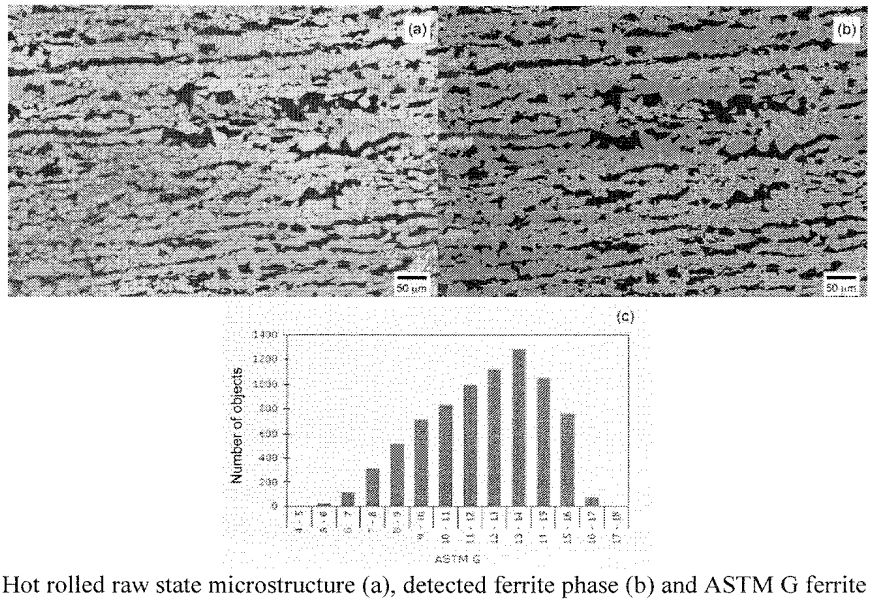

Figure 6: Hot rolled raw state microstructure (a), detected ferrite phase (b) and ASTM G ferrite grain size distribution histogram (c)

Figure 7 shows the microstructure of a sample after being superplastically deformed at 800°C (0.1 mm/min crosshead speed) at a zone 15 mm from the rupture of the specimen. The banded oriented structure has almost disappeared and restored ferrite grains are observed. Also, figure 8, shows characteristics of the structure at the same zone with evidence of decohesion between the ferrite and/or the ferrite-pearlite grains of different types. These are evidence of superplastic mechanisms acting during deformation of the sample [19].

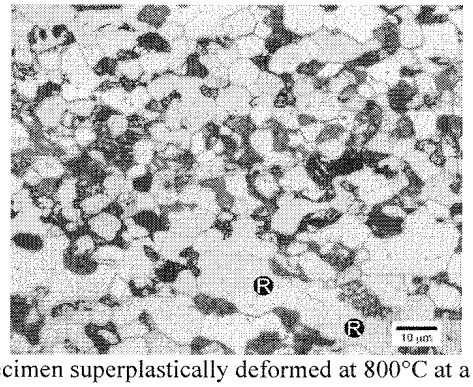

Figure 7: Micrograph of a specimen superplastically deformed at 800°C at a zone close to rupture (15 mm away from it). Restored ferrite (R) is observed.

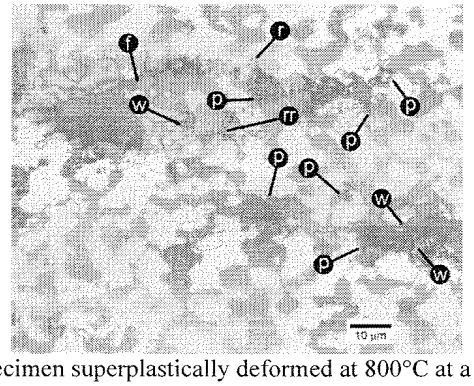

Figure 8: Micrograph of a specimen superplastically deformed at 800°C at a zone close to rupture (15 mm away from it). w-shaped decohesion between ferrite-ferrite-pearlite (w), rr-shaped decohesion between ferrite and pearlite (rr), ferrite-pearlite decohesion (f) and ferrite-ferrite (r) or pearlite-pearlite decohesion (p) are observed.

3. Discussion

The tension testing of the steel at high temperature indicates that both the temperature of the test and the strain rate must be adequate to obtain a superplastic behavior (approximately 200% of elongation). Though the curves shown in figure 1 have the usual shape of a tension test, as strain rate becomes lower (figure 2), uncommon behavior, represented by the formation of more than one neck during plastic deformation, becomes evident. Moreover, it is clear that at 800°C (figures 1, 2 and 3) the material shows elongations with higher values in comparison to other temperatures.

The microstructure of the steel shown in figure 5 is formed by ferrite and pearlite bands, which are features commonly found in construction steels that were modified by a peritectic reaction and solidification under non-equilibrium conditions. As the partition coefficient for carbon, alloying elements (Mn and Si) and impurities (P, S) in this steel, is lower than one, the microstructure cannot be regenerated during soaking treatment before hot-rolling [20]. Figure 9 shows a comparison between the material in its hot rolled raw state (a) and after tension tested (b). In the initial microstructure both ferrite and pearlite grains are continuous and elongated in the rolling direction, while the ferritic volume fraction is higher than the pearlitic one, which is ~30%. On the other hand, the microstructure of the high temperature tested specimen shows the following:

- crystals of ferrite and pearlite, homogeneously distributed as there is a rearrangement of the initial banded structure,
- grain size remains stable (~13 ASTM).

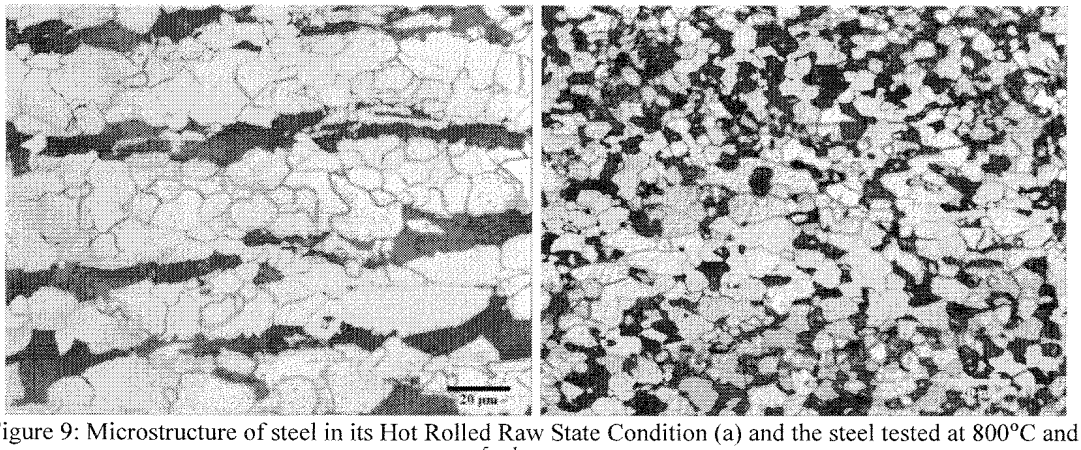

Figure 9: Microstructure of steel in its Hot Rolled Raw State Condition (a) and the steel tested at 800°C and $5.5x10^{-5}$ s^{-1} strain rate (b)

If the superplastic behavior models [21] are used to analyze the relation of stress with strain rate (figure 10), it is evident that:

- A zone II behavior is observed.
- The transition from zone I (creep) to zone II is not evident as tests at lower strain rates should be made in order to observe it.
- At higher strain rates, zone III behavior emerges [6].

The regression lines, also indicated in figure 10a, have slope values of ~0.6 for zone II and ~0.1 for zone III. When the strain rate sensitivity coefficient m lies between 0.3 and 0.7, superplasticity is achieved, figure 10b.

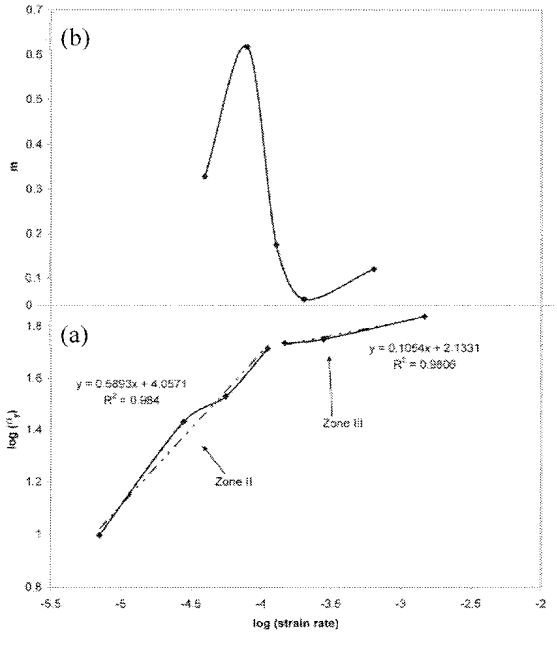

Figure 10: Influence of strain rate on yield stress (a) and superindex m (b) of equation (1) in superplastic behavior at 800°C.

Ashby and Verrall have proposed the following constitutive equation that relates tension, strain rate, grain size and temperature [6]:

$$\dot{\varepsilon} = \frac{98\,\Omega}{k\,T\,d^2}\left[\sigma - \frac{0.72\Gamma}{d}\right] D_v \left[1 + \frac{\pi\,\delta}{d}\frac{D_B}{D_v}\right] \tag{2}$$

where $\dot{\varepsilon}$ is strain rate, Ω atomic volume of ferrite, T absolute temperature, k Boltzmann constant, σ applied stress, Γ interfacial α/α energy, d grain size, D_v diffusion coefficient for the ferrite volume, δ grain boundary thickness and D_B diffusion coefficient for the ferrite grain boundary. For ferrite, at 800°C, the values of D_v, Ω, Γ and δ are approximately $4\text{x}10^{-16}$ m^2/s, $12.2\text{x}10^{-30}$ m^3, 0.6 J/m^2 and $5\text{x}10^{-10}$ m respectively [22].

An approximate value for the diffusion coefficient (equation (2)) can be calculated through data ($\sigma, \dot{\varepsilon}$) of the material deformed in superplastic conditions obtained in tests at 750 and 800°C. An approximation to the previous formula for constant grain size (5μm in this case) is the following:

$$\dot{\varepsilon} \propto \sigma^n \exp\left(-\frac{Q}{RT}\right) \tag{3}$$

where Q is the activation energy for the diffusion, R is the constant for ideal gasses and n is a coefficient approximately equal to $1/m$ [10].

Equation (3) results in:

$$\frac{\dot{\varepsilon}_{800}}{\dot{\varepsilon}_{750}} = \left(\frac{\sigma_{y_{800}}}{\sigma_{y_{750}}}\right)^n \exp\left[-\frac{Q}{R}\left(\frac{1}{1073} - \frac{1}{1023}\right)\right] \tag{4}$$

And using the data: $\dot{\varepsilon}_{800} = 5.56\times10^{-5}s^{-1}$ and $\sigma_{y_{800}} = 34.4MPa$ at 800°C (1073 K) and $\dot{\varepsilon}_{750} = 2.92\times10^{-5}s^{-1}$ and $\sigma_{y_{750}} = 32.47MPa$ at 750°C (1023 K) for $m \approx 0.3$ (superplastic behavior threshold), results in a value of $Q \approx 97050.024$ J/mol [22]. Therefore,

$$D \propto 10^{-4}\left(\frac{m^2}{s}\right)\exp\left(-\frac{97050024}{8.314\cdot1073}\right) = 1.8851\times10^{-9} = 4\times10^{-16}\left(1 + \frac{\pi\left(5\times10^{-10}\right)}{5\times10^{-6}}\frac{D_B}{D_V}\right) \tag{5}$$

where

$$\frac{\pi\delta D_B}{dD_V} \propto \frac{1.8851\times10^{-9}}{4\times10^{-16}}\frac{\pi\left(5\times10^{-10}\right)}{5\times10^{-6}} \propto 1.5\times10^3 \text{ (at 800°C)} \tag{6}$$

In other words, the diffusivity in grain boundaries is three orders of magnitude higher than the bulk diffusivity. This calculation confirms that the diffusion through grain boundaries is the one ruling the process of intergranular sliding in superplasticity, which has also been concluded by other authors [23].

Figure 7 presents the microstructure after deformation: there are ferrite grains of a larger size, slightly elongated in the rolling direction, with evidence (subgrains) of having suffered dynamic recovery during deformation. Furthermore, figure 8 shows:

- decohesions shaped as w and r, mainly located in the ferrite/pearlite (previous austenite grains) interphase, which is an unequivocal proof of intergranular sliding during the deformation process.

- small cavities in the α-pearlite (previous austenite grains) interphase, which shows different deformation capacity for each of these phases.
- null evidence of generalized grain growth during deformation, as grain size is very similar to the original one.
- grain (or grain groups) sliding and rotating, a consequence of superplastic deformation.

During superplastic deformation, the decohesions of the ferrite and pearlite bands occur as a consequence of intergranular sliding of the ferrite within the austenite grains (the two components of the steel at the deformation temperature), as shown in figure 11a by SEM analysis. Superplastic flow stops when the intergranular damage and decohesions between matrix and inclusions take place leading to a ductile fracture (figure 11b).

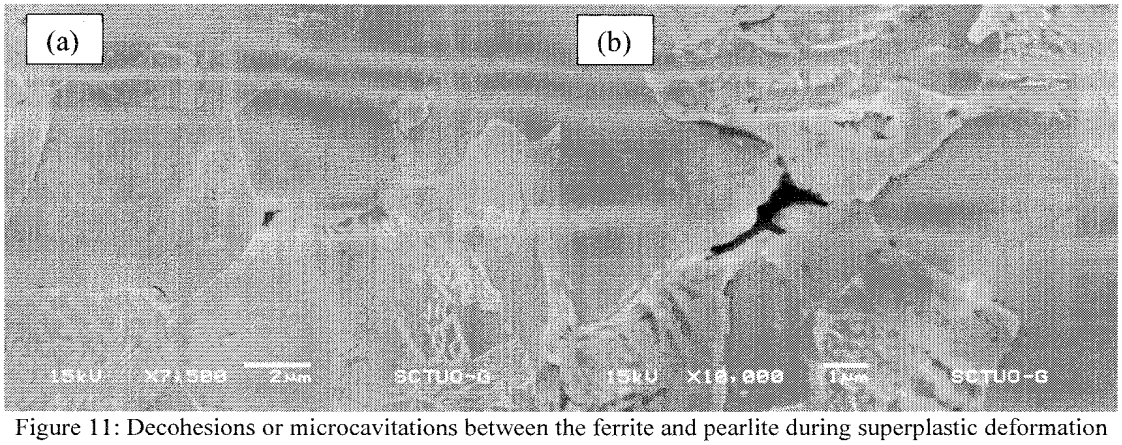

Figure 11: Decohesions or microcavitations between the ferrite and pearlite during superplastic deformation (R-shaped crack) (a) and as a consequence of a conventional high-temperature deformation (decohesions between matrix and hard constituent) (b).

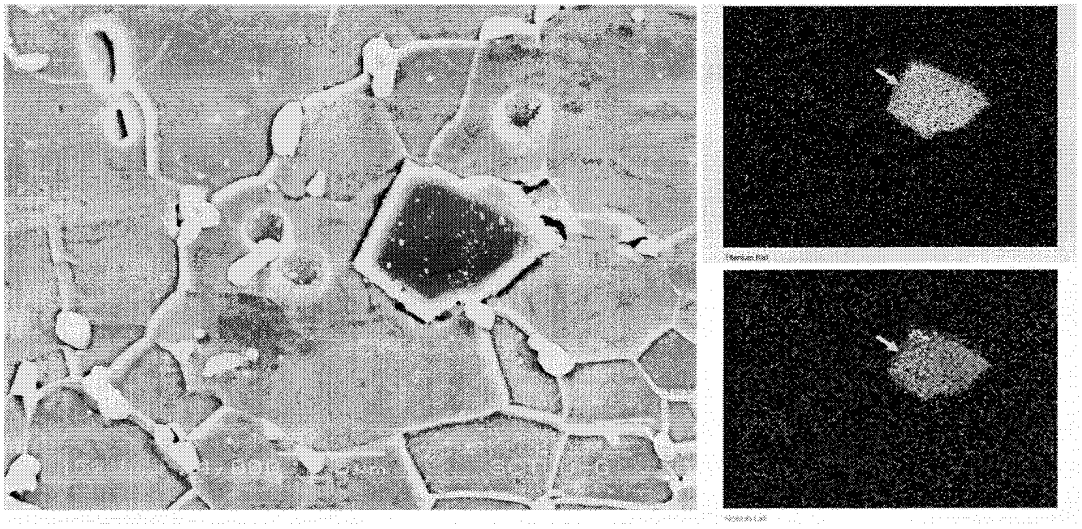

Figure 12: SEM micrograph showing a titanium carbonitride and niobium carbide.

The role of decohesions is evident if the role of Ti and Nb carbides (or carbonitrides) is taken into account as these particles are not dissolved during the 800°C test (figure 12), as these precipitates anchor the grain boundary and prevent the grain growth during rolling, which is accompanied by the formation of γ - pancaked grains and deformation bands. Consequently, a larger number of nucleation sites are made available for the

$\gamma \rightarrow \alpha$ transformation. This allows the formation of an ultrafine microestructure, fulfilling the requirements for both strength and toughness [24,25].

4. Conclusions

Commercial weldable HSLA steels microalloyed with Ti/Nb and obtained by ATMCRP present ultrafine grained microstructures and superplastic behavior (elongations higher than 100%) when deformed in the ferrite-austenite region at temperatures in the range of 750-800^{0}C with strain rates between 10^{-3} and 10^{-5} s^{-1}.

The Ashby-Verrall model is suitable to describe the superplastic behavior of the steel. The most important feature of this model is the grain boundary sliding (GBS) and rotation, along with bulk crystal diffusion to maintain the continuity of the steel. The optimum superplastic behavior is found at 800°C with a strain rate of 10^{-4} s^{-1}.

The Ashby-Verrall Model is confirmed through the existence of decohesions, as a consequence of massive sliding during deformation, leading to localized necking and failure. Though these steels may show superplastic deformation at high temperature, this deformation does not imply a generalized grain coarsening of the microstructure even when the strain rate is very low (10^{-5} s^{-1}).

5. Acknowledgments

The authors thank the Department of Metal Sheet and Hot Coil of Mittal Arcelor of Gijón – Avilés (Asturias, Spain) for providing samples for this research. Also to T. Iglesias and B. Mendieta for the preparation of images and figures.

6. References

[1] Backofen, W.A.; Turner, I.R. and Avery, H. Superplasticity in an Al-Zn Alloy. *Trans ASM*, 1964, vol. 57, pp. 980-990.
[2] Sherby, O.D.; Wadsworth, J. and Oyama, T. Superplasticity: Prerequisites and Phenomenology. U.P. Madrid. Madrid : s.n., 1985. E.T.S.I.C.C.P.
[3] Alden, T.H. *Plastic deformation of materials. Review Topics in Superplasticity,* NY Academic Press, NY, USA, 1975, pp. 225-266.
[4] González, R., García, J.O., Barbés, M.A., Quintana, M.J., Verdeja, L.F., Verdeja, J.I. Ultrafine Grained HSLA Steels for Cold Forming. *J Iron Steel Research Int*, 2010, vol. 17, num. 10, pp. 50-56.
[5] Avery, D.H. and Backofen, W.A. *Trans ASM*, 1965, vol. 58, pp. 551-562.
[6] Ashby, M.F. and Verrall, R.A. Diffusion-accomodated flow and superplasticity, *Acta Metall Mater*, 1973, vol. 21, p. 149.
[7] Pero-Sanz, J.A. *Science and Materials Engineering*, CIE–Dossat 2000, Madrid, Spain, 2006, pp.
[8] Projects: ULSAB, http://www.ulsab.org/Projects/ULSAB.aspx, (2012).
[9] Mukherjee, K.; Hazra, S.S. and Militzer, M. Grain refinement in dual-phase steels, *Met and Mat Trans A*, 2009, vol. 40A, pp. 2145-2159.
[10] Quintana, M.J., Gonzalez, R.; Verdeja, L.F. and Verdeja, J.I. Dual-Phase Ultrafine-Grained Steels Produced by Controlled Rolling Processes, Materials Science and Technology (MS&T) 2011, Ohio, USA, 2011, p. 504
[11] Howe, A.A. Ultrafine grained steels: industrial prospects, *Mater Sci Tech Ser*, 2000, vol. 16, pp. 1264-1266.
[12] Gonzalez, R.; Quintana, M.J.; Verdeja, L.F. and Verdeja, J.I. Ultrafine grained steels and the *n* coefficient of strain hardening, *Memoria de Trabajos de Difusion Cientifica y Tecnica*, 2011, vol. 9, pp. 45-54.
[13] Backofen, W. A.; Turner I. R. and Avery, H. Superplasticity in an Al-Zn Alloy, *Trans ASM*, 1964, vol. 57, pp. 980-990.
[14] Backofen, W. A. Deformation processing, *Met Trans.*, 1973, vol. 4, pp. 2679–2699.
[15] Baudelet, B. La Superplasticite et la mise en Forme des materiaux, Memoires Scientifiques Revue Metalurgie, 1971, vol. 68, pp. 479-487.

[16] Morrison, W.B. Superplasticity of Low-Alloy Steels, Trans ASM, 61 (1968), 423-434.
[17] Reed–Hill, R.E. Creep. Physical Metallurgy Principles, Cengage Learning, Independence, KY, 2nd ed., 1994, pp. 827–887.
[18] Vetrano, J.S. Superplasticity: Mechanisms and applications, JOM, 2001, vol. 3, p. 22.
[19] Pero-Sanz, J. A. Steels: Physical Metallurgy. Selection and Design, CIE–Dossat 2000, Madrid, Spain, 2004. (in Spanish)
[20] Furuhara, T. and Maki, T. Grain boundary engineering for superplasticity in steels, J Mater Sci, 2005, vol. 40, pp. 919-926.
[21] Davies, G.J.; Edington, J.W.; Cutler, C.P. and Padmanabhan, K.A. Superplasticity: A Review, J Mater Sci, 1970, vol. 5, pp. 1091-1102.
[22] Porter, D.A. and Easterling, K.E. Phase Transformations in Metals and Alloys, Chapman & Hall, London, UK, 2nd ed., 1996.
[23] Frommeyer, G. and Jiménez, J.A. Structural Superplasticity at Higher Strain Rates of Hypereutectoid Fe-5.5Al-1Sn-1Cr-1.3C Steel, Met and Mat Trans A, 2005, vol. 36A, pp. 295-300.
[24] Vervynckt, S.; Verbeken, K.; López, B. and Jona, J.J. Modern HSLA steel and role of non – recrystallisation temperature, International Materials Review, 2012, vol. 57, pp. 187-207.
[25] Pero-Sanz, J.A.; Sancho, J.P.; Verdeja, J.I. and L.F. Verdeja, Ferritic grain size: an ignored factor, in fact, in the failure analysis of the sinking of a famous ship, *DYNA*, 2012, vol. 174, pp. 156-161.

Superplastic HSLA steels: microstructure and failure

Sara Fernandez*, María José Quintana**, José Ovidio García*, Luis Felipe Verdeja*, Roberto González**, José Ignacio Verdeja*

*E.T.S.I.M.O., Universidad de Oviedo, Independencia 13, Oviedo 33004, Spain, Tel. (34) 985 10-43-03, Fax. (34) 985 10-42-42, lfv@etsimo.uniovi.es

**School of Engineering, Universidad Panamericana, Augusto Rodin 498, 03920, México, D.F., Mexico, Tel. (52)55 1251-6859, Fax. (52)55 5482-1600 ext. 6101, robglez@up.edu.mx

Abstract

Certain materials can show superplasticity when traction tested at temperatures higher than 50% of their melting point and with low strain rates ($\dot{\varepsilon} < 10^{-2}\ s^{-1}$), showing very high elongations (>100%) without localized necking and mainly intergranular fractures. This behavior requires that the starting grain size is small (<10 μm) so the flow of matter can be non-homogeneous (sliding and rotating of the grain boundaries, accommodated by diffusion).

This works presents the superplastic characteristic of a shipbuilding steel deformed at 800°C and a strain rate slower than $10^{-3}\ s^{-1}$. The fine grain size (5 μm) is obtained when using Nb as a microalloying element and manufactured by controlled rolling processes (3 stages). After the superplastic deformation, the steel presents mixed fractures: by decohesion of the hard (pearlite and carbides) and ductile (ferrite) phases and by intergranular sliding of ferrite/ferrite and ferrite/pearlite, just as it happens in the stage III of the creep behavior. This is confirmed through the Ashby-Verrall model, according to which the dislocation creep (power-law creep) and diffusion creep (linear-viscous creep) occur simultaneously.

Keywords: superplasticity, ultrafine grained, strain rate m coefficient, boundary sliding, high-strength low alloy steels (HSLA steels)

1. Introduction

A material is considered to have superplastic behavior when it shows extremely high and uniform elongations (from 100 to 1000%) under tension stress: a lack of localized necking or a series of diffuse necks along the test zone resulting from a combination of the creep tension stress and the strain rate suffered by the polycrystalline arrangement [1]. Two mechanisms are considered to take place in the material: grain boundary migration and grain boundary shearing/sliding. Theoretical and microstructural models agree that the most important feature of this behavior is the grain boundary sliding (GBS). Nevertheless, dislocations or diffusion in grains or in zones near grain boundaries are necessary in order to maintain the continuity of the material (and avoid ductile decohesions) [2].

Four conditions must be met [3] in order for a material to show superplasticity:

- a stable microstructure of fine equiaxed grains [4],
- m coefficient (strain-rate sensitivity exponent; $\sigma = K \cdot \dot{\varepsilon}^m$) values between 0.3 and 0.7,
- slow strain rates (10^{-3} to 10^{-5} s^{-1}) and
- grain boundaries of the material that allow grain sliding and rotation when stress is applied [5].

In addition to the previous requirements, it is necessary to deform the material at the right temperature which is a fundamental characteristic in some superplastic behavior models, such as the one established by Ashby and Verrall [6]. Their model proposes a theory (Grain Boundary Sliding, Diffusion Accommodated Flow Rate Controlling) to describe superplasticity taking into account two mechanisms:

a) the diffusion-accommodated flow (D-A flow), consisting of GBS along with material transport through grain boundary and bulk crystal diffusion [7] to maintain grain continuity (this phenomena dominates in the low stress regime, strain rates lower than 10^{-5} s^{-1}) and

b) the ordinary power-law creep (dislocation creep) which is a quasi-uniform flow mechanism that results in grain-elongation as dislocations accumulate as cells, storing energy; this last mechanism dominates at sufficient high stresses (strain rates higher than 10^{-3} s^{-1}). In the intermediate stress range, both mechanisms compete in order to achieve the superplastic behavior.

The work presents the high temperature superplastic behavior of an UFG steel microalloyed with Ti-Nb obtained by Advanced Thermomechanical Control Rolling Processes (ATMCRP) at the Arcelor Mittal factory in Veriña (Gijón, Spain), as materials of this type can show this behavior when certain conditions are

met. The characteristics of the steel, delivered in the form of 27.6 mm in thickness sheets (around one inch), are described in the experimental procedure. The HSLA steels described in Euronorms 10149-2 and 10051 are examples of these materials, as well as other construction steels or automotive special steels (just as the ones described in the ultralight steel auto body – ULSAB project), resulting in lower cost materials and a step forward in the research for better materials in industry, such as lightweight structures and components with very good weldability and easier to recycle, all of this, reducing the cost of the alloy and meeting high specifications with steels that have a lower amount of alloying elements and that are considered high-tech [8]. Furthermore, ultrafine grained steels (UFG) may be applied in the future in most of the steel markets and can be used in other industrial applications, such as the ones that require superplastic behavior, just as this work demonstrates.

Ultrafine grained steels (grain size $\overline{d} \approx 1\sim5\mu m$) are currently intensively studied worldwide, as they offer a solution to finding very high strength materials. They also present high toughness and are produced from standard steel compositions (which reflects in low cost) [9]. Recent works have shown that the ultrafine grained structure may be obtained in a hot rolling mill by ATMCRP and not only from small scale laboratory tests [4,10]. However, under some circumstances these materials may present an important disadvantage as they exhibit unstable plasticity upon yielding, severely restricting their potential uses [11]. In order to avoid this instability [12] the mechanical behavior of the steel must show a strain hardening coefficient n (as measured by tension test with the ASTM standard) higher than 0.1, in its hot rolling raw state. If this is achieved, the steel can be used for cold-work operations such as bending, stretching and drawing and in commercial applications such as automotive and other manufacturing industries [4]. Also, in order for the superplastic behavior to show, high strain rate sensitivity, high temperature testing (> ½ T_m), a fine microstructure and a relatively low strain rate are required [13-15].

As an ultrafine grained microstructure is essential to obtain a superplastic behavior, the steel was produced by ATMCRP, which manly consists of three steps:

- roughing (in order to reduce the thickness of the slab),
- delay time (where the material is cooled between 1000 and 850°C) to obtain Ti and Nb carbides and
- finishing (where the deformation is accumulated in the austenite in order to obtain the finest ferrite possible after the allotropic transformation), in the same fashion as described in previous works [10].

In order to achieve this small grain size microstructure, the composition of the steels is very important. Figure 1 shows the changes in grain size during the roughing process for both a steel microalloyed with Nb and one without it. It is clear that the alloying element promotes a smaller grain size and prevents growth after rolling passes. On the other hand, Figure 2 compares the recrystallization kinetics (amount of recrystallized grains) of steels with and without Nb, showing that the microalloying element delays the recrystalization process, and allows the production of steels with smaller (ultrafine) grains [16].

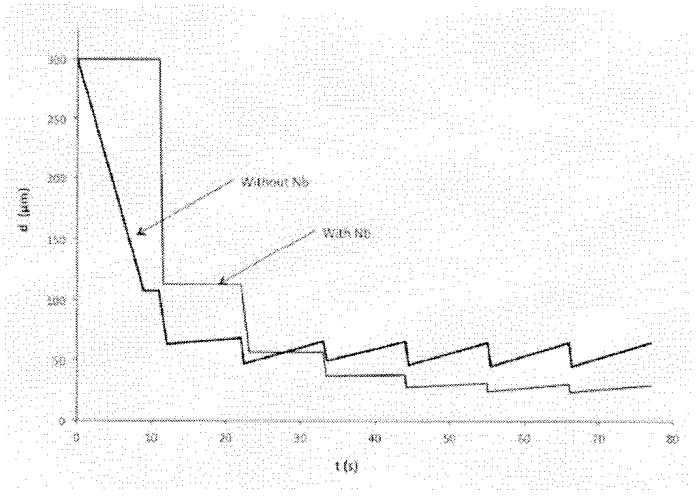

Figure 1. Grain size vs. time in the roughing process of steels with and without Nb

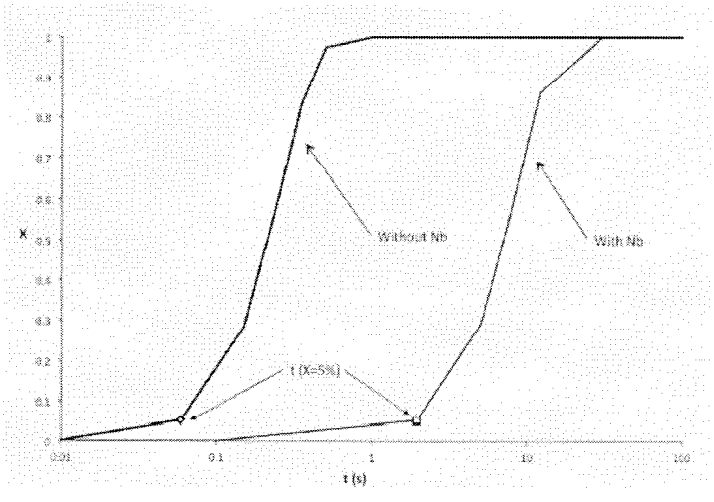

Figure 2. Evolution of recrystallization kinetics during the finishing passes of steels with and without Nb

2. Experimental procedure and Results

The specified chemical composition for this steel (in weight %) according to the Euronorm is: C 0.168, Mn 1.361, Si 0.453, P 0.022, S 0.009, Cu 0.026, As 0.003, Al 0.028, Cr 0.035, **Ti 0.026**, V 0.002, **Nb 0.033**, Mo 0.004, Ni 0.031, Sn 0.002, Al (soluble) 0.027, B 0.0001, N 0.0055, Zr 0.0000, Ca 0.0001, O 0.0000, H 2.00 ppm, B (soluble) 0.0000. In the same way, the specified mechanical properties are: higher yield stress (σ_y) = 447 MPa, ultimate tensile stress (σ_{max}) = 567 MPa, yield elongation with L_0 of 50 mm (El) = 31 % and impact resistance at -20 °C (KCV) = 96 J.

The samples were obtained from the steel sheet in an axis parallel to rolling direction and were machined in a cylindrical shape: 10 mm in diameter and calibrated gage length of either Lo = 57 or Lo = 30 mm (ASTM E21-05 standard). High temperature tension tests were made at different temperatures between 600 and 900°C (50°C intervals) and different crosshead speeds in order to define the temperature interval at which the steel would show a superplastic behavior. After defining a temperature in which the material presented this characteristic, more tests were made using different crosshead speeds in order to determine the optimum strain rate at which the steel behaves superplastically. An INSTRON 1195 model equipment for traction test with a load capacity of 100 kN was used along with an INSTRON 3112 model furnace which allows reaching temperatures as high as 1000°C. The tests were made without a protective atmosphere at speeds between 0.05 and 10 mm/min (strain rates in the range of $10^{-3} - 10^{5} s^{-1}$). Before the tests were performed, uniform heating from room to test temperature was made, lasting 1 hour, followed by a 5~10 min of stabilization. Variations of temperature inside the furnace were of maximum ±10°C.

Figure 3 presents the true tensile curves for samples tested at six different temperatures and a crosshead speed of 5 mm/min. As expected, the higher the temperature the lower the maximum stress the sample may withstand, which for 600°C is above 200 MPa and for 900°C is below 80 MPa. It is noteworthy that at 800°C the steel shows the highest value for true strain (~0.7) and almost steady state regime, like in secondary creep (which is an indication of superplasticity) [17].

Once 800°C was determined as a temperature in which the material may present superplastic behavior, tensile tests at different crosshead speeds were made with this temperature value (Figure 4). Though some ripples are evident during deformation at 5 mm/min, this phenomenon is increased at 0.5 mm/min. The smooth deformation of the samples is only achieved when the crosshead speed is lowered to 0.2 mm/min. For 0.2 and

0.1 mm/min, the true strain of the samples is close to 100%. Table I presents the results obtained from the tensile tests made at 800°C at different strain rates and different types of tests (tension and superplastic tests).

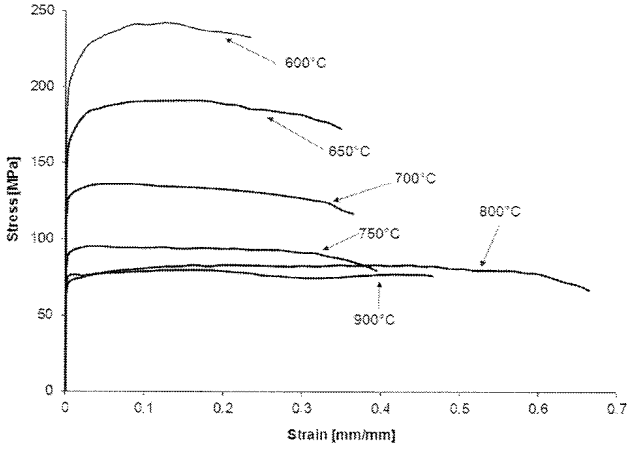

Figure 3: True stress-strain curves at different temperatures and 5 mm/min crosshead speed (L_0 = 57mm)

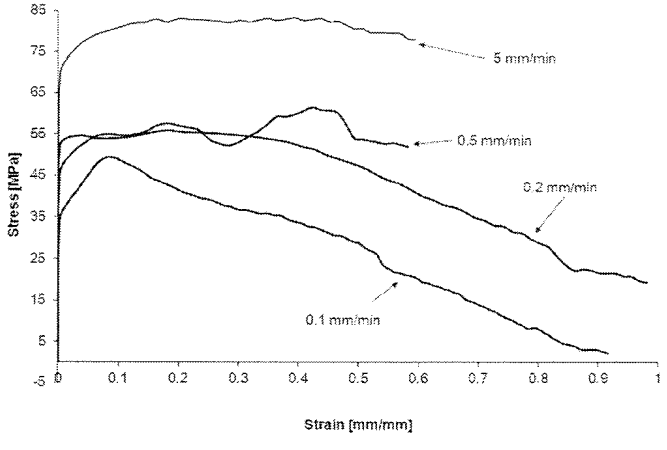

Figure 4: Engineering stress-strain curves at 800°C and different crosshead speeds

Considering the expression (where K is a function of the temperature), the previous deformation the steel may have suffered and the grain size), coefficient m expresses the sensitivity of the applied tension to strain rate as follows:

$$m = \left(\frac{\log\left(\sigma_{y_2} / \sigma_{y_1}\right)}{\log\left(\dot{\varepsilon}_{0_2} / \dot{\varepsilon}_{0_1}\right)} \right)_{T,d,\varepsilon} \tag{1}$$

being σ_y and $\dot{\varepsilon}_0$ the yield stress at 0.2% and the initial strain rate, in tests made at two different strain rates. Figure 5 presents the logarithm of yield stress versus the logarithm of strain rate, where two different slopes of the data may be identified as a zone II and zone III behaviors of the typical sigmoidal high temperature curve [7]. Also figure 5b presents the values of the *m* coefficient with a maximum of ~0.6 which is in the superplastic range, for a strain rate of ~5.5×10^{-5} s^{-1}.

	L (mm)	V_t (mm/min)	σ_y (MPa)	A (%)	$\dot{\varepsilon}$	$\log(\dot{\varepsilon})$	$\log(\sigma_y)$
Non Superplastic tests	57	5	70.0	>109.2	1.46E-03	-2.84	1.845
	30	0.5	57.3	92.7	2.78E-04	-3.56	1.758
	57	0.5	45.8	>111.4	1.46E-04	-3.84	1.660
Superplastic tests	30	0.2	52.8	191.3	1.10E-04	-3.96	1.723
	57	0.2	37.6	>110.0	5.85E-05	-4.23	1.575
	30	**0.1**	**34.4**	**181.7**	**5.56E-05**	**-4.25**	**1.537**
	30	0.05	27.4	137.5	2.78E-05	-4.56	1.438

Table I: Tests made at 800°C using different strain rates

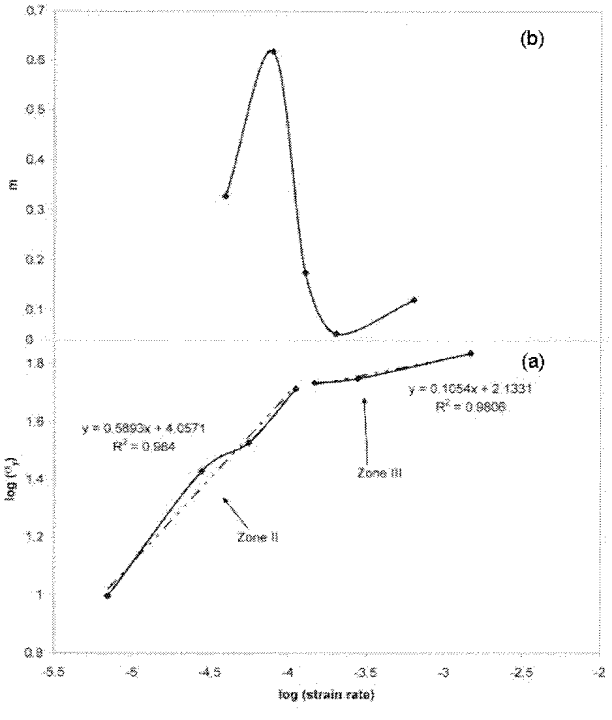

Figure 5. Influence of strain rate on yield stress (a) and super-index (b) in superplastic behavior at 800°C

Metallographic observations were carried out before and after the high temperature tests were made, analyzing the transverse sections of the samples in an axis parallel to the rolling direction. For most of the samples, normal grinding, polishing and etching with Nital-2 solution procedures were used. A Nikon Epiphot metallographic equipment connected to a Buehler Omnimet image analyzer, which allows the automated counting of features using linear intersection techniques and point counting over a mesh superposed to the microstructure image at 400 and 600x were used in the analysis in order to determine the ASTM grain size and its distribution of the ferrite grains. A sufficient amount of micrographs (a minimum of 5), was used during counting. The metallographic observation was also used to analyze different types of structural damages produced during superplastic deformation of selected samples. A scanning electron microscope (SEM) JEOL JSM-5600 with an electroprobe analyzer OXFORD model 6587 was used to observe characteristics such as decohesions and identify small precipitates.

The microstructural analysis of the ferrite grains in the steel in its raw state (Figure 6), along with the analysis of grain size distribution, shows a 13 ASTM G grain size mean value, which corresponds to approximately 5 μm. This value is small enough for the material to show, under the proper conditions of temperature and strain rate, a superplastic behavior. It is also evident from Figure 6 that the hot rolling direction (horizontal axis) produces ferrite and pearlite bands and oriented microstructure.

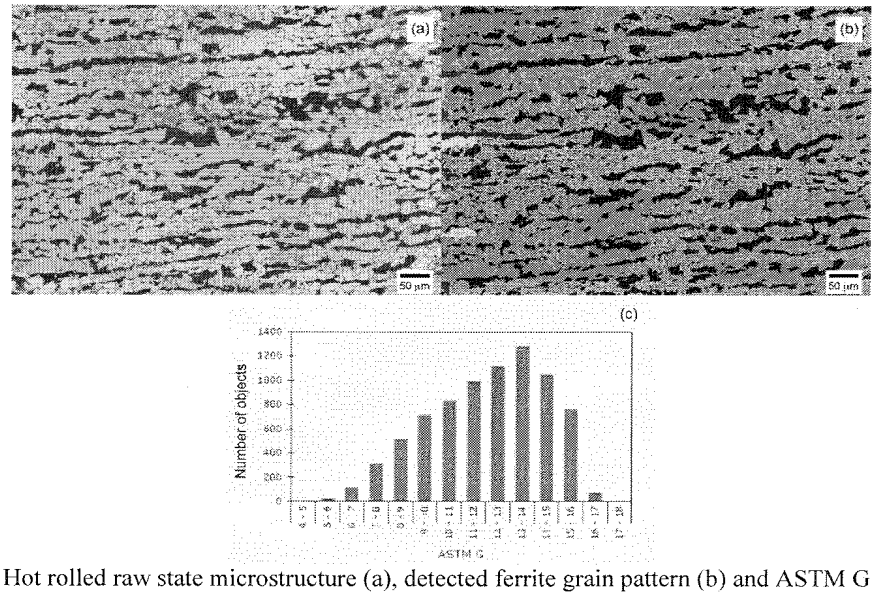

Figure 6: Hot rolled raw state microstructure (a), detected ferrite grain pattern (b) and ASTM G grain size distribution histogram (c)

Figure 7 shows the microstructure of a sample after being superplastically deformed at 800°C (0.1 mm/min crosshead speed) at a zone 15 mm from the rupture of the specimen. The banded oriented structure has almost disappeared and restored ferrite grains are observed. Also, Figure 8 shows characteristics of the structure at the same zone with evidence of decohesion between the ferrite and/or the ferrite-pearlite grains of different types. These are evidence of superplastic mechanisms acting during deformation of the sample [18].

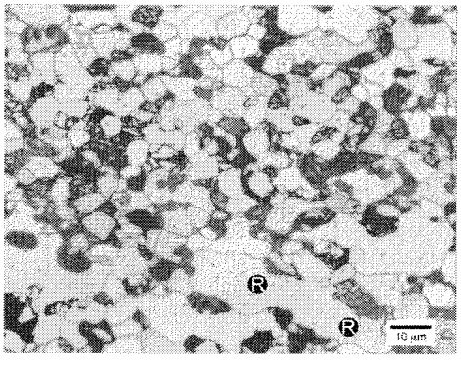

Figure 7: Micrograph of a specimen superplastically deformed at 800°C at a zone close to rupture (15 mm away from it). Restored ferrite (R) is observed.

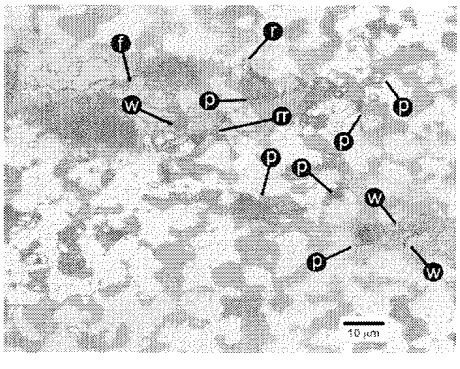

Figure 8: Micrograph of a specimen superplastically deformed at 800°C at a zone close to rupture (15 mm away from it). w-shaped decohesion between ferrite-ferrite-pearlite (w), rr-shaped decohesion between ferrite and pearlite (rr), ferrite-pearlite decohesion (f) and ferrite-ferrite (r) or pearlite-pearlite decohesion (p) are observed.

3. Discussion

The microstructure of the steel shown in Figure 6 is formed by ferrite and pearlite bands, typical in construction steels which have suffered a peritectic reaction and solidification under non-equilibrium conditions. As the partition coefficient for carbon, alloying elements (Mn and Si) and impurities (P, S) in this

steel, is lower than one, the microstructure cannot be regenerated during soaking treatment before hot-rolling [19]. In the initial microstructure both ferrite and pearlite grains are continuous and elongated in the rolling direction, while the ferritic volume fraction is higher than the pearlitic one, which is ~30%.

If the original banded microstructure is compared to the one of the sample tested at 800°C and 0.1 mm/min (Figures 9a and 9b), it is clear that the bands have not completely disappeared though the ferrite phase has suffered restoration without a significant grain size enlargement. If these two microstructures are compared to the sample tested at 750°C and 0.1 mm/min (Figure 9c), a clear difference can be observed, as testing at a lower temperature results in a complete dissapearence of the pearlitic bands, being replaced by ferrite grains and precipitates (mostly carbides).

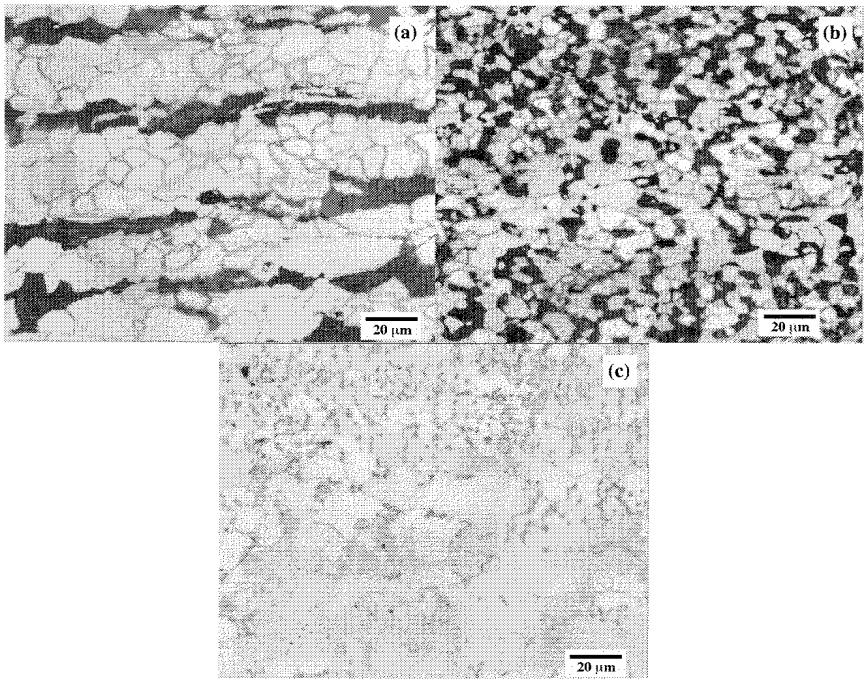

Figure 9. Microstructure of the steel in its hot rolled raw state (a), tested at 800°C and 0.1 mm/min crosshead speed (b) and tested at 750°C and 0.1 mm/min crosshead speed (c)

Figures 7 presents after deformation, ferrite grains of a larger size which are slightly elongated in the rolling direction with evidence (subgrains) of having suffered dynamic recovery during deformation. Furthermore, Figure 8 shows:

- decohesions shaped as w and r, mainly located in the ferrite/pearlite (previous austenite grains) interphase, which is an unequivocal proof of intergranular sliding during the deformation process.
- small cavities in the α-pearlite (previous austenite grains) interphase, which shows different deformation capacity for each of these phases.
- null evidence of generalized grain growth during deformation, as grain size is very similar (or even slightly smaller, <5 μm) to the original one.
- grain (or grain groups) sliding and rotating, a consequence of superplastic deformation.

Figure 10 shows evidence of decohesions which are evidence of superplastic behavior in the steel and consequence of the grain sliding. Also, Figure 11 shows another type of decohesion resulting from boundary sliding of three grains (one grain displaces the other two).

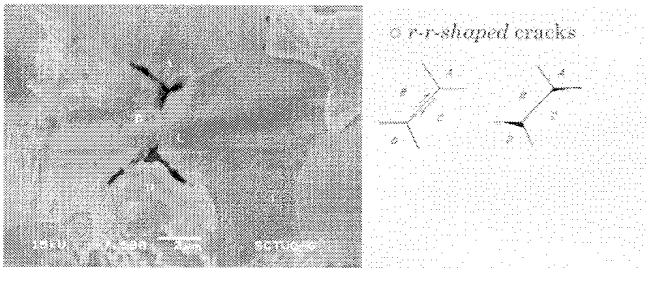

Figure 10. SEM micrograph of the steel tested at 800°C showing a r-r-shaped decohesion

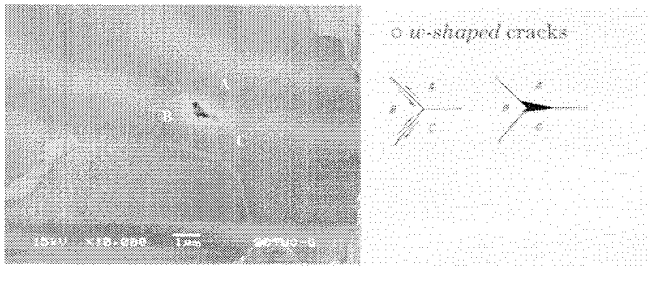

Figure 11. SEM micrograph of the steel tested at 800°C showing a w-shaped decohesion

Furthermore, decohesions between ferrite and pearlite may result in cavities with evidence of ductile deformation of the softer phase, as shown in Figure 12. Superplastic flow stops when the intergranular damage and decohesions between the matrix and inclusions leads to ductile fracture.

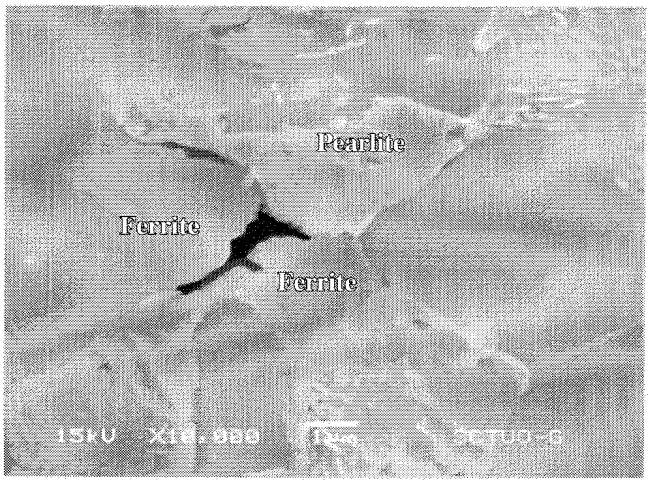

Figure 12. SEM micrograph of the steel tested at 800°C showing a ferrite-pearlite (ductile) decohesion

The importance of decohesions is evident if the role of Ti and Nb carbides (or carbonitrides) is taken into account as these particles are not dissolved during the 800°C test (figure 12): these precipitates anchor the grain boundary and prevent recrystallization and grain growth during rolling at the finishing stage, which is accompanied by the formation of γ - pancaked grains and deformation bands. Consequently, a larger number of nucleation sites are made available for the $\gamma \rightarrow \alpha$ transformation. This allows the formation of an ultrafine microestructure, fulfilling the requirements for both strength and toughness [20,21].

The initial composition (Nb and Ti content) of the steel, and the evidence of an ultrafine microstructure after ATMCRP indicate that the role of NbC and Ti(C,N) are very important during both room temperature and high temperature deformation of the material. Figure 13 shows a particle precipitated at grain boundaries which was initially formed as a titanium carbonitride and then became a substrate for a niobium carbide layer, as confirmed by other authors [20].

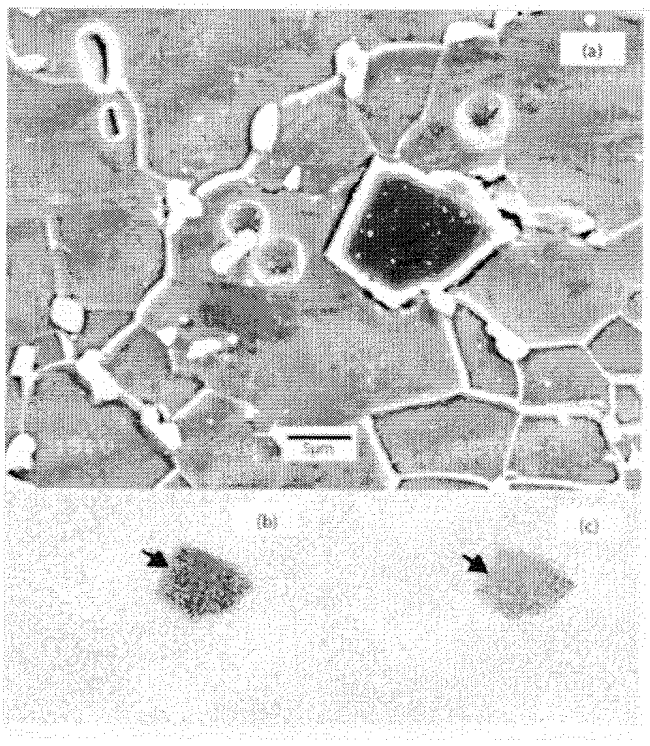

Figure 13. SEM micrograph showing a titanium carbonitride and niobium carbide (a), dot mapping of titanium (b) and dot mapping of niobium (b)

If at a lower magnification, precipitates are observed (Figure 14), it is evident that most of the titanium carbonitrides grow along the former pearlite bands, and as previously mentioned the niobium carbides appear at the same spots using the titanium precipitates as a substrate.

Figure 15 presents curves of the Ashby-Verrall model for a metallic polycrystalline arrangement for grain sizes of 1, 5 and 10 μm. The use of the σ/μ ratio, where μ is the shear modulus, allows the comparison of the experimental data with models for an arrangement of polycrystalline metallic mateials, and where μ (~70 GPa at 800°C in this steel) is a function of the testing temperature [6].The dashed line indicates the values obtained from the high temperature tests of this steel, which lay very closely to the 5 μm curve, though with lower amplitude. This behavior may be explained as a reduction in yield stress caused by the banded structure, even though grains are of the ultrafine type. Consequently, the Ashby-Verrall model seems to be an appropriate description of the relations between temperature, yield stress, strain rate and grain size of the mechanical behavior of this steel.

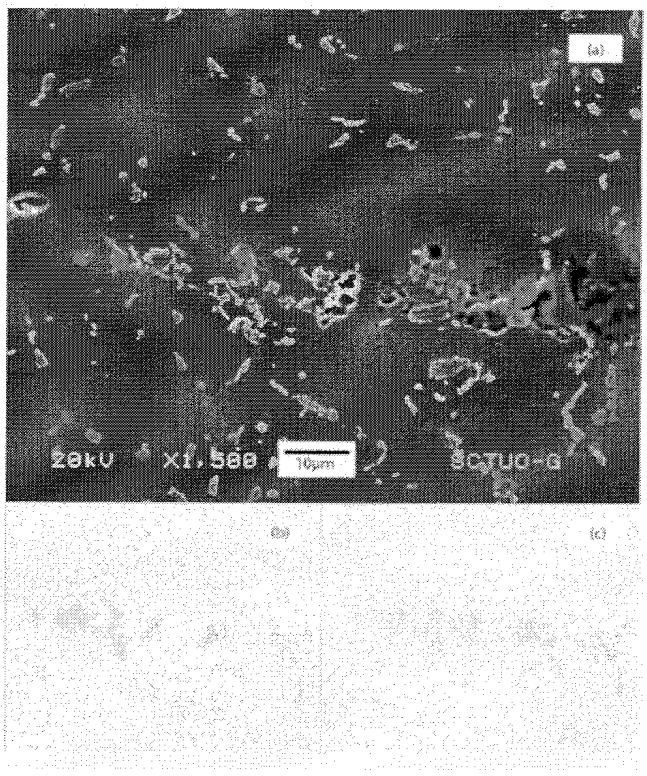

Figure 14. SEM micrograph showing a string of titanium carbonitrides and niobium carbides (a), dot mapping of titanium (b) and dot mapping of niobium (c)

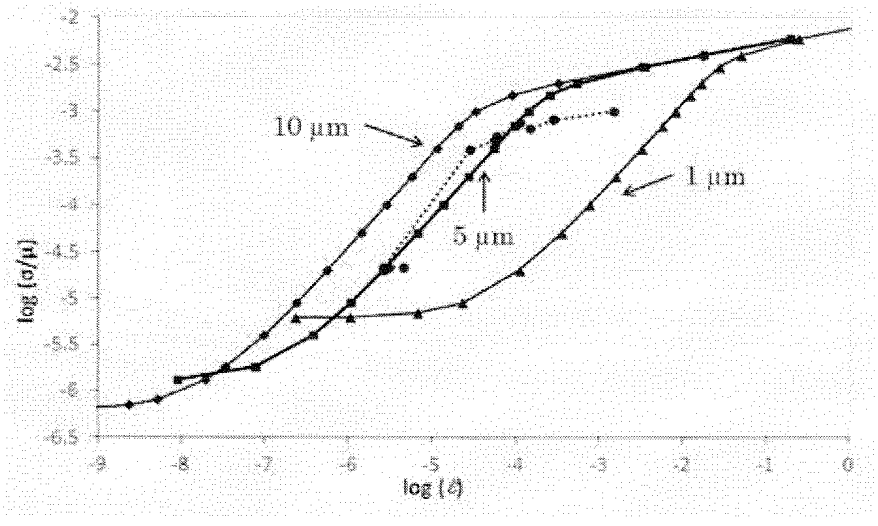

Figure 15. Theoretical curves (Ashby-Verrall model) of logarithm of yield stress/shear modulus vs. logarithm of strain rate considering different grain sizes as well as for the steel investigated (dashed line)

4. Conclusions

Commercial weldable HSLA steels microalloyed with Ti/Nb and obtained by ATMCRP present ultrafine grained microstructures and superplastic behavior (elongations higher than 100%) when deformed in the ferrite-austenite region at 800^0C with strain rates close to $5x10^{-5}$ s^{-1}.

The microstructural analysis of decohesions at the steel after testing confirm grain sliding phenomena described by the model and are also clear evidence of superplasticity. The role of precipitates is not limited to the formation of ultrafine microstructure during ATMCRP, but is also very important during high temperature tests as they prevent grain growth and maintain mechanical strength acting as grain boundary dislocation barriers.

The Ashby-Verrall model is suitable to describe the superplastic behavior of the steel. The most important feature of this model is the grain boundary sliding (GBS) and rotation, along with bulk crystal diffusion to maintain the continuity of the steel.

5. Acknowledgments

The authors thank the Department of Metal Sheet and Hot Coil of Mittal Arcelor of Gijón – Avilés (Asturias, Spain) for providing samples for this research. Also to T. Iglesias and B. Mendieta for the preparation of images and figures.

6. References

[1] W.A. Backofen, I.R. Turner and H. Avery, Superplasticity in an Al-Zn Alloy, Trans. ASM, vol. 57, 1964, p 980-990.

[2] O.D. Sherby, J. Wadsworth and T. Oyama, Superplasticity: Prerequisites and Phenomenology, Universidad Politécnica de Madrid E.T.S.I.C.C.P., 1985.

[3] T.H. Alden, Plastic deformation of materials. Review Topics in Superplasticity, NY Academic Press, NY, USA, 1975, p 225-266.

[4] R. González, J.O. García, M.A. Barbés, M.J. Quintana, L.F. Verdeja and J.I. Verdeja, Ultrafine Grained HSLA Steels for Cold Forming, J. Iron Steel Res. Int., vol. 17 (no. 10), 2010, pp. 50-56.

[5] D.H. Avery and W.A. Backofen, Trans. ASM, vol. 58, 1965, p 551-562.

[6] M.F. Ashby and R.A. Verrall, Diffusion-accomodated flow and superplasticity, Acta Metall. Mater., vol. 21, 1973, p 149.

[7] J.A. Pero-Sanz, Science and Materials Engineering, CIE–Dossat 2000, Madrid, Spain, 2006 (in Spanish)

[8] C.T. Broek, FutureSteelVehicle: leading edge innovation for steel body structures, Ironmaking Steelmaking, vol. 39 (no. 7), 2012, p 477-482.

[9] K. Mukherjee, S.S. Hazra and M. Militzer, Grain refinement in dual-phase steels, Met. and Mat. Trans. A, vol. 40A, 2009, p 2145-2159.

[10] M.J. Quintana, R. Gonzalez, L.F. Verdeja and J.I. Verdeja, Dual-Phase Ultrafine-Grained Steels Produced by Controlled Rolling Processes, Oct 16-20, 2011 (Ohio, USA), Materials Science and Technology (MS&T), 2011, p 504

[11] A.A. Howe, Ultrafine grained steels: industrial prospects, Mater. Sci. Tech. Ser., vol. 16, 2000, p 1264-1266.

[12] R. Gonzalez, M.J. Quintana, L.F. Verdeja and J.I. Verdeja, Ultrafine grained steels and the n coefficient of strain hardening, Memoria de Trabajos de Difusion Cientifica y Tecnica, vol. 9, 2011, p 45-54.

[13] W.B. Morrison, Superplasticity of Low-Alloy Steels, Trans. ASM, vol. 61, 1968, p 423-434.

[14] R.E. Reed–Hill, Creep. Physical Metallurgy Principles, 2nd ed., Cengage Learning, Independence, KY, 1994, p 827–887.

[15] J.S. Vetrano, Superplasticity: Mechanisms and applications, JOM, vol. 3, 2001, p 22.

[16] C. Capdevila, V. Amigo, F.G. Caballero, C. García de Andres and M.D. Salvador, Influence of microalloying elements on recristallization texture of warm-rolled interstitial free steels, Mater. Trans., vol 51 (no. 4), 2010, p 625-634.

[17] Y. Motohashi, V. Ryukhtin, S. Takaaki and J. Saroun, Influence of flat cavity formation on stress vs. strain and strain rate relations of superplastic deformation in 3Y-TZP, Mater. Trans., vol. 51 (no. 3), 2010, p 567-573.

[18] J.A. Pero-Sanz, Steels: Physical Metallurgy. Selection and Design, CIE–Dossat 2000, Madrid, Spain, 2004 (in Spanish)

[19] T. Furuhara and T. Maki, Grain boundary engineering for superplasticity in steels, J. Mater. Sci., vol. 40, 2005, p 919-926.

[20] S. Vervynckt, K. Verbeken, B. López and J.J. Jonas, Modern HSLA steel and role of non – recrystallisation temperature, Int. Mater. Rev., vol. 57, 2012, p 187-207.

[21] J.A. Pero-Sanz, J.P. Sancho, J.I. Verdeja and L.F. Verdeja, Ferritic grain size: an ignored factor, in fact, in the failure analysis of the sinking of a famous ship, DYNA, vol. 174, 2012, p 156-161.

Structural ultrafine grained steels obtained by advanced controlled rolling

R.González[1], J.O.García[2], M.A.Barbés[2], M.J.Quintana[1], L.F.Verdeja[2], J.I.Verdeja[2]

([1]School of Engineering, Universidad Panamericana, Augusto Rodin 498, 03920, Mexico; [2]E.T.S.I.M.O., Universidad de Oviedo, Independencia 13, Oviedo 33004, Spain)

Abstract:

Steels with ultrafine grains (lower than 5 μm), usually known as ultrafine ferrite or ultrafine grained materials, are presently the object of intense research, because of the improvement in resistance and fracture toughness they may reach compared to conventional steels (with grain sizes above this value). This work shows that the forenamed steels designated in the Euronorm EN 10149-2, manufactured by advanced techniques of controlled rolling and mainly used in automotive industry, have an ultrafine grain size, in the range of 2.5 to 3.5 μm, with elastic yield stresses higher than 400 MPa. Based on the Morrison-Miller criterion, it is shown that values of the strain hardening "n" coefficient lower than 0.08 would make the industrial application of these steels unfeasible.

Key words: ultrafine grained steels, mechanical properties, manufacturability, strain-hardening.

1. Introduction

In recent years an increasing interest has been developed in both industrial and laboratory levels, for the production of none-alloyed, low-alloyed and micro-alloyed steels with ultrafine grains (UFF-ultrafine ferrite, UFG-ultrafine grained) defining these steels as those with ASTM G grain size higher than 12 (5μm or less)[1-2]. It is expected from this new generation of steels, a higher resistance and fracture toughness at temperatures below 0°C. Two tendencies appear as fundamental: laboratories dedicated to scientific research and not connected to the steelmaking industry, that pursue this objective using techniques that involve large deformations (SPD process: severe plastic deformation) with deformations $\varepsilon \approx 4$, and that of labs directly inside or linked to the industrial process -which is the case of the Sid-met-mat group of ETSIMO (Spain)- that use advanced technologies in thermomechanical controlled rolling processes (ATMCRP) and propose an alternative in the mass production of UFF (or UFG) steels. This is possible[3] due to recent advancements in the steelmaking industry: improvements in both information technologies and process automation have allowed the crossover from laboratory to industrial level of UFG steels, now commonly used (particularly in the automotive sector).

The present work shows that steels specified in Euronorm UNE – EN 10149-2 are in fact UFF steels which ArcelorMittal de Asturias (Spain) produced 305,000 Tons of hot rolled structural strip steels in 2010, and from those, 60,000 Tons were delivered in raw hot-rolled conditions in different specifications indicated by the Euronorm. Tables I and II, with data extracted from the mentioned standard, indicate the range of chemical composition and mechanical properties expected from these steels.

Biography: R.González (1967 -), Male, PhD. in Materials Science, full time researcher at the School of Engineering of Panamerican University and member of The Mineral, Metals & Materials Society, **E-mail:** robglez@up.edu.mx, **Received Date:**

2. Experimental Work and Results

This work contemplates four steels included in the Euronorm and detailed in Tables I and II: S315, S420, S500 and S600, respectively alloyed with Nb or Nb/Ti, in the form of steel sheet and with thickness below or equal to 5 mm obtained by ATMCRP (hot-rolled raw state) in the factory of ArcelorMittal in Avilés (Oviedo, Spain). This process consists in the control of the speed and amount of deformation of sheets at adequate times and temperatures to achieve the UFG microstructure, in the following steps:

1. *Homogenization.* The slabs obtained by continuous casting (approximately 230x1580x7120 mm) are maintained at temperatures of 1200~1250°C to start with a recrystallized structure.
2. *Roughing.* In reversible rolling trains (husk tool and roughing tool), approximately 10 passes (with rolling speeds between 2~3.25 m/s) are made to reduce the thickness to ~40 mm (approximately 20 mm per pass) and maintaining a temperature of 1200~1100°C.
3. *Waiting.* Before the finishing train, the material is cooled to 1100~1000°C.
4. *Finishing.* Consists in a train of hot or semicontinuous bands (7 boxes). The temperature drops to 850°C, obtaining a thickness of ~5 mm.
5. *Controlled cooling.* Atomized water is used as a cooling method until it reaches coiling temperature (~600°C).
6. *Coiling.* The sheet is coiled at a temperature of ~600°C. It is very important that the coiling cooling rate results in a ferritic-pearlitic ultrafine structure.

The laboratory chemical analysis (Table III), performed on two samples for each steel, included the following: C and S were analyzed by combustion in a LECO CS-200 equipment; the remaining elements by optic emission spectrometry in an ARL 3460 system. As expected from the Euronorm specification and manufacturing process, S500 and S600 are microalloyed with Nb/Ti and high Mn within the specification range.

Name	Material number	C% max	Mn% max	Si% max	P% max	S% max[1)]	Al total % min	Nb% max[2)]	V% max[2)]	Ti% max[2)]	Mo% max	B% max
S315	1.0972	0.12	1.30	0.50	0.025	0.020	0.015	0.09	0.20	0.15	--	--
S355	1.0976	0.12	1.50	0.50	0.025	0.020	0.015	0.09	0.20	0.15	--	--
S420	1.0980	0.12	1.60	0.50	0.025	0.015	0.015	0.09	0.20	0.15	--	--
S460	1.0982	0.12	1.60	0.50	0.025	0.015	0.015	0.09	0.20	0.15	--	--
S500	1.0984	0.12	1.70	0.50	0.025	0.015	0.015	0.09	0.20	0.15	--	--
S550	1.0986	0.12	1.80	0.50	0.025	0.015	0.015	0.09	0.20	0.15	--	--
S600	1.8969	0.12	1.90	0.50	0.025	0.015	0.015	0.09	0.20	0.22	0.50	0.005
S650	1.8976	0.12	2.00	0.60	0.025	0.015	0.015	0.09	0.20	0.22	0.50	0.005
S700	1.8974	0.12	2.10	0.60	0.025	0.015	0.015	0.09	0.20	0.22	0.50	0.005

Table I. Chemical composition of thermomechanically rolled steels.
Note: 1) If ordered, the sulphur content shall be max. 0.01%. 2) The sum of Nb, V and Ti shall be max. 0.22%.

Tension testing was made in longitudinal samples extracted from the steel sheet, with calibrated length L_0 in accordance to UNE-EN 10002-1 standard. The equipment used was an INSTRON 5583 machine, with a 150 kN capacity load cell, specially adapted for tension testing of either hot or cold rolled plane products. The parameters evaluated (Table IV) were: higher yield stress, lower yield stress, yield elongation, rupture stress, elongation before rupture, lower yield/rupture stress ratio and strain hardening coefficient *n*. All the steels comply with the specifications of the EN 10149-2 standard, with the exception of the S600 yield stress which is at the limit of the specification. Engineering stress-strain curves for the samples are presented in Figure 1 adding as comparison the ones for ULC steel (0.003% C, 0.15% Mn, 0.07% Ti) indicated as IF and with extra-deep-drawing quality (n=0.25); and a dual phase steel (0.1% C, 0.55% Si, 1.6% Mn, 0.005% B), indicated as DP with commercial quality (n=0.22).

Name	Material number	Minimum yield strength [MPa]	[1)]Tensile strength [MPa]	Min percentage elongation at fracture		Bending at 180° min. mandrel diameter
				If t <3 [2)]L_0=80 mm	If t≥3 [3)]$L_0=5.65\sqrt{S_0}$	
S315	1.0972	315	390 – 510	20	24	0t
S355	1.0976	355	430 – 550	19	23	0.5t
S420	1.0980	420	480 – 620	16	19	0.5t
S460	1.0982	460	520 – 670	14	17	1t
S500	1.0984	500	550 – 700	12	14	1t
S550	1.0986	550	600 – 760	12	14	1.5t
S600	1.8969	600	650 – 820	11	13	1.5t
S650	1.8976	650	700 – 880	10	12	2t
S700	1.8974	700	750 - 950	10	12	2t

Table II. Mechanical properties for thermomechanically rolled steels.

Note: 1) The values for the tensile test apply to longitudinal test pieces. The values for the bent test apply to transverse test pieces. For thickness t>8 mm, min. yield strength can be 20 MPa lower. 2) L_0 is the initial length of the tension test sample. 3) S_0 is the initial width of the tension test sample.

Sample	C	Mn	Si	S	P	Ti	Nb	Al
S315	0.07	0.33	0.01	0.013	0.008	--	0.023	0.042
S420	0.10	0.47	0.01	0.010	0.016	--	0.044	0.029
S500	0.09	1.41	0.02	0.012	0.019	0.075	0.047	0.031
S600	0.09	1.45	0.02	0.008	0.019	0.074	0.047	0.026

Table III. Chemical analysis of the four steel samples tested

Sample	S315	S420	S500	S600
Thickness/mm	4.0	5.2	4.5	2.3
Higher yield stress/MPa	369	465	630	585
Lower yield stress/MPa	357	449	618	581
Yield elongation/%	0.5	2.0	2.3	0.6
Rupture stress/MPa	421	534	678	661
Elongation before rupture/%	20	27	26	16
Lower yield/rupture stress ratio	0.85	0.84	0.91	0.88
Strain hardening coefficient	0.19	0.16	0.10	0.10
$\overline{G}$ **(ASTM)**	13.0	13.3	14.2	13.9
σ_G **(ASTM)**	1.50	1.47	1.05	1.20
$\overline{L}$ **(μm)**	3.5	3.1	2.3	2.5

Table IV. Mechanical properties and quantitative metallographic results.

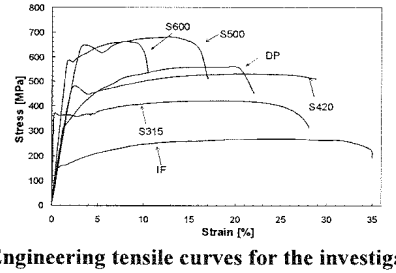

Figure 1. Engineering tensile curves for the investigated steels.

Metallographic analysis were carried out in the transverse section of the steel sheet parallel to the rolling direction, followed by mechanical grinding, 6 and 1 μm diamond paste polishing and using a 0.05 μm γ-alumina solution to achieve mirror finish. The etch to reveal microstructures was Nital-2, a 2% nitric acid solution in alcohol. Quantitative metallography was made using a Nikon-Epiphot equipment and, because

these are UFF steels, to evaluate the ASTM G grain size, optical objectives Mx higher than 100x were used, just as recommended by the ASTM E-112 standard. The formula[4]:

$$G = G' + 6.64 \log\left(\frac{Mx}{100}\right) \quad (1)$$

was used to convert grain size. To quantitatively determine the statistical distribution of grain sizes (mean linear intercept $\bar{L}$), a Buehler Omnimet image analyzer connected to the Nikon-Epiphot microscope was used, in accordance to the already quoted E 112 standard, and to the extended E 1181-02 version.

The intercept measurements are automatically made by the equipment with lines traced over the micrograph at 0, 45, 90 and 135 degrees of the rolling direction. The distribution of grain sizes (histogram) follows a log-normal law. As the relation between ASTM G number and linear intercept sizes is:

$$G = -3.356 - 6.644 \log \bar{L}(\text{mm}) \quad (2)$$

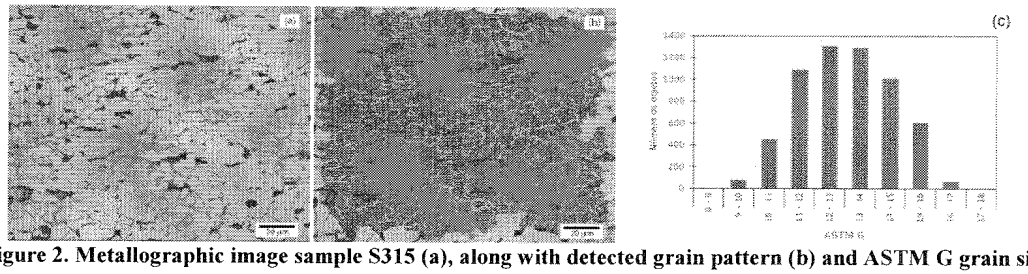

Figure 2. Metallographic image sample S315 (a), along with detected grain pattern (b) and ASTM G grain size distribution histogram (c).

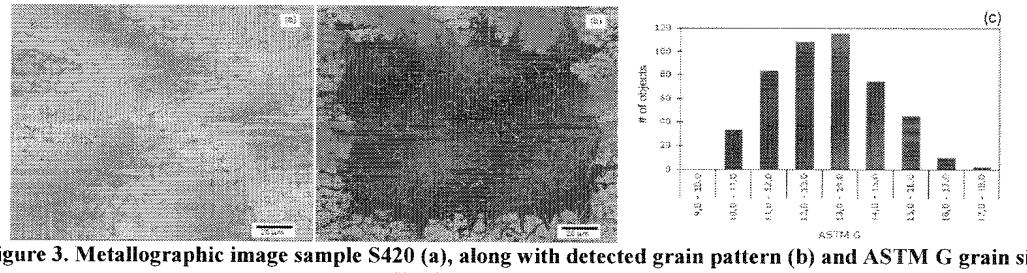

Figure 3. Metallographic image sample S420 (a), along with detected grain pattern (b) and ASTM G grain size distribution histogram (c).

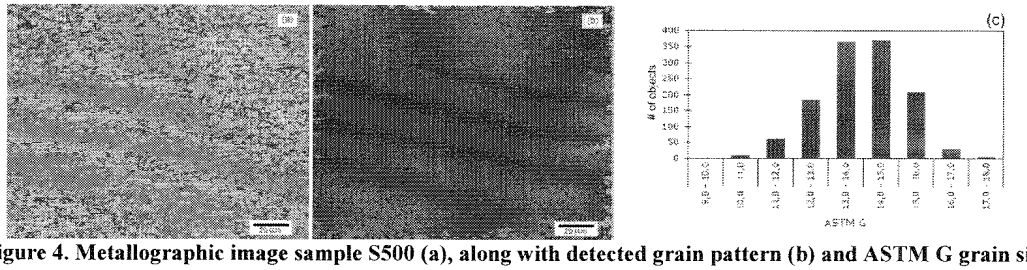

Figure 4. Metallographic image sample S500 (a), along with detected grain pattern (b) and ASTM G grain size distribution histogram (c).

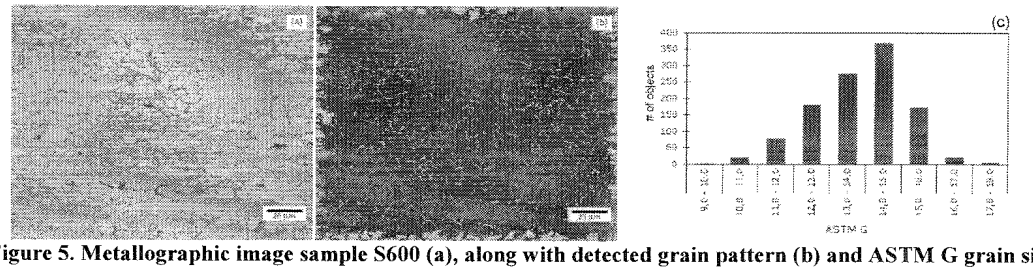

Figure 5. Metallographic image sample S600 (a), along with detected grain pattern (b) and ASTM G grain size distribution histogram (c).

The statistical distribution of frequency versus G size is of the normal type. Thus, the mean grain size G and standard deviation σ_G were determined using 6 micrographs for each steel and reporting the average value and standard deviation (Table IV). The values indicate (Figures 2, 3, 4 and 5) that these are in fact UFF steels with mean grain size values in the range of 13~14 ASTM (3.5 ~ 2.5 μm).

The optical micrographs of these steels, have the following common characteristics:

- Slight banding of the ferrite-pearlite structure in the rolling direction, where the volume fraction of pearlite, also quantitatively analyzed, never surpasses 5%, therefore making the structure, from a mechanical point of view, as single-phased.
- "Pancake" structure of the ferrite phase, inherited from the controlled rolling process, with elongated grains in the rolling direction, which makes indispensable, as indicated before, to measure intercepts in lines with different angles to obtain a correct $\bar{L}$ value.
- The structures are recrystallized, though no evidence of sub-grains was found, typical in restored states.

Discussion

As already indicated, the works published in the last decade on UFF steels are abundant, using different technologies, all of them developed until now in a laboratory level, with examples such as:

- Hot-rolling processes, followed by large deformations in warm temperature and rapid cooling developed at the Max Planck Institute (Germany), have produced grain sizes close to 1.6 μm [5].
- Dynamic Strain Induced Transformation - DSIT processes of hot-rolled sheets performed at Deakin University, Australia, with large deformations ($\varepsilon \approx 3$) in the $A_3 - A_{3r}$ interval, followed by controlled cooling, reaching grain sizes close to 0.5 μm [6-7].
- Severe Plastic Deformation - SPD and Accumulative Roll Bonding - ARB on steel and aluminum sheets at the Universities at Osaka and Tokyo, Japan, subjected to various cycles of deformation (cumulative deformation $\varepsilon_{Total} \approx 5$) and subcritic annealing. Grain sizes of 0.2 μm may be reached [8-10].
- Rapid Transformation Annealing - RTA processes which consist in large cold reductions of thickness in steel sheets ($1 < \varepsilon < 3$), followed by flash-annealing (lasting a few seconds) at subcritic ($<A_{c1}$), intercritic ($A_{c1}<T<A_{c3}$) or complete austenization temperatures. The University of Aachen, Germany and CEIT de Guipuzcoa, Spain have obtained grain sizes with values of 2 to 3 μm[11]. Similar procedures have been used in the R&D division of Tata Steel (India), working with low carbon martensitic steels[12].

All the research groups just mentioned have found what Howe[13], very wisely, has defined as the Achilles' heel of the UFF materials: there is an inferior limit for the grain size of these steels below which they are not able to homogenously strain-harden and are, therefore, unviable for processes of drawing and/or expansion cold-forming. The demonstration of this, is based in the works of Morrison[14] and Morrison and Miller[15] and focuses on the *n* coefficient of strain hardening, quoted in texts on metallic materials[16-23], and its correlation to grain size. In a resumed way, the argument is the following: when tested in tension, ductile materials -such as steel- show a response in the uniform deformation plastic zone that fits a Ludwik-Hollomon law type:

$$\sigma = K\varepsilon^n \tag{3}$$

where σ is the true tension stress, ε the true strain, K a proportional constant and n the strain hardening coefficient.

Figure 6 presents the σ/K value plotted versus ε for the investigated steels. On the other hand, ductile materials (steels included) also show a relation -based on deformation by dislocation movement- between yield stress s_y and grain size, consistent with the Hall-Petch formula:

$$s_y = s_0 + kd^{-1/2} \tag{4}$$

where s_y is the engineering lower yield stress, s_0 is the Peierls tension or resistance of the crystal lattice to the movement of dislocations, k is a constant function of the chemical composition of the steel and d is the grain size, usually expressed in mm.

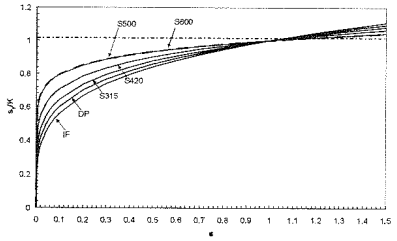

Figure 6. s_y/K as a function of ε

There are numerous theories (and formulas) to correlate composition, structure and mechanical properties of low, medium and high C steels, as well as stainless steels[17,19,23,24], all of them considering as starting point the Hall-Petch law and using linear regression multivariable methods: a relation is established between the yield stress s_y and the inverse square root of grain size. This law may also be applied to the fracture stress s_u and transition temperature (ITT), both of them very important in the design and application of structural steels, as the following examples show:

1) According to Pickering[17] for low C, ferritic-pearlitic, weldable steels, the formulas may be:

$$s_y(MPa) = 54 + 32(\%Mn) + 83(\%Si) + 354(\%N_f) + 17d^{-1/2} \quad (5)$$

$$s_u(MPa) = 295 + 28(\%Mn) + 83(\%Si) + 4(\%pearlite) + 8d^{-1/2} \quad (6)$$

with the alloying elements and pearlite expressed in weight percentage and grain size in mm. Not considering (as a first approximation) the influence of alloying elements:

- 0% pearlite steel (pure ferrite) as in an IF steel

$$s_y(MPa) \approx 54 + 17d^{-1/2} \quad (7)$$

$$s_u(MPa) \approx 295 + 8d^{-1/2} \quad (8)$$

$$s_y = s_u \rightarrow d^{-1/2} = 26.8 \rightarrow d = 1.4\mu m \quad (9)$$

Substituting in formulas (7) and (8):

$$s_y = s_u \approx 510MPa \quad (10)$$

- 15% pearlite steel (~0.1% C) as in low-carbon mild steel

$$s_y = s_u \rightarrow d^{-1/2} \approx 33.4 \rightarrow d = 0.9\mu m \quad (11)$$

$$s_y = s_u \approx 620MPa \quad (12)$$

- 25% pearlite steel (~0.2% C) as in structural steel

$$s_y = s_u \rightarrow d^{-1/2} \approx 37.9 \rightarrow d = 0.7\mu m \quad (13)$$

$$s_y = s_u \approx 700MPa \quad (14)$$

If s_y (and s_u) are plotted against $d^{-1/2}$ or d, it follows that the minimum grain size (critical size) that cancels the ductility of the steel is close to 1 μm.

2) According to Gawne and Lewis[24] the correlations would be the following:

$$s_y(MPa) = 27 + 22d^{-1/2} + 165(\%C) + 470(\%P) + 3000(\%N_f) + 60(\%Si) - 665(\%S) \quad (15)$$

$$s_u(MPa) = 150 + 16d^{-1/2} + 335(\%C) + 600(\%P) + 4505(\%N_f) + 77(\%Si) - 845(\%S) \quad (16)$$

with the numbers expressed in the same way as formulas (5) and (6). Using the same assumptions as in the previous case:

- 0% pearlite steel (pure ferrite) as in a IF steel

$$s_y(MPa) \approx 27 + 22d^{-1/2} \quad (17)$$

$$s_u(MPa) \approx 150 + 16d^{-1/2} \quad (18)$$

$$s_y = s_u \rightarrow d^{-1/2} = 20.5 \rightarrow d = 2.4\mu m \quad (19)$$

Substituting in formulas (15) and (16):

$$s_y = s_u \approx 480MPa \quad (20)$$

- 15% pearlite steel (~0.1% C) as in low-carbon mild steel

$$s_y = s_u \rightarrow d^{-1/2} \approx 23.7 \rightarrow d = 1.8\mu m \quad (21)$$

$$s_y = s_u \approx 565MPa \quad (22)$$

- 25% pearlite steel (~0.2% C) as in structural steel

$$s_y = s_u \rightarrow d^{-1/2} \approx 26.83 \rightarrow d = 1.4\mu m \quad (23)$$

$$s_y = s_u \approx 650MPa \quad (24)$$

In other words, the resulting critical grain sizes are above 1 μm and, therefore, mechanical resistances lower than those predicted by Pickering[17]. In any case, both works agree in a ferrite critical grain size of about 1 μm that will annul ductility. A 2.5 μm grain size (ASTM 14) would be a more conservative value, and in this case, the presence of a hardening phase (pearlite) diminishes the critical grain size. These two conclusions are very important in the process of designing UFF steels.

By accepting expressions (3) and (6), it may also be deduced the existence of a functional relation between the strain hardening coefficient *n* and grain size *d*, known as the Morrison law[14]:

$$n = 5/(10 + d^{-1/2}) \quad (25)$$

with *d* as grain size in mm. This formula, which establishes an inverse proportional relation between *n* and *d*, is particularly relevant for UFF (UFG) steels.

Steels that present a tensile curve with a higher yield stress, lower yield stress (s_y) and yield elongation by propagation of Lüders bands (plastic instability prior to uniform deformation), of ε_L value (true Lüders strain), may loose their capacity for homogenous deformation if the following condition[15] is verified:

$$\varepsilon_L = n \quad (26)$$

Therefore, non-homogenous Lüders deformations eliminate the capacity for strain hardening of the steel. Applying formulas (3) and (26) and relationships between engineering and true stress, it follows that:

$$s_y(1 + e_L) = K\varepsilon_L^n \quad (27)$$

where, taking logarithms in both sides of the equation and regrouping, leads to the expression:

$$\ln\frac{K}{s_y} = \varepsilon_L - n\ln\varepsilon_L = n(1 - \ln n) \quad (28)$$

Figure 7 presents the analytical expression for this last formula, where the limit curve, which corresponds to the $\varepsilon_L = n$ criterion is plotted, and separates the upper part of stable steels ($n > \varepsilon_L$) from the unstable ones ($n < \varepsilon_L$). The first ones overpass the yield elongation and strain harden, while the second ones ($n \leq \varepsilon_L$) fail to accomplish these aspects. On the figure, the UFF steels investigated in this work are presented, along with the reference DP and IF steels, all of them in the stable plastic deformation zone.

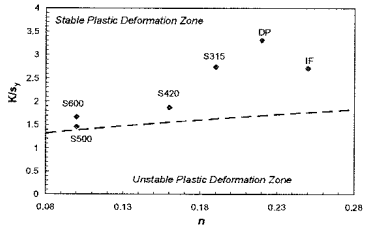

Figure 7. K/s_y in accordance to eq 28

From these considerations it may be deduced that there is a "natural" inferior limit imposed to UFG steels and their corresponding grain size d and homogenous deformation n, utterly connected to the deformation by dislocation movement and pile-up strengthening behavior[18]. In all cases the n coefficient should be higher than 0.08 (as may be seen in Figure 8). For n=0.1, the Morrison law (equation 25) requires a 0.6 μm grain size that seems excessively small, though, as reported by Tsuji et al.[8] in an exhaustive work carried out on commercial aluminum alloys (1100 quality) and ULC IF steels (%C<0.003, microalloyed with Ti), the critical grain size in these materials is close to 1 μm, beneath which the yield stress and tensile stress match up, making uniform deformation impossible, at least at room temperature. Figure 9 presents both the ASTM G grain size (on the left) and the mean linear intercept $\overline{L}$ in μm (on the right) as a function of the n coefficient for the four steels investigated. In the case of $\overline{L}$ (lower part of the figure) a second-degree-fit curve indicates a value below 2 μm for the 0.08 n coefficient limit. In a similar way (upper part of the figure), the ASTM G grain size is shown, along with the upper and lower limits for a 95% confidence level of these measurements. The second-degree-fit curves indicate that for an n value of 0.08, the corresponding mean grain size is close to 14.

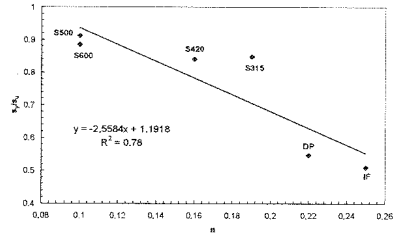

Figure 8. s_y/s_u as a function of n

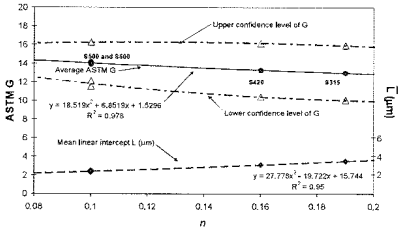

Figure 9. Mean linear intercept $\overline{L}$ grain size as a function of strain hardening coefficient n, and also average ASTM G number, along with 95% confidence level upper and lower limits for the four ultrafine grained steels investigated.

To conclude, as there is a correlation between the value of the s_y/s_u ratio and the n coefficient (as shown in Figure 8) there is a minimum value $n \approx 0.08$ for which s_y/s_u has a value lower than 1 and a threshold for uniform plastic deformations. Thus, microalloyed UFF ferrite-pearlite steels obtained by ATMCRP may reach 600 MPa in yield stress with limit values of $n \approx 0.1$ and $d \approx 2.5\ \mu m$. Increasing the yield stress over 600 MPa (S650 and S700 steels of the EN 10149-2 standard) would imply a raise in the Mn content, addition of Mo and microalloying B (besides Ti/Nb). These steels, after controlled rolling and rapid cooling will present, in the hot rolling raw state, ferritic-pearlitic-bainitic-martensitic structures: they are dual and multi-phase steels with ultrafine grain sizes below 2 μm. The work "Fundamentals of Dual-Phase steels"[25] explains the possibilities of strain hardening and cold work manufacturing on these materials, product of the increase in the n coefficient[26]. These dual-phase steels are a new class of high-strength low alloy (HSLA) materials characterized by a microstructure consisting of a dispersion of about 20 – 30 % of hard martensite islands in a soft, ductile ferrite matrix, although small amounts of bainite, pearlite, and retained austenite may also be

present. These steels have a number of unique properties (sometimes called multi-phase properties), which include:

- continuous yielding behavior (no yield point and ludering elongation),
- a low 0.2 percent offset yield strength (≈ 300 MPa),
- a high tensile strength (≈ 600 MPa),
- a high work hardening rate,
- an unusually high uniform and total elongation. The high work-hardening rate results in a yield strength of 500 MPa after only 5 ~ 10 % deformation.

As a result, in formed parts dual-phase steels have a yield strength comparable to that of other 600 MPa HSLA steels (S600) and much better ductility. More importantly, the high work-hardening rate, combined with the high uniform elongation of these steels, gives them a formability equivalent in stretching to that of much lower strength sheet steels (deep-drawing quality and drawing-quality). As a result these steels are an attractive material for weight-saving applications in automobiles.

Dual-phase steels can be produced either in the hot-rolled state (S650 and S700) or by intercritical heat treatment with either continuous annealing or box annealing technologies. Actual production has concentrated on using continuous-annealing processing lines because of higher production rates, better uniformity of properties, and the possibility to use lower alloy steels [26-27].

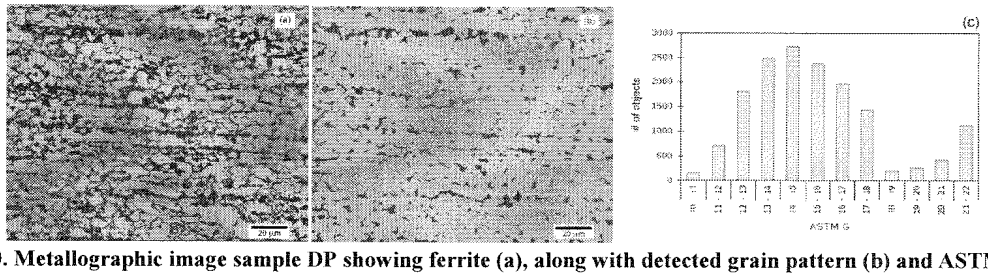

Figure 10. Metallographic image sample DP showing ferrite (a), along with detected grain pattern (b) and ASTM G grain size distribution histogram (c)

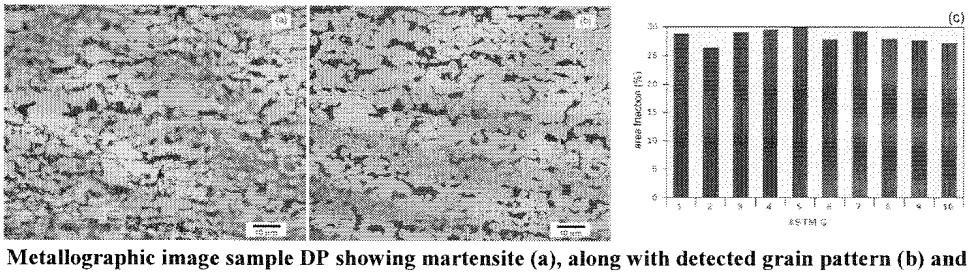

Figure 11. Metallographic image sample DP showing martensite (a), along with detected grain pattern (b) and martensite volume fraction histogram (c)

Figures 10 and 11 show the micrograph, ASTM grain size distribution and presence of ferrite and martensite respectively in a DP600 (in hot rolled state as demanded by RUR Group) steel, which has been used as a reference in this work. This material is also an ultrafine grained steel, and the reason for its low s_y/s_u ratio (high ductility) is the residual stresses introduced by the austenite during the martensitic transformation, after cooling into a ferritic matrix. In other words, the transformation occurs at low temperature (below 500°C) causing the ferritic phase to withstand the volume expansion (2~4 %). As a result, both a high dislocation density and residual stresses are generated at the ferritic phase surrounding martensite. In a simplified interpretation of the phenomena, the deformation pattern takes the form of thin bands of alternated deformed and not-deformed regions, parallel to the rolling direction. This pattern causes continuous yielding, which is a consequence of its yielding nucleation at many points in the sheet[19,21,25]. This mechanical behaviour is similar

to pre and post-tensioned steel reinforced concrete: steel bars work in tension (like ferrite) and bainite and martensite in compression (like concrete), increasing ductility and delaying fracture of the composite.

3. Conclusions

Low C steels microalloyed with Nb/Ti and ferritic-pearlitic structures standardized by UNE EN 10149-2, manufactured by ATMCRP in the ArcelorMittal de Asturias (Spain) factories are mainly used in automotive applications (fittings and reinforcement parts).

Denominations S315 to S600 investigated in this work have grain sizes lower than 5 μm (12 ASTM) and may be classified as UFF steels. Grain size is mainly in the 13~14 ASTM (3.5 to 2.5 μm) interval.

The strain hardening coefficient n is, in all cases, higher than 0.1, which makes them suitable for not-too-demanding cold work (bending and drawing), as indicated by the mentioned Euronorm.

If an excessive grain size refinement (reaching values close to 1 μm) results in a coefficient n value lower than 0.08, the steel would be plastically unstable (Lüders deformations): strain hardening would be impossible and the material industrially (in practice) unacceptable.

Microalloyed ferritic-pearlitic ultrafine grained steels with yield stresses higher than 600 MPa (including dual and multiphase steels), slightly alloyed with Mn/Mo, microalloyed with Ti/Nb/B and manufactured by ATMCRP, present second phases of the bainitic-martensitic type and reach values of $n > 0.1$, and thus, higher than the n=0.08 critical value.

The authors wish to thank the Research and Hot Coil Products Department of the ArcelorMittal in Asturias (Spain) Factories (formerly Ensidesa, CSI Planos, Aceralia and Arcelor). They also acknowledge Ms. Teresa Iglesias and Ms. Bertha Mendieta for their invaluable help in experimental work and text and figures revisions.

References:

[1] Special Issue on Ultrafine Grained Steels [M]. Tadashi Furuhara. Japan: ISIJ International, 2008.
[2] González, R., García, J.O., Barbés, M.A., Quintana, M.J., Verdeja, L.F., Verdeja, J.I. Ultrafine Grained HSLA Steels for Cold Forming [J]. Journal of Iron and Steel Research International, 2010, 17 (10): 50-56.
[3] Eager, T. The quiet revolution in materials manufacturing and production [J]. Journal of Metals, 1998, 50 (4): 19–26.
[4] VanderVoort, G.F. Metallography. Principles and Practice [M]. Ohio: ASM International, 1999.
[5] Morgan, P., Rickinson, B. Advances in the hot rolling of steels – Conference Report [C]. UK: Ironmaking and Steelmaking, 2004. 8–13.
[6] Beladi, H., Kelly, G.L., Hodgson, P.D. The Effect of Multiple Deformations on the Formation of Ultrafine Grained Steels [J]. Metallurgical and Materials Transactions A, 2007, 38A (3): 450–463.
[7] Beladi, H., Kelly, G.L., Hodgson, P.D. Ultrafine grained structure formation in steels using dynamic strain induced transformation processing [J]. International Material Review, 2007, 52 (1): 14–28.
[8] Tsuji, N., Ito, I., Saito, Y., Minamino, Y. Strength and ductility of ultrafine grained aluminum and iron produced by ARB and annealing [J]. Scripta Materialia, 2002, 47 (12): 893–899.
[9] Sakai, T., Belyakov, A., Miura, H. Ultrafine Grain Formation in Ferritic Stainless Steel during Severe Plastic Deformation [J]. Metallurgical and Materials Transactions A, 2008, 39 (9): 2206–2214.
[10] Okitsu, Y., Takata, N., Tsuji, N. A New Route to Fabricate Ultrafine Grained Structures in Carbon Steels without Severe Plastic Deformation [J]. Scripta Materialia, 2009, 60 (2): 76–79.
[11] Lesch, C., Alvarez, P., Bleck, W., Gil–Sevillano, J. Rapid Transformation Annealing: a Novel Method for Grain Refinement of Cold-Rolled Low-Carbon Steels [J]. Metallurgical and Material Transactions A, 2007, 38 (9): 1882–1890.
[12] Ghosh, C., Haldar, A., Ghosh, P., Ray, R.K. Microstructure, Texture, Grain Boundary Characteristics and Mechanical Properties of a Cold Rolled and Annealed Martensitic Steel [J]. ISIJ International, 2008, 48 (11): 1626–1634.
[13] Howe, A.A. Ultrafine grained steels: industrial prospects [J]. Materials Science and Technology, 2000, 16 (11-12): 1264–1266.
[14] Morrison, W.B. The Effect of Grain Size on the Stress-Strain Relationship in Low-Carbon Steel [J]. Transactions of the ASM, 1966, 59: 824–846.
[15] Morrison, W.B., Miller, R.L. The ductility of ultra-fine-grain alloys. Ultrafine–grain Metals [M]. NY, USA: Syracuse University Press, 1970.
[16] Backofen, W.A. Deformation processing [J]. Metallurgical Transactions, 1973, 4B (12), 2679–2699.
[17] Pickering, F.B. Physical Metallurgy and the Design of Steels [M]. London, UK: Applied Science Publishers, 1978.
[18] Dieter, G.E. Mechanical Metallurgy [M]. London, UK: McGraw–Hill Series in Materials Science and Engineering, 1981.
[19] Leslie, W.C. The Physical Metallurgy of Steels [M]. London, UK: McGraw–Hill. International Book Company, 1981.
[20] Llewellyn, D.T. Steels: Metallurgy and Applications [M]. Oxford, UK: Butterworth–Heinemann Limited, 1992.
[21] Pero-Sanz, J.A. Steels: Physical metallurgy. Selection and Design [M]. Madrid: CIE–Dossat 2000 (in Spanish), 2004.
[22] Hosford, W.F. Physical Metallurgy [M]. London:CRC Press, 2005.
[23] Pero-Sanz, J.A. Science and Materials Engineering [M]. Madrid: CIE–Dossat 2000 (in Spanish), 2006.
[24] Gawne, D.T., Lewis, G.M.H. Strain Hardening of High Strength Steels [J]. Materials Science and Technology, 1985, 1 (2): 128-135.

[25] Speich, G.R. Physical Metallurgy of dual–phase steels [C]. Pennsylvania: The Metallurgical Society of AIME, 1981. 3–45.
[26] Verdeja, J.I., Busto, A.G., García, J.O., Sancho, J.P. Iron and steel making in the third millennium [J]. CIM Bulletin, 2006, 99 (1097): 1–4.
[27] Verdeja, J.I., Pero-Sanz, J.A., Asensio, J. Multiphase Steels: Structure-Mechanical Properties Relationships in the Cold Rolled and Continuous Annealed Condition [C]. Switzerland: Materials Science Forum, 2005, 429-435.